universität wien

DISSERTATION / DOCTORAL THESIS

Titel der Dissertation /Title of the Doctoral Thesis

Generation and application of polyethylenimine based nanoparticulate systems for topical nucleic acid delivery to lung

verfasst von / submitted by

Mag. pharm. Alexander Taschauer

angestrebter akademischer Grad / in partial fulfilment of the requirements for the degree of

Doktor der Naturwissenschaften (Dr.rer.nat.)

Wien, 2019 / Vienna 2019

Studienkennzahl lt. Studienblatt / degree programme code as it appears on the student record sheet:	A 796 610 449
Dissertationsgebiet lt. Studienblatt / field of study as it appears on the student record sheet:	Pharmacy / Pharmazie
Betreut von / Supervisor:	Univ. Prof. Dipl. Ing. Dr. Manfred Ogris

To my grandfather

Acknowledgements

First, I would like to thank my supervisor Manfred Ogris for all his advices and for giving me the opportunity to work in his research group. Besides all the scientific freedom he also gave me the honor of being part during this advantageous phase of starting up a whole new lab.

Special thanks go to Haider Sami. Oh captain, my captain! Thank you for showing me what it needs to be a good scientist. Thanks for all those nice discussions about everything imaginable, natural and even supernatural. Your motivational speeches and quotations from our conversations like “we stand and fall together till this paper is submitted” are only two of many reasons why this friendship means that much to me.

My deepest gratitude goes to my diploma students Jakob, Martina, Viktoria, Emanuela, Simon , Stefan and Slavica for their scientific help but also all the lessons they taught me about life. I also thank all the other students in our lab for all the nice discussions we had and for their help during sometimes occurring stressful situations.

I also want to thank our “shadow in the dark”, Susi, for organizing everything in the lab that perfectly. Thank you for your openness and for giving me the opportunity to improve my “stuasteirisch”.

During this period of life I had the fortune to spend my time in the lab with the most amazing co-workers and friends somebody can have. Magda, Julia and Antonia, you made this whole journey something truly special.

At the last stage of my PhD thesis I had the honor of being founder member of a highly philosophical brotherhood. Thank you, Simon, Wolfram, Benjamin and Hermann for all the constructive input you give me.

Finally, I want to thank my family. Without your continuous help all of this wouldn´t have been possible.

Contents

I. Abstract

Gene therapy offers the possibility to treat the root cause of cancer, namely a genetic predisposition. Efficient transfer of nucleic acids can be achieved by both viral and non-viral delivery agents. In contrast to virus based formulations, non-viral vectors are characterized by their simple synthesis, low cost and the possibility of delivering a high amount of nucleic acid. In this PhD thesis, the focus lays on the modification and application of nucleic acid delivery agents based on linear polyethylenimine (LPEI). The thesis is divided into three main parts as described below.

Part One is mainly dedicated to the establishment of an up-scaled synthesis method for preparing polyplexes based on LPEI and pDNA. Manual mixing by flash pipetting shows certain drawbacks like its limitation to relatively small synthesis volumes and distinct batch-to-batch variability. By using a syringe pump based system, we could overcome these shortcomings: well-defined nanoparticles with consistent physical properties and good *in vitro* and *in vivo* transfection abilities were obtained.

In **Part Two** LPEI polyplexes were used for topical non-targeted and targeted treatment of CD49f overexpressing lung metastasis by aerosolization. *In vivo* experiments with Balb/c mice bearing iRFP720 labelled tumors demonstrated the possibility of co-localizing the fluorescence signal of iRFP720 and bioluminescence signals created by sufficient tissue transfection with polyplexes. The influence of introducing PEG and a CD49f targeting domain on physical and biological properties of polyplexes was extensively tested by nanoparticle tracking analysis (NTA), *in vitro* and *in vivo* assays. Physical evaluation of polyplexes showed high stability of nanoparticles after aerosolization. Shielding of LPEI with PEG resulted in an enhancement of the transfection efficiency *in vivo*. Additionally, a significant improvement of cell association, uptake and transfection was observed with the CD49f targeted conjugate.

In **Part Three** we developed a new gene carrier system based on gold nanoparticles (AuNP), small interfering RNA (siRNA) and LPEI, termed as auropolyplexes. Cationic gold nanoparticles could be generated by chemisorption of LPEI with a terminal mercapto moiety. Auropolyplexes were synthesized by mixing cationic gold nanoparticles with siRNA followed by additional LPEI. The product showed high physical stability and good knock-down efficiency *in vitro*. *In vivo* biodistribution studies revealed an efficient release of siRNA after i.t. administration. The flexibility of the formulation was shown by using LPEI with different molecular weights and PEGylated LPEI for the last complexation step.

II. Zusammenfassung

Gentherapie ermöglicht die Behandlung der Grundursache von Krebs, nämlich eine genetische Veranlagung. Der effiziente Transfer von Nukleinsäuren kann sowohl mit viralen als auch non-viralen Gentransferkomponenten erzielt werden. Im Gegensatz zu viral basierten Formulierungen sind non-virale Vektoren durch ihre einfache Synthese, geringe Kosten und die Möglichkeit der Übertragung hoher Mengen von Nukleinsäuren charakterisiert. Der Hauptfokus dieser Doktorarbeit liegt auf der Modifikation und Anwendung von Nukleinsäuretransferkomponenten basierend auf lineares Polyethylenimin (LPEI). Die Arbeit ist, wie folgt beschrieben, in drei Hauptteile aufgeteilt:

Teil Eins widmet sich hauptsächlich der Entwicklung einer hochskalierten Synthesemethode für die Herstellung von Polyplexen basierend auf LPEI und pDNA. Manuelles Mischen durch "rasches Pipettieren" zeigt bestimmte Nachteile wie dessen Limitierung auf relativ kleine Synthesevolumina und deutliche Chargenvariationen. Durch die Verwendung eines spritzenpumpenbasierten Systems konnten wir diese Mängel beheben: Gut definierte Nanopartikel mit konsistenten physikalischen Eigenschaften und guten *in vitro* und *in vivo* Transfektionsfähigkeiten wurden erhalten.

In **Teil Zwei** wurden LPEI-Polyplexe für die topische ungezielte und gezielte Behandlung von CD49f-überexprimierenden Lungenmetastasen durch Aerosolisierung verwendet. *In vivo* Experimente mit iRFP720 markierten tumortragenden Balb/c-Mäusen demonstrierten die Möglichkeit der Co-Lokalisierung des Fluoreszenzsignals von iRFP720 und Biolumineszenzsignalen erzeugt durch die erfolgreiche Gewebstransfektion mit Polyplexen. Der Einfluss der Einführung von PEG und einer CD49f-Zielrichtungsdomäne auf die physikalischen und biologischen Eigenschaften von Polyplexen wurde eingehend mittels "nanoparticle tracking analysis" (NTA), *in vitro* und *in vivo* Untersuchungen getestet. Die physikalische Überprüfung von Polyplexen zeigte eine hohe Stabilität der Nanopartikel nach Aerosolisierung. Die Abschirmung von LPEI mit PEG resultierte in einer Steigerung der Transfektionseffizienz *in vivo*. Zusätzlich wurde eine signifikante Verbesserung der Zellassoziation, der Aufnahme und Transfektion mit dem CD49f-zielgerichteten Konjugat beobachtet.

In **Teil Drei** entwickelten wir ein neues Genüberträgersystem basierend auf Goldnanopartikel (AuNP), kleiner interferierender RNA (siRNA) und LPEI, auch als Auropolyplexe bezeichnet. Kationische Goldnanopartikel konnten durch Chemisorption von LPEI mit terminaler Mercaptogruppe hergestellt werden. Auropolyplexe wurden durch das Mischen von

kationischen Goldnanopartikeln mit siRNA gefolgt von zusätzlichem LPEI generiert. Das Produkt zeigte eine hohe physikalische Stabilität und eine gute Knock-down Effizienz *in vitro*. Die *in vivo* Bioverteilung zeigte die effiziente Freisetzung von siRNA nach i.t. Verabreichung. Die Flexibilität der Formulierung wurde durch die Verwendung von LPEI mit unterschiedlichem Molekulargewicht und PEGyliertem LPEI für den letzten Komplexierschritt gezeigt.

III. Introduction

1. Gene therapy for cancer treatment

The standard of care in cancer therapy is a combination of surgery, radiation treatment and chemotherapy.[1] However, the fact that this schedule is often confronted with resurgence of the disease leads to other therapeutical approaches coming into focus for cancer treatment.[2] One of them is gene therapy, which mainly concentrates on the fact that generation and progression of cancer diseases are based on a genetic predisposition.[3] Cancer is a multistage process leading to an accumulation of mutations within proto-oncogenes and tumor suppressor genes followed by uncontrolled tissue proliferation due an imbalance in the cell cycle.[4, 5] Lack or dysfunction of tumor suppressors and an amplification of growth promoting signals are the basis of the chronic proliferation and progression of tumor tissue, hence important targets for gene therapy.[6, 7]

In general, gene therapy is a prodrug based approach characterized by high specificity. Due to the rather high molecular weight of nucleic acids applied, it is not affected by certain shortcomings like efflux mediated drug resistances, which can limit the treatment efficiency of small molecular weight cytostatic drugs. However, direct administration of naked nucleic acids is not efficient due to fast enzymatic degradation by nucleases and low uptake into target tissue mainly because of their polyanionic character.[8-10] The development of gene therapy started with the application of viral vectors as vehicles for nucleic acids.[11] Efficient transfer of genes into target tissue showed clear advantages over other therapeutic approaches.[12, 13] Compared to both physical and chemical based transfection methods, the application of viral vectors often results in relatively high transgene expression. Modifications of viral vectors can be conducted in order to improve both efficiency and tissue specificity and reduce toxicity. For example, introduction of polyethylene glycol (PEG) combined with the addition of targeting moieties like transferrin on the capsid surface could be applied for sufficient retargeting of the virus.[14] For monogenetic diseases and/or *ex vivo* approaches, adeno associated virus (AAV) and lentivirus, respectively, show in general high and stable gene transfer combined with good biocompatibility and are therefore used as main compounds in clinically approved gene therapeutics (e.g. Glybera® (AAV), Luxturna® (AAV) and Kymriah® (lentivirus)).[15] On the other hand, oncolytic vectors (e.g. Imlygic® (herpes simplex)) can be used for combining high tumor cell specificity with an activation of antitumor immune reactions.[16]

Nevertheless, the immunogenicity of viral vectors limits the efficacy of repeated systemic administration, and risks related to fatal systemic immune reactions, or, in case of integrating vectors, insertional mutagenesis remain.[17, 18]

2. Non-viral gene delivery agents

Delivery of genes into target tissue through the application of naked nucleic acids shows low efficiency because of their high molecular weight and their negative charge.[19] Besides their low cellular uptake especially unmodified nucleic acids are also prone to fast degradation after *in vivo* administration.[9, 20, 21] Chemical modification of short, synthetic nucleic acids, like oligonuclecotides and small interfering RNA (siRNA) molecules can improve both enzymatic stability and cell uptake.[9] Drisapersen, for example, is a 2'-O-methyl-phosphorothioate modified RNA molecule which shows promising results in the treatment of Duchenne muscular dystrophy.[22] Such phosphorothioate modifications enhance the binding of oligonucleotides to plasma proteins and cells. A further approach to enhance cellular binding and uptake is the direct conjugation of oligonucleotides to peptide/protein based ligands.[23]

Non-viral gene delivery vectors can be used for efficient complexation and protection of nucleic acids in order to overcome above described biological barriers.[24] Non-viral vectors are in general positively charged macromolecules which condense nucleic acids into virus like particles.[25, 26] Compared to viral vectors, non-viral gene transfer agents are rather simple chemicals. Both synthesis and modifications of such compounds can be easily accomplished. Additionally, non-viral gene delivery vehicles like cationic lipids and polycationic compounds are able to complex large quantities of nucleic acids.[19] Complexation of nucleic acids mainly works via electrostatic interaction followed by hydrophobic collapse resulting in nano-sized particles characterized by surplus of positive charge.[19] Based on their positive charge those so-called nanoplexes are able to electrostatically interact with negatively charged molecules such as glycosaminoglycanes located on the cellular surface which leads to endocytosis.[1, 27, 28]

2.1. Lipoplexes

Lipid based gene delivery systems, so called lipoplexes, are the most commonly used transfection agents for both DNA and RNA delivery.[13, 29, 30] The chemical structure of such lipids is characterized by a hydrophobic tail and a positively charged hydrophilic head group which is usually based on functional groups with a basic character such as amine, quarternary ammonium and guanidinium moieties as well as peptide and heterocyclic structures.[31] The backbone of such lipids connects the hydrophilic cationic moiety with the hydrophobic part and can be composed

of functionalities like peptides, phosphate, phosphonate linkers and aromatic compounds. Cationic lipids like N-[1-(2,3-Dioleoyloxy)propyl]-N,N,N-trimethylammonium (DOTAP) are connected via ester groups which show a relatively low chemical stability (Figure 1).[32] In contrast 1,2-di-O-octadecenyl-3-trimethylammonium propane (DOTMA) which is bound via ether functionalities is characterized by high chemical stability without biodegradability. Because of the versatile chemical structure of linker compounds modifications based on the introduction of amide or carbamate functionalities can be used for changing chemical stability and biocompatibility of the final product. In order to improve both physical and biological properties of the final complex with nucleic acids, lipoplexes are often generated combining cationic lipids with neutral helper lipids, like cholesterol and 1,2-Dioleoyl-sn-glycero-3-phosphoethanolamine (DOPE).[33] The application of cholesterol for the synthesis results in the formation of lipoplexes characterized by high stability under physiological conditions.

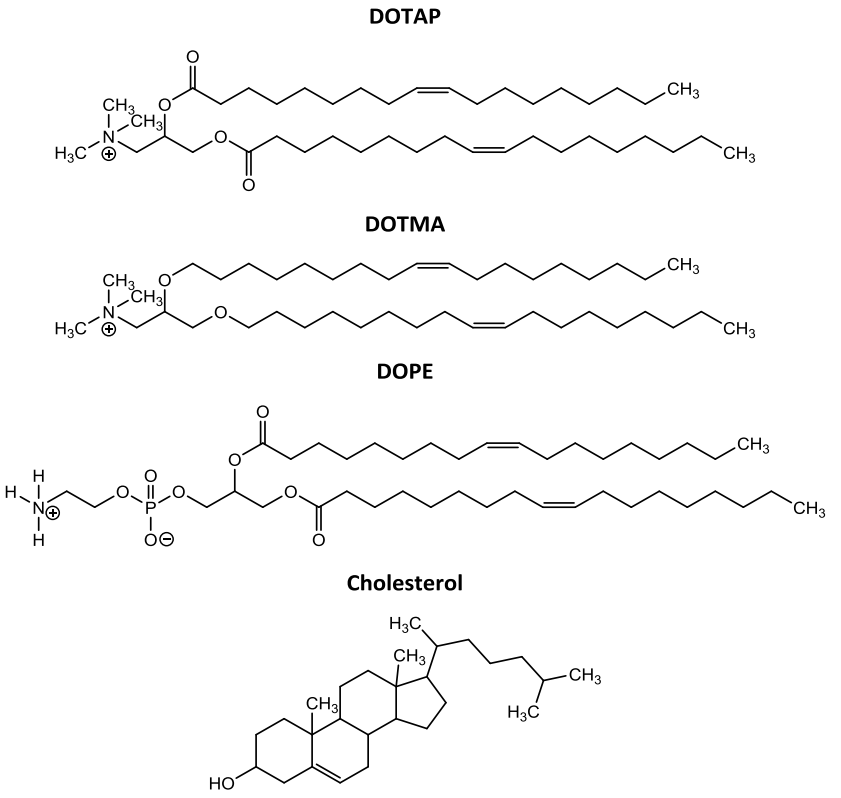

Figure 1: *Examples for positively charged (DOTAP, DOTMA) and neutral/uncharged lipids (DOPE, cholesterol) often used for lipoplex formation*

Based on their composition lipoplexes can show different structural characteristics which could be revealed by X-ray diffraction analysis. Both multilamellar structures with alternating lipid bilayers and nucleic acid based monolayers as well as inverted hexagonal structures with cylinder-like lipid structures with a nucleic acid core could be detected.[31] Major drawbacks of

lipoplex formulations when applied *in vivo* are inflammatory reactions due to high toxicity and formation of aggregates due to non-specific interactions with blood components.[34]

2.2. Inorganic nanoparticle formulations

Nanoparticles derived from heavy metals such as gold and iron can be applied as template material for non-viral gene delivery as their physical and biological properties can simply be changed by introducing surface modifications.[35, 36] Products characterized by relatively small hydrodynamic diameters with low polydispersity can be reproducibly generated following simple synthesis routes ensuring the generation of well-defined formulations. Especially particles characterized by small size and high stability can easily be internalized by cells.[34]

In general there are two different approaches to generate inorganic nanomaterial, namely the top-down and the bottom-up approach.[37] The top-down approach describes the procedure of creating nanoparticles starting with bulk material through the application of methods like etching and lithiography. The main disadvantage of such techniques is the creation of particles often characterized by high heterogeneity. The bottom-up approach is about the assembly of single atoms or molecules into nanostructures which often results in a product with low polydispersity. This can, for example, be done by simple chemical reduction of the initiating compounds.[38]

One of the most commonly used methods for generating spherical and rod-shaped gold nanoparticles is the application of sodium citrate as initiator in a certain ratio to $HAuCl_4$ where sodium citrate acts as reducing agent, stabilizer and pH mediator.[39, 40] Size of the resulting particles can be controlled based on the ratio between gold and sodium citrate. The size dependent uptake of citrate capped gold nanoparticles has been evaluated by Chithrani et al. who found out that especially particles with a mean diameter of 50 nm show efficient internalization into cells despite their negative surface charge.[41] They hypothesized that non-specific interactions with proteins in the cell culture medium might play an important role during cell uptake.

In case of gold nanoparticles, compounds containing thiol, phosphine and amine functionalities attach by chemisorption which enables modifications of the gold nanoparticle surface. Based on that, fast and efficient coupling of targeting peptides, antibodies and nucleic acids can be conducted for generating gold nanoconjugates.[36, 42] Such formulations can be applied for tissue specific gene delivery but also as contrast agents for X-ray and computed tomography (CT) imaging due to the high mass attenuation coefficient of gold. Surface modifications with

peptides and antibodies resulted in efficient targeting of tumor tissue, liver, lymph nodes etc.[43-45] Besides their high electron density, which enables detection by transmission electron microscopy, gold nanoparticles are also characterized by surface plasmon resonance.[46] Based on that, a suspension of spherical unmodified gold nanoparticles shows light absorption at a wavelength between 510 nm and 540 nm depending on the particle size.[47] Therefore modifications which result in an increase of particle size can be detected by a shift of the absorption of light towards a longer wavelength.

2.2.1. Gold nanoparticles for nucleic acid delivery

Gold nanoparticles can be used as template for the development of formulations for nucleic acid delivery. Wurster et al. used a combination of gold nanoparticles as template compound with BPEI and siRNA for efficient gene transfer.[47] In their protocol they functionalized citrate capped gold nanoparticles by thiol exchange with 11-mercaptoundecanoic acid. The resulting negatively charged surface was used as starting point for generating alternating layers of BPEI and siRNA by electrostatic interaction. This principle is also termed as layer-by-layer assembly.[48, 49] One of the major disadvantages of this approach is that every coating procedure is followed by purification steps in order to remove excessive unbound polymer which is automatically related to significant product loss.[50] This and the batch dependent loading with siRNA and therefore lack of reproducibility of the synthesis are major points why other synthetic approaches are needed for nucleic acid delivery based on gold nanoparticles as template material.[51, 52]

Another possibility for surface modifications of gold nanoparticles is the direct coupling of alkanethiol modified oligonucleotides.[53] With that method coupling of approx. 250 oligonucleotides per nanoparticle with a size of 15 nm could be achieved.[54] Oligonucleotides bound to the gold surface showed high stability against nucleases which could be due to steric hindrance because of the dense packing of the nucleotides.[55] Interestingly, despite their highly negatively charged surface oligonucleotide modified gold nanoparticles showed good cellular uptake. Same as described above for citrate capped gold nanoparticles also here efficient cell uptake might be due to changes in both particle size and ζ-potential through non-specific adhesion of positively charged serum proteins. Important, due to the direct coupling of oligonucleotides to the gold surface by chemisorption approx. 60 % of the nucleic acid remained bound on the nanoparticles and might therefore not show any effect on target cells/tissue.[56]

2.3. PAMAM dendrimers

In case of polycationic compounds the interaction of the delivery agent with the nucleic acid is based on electrostatic interaction. Amongst those compounds, especially polyamidoamine (PAMAM) dendrimers and polyethylenimine (PEI) showed high efficiency both for complexation and the delivery of nucleic acids.[19] One major advantage of PAMAM is the synthetic strategy which leads to a relatively monodisperse product.[57] The chemical structure of PAMAM dendrimers is in general based on a multifunctional core, a repetitive branching amidoamine based internal structure and a modifiable surface which in a simple form can be based on primary amine groups (Figure 2).[58, 59] Generation of the branched internal structure is done by Michael addition of a "core" compound like ethylenediamine to methyl acrylate followed by amidation of the ester functionality with ethylenediamine.[57] With ethylenediamine as core four branches per reaction can be created. Repetition of those reactions leads to different generations of PAMAM dendrimers and therefore an increase of both molecular weight and the total amount of functional surface groups of the final product. Especially higher generation PAMAM dendrimers are characterized by their high efficiency regarding complexation of big amounts of nucleic acids forming compact and highly stable particles.[60]

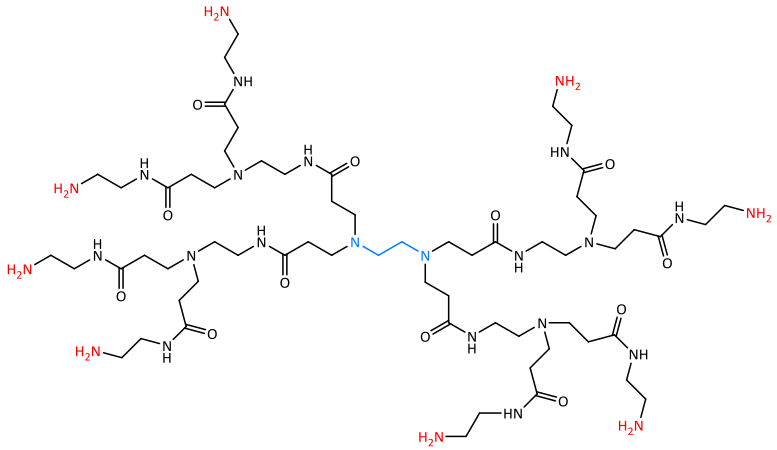

Figure 2: *Generation 1 PAMAM with an ethylendiamine "core" unit (blue) and in total 8 amino surface groups (red)*

Cationic PAMAM dendrimers show relatively high toxicity when compared to their uncharged or negatively charged equivalents. The strong electrostatic interaction of those compounds with the cellular surface increases the risk for lysis and therefore high cell toxicity.[61, 62] *In vivo* experiments on embryonic zebrafish with unmodified primary amine terminated PAMAM dendrimers revealed increased mortality with decreasing generation which could be due to reduced stability of polyplexes.[63] Side effects like the formation of pericardial edema could be observed.

2.4. Polyethylenimine

2.4.1. Branched polyethylenimine

Branched PEI (BPEI) was first used in 1995 as transfection agent for delivering pDNA *in vitro* and *in vivo*.[64] Due to its high density of positive charges based on protonable primary, secondary and tertiary amino groups it can be used for condensation of high amounts of nucleic acid.[65] The synthesis of BPEI is based on a cationic ring opening polymerization of aziridine as starting material (Figure 3).[66, 67] Under acidic conditions an aziridinium ion is formed and attacked by another aziridine monomer. In this synthesis approach "propagation" and "branching" reactions occure. With this strategy generation of BPEI with a molecular weight even higher than 800 kDa is possible.[65] However, the principle of its generation also leads to a variable and incontrollable total amount of primary, secondary and tertiary amino groups which has major impact on polymer properties when it comes to complexation of nucleic acids and toxicity.[67, 68]

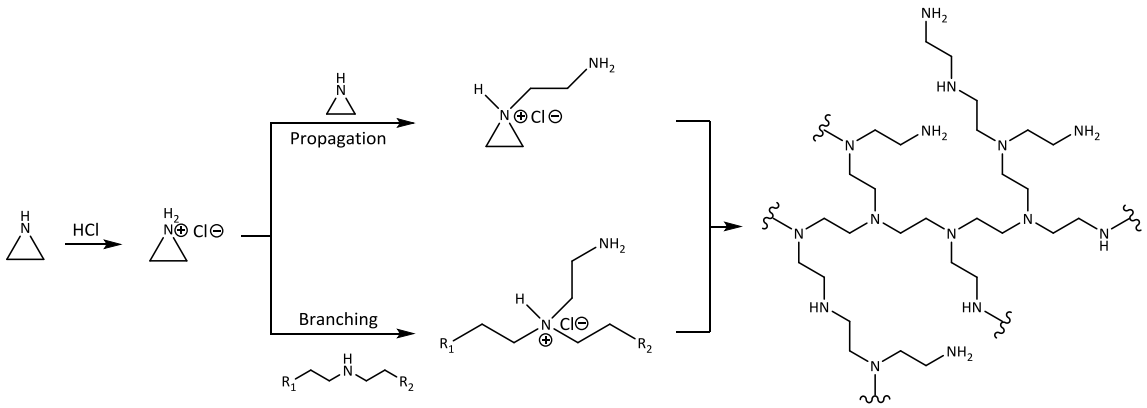

Figure 3: *Synthesis of BPEI with aziridine under acidic conditions (here HCl). Propagation and branching reaction result in the formation of a branched structure with primary, secondary and tertiary amino groups.*

At physiological pH, approx. 50 % of the amino groups are protonated.[1, 69] Like other positively charged non-viral gene delivery agents, PEI based polyplexes interact with negatively charged compounds on the cellular surface leading to endocytosis. In literature, both adsorptive and fluid-phase endocytosis have been described for PEI polyplexes.[70, 71] The endosomal release is based on the high buffering capacity of PEI which leads to an active transport of protons into the endosome, also known as "proton sponge" effect. The following passive transport of chloride and water into the endosome results in rupture of the endosomal membrane and the release of the particles into the cytosol.[72]

Both physical and biological properties of PEI based polyplexes are dependent on the molecular weight and the ratio between nitrogen groups of PEI and phosphate groups of the nucleic acid, also known as N/P ratio.[19] Formation of stable polyplexes starts with N/P 2-3.[73] Erbacher et al. showed that with PEI with a molecular weight of 25 kDa an increase of the N/P ratio leads to a reduction of the particle size from >1000 nm for N/P 2 to 100-200 nm for N/P 20.[74] In other words, N/P ratios close to electroneutrality lead to a high tendency for aggregate formation. With increasing N/P ratio also the total amount of free PEI necessary for particle stabilization and transfection efficiency increases.[75]

2.4.2. Linear polyethylenimine

In contrast to branched PEI, linear PEI (LPEI) shows a backbone with only secondary amino groups. LPEI is usually synthesized by acidic hydrolysis of poly(2-alkyl-2-oxazoline) (e.g. poly(2-ethyl-2-oxazoline)).[76, 77] Poly(2-ethyl-2-oxazoline) is generated by cationic ring opening polymerization of its monomer (Figure 4). The polymerization degree can be controlled by the ratio between the initiator compound and the monomer. Variations of reagents which are used for initiation and termination of the polymerization give the possibility of changing the structure of both α- and ω-terminus of the product. As initiator strong alkylating agents like tosylate compounds can be used under water free conditions.[78] Termination is conducted with nucleophilic compounds like methanolic KOH, ammonia or piperidine.[78, 79] Figure 4 shows the polymerization mechanism using methyl tosylate as initiating compound and methanolic KOH as terminating agent. Deacylation of poly(2-ethyl-2-oxazoline) can be done under strong acidic conditions with HCl. During this procedure both concentration of HCl and duration of the reaction process can be changed in order to synthesize either LPEI or partially deacylated poly(2-ethyl-2-oxazoline) giving the possibility to change nucleic acid complexation properties, toxicity and transfection behaviour of resulting polyplexes.[76]

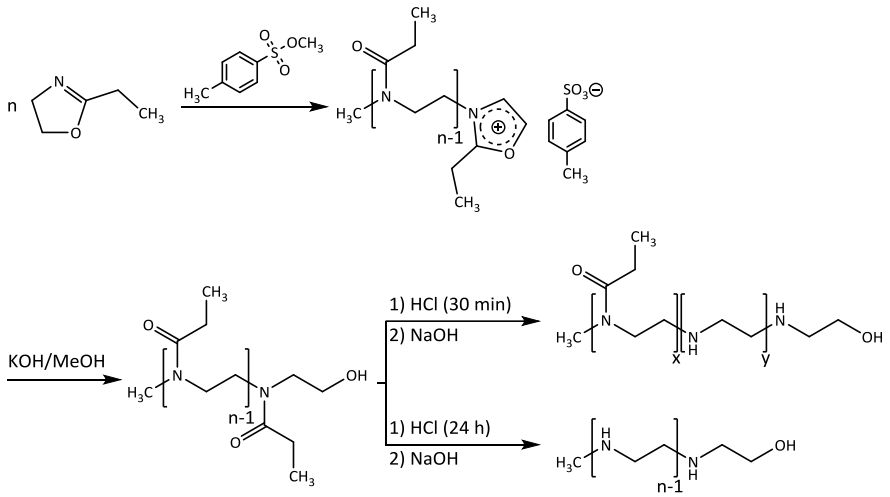

Figure 4: *LPEI synthesis scheme showing the generation of poly(2-ethyl-2-oxazoline) with n Mol 2-ethyl-2-oxazoline as monomer and methyl tosylate as initiator. Termination is done with methanolic KOH. Through variations in HCl concentration and the total duration of dealkylation either partially hydrolyzed poly(2-ethyl-2-oxazoline) or LPEI can be generated*

2.4.3. Manual versus automated polyplex generation

In general, one major disadvantage of polyplex formulations are variations amongst different synthesis batches regarding physical particle properties which might negatively affect their biological activity.[80] This is mainly due to the standard procedure applied for particle preparation which is based on manual mixing of the components by pipetting. Being limited to relatively small volumes this method also tends to result in operator specific variations of the final product with a high risk for irreproducible gene delivery.[81] Kasper et al. described the possibility of polyplex generation with a syringe pump based system which enabled automated and controlled mixing of polycation and nucleic acid containing solutions.[82] The whole procedure ensured both reproducible generation of gene delivery particles and the possibility of creating bigger product volumes. Based on the same principle the Gill and Hyde group established a device for the production of sample volumes up to 100 mL.[83]

2.4.4. Toxicity of PEI

PEI in general shows toxicity characterized by the generation of intracellular stress when released into the cytoplasm through its influence on mitochondrial pathways.[84] Moghimi et al. described PEI derived cytotoxicity as a two-stage process where mitochondrial mediated apoptosis follows damage of the cellular membrane.[85] Both *in vivo* and *in vitro* toxicity of PEI seems to directly correlate not only with the total amount of the compound applied but also with its molecular weight.[86] It is thereby necessary to use PEI with a molecular weight which ensures optimal condensation and transfer of the nucleic acid but still shows controllable

toxicity. Additionally, PEI with a branched chemical structure is characterized by significantly higher cytotoxicity compared to linear PEI.[87, 88]

2.4.5. Comparison of LPEI and BPEI based delivery of pDNA

LPEI shows overall better performance in pDNA delivery both *in vitro* and *in vivo* compared to BPEI.[89-92] *In vitro* experiments of different cancer cell lines done by Wightman et al. resulted in a clear improvement of transgene expression after LPEI treatment at N/P ratios ranging from 3.5 to 8 compared to BPEI polyplexes at same N/P ratios.[93] Experiments were conducted in salt containing buffer (HBS; HEPES buffered saline). In general, BPEI and LPEI based polyplexes prepared under low salt conditions (e.g. 5% glucose at pH 7.4) are characterized by small size and high stability. However, due to their small size those particles showed limited ability to accumulate on the cellular surface requiring either an increased treatment concentration or prolonged treatment duration to achieve good transfection efficiency. As BPEI creates highly stable particles even in salt containing buffers formation of particle accumulation on the cellular surface and therefore cell uptake was significantly reduced when compared to its linear polymer version. This relation between transfection efficiency, particle size and particle sedimentation was also investigated by Pezzoli et al.[94] In their protocol they increased the sedimentation of small particles by centrifugation and with that significantly improved their transfection efficiency. Same could be observed *in vivo*. After intravenous (i.v.) injection unmodified LPEI polyplexes showed significant particle aggregation because of interaction with blood components, such as serum proteins and platelets.[89, 90, 95] Intravenous administration of LPEI based particles resulted in high transfection of lung tissue, especially of endothelial cells in the lungs and type I and type II pneumocytes.[96] Experiments based on the i.v. administration of BPEI polyplexes with comparable molecular weight prepared at the same concentration and N/P ratio showed rather low transgene expression and significantly higher toxicity when compared to LPEI.[93]

2.4.6. Comparison of PEI complexation efficiency for pDNA and siRNA

Due to its good complexation abilities PEI can also be used as delivery agent for relatively small nucleic acid types, such as siRNA.[3, 97] In general RNA interference is known to play an important role in the control of cell growth and development through post transcriptional gene silencing. Furthermore, it is part of protection mechanisms against double stranded RNA derived by viruses.[98, 99] Therefore, delivering siRNA for the down regulation of genes which, for example, are responsible for tumor progression is an important approach in cancer therapy. In short,

double stranded siRNA works through the incorporation into the RNA-induced silencing complex (RISC).[100] After removal of the sense strand the antisense strand directs RISC to the target mRNA which gets cleaved by so called Argonaute proteins.[101]

With a size of 21-23 nucleotides siRNA molecules are relatively small when compared to other nucleic acid types like pDNA.[102] Therefore, good complexation properties and efficient protection of the payload are major criteria for non-viral gene delivery agents. PEI polyplexes based on pDNA show in general higher stability compared to those based on siRNA.[103, 104] Especially LPEI shows low complexation and transfection abilities for siRNA.[86] Reason for that are structural differences and the high molecular weight, hence the total amount of negative charges of pDNA compared to siRNA. Investigations based on molecular dynamics simulations were conducted in order to show the difference of the interaction of LPEI with DNA and siRNA.[105] Those experiments revealed that DNA shows interaction with more protonated nitrogens of the LPEI molecule compared to siRNA. Besides that, a reduction of the configurational entropy of siRNA when condensed in polyplexes seems to make the whole complexation process during particle formation less energetically favorable. This is confirmed by *in vitro* experiments which showed insufficient siRNA delivery with unmodified LPEI of different molecular weights.[106, 107] Compared to LPEI/siRNA polyplexes those based on BPEI were characterized by higher transfection efficiency. This is most probably due to both the branched chemical structure of BPEI and its composition of primary, secondary and tertiary amines which enhances electrostatic interactions between the polycation and the nucleic acid.[86]

Further investigations showed, also in case of BPEI/siRNA polyplexes, the influence of the molecular weight of the polycation on physical particle properties. BPEI with a high molecular weight required lower N/P ratios for good transfection efficiency compared to low molecular weight BPEI.[87, 108] However, due to the positive correlation of reduced cytotoxicity with decreasing molecular weight of the polycation Werth et al. investigated the efficiency of low molecular weight fractions of BPEI obtained by size exclusion chromatography.[8] Cell treatment with polyplexes based on such low molecular weight fractions showed sufficient transfection together with higher cell viability. Same as with pDNA based complexes a significant impact of the synthesis medium on physical and biological properties of BPEI/siRNA polyplexes could be found. In general, BPEI/siRNA polyplexes prepared in 5 % (w/V) glucose showed higher stability and biological activity even after lyophilization compared to particles generated in 150 mM NaCl.

2.5. Evaluation of transfection efficiency in vitro and in vivo with reporter genes

Biological properties of both viral and non-viral gene delivery agents can be analyzed by the application of nucleic acid based reporter constructs. Such reporters consist of two parts, namely a promoter and the reporter gene.[109, 110] Promoters show either inducible or constitutive activity. Analysis of transfection efficiency with constitutively active promoters is done in order to evaluate reporter gene expression without regulation by cell processes. Typical examples are the promoters of the simian virus 40 (SV40), the human elongation factor 1α (EF1α) and the immediate-early cytomegalovirus promoter (CMV).[111] Important, amongst different cell lines variations in the activity of such constitutively active promoters could be found.[112] Therefore, detailed investigations have to be done for finding the optimal promoter for transfection assays.

Monitoring of gene delivery efficiency both *in vitro* and *in vivo* could be conducted with reporter genes encoding for fluorescent and luminescent proteins. Two examples for such fluorescent reporter proteins are the enhanced green fluorescent protein (EGFP) with an excitation maximum at 488 nm and emission maximum at 509 nm and the near-infrared (NIR) fluorescent proteins (iRFP) like iRFP720 with an excitation maximum at 702 nm and emission maximum at 720 nm.[113-115] EGFP shows limited usability for *in vivo* imaging as its emitted light gets almost completely absorbed by hemoglobin and melanin. The excitation and emission profile of NIR fluorescent proteins lies in an “optical window” between 650 nm and 900 nm where body tissue shows the highest transparency to light.[116] Therefore, iRFPs can be applied for deep optical imaging.

Compared to fluorescent proteins the application of bioluminescence reporters does not require excitation light which reduces background signals and therefore results in higher sensitivity.[117] This is especially needed for the evaluation of the influence of targeting moieties on the transfection efficiency of gene delivery agents. The light signal generated by luciferases is based on the enzymatic oxidation of a substrate, like luciferin for firefly luciferase and coelenterazine for Gaussia luciferase.[118] In contrast to firefly luciferase which stays intracellularly after expression and creates its light signal dependent on ATP Gaussia luciferase gets secreted and catalyses the conversion of its substrate ATP indepently.[118-120] Therefore, using Gaussia luciferase for *in vitro* experiments does not require cell lysis enabling further evaluations of treatment effects on cells based on techniques like flow cytometry.

2.6. Generation of LPEI based conjugates with enhanced biological properties

2.6.1. Introduction of a shielding domain

As mentioned in section 2.4.1. PEI based polyplexes are characterized by more or less intense positive surface charge depending on the N/P ratio applied for particle formation and therefore interact with blood components after systemic administration subsequently followed by particle aggregation.[73, 121-124] Reduction of such interactions and therefore prolonging the blood circulation time of polyplexes can be achieved by introducing a shielding domain which efficiently reduces the ζ-potential and improves physical stability of the particles.[125] Schaffert et al. coupled PEG to LPEI by N-hydroxysuccinimide (NHS) based chemistry to secondary amino groups of LPEI via a carboxamide functionality.[125] They found a significant decrease of ζ-potential using PEG with a molecular weight ranging from 2 kDa to 10 kDa. Introduction of 10 kDa PEG resulted in complete loss of transfection activity of polyplexes whereas in case of 2 kDa PEG significantly reduced but still remaining activity could be detected compared to unmodified LPEI polyplexes. In general, PEGylation of LPEI led to reduced cytotoxicity. This correlation between efficient shielding and a reduction of the biological efficiency of the formulation is termed as "PEG dilemma".[126] Nevertheless, PEGylation could be employed for reducing non-specific interaction of LPEI based polyplexes with the cellular surface and therefore used for synthesizing a LPEI-PEG platform for the introduction of targeting moieties against tumor antigens.

2.6.2. Tumor targeting with LPEI-PEG-PEPTIDE constructs

A heterobifunctional PEG with 3-(2-pyridyldithio)propionamide (OPSS) on the α-terminus and N-hydroxysuccinimide (NHS) on the ω-terminus could be applied for coupling a targeting peptide via a disulfide bridge.[125, 127] This enabled the functionalization of LPEI-PEG with thiol modified peptides like epidermal growth factor (EGF) which brought a significant enhancement of transfection efficiency. However, as expected cell treatment with EGF functionalized polyplexes resulted in an activation of epidermal growth factor receptor (EGFR) linked to mitogenic effects through receptor autophosphorylation and increased downstream signaling leading to enhanced tumor progression.[128] Therefore, it is important that LPEI-PEG-PEPTIDE constructs are used that avoid receptor activation but still mediate sufficient gene transfer.

2.7. Development of tumor targeting peptides

2.7.1. Phage display

Since its first use in 1985 phage display showed high potential for finding peptide and protein sequences for efficient tumor targeting.[129, 130] This technique is based on a ligand which is displayed on the phage surface after introducing its gene to the phage genome. Testing the interaction between phage and the selected target allows fast screening of libraries. This makes phage display a powerful route for screening a high number of ligands against one antigen in a relatively short amount of time. However, it is of great importance to conduct further evaluations of the pure ligands found during phage display based on other techniques such as surface plasmon resonance (SPR) which give more insights on biophysical properties.

A typical example where the results of further binding studies with the pure peptide stood in direct contrast to the results generated by phage display was the EGFR targeting peptide GE11.[128] Despite its high efficiency in phage display studies radioactive binding assays showed low binding affinity of the peptide when compared to EGF.[131] Investigations based on SPR revealed a low equilibrium dissociation constant (K_D) value of $1.8x10^{-7}$ M for GE11. As comparison, in the same experimental setup EGF showed a K_D value of $4.6x10^{-4}$ M.[132] However, transfection experiments with LPEI-PEG-PEPTIDE constructs showed a clear improvement of transgene expression using GE11 as targeting moiety compared to EGF which implies that GE11 reveals its high potential in nanoparticular formulations where a high number of peptide molecules per particle can be found.[127, 131] This suggests that GE11 leads to EGFR mediated cell uptake through both receptor binding and receptor crosslinking.[133] Mickler et al. revealed a further mechanism where GE11 based nanoparticle uptake works via an actin dependent pathway after binding to EGFR.[134]

2.7.2. Rational design of targeting peptides

Besides phage display computational based peptide design also represents an efficient strategy for finding peptides which can be used for receptor targeting. Protein databases enable de novo design of peptide ligands based on the known structure of antigens.[135] Besides that, docking simulations can be employed for finding possible binding sites. In general, such techniques can be used for extensive evaluations of the mechanism of interaction between a targeting peptide and its antigen. However, as this only gives theoretical information about the targeting and binding efficiency of molecules further investigations for proving the biological usability of the compound have to be done.

Rational peptide design was for example used for finding a further EGFR targeting peptide with the amino acid sequence LARLLT.[136] Compared to GE11 which interacts with the binding pocket of the receptor computational docking simulations showed that LARLLT binds on a receptor region outside the binding pocket. SPR based investigations on the EGFR binding activity of LARLLT showed a K_D value of $8.7x10^{-6}$ M. Based on that LARLLT is characterized by an almost 50fold stronger binding intensity to EGFR compared to GE11.[137] Gene delivery experiments on EGFR overexpressing tumor cells which compared lipoplexes with either GE11 or LARLLT as targeting moiety revealed a clear enhancement of transfection efficiency with LARLLT.[138]

2.8. CD49f as target for efficient gene delivery

Targeting of certain integrin types seems to be a promising tool for specific gene transfer into cancer cells. LPEI conjugates functionalized with a RGD moiety have already shown high efficiency for targeting integrin $\alpha_v\beta_3$.[139, 140] Furthermore, integrin α6 (CD49f) which is, for example, expressed in skin tissue shows considerable expression levels as α6β1 heterodimer in many tumor cell types where it seems to be directly involved in tumor cell migration.[141, 142] As it is also known as a tumor stem cell marker targeting CD49f for specific gene delivery could be a promising approach.[143, 144] Based on initial findings that laminin binds by interaction of the IKVAV motif found in the E8 region on the laminin α1 chain with α6 integrin Stevenson et al. utilized the peptide YESIKVAVS for modifying the surface of luciferase expressing adenovirus (Adluc).[141] Comparison with unmodified Adluc showed a clear improvement of transduction properties of the virus. Targeting specificity could be shown with the scrambled version IVVSYAKSE. However, at high concentrations (>0.1 mM) the interaction of the IKVAV motif with CD49f results in activation of extracellular signal-regulated kinase (ERK) 1/2 signaling which promotes tumor growth.[145] Therefore, it is important to use YESIKVAVS in low non-activating concentrations.

3. Topical lung delivery of nanoparticles

Besides systemic application *in vivo* topical administration into lungs can be employed as efficient alternative for nanoparticle formulations and comprises three different routes, namely intranasal, intratracheal and inhalation. The intranasal route is mainly characterized by simple administration of nasal suspensions but also results in a rather low amount of the applied formulation reaching the lung tissue.[146] Especially lung tumors which showed better accessibility from the apical site could be treated through local delivery by inhalation or instillation.[147] *In vivo* experiments based on intratracheal aerosolization already brought good results with BPEI polyplexes.[148] Important, in case of the intranasal and the intratracheal route care has to be taken, as both techniques are often found to be less tolerated during *in vivo* experiments.[149]

Topical lung administration is also confronted with several biological barriers such as fast clearance. Lung tissue is characterized by mucus production which serves as a protective agent for airways. The gel-like structure of mucus is created by highly glycosylated proteins with a molecular weight of 10-40 MDa, also termed as mucins.[150, 151] Physicochemical properties of mucus highly depend on the ratio between mucins, electrolytes, globular proteins, lipids, cellular debris and water. This leads to the generation of both steric and adhesive hindrance for particle formulations. Mucus gets continuously secreted forming a layer with a thickness ranging from 5 to 15 µm in the nasal cavity, 10-30 µm in trachea and 2-5 µm in bronchi and participates in the fast elimination of particles and pathogens.[152, 153] Therefore, overcoming the mucosal barrier and the efficient protection of the payload from mucosal components are major criteria used for the design of nanoparticular formulation for local lung administration. One possiblity to overcome this barrier is the application of physical methods, such as magnetic based targeting.[154] In this approach an aerosol of a mixture of PEI/pDNA polyplexes with superparamagnetic iron oxide nanoparticles was administered followed by the application of an external magnetic field. Compared to pure PEI/pDNA particles this resulted in a clear improvement of transgene expression in lung tissue.

3.1. PEGylation for improving particle performance after i.t. administration

Surface functionalization of nanoparticles with PEG often resulted in significant enhancement of the transfer of the formulation through mucus. This is mainly because the particle shielding through surface PEGylation reduces adhesion properties of particles and therefore decreases unwanted non-specific interactions of the formulation with the mucus environment. Important, Schuster et al. found out that mucus of different body compartments sometimes show tremendous differences in terms of viscosity.[155] As an example they brought PEGylated polystyrene particles with a size of 500 nm which were able to pass through cervicovaginal mucus but showed almost complete immobilization in airway mucus. However, PEGylated particles with a size ranging from 100 nm to 200 nm showed a significantly improved diffusion rate compared to bigger particles and particles of the same size but without surface modification. Therefore, shielding of gene delivery particles with PEG might also be an efficient approach for improving properties of gene delivery particles when applied intratracheally.

IV. Aims of the thesis

The primary aim of this PhD thesis was the design, synthesis and evaluation of novel LPEI based gene transfer particles suitable for pDNA and siRNA delivery. Main focus was set on the synthesis of uniform and stable non-targeted and targeted particles for direct lung administration. Overall, three main targets where followed, namely the establishment of a reproducible method for polyplex generation, the synthesis of PEGylated LPEI conjugates for active tumor targeting and the combination of LPEI with gold nanoparticles for sufficient siRNA delivery.

1. **Optimization of an automated and scalable synthesis of LPEI polyplexes via syringe pump based mixing (Figure 5).**
   1.1. High resolution evaluation of particle properties (hydrodynamic diameter and ζ-potential) by nanoparticle tracking analysis (NTA).
   1.2. Testing transfection efficiency of particles prepared at different N/P ratios with both firefly luciferase and Gaussia luciferase based *in vitro* assays.
   1.3. Evaluating cellular toxicity by flow cytometry.
   1.4. Testing transfection efficiency of polyplexes *in vivo* after i.v. administration

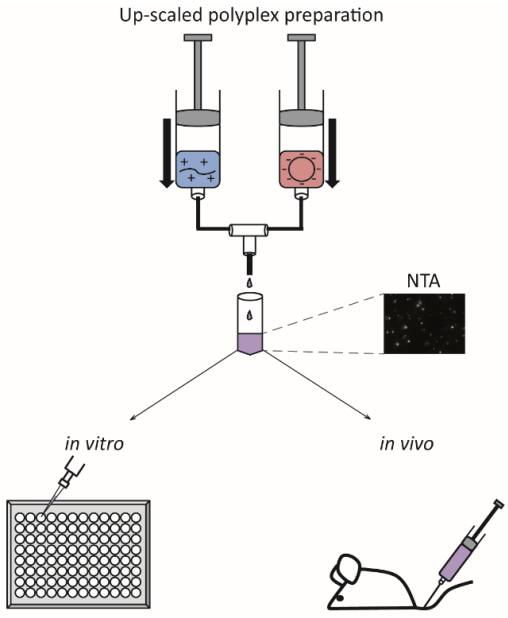

Figure 5: *Scheme of up-scaled polyplex generation evaluated by NTA and used for in vitro and in vivo gene delivery experiments (graphics taken from "Up-Scaled synthesis and characterization of nonviral gene delivery particles for transient in vitro and in vivo transgene expression"; see section 2.1 (chapter "Results"))*

2. **Administration of non-targeted and targeted LPEI polyplexes by i.t. aerosolization for treating lung metastasis.**

2.1. Synthesis of CD49f targeting peptide (CYESIKVAVS).[141]

2.2. Generation of LPEI-PEG-CYESIKVAVS (Figure 6) for active tumor targeting.

2.3. Characterization of physical properties of particles based on LPEI-PEG and LPEI-PEG-CYESIKVAVS in comparison to LPEI.

2.4. Evaluation of cell binding and transfection properties of pDNA based gene delivery particles.

2.5. Investigation of the impact of aerosolization on hydrodynamic diameter, stability and biological activity of particles.

2.6. Analysis of *in vivo* transfection efficiency and tumor specificity of particles.

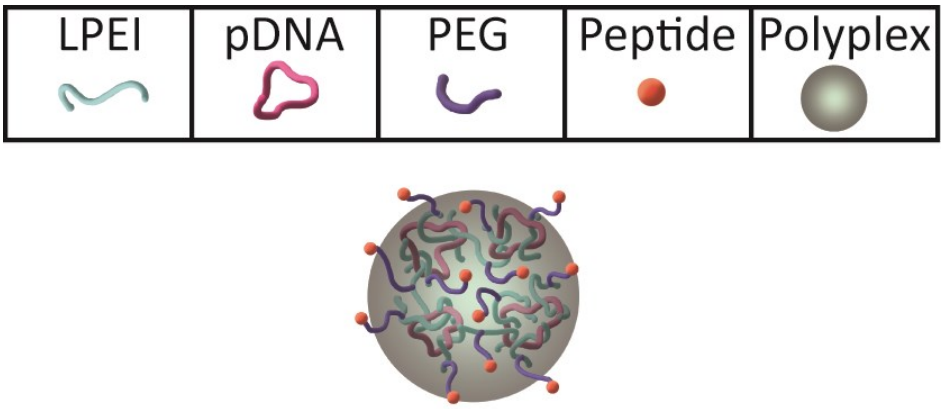

Figure 6: *Scheme of a polyplex particle based on LPEI-PEG-CYESIKVAVS*

3. Generation of a siRNA delivery platform based on LPEI and gold nanoparticles (Figure 7).

3.1. Synthesis of stable cationic gold nanoparticles by chemisorption of thiol terminated LPEI.

3.2. Generation of siRNA based complexes (auropolyplexes) using cationic gold nanoparticles as starting material and additional free LPEI to improve particle stability and transfection efficiency.

3.3. Physical evaluation of particles by NTA and transmission electron microscopy (TEM)

3.4. Analysis of cell association and uptake by CLSM and flow cytometry.

3.5. Investigation of *in vitro* knock-down efficiency of firefly luciferase expression.

3.6. Showing versatility of auropolyplex platform by exchanging LPEI used for the last complexation step with unmodified LPEI with different molecular weight or PEGylated LPEI.

3.7. Monitoring *in vivo* biodistribution after i.t. administration of the formulation based on fluorescence signal derived by AlexaFluor® 750 labelled siRNA and localization of gold by inductively coupled plasma mass spectrometry (ICP-MS).

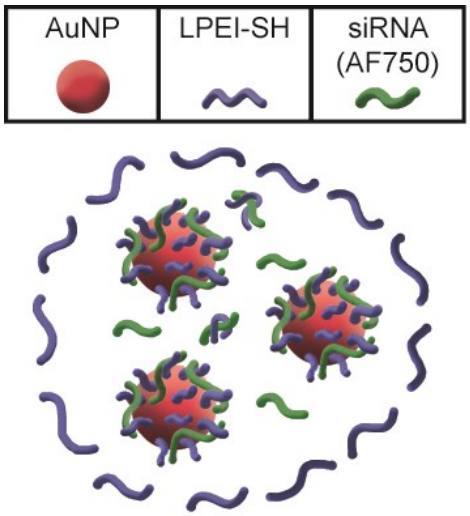

Figure 7: *Scheme of an auropolyplex (from "Auropolyplex: a versatile nanotherapeutic platform for efficient nucleic acid delivery in vitro and in vivo"; see section 2.4. (chapter "Results"))*

V. Results

1. List of publications/submissions and Contribution

Up-Scaled synthesis and characterization of nonviral gene delivery particles for transient *in vitro* and *in vivo* transgene expression

Journal	Human Gene Therapy Methods
Issue	2016; Volume 27; Number 3
DOI	10.1089/hgtb.2016.027
First author	Alexander Taschauer
Co-author	Antonia Geyer, Sebastian Gehrig, Julia Maier, Haider Sami,* Manfred Ogris
Contribution	Project planning; Synthesis of compounds; Establishment of up-scaled generation of polyplexes; Physical evaluation of nanoparticles; *In vitro* evaluation; Data analysis

Multimodal fluorescence and bioluminescence imaging reveals transfection potential of intratracheally administered polyplexes for breast cancer lung metastases

Journal	Human Gene Therapy
Issue	2017; Volume 28; Number 12
DOI	DOI: 10.1089/hum.2017.137
First authors (equal contribution)	Antonia Geyer, Alexander Taschauer
Co-author	Fatih Alioglu, Martina Anton, Julia Maier, Elisabeth Drothler, Manuela Simlinger, Sümeyye Yavuz, Haider Sami, Manfred Ogris
Contribution	Project planning; Synthesis of compounds; Physical evaluation of nanoparticles; Cell characterization; *In vitro* evaluation of particles; Data analysis

Peptide-targeted polyplexes for aerosol mediated gene delivery to CD49f overexpressing tumor lesions in lung

Journal	Molecular Therapy – Nucleic Acids
Date of submission	26.05.2019
Manuscript number	MTNA-19-1776
Status	In submission
First author	Alexander Taschauer
Co-authors	Wolfram Polzer, Fatih Alioglu, Magdalena Billerhart, Simon Decker, Theresa Kittelmann, Emanuela Geppl, Salma Elmenofi, Martin Zehl, Ernst Urban, Haider Sami, Manfred Ogris
Contribution	Project planning; Synthesis of compounds; Physical evaluation of nanoparticles; *In vitro* evaluation; Data analysis

Auropolyplex: a versatile nanotherapeutic platform for efficient nucleic acid delivery *in vitro* and *in vivo*

Journal	Journal of Controlled Release
Date of submission	22.10.2018
Manuscript number	JCR-D-18-01608
Status	Revision
First authors	Alexander Taschauer
Co-author	Wolfram Polzer, Stefan Pöschl, Slavica Metz, Nathalie Tepe, Simon Decker, Norbert Cyran, Julia Maier, Hermann Bloß, Martina Anton, Thilo Hofmann, Manfred Ogris, Haider Sami
Contribution	Project planning; Synthesis of compounds; Physical evaluation of nanoparticles; *In vitro* evaluation; Data analysis

2. Publications/Submissions

2.1. Up-scaled synthesis and characterization of nonviral gene delivery particles for transient in vitro and in vivo transgene expression

PROTOCOL

Up-Scaled Synthesis and Characterization of Nonviral Gene Delivery Particles for Transient *In Vitro* and *In Vivo* Transgene Expression

Alexander Taschauer, Antonia Geyer, Sebastian Gehrig, Julia Maier, Haider Sami,* and Manfred Ogris

MMCT Laboratory of Macromolecular Cancer Therapeutics, Department for Pharmaceutical Chemistry, Faculty Center for Pharmacy, University of Vienna, Vienna, Austria.

Polyethylenimine-based polyplexes are promising nonviral gene delivery systems for preclinical and clinical applications. Pipette-based polyplexing is associated with several disadvantages, such as batch-to-batch variability, restriction to smaller volumes, and variable gene delivery results. The present protocol describes syringe-pump-mediated upscaled synthesis of well-defined gene delivery nanoparticles capable of efficient *in vitro* and *in vivo* gene delivery. Syringe-pump-based synthesis ensures controlled mixing, upscaling, and reproducible gene delivery. Nanoparticle tracking analysis of the upscaled formulations involved single nanoparticle tracking, thereby generating highly resolved biophysical characterization. Gene delivery performance was investigated by luciferase gene expression in cells and three-dimensional bioluminescence imaging in mice.

INTRODUCTION

DELIVERY OF GENES TO CELLS is a key step in gene therapy, which is achieved by both viral and nonviral gene carriers.[1] The latter category of gene carriers offers various advantages, including tunable biosafety profile, lack of immunogenicity, and programmability for multiple functions. In addition, owing to the multiple possibilities offered by nanotechnology, development of efficient nonviral gene carriers for preclinical and clinical research is highly promising. Accomplishment of successful and reproducible *in vitro* and *in vivo* gene expression via nonviral gene nanocarriers is a challenging task; it needs fine control on the synthesis of nanocarriers, upscaled synthesis methods, detailed characterization of nanoparticles, and sensitive *in vitro*/*in vivo* gene expression techniques.

The classical method of generating polyplexes by flash pipetting is often characterized by a distinct batch-to-batch variability of the product.[2] Furthermore, it must be considered that formation of polyplexes using a pipette is limited to relatively small volumes.[3] Moreover, it is also susceptible to operator-induced variability, thereby leading to irreproducible gene delivery. Fine control on the synthesis of polyplexes can be achieved by employment of a syringe pump for controlled mixing of the two components needed for polyplex synthesis, that is, plasmid DNA (pDNA) and the transfection agent (linear polyethylenimine, LPEI).[4] Similarly, a mixing device has been reported for lipid-DNA complexes to generate formulations with reproducible attributes.[5] Also, syringe-pump-mediated polyplex synthesis ensures an upscaled production, characterized by a controlled and reproducible mixing, resulting in nanoparticles with narrow size distribution.[4] Detailed characterization of biophysical properties of the nanoparticle formulations is another key aspect for designing efficacious gene delivery particles. Nanoparticle tracking analysis (NTA) is a relatively recent technique that tracks single nanoparticles via light scattering and brownian motion combined with a video camera, thereby giving more detail on nanoparticle population characteristics for size and zeta potential (ζ-potential), when compared with the routinely used dynamic light scattering system.[6] Because of its ability of detecting individual nanoparticles, NTA results in a high-resolution measurement of both particle size and ζ-potential, even of samples characterized by high polydispersity.[6] Another key

*Correspondence: Dr. Haider Sami, MMCT Laboratory of Macromolecular Cancer Therapeutics, Department for Pharmaceutical Chemistry, Faculty Center for Pharmacy, University of Vienna, Althanstraße 14, A-1090 Vienna, Austria. E-mail: haider.sami@univie.ac.at

DOI: 10.1089/hgtb.2016.027

parameter affecting the gene delivery process of polyplexes is their biophysical stability, which is directly dependent on the solvent used during polyplexing. For example, an increasing concentration of NaCl in the solution results in an enhanced tendency of LPEI-pDNA complexes to form larger aggregates that would finally affect the transfection efficiency.[7–9] HEPES buffered glucose (HBG) shows a stabilizing effect on the physicochemical properties and therefore leads to a more reproducible quality of the resulting nanoparticles.[7,8,10] Other factors affecting transfection efficiency of polyplexes include size, charge, and amount of DNA within the polyplex formulation.[11–13] However, the amount of pDNA that can be used for transient transfection *in vitro* and *in vivo* is strongly limited by the quantity of LPEI needed for complexation because of its cellular toxicity. Apart from chemical and biophysical properties of polyplexes, the success of transient transfection is also influenced by genotypic and phenotypic properties of different cell types.[14] Therefore, it is important that the whole transfection process is optimized for every individual cell type. Upscaling of the polyplexation is more important for *in vivo* gene delivery owing to the high amounts needed in preclinical gene delivery studies. Upon intravenous administration, LPEI polyplexes tend to interact with blood components leading to the formation of aggregates and thereby transfection of lung tissue (after crossing of pulmonary–endothelial barrier).[15,16]

Here we describe a method for syringe-pump-mediated upscaled production of gene delivery nanoparticles for efficient *in vitro* and *in vivo* transient transgene expression (Fig. 1). LPEI was employed as the transfection reagent owing to its higher biocompatibility in comparison to the branched versions.[7–10] This protocol can be used for delivery of transgenes with both intracellular and secreted protein products *in vitro*. *Firefly luciferase* (intracellular) and *Gaussia luciferase* (secreted) were selected as model/reporter genes for delivering them *in vitro* and investigating luciferase expression as parameter of successful gene delivery. Similarly, by employing the same gene delivery nanoparticles, firefly luciferase was delivered *in vivo* and transient transfection of lung tissue was monitored by bioluminescence imaging. Quality control of the nanoparticle formulations was done by NTA to ensure narrow size distribution.

1. MATERIALS

1.1. Reagents

All reagents are enlisted in Table 1.

1.2. Equipment

1. KDS Legato 210 syringe pump system
2. Nanosight NS500 (Malvern)
3. Tecan Infinite M200 pro
4. MacsQuant VYB
5. Inverted microscope
6. Biological safety cabinet
7. Magnetic stirrer
8. pH Meter
9. Arium Pro VF (Sartorius)
10. Vortex mixer
11. Shaking platform
12. Water bath
13. Incubator 37°C, 5% CO_2
14. Refrigerator (4°C)

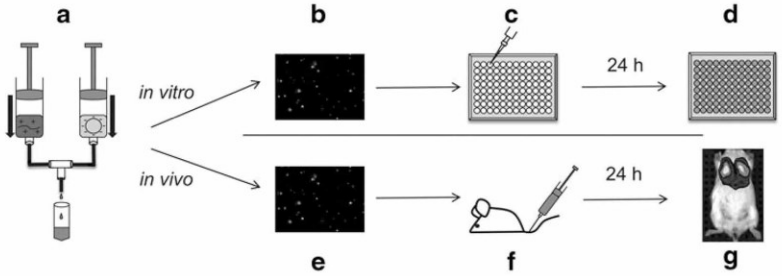

Figure 1. Experimental procedure. **(a)** Prepare polyplexes by mixing equal volumes of pDNA and LPEI-containing solutions using a syringe-pump-based system. **(b, e)** Analyze biophysical properties (particle size; ζ-potential) of polyplexes by NTA. **(c)** For *in vitro* evaluation add polyplexes and control substances (e.g., Lipofectamine 2000 and jetPRIME) to cells. **(d)** Measure luminescence activity after 24 hr. Luminescence signal can be normalized using BCA protein assay or flow cytometry. **(f)** For *in vivo* evaluation, inject polyplex-containing solution into the tail vein of mice. **(g)** After 24 hr measure bioluminescence after s.c. D-luciferin injection and correlate luciferase activity with photons/sec. LPEI, linear polyethylenimine; NTA, nanoparticle tracking analysis.

Table 1. *Reagents*

Reagents	*Supplier*	*Specific handling*	*Storage conditions*
Poly(2-ethyl-2-oxazoline) 50 kDa	Sigma-Aldrich Cat. No. 372846 Lot. No. 09410LH		Room temperature; protected from light in a desiccator
pCMV-Gluc	New England Biolabs Cat. No. N8081S		–20°C
pCpG-hCMV-EF1α-LucSH	Available on request from the authors		–20°C
N-(2-Hydroxyethyl)piperazine-N′-(2-ethanesulfonic acid) (HEPES)	AppliChem Cat. No. A3724,0500		Room temperature
D(+)-Glucose	Merck Millipore Cat. No. 1.08337.1000		Room temperature
Hydrochloric acid 37%	Sigma-Aldrich Cat. No. 30721		Room temperature
Sodium hydroxide	AppliChem Cat. No. A6829,1000		Room temperature
Ethanol absolute	Merck Millipore Cat. No. 1.11727.2500		Room temperature
Cell line: A549 (lung adenocarcinoma)	ATCC		–150°C
RPMI-1640 Medium	Sigma-Aldrich Cat. No. R0883		+4°C
Fetal bovine serum (FBS)	Sigma-Aldrich Cat. No. F7524		–20°C
L-Glutamine 200 m*M*	Sigma-Aldrich Cat. No. G7513		–20°C
Dulbecco's phosphate buffered saline (DPBS)	Sigma-Aldrich Cat. No. D8537		Room temperature
TrypLE express enzyme with phenol red	Gibco Cat. No. 12605–036		Room temperature
2-(4-Amidinophenyl)-6-indolecarbamidine dihydrochloride (DAPI)	Sigma-Aldrich Cat. No. D9542		+4°C; protected from light Aqueous solutions should be stored at –20°C
BCA Compat-Able Protein Assay Kit	Pierce Cat. No. 23229	Danger: reagents can cause severe skin burns and eye damage	Room temperature
Dual-Luciferase Reporter Assay System	Promega Cat. No. E1960		–20°C; once reconstituted the luciferase assay substrate should be stored at –70°C (max. 4 weeks) and the Stop & Glo Reagent at –20°C (max. 15 days)
MACSQuant Running buffer for flow cytometry	Miltenyi Biotec Cat. No. 130-092-747		Room temperature
Beetle luciferin, sodium salt	Promega Cat. No. E464X		–80°C
Isoflurane	CP Pharma Cat. No. 798–932		Room temperature, protected from light
Oxygen	Air liquid—Alphagaz		Room temperature
Scanlux 300	Sanochemia Diagnostics Approval No. 1–23236		Room temperature, protected from light

15. Freezer (–20°C, –80°C, –150°C)
16. IVIS SpectrumCT Preclinical *In vivo* Imaging System (Perkin Elmer)
17. Computer equipped with FlowJo, Microsoft Excel, Living Image, and GraphPad Prism

1.3. Supplies

1. Eppendorf tubes
2. 15 ml centrifuge tubes (Starlab)
3. Syringes:
   a. 3 ml OmniFix (BBraun)
   b. 1 ml Omnican 100 (BBraun)
4. Components of tubing system used for polyplex generation:
   a. Flangeless Nut Delrin 1/4-28 1/16″ Red with Ferrule (Kinesis Abimed)
   b. Female Luer to 1/4-28 Female PEEK (Kinesis Abimed)
   c. Tee HP PEEK 1/16″ (Kinesis Abimed)
   d. PEEK tubing (OD 1/16″) (GE Lifesciences)
5. Pasteur pipettes
6. Pipette tips
7. White 96-well flat-bottom microplate, transparent bottom, sterile (Greiner)

8. Transparent 96-well flat-bottom microplate, sterile (Greiner)
9. Reagent reservoirs

1.4. Reagent setup

HEPES buffered glucose (20 mM HEPES/5% [w/V] glucose). Dissolve 0.4766 g of HEPES and 5 g of glucose in 80 ml ddH_2O; adjust pH to 7.4 by using HCl/NaOH; add ddH_2O to reach a final volume of 100 ml; pass the final solution through a 0.22 μm filter under a biological safety cabinet.

This solution can be made in advance and stored at +4°C for up to 6 months.

Linear polyethylenimine. Linear polyethylenimine (LPEI) with an average molecular weight of 10 kDa was synthesized based on the instructions described by Rödl et al. using poly(2-ethyl-2-oxazoline) as initial compound.[16]

Because of significant batch-to-batch variability of commercially available poly(2-ethyl-2-oxazoline), both ^{1}H-NMR and gel permeation chromatography (GPC) should be conducted for characterizing the product.

LPEI solution in HBG (1 mg/ml). Resuspend 5 mg of LPEI in 4 ml of HBG and readjust the pH to 7.4 with HCl/NaOH under vigorous vortexing to avoid the formation of LPEI precipitates; add HBG to reach a final volume of 5 ml; pass the final solution through a 0.22 μm filter under a biological safety cabinet. Filtering LPEI-containing solutions can cause a reduction of the polymer concentration. Therefore, it is obligatory to quantify the LPEI concentration post-filtration by conducting a copper assay described by Ungaro et al.[17] LPEI-containing stock solutions can be stored at +4°C for up to 2 months and at –80°C for long-term.

Cell culture medium. 500 ml RPMI-1640 is supplemented with 10% (V/V) FBS and L-glutamine at a concentration of 0.3 g/liter. Cell culture medium should be stored at +4°C for up to 2 months. Storing cell culture medium in small aliquots avoids frequent warm-up cycles, which can negatively influence the quality of cell culture medium.

2. EXPERIMENTAL PROCEDURE

2.1. Syringe-pump-based synthesis system for controlled mixing[4]

1. As shown in Fig. 2, connect two 3 ml syringes to a T-connector via polyetherketone tubings with a length of 10 cm, respectively. One syringe is for LPEI and the other syringe is for pDNA.
2. Use one further polyetherketone tubing (5 cm) connected to the T-connector as an outlet tubing.
3. The product can be collected in a centrifuge tube.

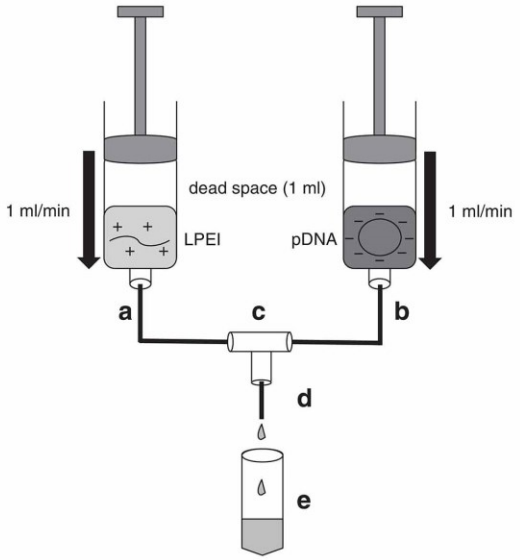

Figure 2. Scheme of syringe-pump-based polyplex generation. Load LPEI- and pDNA-containing solutions into two separate syringes. A dead space of 1 ml in both syringes avoids loss of volume during polyplex generation. Use polyetherketone tubings **(a, b)** to connect both syringes to a T-connector **(c)**. After starting the syringe pump at a flow rate of 1 ml/min, LPEI and pDNA solutions are mixed in the T-connector. The product solution flows through a further polyetherketone tubing **(d)** into a centrifuge tube **(e)**.

2.2. Polyplex formation

1. pDNA and LPEI solutions have to be prepared in different tubes and in same volume as described in steps 2.2.2. and 2.2.3. below.
2. Dilute pDNA (*pCpG-hCMV-EF1α-LucSH* or *pCMVGLuc*) in HBG buffer (20 m*M* HEPES, 5% glucose) to a final concentration of 40 μg/ml for *in vitro* assays or 400 μg/ml for *in vivo* assays.
   a. Note: Generating polyplexes is normally done by mixing equal volumes of pDNA- and LPEI-containing solutions finally resulting in a pDNA concentration of 20 μg/ml for *in vitro* or 200 μg/ml for *in vivo* experiments.

3. The appropriate amount of LPEI according to the total amount of pDNA and the desired N/P ratio can be calculated by using the following equation:

$$m(\text{LPEI}) = \frac{m\ (\text{pDNA}) \times 43 \times \text{N/P}}{330}$$

   a. 43 g/mol is the molecular weight of one subunit in the molecular structure of LPEI and 330 g/mol is the average molecular weight of one nucleotide.
   b. Example: for preparing 500 μl of a polyplex solution with a pDNA concentration of 20 μg/ml and an N/P ratio of 6:
      i. m (pDNA) = 10 μg
      ii. $m(\text{LPEI}) = \frac{10 \times 43 \times 6}{330} = 7.82\ \mu\text{g}$
   c. LPEI has to be diluted in HBG buffer in same volume as used for pDNA.
4. Let both (pDNA solution prepared in 2.2.1. and LPEI solution prepared in 2.2.2.) solutions equilibrate at room temperature for at least 5 min.
   a. Note: For investigating pDNA recovery it is necessary to measure pDNA concentration before and after complexation with LPEI. pDNA concentration and recovery are calculated by using the following equations:

$$c(\text{pDNA};\ \mu\text{g/ml}) = [\text{Abs}(260\ \text{nm})\text{-Abs}(320\ \text{nm})] \cdot 50$$

$$\text{pDNA recovery}\ (\%) = \frac{c(\text{pDNA;\ after polyplexing})}{[c\ (\text{pDNA;\ before polyplexing})/2]} \times 100$$

5. Transfer each solution into 3 ml syringes
   a. Note: To avoid loss of volume during the mixing process, using a dead space of 1 ml in each syringe is advised.
6. Attach both syringes to the tubing system as shown in Fig. 2 and described in Sec. 2.1, and fix them in the syringe pump.
   a. Note: Controlled mixing should be done by using a flow rate of 1 ml/min.
7. Start the syringe pump to start the polyplexation process and collect the polyplex product in a centrifuge tube after the mixing cycle is complete.
   a. Note: Incubating polyplex-containing solutions over time would result in an increased aggregate formation, which would negatively influence the transfection efficiency of the sample. Therefore, it is advisable to do the biophysical as well as the biological evaluation of LPEI-based polyplexes immediately after generating them.

2.3. Biophysical evaluation by NTA

1. Before doing the first NTA measurement it is necessary to prepare the NanoSight NS500 as follows:
   a. Prime the fluidics with ddH_2O
   b. Before measuring a sample it is mandatory to load the system (at least two times) with the solvent used for diluting the sample to avoid particle movement caused by differences of the ionic strength within the fluidics system.
   c. It is necessary to flush the system 2–3 times between each measurement with ddH_2O for removing remaining particles of the previous sample.
2. NTA measurements require an appropriate dilution of each sample to reach an optimal concentration of 10^8–10^9 particles/ml, which correlates to 10–100 particles in the field of view.
   a. Use either HBG or RPMI 1640 as a diluent for size measurements.
      i. Note: The particle concentration of the prepared polyplex solution correlates directly with both pDNA concentration and N/P ratio. The dilution factors used for this protocol are enlisted in Sec. 4 (troubleshooting).
      ii. Note: Basal RPMI 1640 is used as transfection medium for *in vitro* assays with A549 cells and can therefore be employed as a diluent for the biophysical evaluation to investigate changes in the size of polyplexes that may occur during cell treatment.
   b. Use 2.5 m*M* NaCl as a diluent for investigating the ζ-potential.
      i. Note: The parabolic profile of the particle drift should have a coefficient of determination (R^2 value) of at least 0.95.
   c. Use NTA settings as described in Table 2.

2.4. Reporter activity assay to monitor *in vitro* transgene expression

1. Seed 10,000 cells suspended in 200 μl of complete cell culture medium into each well of a flat-bottom 96-well tissue culture plate.

Table 2. *NTA settings*

Size measurements	*ζ-potential measurements*
Number of captures: 5	Capture duration: 90 sec
Capture duration: 60 sec	Secondary duration: 30 sec
Temperature control: 25.0°C	Applied voltage: 24 V
	Temperature control: 25.0°C

Gently agitate the plate to ensure an even distribution of the cells throughout the whole well surface.

a. Note: The whole *in vitro* transfection protocol is optimized for A549 lung adenocarcinoma cells that have a doubling time of approximately 22 hr. Seeding density and duration should be optimized individually for different cell types.

2. Incubate the cells overnight in a 37°C/5% CO_2 incubator for approximately 16 hr.
3. Check the appearance of the cells under a microscope for morphology and confluence. For efficient transfection, it is advisable that cells are 70–80% confluent at the time of addition of polyplexes (see note in Sec. 2.4.1)
4. Before starting with addition of polyplexes, aspirate the medium of each well and add 90 μl of RPMI-1640 (without FBS) directly on the cells.
5. Add 10 μl of a polyplex solution (containing 20 μg/ml pDNA concentration) to each well containing the 90 μl RPMI-1640.
   a. Note: Always keep untreated cells and cells treated only with pDNA as negative controls. Commercially available transfection agents such as Lipofectamine 2000 or jetPRIME can be used as positive controls.
6. After 4 hr, add 100 μl of complete cell culture medium into each well.
7. Total transfection time (starting from step 5) of 24 hr was followed before investigating the transgene expression.
8. In case of transgenes with intracellular protein products, the procedure described in Sec. 2.5 was followed. For transgenes with secretory protein products, the procedure described in Sec. 2.6 was followed.

2.5. Evaluation of *in vitro* transfection efficiency of intracellular expressed firefly luciferase:

1. After step 7 of 2.4, aspirate the cell culture medium from each well and wash the cells one time with 200 μl DPBS.
2. Lyse the cells using Passive Lysis Buffer (Promega) as per manufacturer's instructions.
3. Use 50% of the total volume of cell lysate for measuring the luminescence of the luciferase protein from the reporter gene.
   a. Apply the following plate reader settings for luminescence measurement:
      i. Substrate volume (Luciferase Assay reagent II; included in Dual-Luciferase Reporter Assay System; Promega): 50 μl
      ii. Integration time: 10,000 msec
      iii. Waiting time (between wells): 2 sec
4. Normalization of the luminescence values based on the amount of protein per well:
   a. Use the remaining 50% of cell lysate for determining the protein concentration by using a BCA protein assay kit.
   b. Mix every sample with 200 μl of BCA working reagent and place the plate in a 37°C/5% CO_2 incubator for 30 min.
      i. Note: While mixing the sample with BCA working reagent, avoid generating air bubbles in the sample as the air bubbles might give rise to erroneous absorption measurements.
   c. After cooling the plate to room temperature measure the absorption of each sample by using the following plate reader settings:
      i. Wavelength: 562 nm
      ii. Bandwidth: 9 nm
      iii. Number of flashes: 25
   d. Note: Use a bovine serum albumin (BSA) standard curve for calculating the protein amount in the cell lysates.

2.6. Evaluation of *in vitro* transfection efficiency of secreted Gaussia luciferase:

Compared with intracellular expressed reporter proteins, secreted reporters offer several advantages, such as the possibility of monitoring transient transfection over a longer duration. Since the luciferase expression is measured only in the medium, the remaining and intact cells can be employed for further analysis, such as the evaluation of cellular toxicity of the transfection reagents by flow cytometry and normalizing the luminescence values by the total number of living cells per well.[18,19]

1. After step 7 of Sec. 2.4, transfer 20 μl of the cell culture medium from each well into a white 96-well flat-bottom microplate for luminescence measurement. Therefore, it is necessary

to use a plate reader for luminescence measurements with the following settings:

a. Substrate volume (Stop & Glo Reagent; included in Dual-Luciferase Reporter Assay System; Promega): 50 μl
b. Integration time: 10,000 msec
c. Waiting time (between wells): 2 sec

2. Normalization of the luminescence values based on absolute cell count per well by flow cytometry:
   a. Aspirate the cell culture medium from the cells and wash them with 200 μl DPBS.
   b. Detach the cells by adding 20 μl of TrypLE to each well and incubating the plate for 5 min in an incubator (37°C/5% CO_2).
   c. Once cells are detached from the surface, resuspend them in 140 μl DPBS.
   d. Add 40 μl of DAPI-HCl dissolved in DPBS (5 μg/ml) to each sample directly before starting the flow cytometer measurement for counting dead and live cells.
      i. Note: Exclude duplicates from your cell population.
      ii. Note: Voltage settings have to be adjusted in a way to set the peak created by the living cells between 10^0 and 10^1.

Note: For normalizing the luminescence to the protein amount, use the protocol described in step 2.5.4.

2.7. Evaluation of *in vivo* transfection efficiency of intracellular expressed firefly luciferase

Balb/c mice were used as models for transfection with firefly luciferase-based polyplexes and bioluminescence imaging studies were performed to investigate the reporter transgene expression *in vivo*. The whole process was carried out in a way similar to the *in vitro* experiments described above.

1. Prepare polyplexes as described in Sec. 2.2. with a final pDNA concentration of 200 μg/ml.
   a. Note: Before injecting, evaluation of biophysical properties of polyplexes such as size and ζ-potential should be conducted to ensure high quality and good transfection efficiency (see Sec. 2.3.).
2. Inject the polyplex product intravenously (tail vein) at a dose of 2.5 mg of pDNA per kg body weight.[13]
3. After 24 hr of polyplex treatment, perform bioluminescence imaging (under anesthesia) as described in steps 4–7.
   a. Note: Induce anesthesia by applying 5% isoflurane in oxygen using a precision vaporizer. Anesthesia can be maintained using 1.5–2% isoflurane in oxygen.
4. Inject D-luciferin (dissolved in DPBS with a concentration of 30 mg/ml) subcutaneously at a dose of 150 mg per kg body weight. Place the animal in the imager in a ventral position and start with bioluminescence imaging after 10 min of luciferin injection. Depending on the imaging device, the bioluminescence can be acquired in either two-dimensional (2D) mode or both 2D and 3D modes.
   a. Use the following Caliper Ivis settings for acquiring 2D bioluminescence images:
      i. Emission open
      ii. Excitation blocked
      iii. Exposure time: 60 sec

Table 3. *Timelines for* in vitro *and* in vivo *transfection*

Task	*Steps*	*Duration*
Timeline for in vitro *transfection*		
Cell seeding for transfection	Sec. 2.4, step 1	30–45 min for cell seeding pprox. 12 hr incubation for cell attachment
Polyplex preparation	Sec. 2.2, steps 1–7	15 min per sample
Biophysical evaluation	Sec. 2.3, steps 1–2	60 min per sample
Cell treatment	Sec. 2.4, steps 3–5	10 min
Reporter activity assay for intracellular luciferase types	Sec. 2.5, steps 1–3	60–90 min
Reporter activity assay for secreted luciferase types	Sec. 2.6, step 1	30–60 min
Normalization via:		
1. Evaluation of the amount of protein per well, or	Sec. 2.5, step 4	90–120 min
2. Absolute count of living cells	Sec. 2.6, step 2	30–60 min
Timeline for in vivo *transfection*		
Polyplex preparation	Sec. 2.2, steps 1–7	30 min
Biophysical evaluation	Sec. 2.3, steps 1–2	30 min
i.v. injection into tail vein	Sec. 2.7, step 2	5 min per mouse
Bioluminescence imaging	Sec. 2.7, steps 3–7	60 min per mouse

Table 4. *Troubleshooting*

Problem	*Possible reason(s)*	*Solution(s)*
ζ-potential measurement shows parabolic drift profile with a coefficient of determination of less than 0.95	Particle concentration too low Measuring chamber of the NTA system is coated with LPEI-based particles.	Increase the concentration of the sample used for ζ-potential measurement. The NTA software needs at least 100 particle tracks per video. The dilution factors that showed optimal measurement conditions are listed in Table 5. Disassemble and clean the chamber as per instructions from the manufacturer.
High toxicity after cell treatment with polyplexes	LPEI concentration too high	Perform cell treatment with different N/P ratios and cell densities for determining the least toxic amount of LPEI.
Low pDNA recovery after polyplex formation	N/P ratio too low	Increase the amount of LPEI used for complexing pDNA.
Low luciferase signal *in vitro*	Low transfection efficiency of polyplexes	Evaluate the biophysical properties of used polyplexes. Aggregate formation could lead to reduced transfection of cells.
	Usage of overgrown cell passage for transfection assay	Subculture cells for regaining optimal cell growth.
	Cells may not be completely lysed	Increase the incubation time for the lysis step.
Low/no luciferase activity after animal treatment detected	Bradycardia induced through anesthesia during injecting of polyplex-containing solution	Side effects like bradycardia may lead to a reduced transfection of lung tissue. Injection without anesthesia is advised.
	Time between subcutaneous injection of D-luciferin and bioluminescence imaging	Optimal duration between injecting D-luciferin and luciferase detection *in vivo* is 10–15 min.
	Exposure time and binning are too low.	Readjust exposure time and binning as per instructions from the manufacturer.

LPEI, linear polyethylenimine; NTA, nanoparticle tracking analysis.

iv. F/stop: 1
v. Binning: 8
vi. Field of view (FOV): 13.4 cm^2

b. Use the following Caliper Ivis settings for acquiring 3D bioluminescence images:
i. Emission filter set range: 560–640 nm
ii. Excitation blocked
iii. Binning: 8
iv. F/stop: 1
v. Filter position: 60 sec
vi. Field of view (FOV): 13.4 cm^2

c. Acquiring 3D reconstructions requires a number of photon counts of 600–60,000 in at least 3 filters (600–640 nm), which cannot be achieved with polyplexes prepared at an N/P ratio of 6.

5. Image processing can be conducted using a program such as Living image.
6. Define the region of interest (ROI) in 2D images around the lung tissue using an automated contour drawing function for analyzing only the intensity of the bioluminescence signal that is significantly higher than the background.
7. Luciferase activity can be correlated with photons/sec.

3. TIMING

All time points are listed in Table 3.

4. TROUBLESHOOTING

Troubleshooting is shown in Tables 4 and 5.

ANTICIPATED RESULTS

Applying a syringe-pump-based controlled mixing method for pDNA/LPEI complexation results in reproducibly controlled formation of nanoparticles with a narrow size distribution as shown in Fig. 3. NTA was used for high-resolution analysis of both size and ζ-potential of the nanoparticulate polyplexes. For investigating changes in polyplex characteristics as a function of solvent used for polyplexing/transfection, the particle size was analyzed after diluting the polyplexes in HBG/serum-free medium (RPMI 1640), respectively (shown in Fig. 3a).

The positive correlation between DNA complexation and the N/P ratio is shown in Fig. 4 in

Table 5. *Troubleshooting: suggested dilution factors for size and ζ-potential measurements by NTA*

	Dilution factor (for samples prepared at final pDNA conc. of 20 μg/ml)		*Dilution factor (for samples prepared at final pDNA conc. of 200 μg/ml)*	
N/P ratio	*HBG*	*RPMI 1640*	*HBG (for size measurement)*	*2.5 mM NaCl (for ζ-potential measurement)*
3	1/10	1/10	—	—
6	1/50	1/50	1/500	1/40
9	1/100	1/100	1/500	1/40

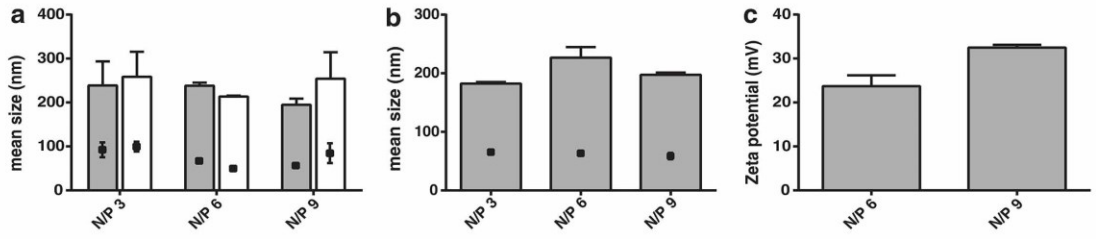

Figure 3. Evaluation of biophysical properties of LPEI-based polyplexes by NTA. All experiments are presented as mean ± SD ($n=3$). **(a)** Size measurement of polyplexes prepared at a final pDNA concentration of 20 μg/ml for *in vitro* transfection. Polyplexes were prepared at different N/P ratios in HBG by controlled mixing and analyzed without incubation time. To investigate changes in the particle size as a function of solvent used for polyplexing/transfection, both HBG (gray bars) and RPMI 1640 (white bars) were used as diluents for NTA measurements. Bars indicate the mean size, and black squares (within each bar) indicate the standard deviation calculated by the NTA software. **(b)** Size measurement of polyplexes prepared at a final pDNA concentration of 200 μg/ml for *in vivo* transfection. All samples were diluted with HBG. Bars indicate the mean size, and black squares (within each bar) indicate the standard deviation calculated by the NTA software. **(c)** ζ-potential measurements were done with samples prepared at 200 μg/ml using 2.5 m*M* NaCl as diluent.

terms of DNA recovery after polyplexation. N/P 3 already leads to full complexation of pDNA at a concentration of 20 μg/ml as indicated by the pDNA recovery of nearly 100%. In case of N/P 3 at a pDNA concentration of 200 μg/ml, the polyplexes precipitated immediately during polyplexation, indicating lower stability. As observed in Fig. 4, the pDNA recovery was also very low in this case, which might be because of lack of full complexation of pDNA, also indicated by precipitation. At higher N/P ratios, the pDNA recovery was 100% irrespective of the pDNA concentration. This indicates the need for applying a certain amount of free LPEI, which is necessary not only to complex pDNA and stabilize the nanoparticles but also to enhance their ability to effectively transfect cells.[13] Therefore, measuring recovery of pDNA after polyplex generation is an important tool for quality assurance.

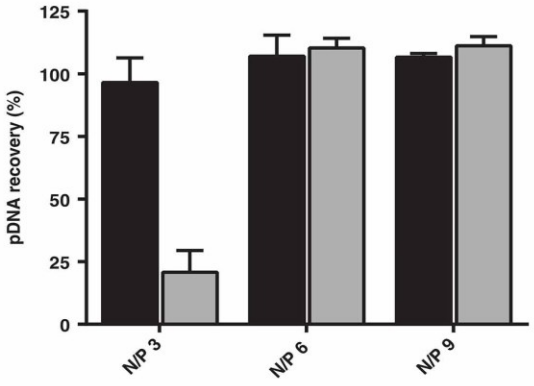

Figure 4. pDNA recovery after polyplex formation. All experiments are presented as mean ± SD ($n=3$). pDNA recovery was evaluated by calculating the percentage ratio between pDNA concentration before and after polyplex formation (black columns: polyplexes prepared at a pDNA concentration of 20 μg/ml; gray columns: polyplexes prepared at a pDNA concentration of 200 μg/ml).

The upscaled polyplex nanoparticles were investigated for efficiency of gene delivery both *in vitro* and *in vivo* models. The optimized *in vitro* transfection protocol was used for A549 lung adenocarcinoma cells just as a model cell type and is expected to work for a broad spectrum of cell lines (with differing transfection efficiency depending on the cell type), as demonstrated in other cell types.[4,20,21] For *in vitro* studies, intracellular and secreted luciferase reporter genes were employed, and expression of respective luciferase proteins was studied as shown in Fig. 5. The upscaled nanoparticles at N/P 6 and N/P 9 showed transfection efficiency comparable to the commercially available transfection agents for both types of luciferases as shown in Fig. 5a and 5b. Activity of intracellularly expressed luciferases needs normalization based on total protein amount. On the other hand, using of secreted luciferases offers advantages of evaluation of the cellular toxicity (Fig. 5c) and total cell count-based normalization of luciferase activity. Upscaled polyplexes (based on firefly luciferase reporter gene) at two different N/P ratios (N/P 6 and 9) were used for monitoring transfection efficiency *in vivo*. Bioluminescence measurement 24 hr post-injection shows a distinct luciferase activity in the chest area (Fig. 6a and 6b), indicating successful gene delivery by the upscaled nanoparticles. Bioluminescence imaging in combination with CT (i.e., 3D mode of acquisition) offers the advantage of localizing the luminescence signal to the lungs of the animal (Fig. 6c). PEI-based polyplexes have been demonstrated to cross pulmonary–endothelial barrier and transfect the

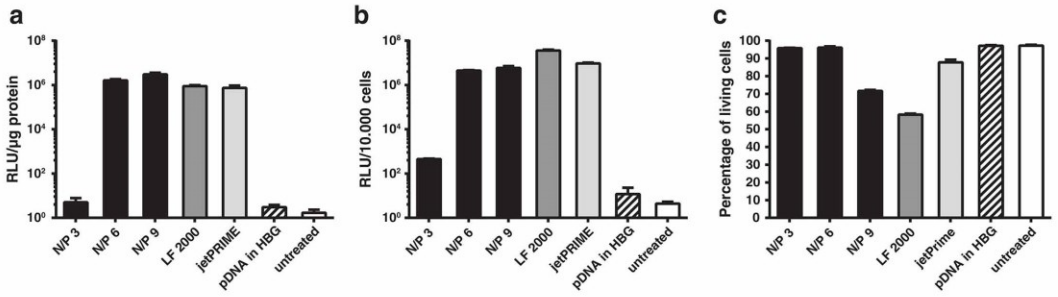

Figure 5. *In vitro* expression of *firefly* and *Gaussia luciferase* reporter transgenes. A549 cells (10,000) were seeded into a 96-well plate and treated with 200 ng pDNA complexed with LPEI (10 kDa) at three different N/P ratios (N/P 3, 6 and 9; prepared at 20 μg/ml) in serum-free medium (RPMI 1640). After 4 hr, RPMI 1640/10% FCS was added to reach a final volume of 200 μl in each well. Both Lipofectamine 2000 (LF 2000) and jetPRIME were used as positive controls. Only pDNA in HBG was used as a negative control. Reporter activity was measured 24 hr after starting the cell treatment ($n=3$). **(a)** Expression of firefly luciferase (*pCpG-hCMV-EF1α-LucSH*) at different N/P ratios: It was detected by lysing the cells followed by measuring luciferase activity. Luciferase activity was normalized according to the amount of protein per well. **(b)** Expression of Gaussia luciferase (*pCMV-Gluc*) at different N/P ratios: It was analyzed in 20 μl of the supernatant. Gaussia luciferase activity was normalized to the total count of living cells per well determined by flow cytometry. The percentage of living cells per well was evaluated using DAPI staining of dead cells as shown in **(c)**.

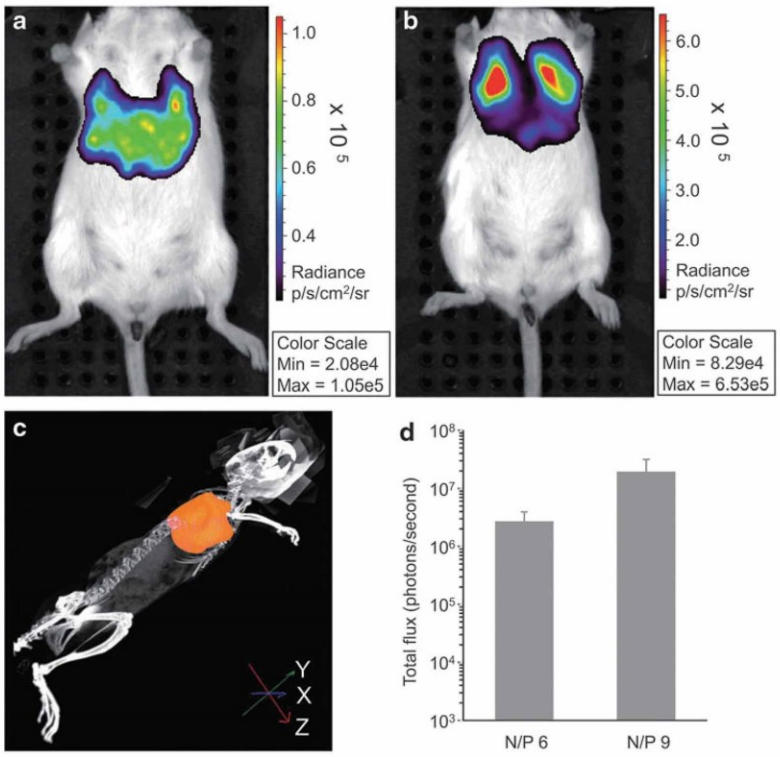

Figure 6. *In vivo* lung expression of firefly luciferase reporter transgene. Polyplexes were prepared at a pDNA concentration of 200 μg/ml using N/P 6 and N/P 9 and immediately injected into the tail vein of BALB/cByJRj mice using a dosage of 2.5 mg/kg. Control mice were injected with 250 μl HBG (n=3). After 24 hr of polyplex injection, bioluminescence was measured after administration of D-luciferin (150 mg/kg). CT-based 3D reconstruction enabled localizing the luminescence signal to the lungs. Panels **(a)** and **(b)** show representative 2D bioluminescence images of animals treated with polyplexes at N/P 6 and N/P 9. Panel **(c)** shows representative 3D surface reconstruction of the luminescence signal of an animal treated with polyplexes at N/P 9. Luciferase activity was calculated as photons/sec detected in the region of interest **(d)**.

pulmonary cells as reported in earlier studies.[15,16] Total flux measured in 2D bioluminescence increases with the total amount of polymer used for complexing pDNA as seen in Fig. 6d.

ACKNOWLEDGMENTS

Parts of this work have received support from the EU/EFPIA Innovative Medicines Initiative Joint Undertaking COMPACT Grant No. 115363. J.M. is supported by the uni:docs—fellowship program for doctoral candidates of the University of Vienna.

AUTHOR DISCLOSURE

No competing financial interests exist.

REFERENCES

1. Gehrig S, Sami H, Ogris M. Gene therapy and imaging in preclinical and clinical oncology: Recent developments in therapy and theranostics. Ther Deliv 2014;5:1275–1296.
2. Talsma H, Cherng J, Lehrmann H, et al. Stabilization of gene delivery systems by freeze-drying. Int J Pharm 1997;157:233–238.
3. Anchordoquy TJ, Koe GS. Physical stability of nonviral plasmid-based therapeutics. J Pharm Sci 2000;89:289–296.
4. Kasper JC, Schaffert D, Ogris M, et al. The establishment of an up-scaled micro-mixer method allows the standardized and reproducible preparation of well-defined plasmid/LPEI polyplexes. Eur J Pharm Biopharm 2011;77:182–185.
5. Hirota S, de Ilarduya CT, Barron LG, et al. Simple mixing device to reproducibly prepare cationic lipid-DNA complexes (lipoplexes). Biotechniques 1999;27:286–90.
6. Filipe V, Hawe A, Jiskoot W. Critical evaluation of nanoparticle tracking analysis (NTA) by NanoSight for the measurement of nanoparticles and protein aggregates. Pharm Res 2010;27:796–810.
7. Wightman L, Kircheis R, Rossler V, et al. Different behavior of branched and linear polyethylenimine for gene delivery *in vitro* and *in vivo*. J Gene Med 2001;3:362–372.
8. Goula D, Benoist C, Mantero S, et al. Polyethylenimine-based intravenous delivery of transgenes to mouse lung. Gene Ther 1998; 5:1291–1295.
9. Ferrari S, Moro E, Pettenazzo A, et al. ExGen 500 is an efficient vector for gene delivery to lung epithelial cells *in vitro* and *in vivo*. Gene Ther 1997;4:1100–1106.
10. Goula D, Remy JS, Erbacher P, et al. Size, diffusibility and transfection performance of linear PEI/DNA complexes in the mouse central nervous system. Gene Ther 1998;5:712–717.
11. Di Gioia S, Conese M. Polyethylenimine-mediated gene delivery to the lung and therapeutic applications. Drug Des Devel Ther 2009;2:163–188.
12. Khalil IA, Kogure K, Akita H, et al. Uptake pathways and subsequent intracellular trafficking in nonviral gene delivery. Pharmacol Rev 2006;58:32–45.
13. Boeckle S, von Gersdorff K, van der Piepen S, et al. Purification of polyethylenimine polyplexes highlights the role of free polycations in gene transfer. J Gene Med 2004;6:1102–1111.
14. von Gersdorff K, Sanders NN, Vandenbroucke R, et al. The internalization route resulting in successful gene expression depends on both cell line and polyethylenimine polyplex type. Mol Ther 2006;14:745–753.
15. Goula D, Becker N, Lemkine GF, et al. Rapid crossing of the pulmonary endothelial barrier by polyethylenimine/DNA complexes 965. Gene Ther 2000;7:499–504.
16. Rödl W, Schaffert D, Wagner E, et al. Synthesis of polyethylenimine-based nanocarriers for systemic tumor targeting of nucleic acids. Methods Mol Biol 2013;948:105–120.
17. Ungaro F, De Rosa G, Miro A, et al. Spectrophotometric determination of polyethylenimine in the presence of an oligonucleotide for the characterization of controlled release formulations. J Pharm Biomed Anal 2003;31:143–149.
18. Tannous BA. Gaussia luciferase reporter assay for monitoring biological processes in culture and *in vivo*. Nat Protoc 2009;4:582–591.
19. Tannous BA, Kim DE, Fernandez JL, et al. Codon-optimized Gaussia luciferase cDNA for mammalian gene expression in culture and *in vivo*. Mol Ther 2005;11:435–443.
20. Lenter MC, Garidel P, Pelisek J, et al. Stabilized nonviral formulations for the delivery of MCP-1 gene into cells of the vasculoendothelial system. Pharm Res 2004;21:683–691.
21. Kopp F, Schnoedt M, Haase R, et al. De-targeting by miR-143 decreases unwanted transgene expression in non-tumorigenic cells. Gene Ther 2013;20:1104–1109.

Received for publication February 26, 2016; accepted after revision May 10, 2016.

Published online: May 11, 2016.

2.2. Multimodal fluorescence and bioluminescence imaging reveals transfection potential of intratracheally administered polyplexes for breast cancer lung metastases

Multimodal Fluorescence and Bioluminescence Imaging Reveals Transfection Potential of Intratracheally Administered Polyplexes for Breast Cancer Lung Metastases

Antonia Geyer,[1,†] Alexander Taschauer,[1,†] Fatih Alioglu,[1] Martina Anton,[2] Julia Maier,[1] Elisabeth Drothler,[1] Manuela Simlinger,[1] Sümeyye Yavuz,[1] Haider Sami,[1,*] and Manfred Ogris[1,*]

[1]*Laboratory of MacroMolecular Cancer Therapeutics (MMCT), Center of Pharmaceutical Sciences, Department of Pharmaceutical Chemistry, University of Vienna, Vienna, Austria;* [2]*Institutes of Molecular Immunology and Experimental Oncology, Klinikum rechts der Isar, Technische Universität München, Munich, Germany.*
[†]*These authors contributed equally to this work.*

Local delivery of anticancer agents or gene therapeutics to lung tumors can circumvent side effects or accumulation in non-target organs, but accessibility via the alveolar side of the blood–air barrier remains challenging. Polyplexes based on plasmid and linear polyethylenimine (LPEI) transfect healthy lung tissue when applied intravenously (i.v.) in the mouse, but direct delivery into the lungs results in low transfection of lung tissue. Nevertheless, LPEI could offer the potential to transfect lung tumors selectively, if accessible from the alveolar side. This study combined near infrared fluorescent protein 720 (*iRFP720*) and firefly luciferase as reporter genes for detection of tumor lesions and transfection efficiency of LPEI polyplexes, after intratracheal microspraying in mice bearing 4T1 triple negative breast cancer lung metastases. Simultaneous flow cytometric analysis of iRFP720 and enhanced green fluorescent protein expression *in vitro* demonstrated the potential to combine these reporter genes within transfection studies. Polyplex biophysics was characterized by single nanoparticle tracking analysis (NTA) to monitor physical integrity after microspraying *in vitro*. 4T1 cells were transduced with *iRFP720*-encoding lentivirus and evaluated by flow cytometry for stable iRFP720 expression. Growth of 4T1-iRFP720 cells was monitored in Balb/c mice by tomographic near infrared imaging, tissue and tumor morphology by computed tomography and magnetic resonance imaging. In 4T1-iRFP720 tumor-bearing mice, intratracheal administration of luciferase-encoding plasmid DNA by LPEI polyplexes resulted in successful tumor transfection, as revealed by bioluminescence imaging.

Keywords: plasmid DNA, linear polyethylenimine, intratracheal lung delivery, near infrared imaging, bioluminescence imaging, breast cancer

INTRODUCTION

LINEAR POLYETHYLENIMINE (LPEI), albeit having its drawbacks of being a non-biodegradable polymer, still has the advantage of being one of the most efficient transfection reagents, both *in vitro* and *in vivo*. Several clinical trials have already been conducted, and all of them have concentrated on localized delivery, for example for the treatment of superficial bladder cancer (https://clinicaltrials.gov/ct2/show/NCT00595088), but LPEI is also suitable for local gene therapy of the lungs.[1] Pulmonary delivery of macromolecules such as nucleic acids and nanoparticulate formulations is challenging because of the biological barriers such as distribution into the deep lung, overcoming the mucus layer,[2] and rapid clearance from the lungs.[3] The presence of lung tumors, either primary ones or lung metastases arising from breast, colon, and other cancers, changes lung morphology, and such tumors are in principle accessible from the apical site, for example by inhalation or instillation of drug carriers.[4] For PEI-based gene carriers, it was demonstrated that

*Correspondence: Dr. Haider Sami and Prof. Manfred Ogris, Laboratory of MacroMolecular Cancer Therapeutics (MMCT), Center of Pharmaceutical Sciences, Department of Pharmaceutical Chemistry, University of Vienna, Althanstrasse 14, A-1090 Vienna, Austria. E-mail: haider.sami@univie.ac.at; m.ogris@univie.ac.at

DOI: 10.1089/hum.2017.137

lung tumors can be transfected when applied as an aerosol,[5] although this also depends on the tumor type and potential restricted access.[6] In order to optimize application routes and delivery agents, optical *in vivo* imaging can help to identify bottlenecks, with respect to both nucleic acid delivery and transgene expression. To this end, near infrared (NIR) fluorescent dyes have been used directly attached to either the nucleic acid or to the carrier system to monitor the biodistribution and potential redistribution dynamics.[3,7–9] When using suitable imaging systems, both biodistribution and transgene expression can be monitored by using bioluminescence imaging (BLI) to track luciferase reporter gene expression.[7] On the other hand, simultaneous tracking of both tumor growth and transfection requires multiple imaging modalities. BLI of tumor cells, stably transduced with luciferase reporter, is one of the most sensitive methods, allowing the detection of <100 luciferase positive cells.[10] To allow three-dimensional (3D) imaging of the BLI signal, a method based on wavelength-dependent absorption of luciferase emitted light was developed, which together with the reconstruction of a virtual surface enables tomographic analysis.[11] In combination with morphological imaging, for example computed tomography (CT) and suitable CT contrast agents, this method enables precise allocation of tumor nodules to organ structures (Gehrig *et al.*, in preparation). As an alternative to luciferase labeling, fluorescent reporter gene products can also be used. However, *in vivo* tissue absorption poses challenges for their usage. For instance, fluorescent proteins emitting in the green–yellow–orange part of the spectrum are most suited for labeling of only superficial tumors, for example subcutaneously (s.c.) implanted tumors.[12] More recently, the Verkhusha lab developed a protein series, termed iRFPs, with strong far-red and NIR-shifted excitation and emission maxima.[13] Due to their efficient tissue penetration, fluorescence imaging tomography (FLIT) for 3D-signal reconstruction is feasible.

The present study combines NIR fluorescent protein *iRFP720* and firefly luciferase–based reporter genes for detection of tumor lesions and monitoring *in vivo* transfection efficiency of LPEI polyplexes (after microspray-based intratracheal administration), respectively. Influence of microspraying on size and *in vitro* transfection efficiency of LPEI polyplexes was investigated by nanoparticle tracking analysis and luciferase reporter gene assay, respectively. LPEI polyplexes were intratracheally administered in mice bearing lung metastases of syngeneic 4T1 breast cancer cells, and their transfection profile was investigated by BLI in combination with fluorescence imaging–based visualization of 4T1-iRFP720 tumors.

MATERIALS AND METHODS

Transfection and transduction reagents

The CpG-free plasmid *pCpG-hCMV-EF1α-LucSH* expresses luciferase-bleomycin fusion protein under the control of the human elongation factor alpha promoter.[8] The iRFP720-encoding plasmid *piRFP720-N1* was a gift from Vladislav Verkhusha (Addgene plasmid # 45461). *pEGFP-N1* was bought from Clontech (now TaKaRa Bio USA, Inc., Mountain View, CA). Plasmids were expanded using either *Escherichia coli* DH5α (pEGFP-N1 based) or GT115 (pCpG based), as described elsewhere,[8] and purified using commercial kits (GeneJET Plasmid Maxiprep Kit; Thermo Fisher Scientific, Schwerte, Germany; and NucleoBond® PC 10,000; Macherey-Nagel, Dueren, Germany). LPEI (10 kDa) was synthesized and used as described earlier.[14] The VSV-G pseudotyped, self-inactivating lentivirus expresses *iRFP720* under the control of the constitutively active phosphoglycerol (PGK) promoter. The *iRFP720* cDNA was excised from *piRFP720-N1* by XbaI and inserted into pHIV-7 carrying the PGK promoter. Lentiviral vector production was performed in 293T cells, as described earlier.[15]

Cell culture and transductions

4T1 murine triple negative breast cancer cells (CRL-2539) and human lung adenocarcinoma A549 cells (CRM-CCL-185) were obtained from ATCC (LGC Standards GmbH, Wesel, Germany) and cultured in RPMI1640 (supplemented with 10% fetal bovine serum, L-glutamine, and antibiotics). 4T1 cells were lentivirally transduced with polybrene, as described earlier,[15] and sorted for iRFP720 expression on a FACS Aria III (BD Biosciences, San Jose, CA) using 633 nm excitation and a 780/60 bandpass emission filter to obtain 4T1-iRFP720 cells. 4T1-Luc cells were bought from PerkinElmer (Waltham, MA).

Polyplex synthesis

All polyplex solutions were prepared by flash pipetting based on the protocol by Rödl *et al.*[16] For *in vitro* transfection experiments, polyplexes were prepared at different N/P ratios (six or nine) at pDNA concentration of 20 μg/mL (for transfection experiment with *piRFP720-N1* and *pEGFP-N1*) or 267 μg/mL (for microspraying of polyplexes *in vitro*) in HEPES-buffered glucose (HBG buffer; 20 mM HEPES, 5% [w/V] glucose, pH 7.4, sterile filtered). Polyplexes for *in vivo* application were generated at a N/P of 9 at a final pDNA concentration of 267 μg/mL in HBG buffer.

In vitro transfections with piRFP720-N1 and pEGFP-N1

A549 cells (10,000 cells/well) were seeded in 200 μL of medium onto a 96-well plate. After 24 h, the medium was replaced with 80 μL of RPMI1640 (without supplements) and 20 μL of of polyplex solution (containing 400 ng of *piRFP720-N1*, or 400 ng of *pEGFP-N1*, or a mixture of 200 ng of *piRFP720-N1* and 200 ng of *pEGFP-N1* complexed at a N/P of 9) was added per well. After 4 h of treatment with polyplexes, 100 μL of complete medium was added. For flow cytometric analysis, cells were detached after 24 h total transfection time using 30 μL of TrypLE (Thermo Fisher Scientific) and then re-suspended in 130 μL of phosphate-buffered saline (PBS; Dulbecco's PBS; Sigma–Aldrich, Darmstadt, Germany). DAPI (2-[4-amidinophenyl]-6-indolecarbamidine dihydrochloride; Sigma–Aldrich) was used for distinguishing between live and dead cells at a final concentration of 1 μg/mL. One hundred microliters of each cell suspension was analyzed using a MacsQuant Analyzer 10 flow cytometer (Miltenyi Biotec GmbH, Bergisch Gladbach, Germany). During flow cytometry analysis, cells were permanently cooled at 4°C using a Inheco CPAC unit (INHECO, Planegg, Germany). DAPI was excited with 405 nm, and emission was detected with a 450/50 nm band pass filter. Enhanced green fluorescent protein (EGFP) was excited with 488 nm and detected with a 525/50 nm band pass filter. iRFP720 was excited with 635 nm and detected with a 655–730 nm band pass filter. For evaluating expression levels of EGFP and iRFP720, dead cells were excluded.

Microspraying of polyplexes *in vitro*: biophysical characterization and cell transfection

After polyplex preparation, 75 μL of polyplex solution (generated at N/P ratios of 6 and 9) was microsprayed into 1.5 mL centrifuge tubes using a MicroSprayer®/Syringe Assembly (MSA-250-M; Penn-Century, Inc., Wyndmoor, PA). For evaluating the influence of microspraying on nanoparticle properties, microsprayed and non-microsprayed polyplexes were investigated for *in vitro* transfection efficiency in 4T1 and A549 cells by firefly luciferase assay and for size by nanoparticle tracking analysis (NTA; NanoSight NS500, Malvern, United Kingdom). Size evaluation of microsprayed and non-microsprayed polyplexes was done by NTA using a procedure described earlier.[14]

Within *in vitro* transfection assay (based on firefly luciferase reporter gene), A549 and 4T1 cells (10,000 cells/well) were seeded onto a 96-well plate. After 24 h, the medium was replaced with RPMI1640 (without supplements), and 10 μL of polyplex solution (containing 200 ng of *pCpG-hCMV-EF1α-LucSH*, at N/Ps of 6 and 9) was added per well. After 4 h of treatment with polyplexes, 100 μL of RPMI1640 (with supplements) was added. After 24 h of addition of polyplexes, supernatant was removed, and cells were lysed using 30 μL of passive lysis buffer (Promega, Mannheim, Germany). For evaluating luciferase expression, 100 μL of homemade D-luciferin solution (based on sodium salt of luciferin; Promega) was added to 10 μL of cell lysate using the Tecan Infinite M200Pro equipped with auto-injectors, and luminescence (integration time: 10,000 ms; waiting time: 2 s) was measured; 1 nanogram of recombinant luciferase protein corresponds to 10^6 light units. Relative light unit values were normalized based on total protein amount per well. Protein quantification was done for rest of the cell lysate using a BCA assay kit (Pierce; Thermo Fisher Scientific) following the manufacturer's instructions.

Tumor models, intratracheal application

Mice (Balb/cJRj, female; purchased from Janvier Labs, Le Genest-Saint-Isle, France) were housed in individually ventilated cages (Type 2L; Tecniplast, Hohenpeißenberg, Germany) under specified pathogen-free conditions and allowed to acclimatize for at least 10 days prior to experiments. Autoclaved water and food (standard rodent diet; SSniff, Soest, Germany) were provided *ad libitum*. Low fluorescent diet (AIN-76A; Brogaarden Korn & Foder ApS, Lynge, Denmark) was used for at least 7 days prior to the experiments. All procedures were approved by local ethics committee and are in accordance with the Austrian law for the protection of animals and the EU directive 2010/63/EU for animal experiments.

For 4T1-Luc tumor model generation, 4T1-Luc cells were harvested with TrypLE (Thermo Fisher Scientific), washed, and re-suspended in PBS; 10^5 cells (counted by MacsQuant Analyzer 10 flow cytometer) in 100 μL of PBS were injected into the lateral tail vein of mice ($n=3$). For 4T1-iRFP720 tumor model generation, 4T1-iRFP720 cells were harvested with TrypLE, washed, and re-suspended in PBS; 10^5 cells (counted by MacsQuant Analyzer 10 flow cytometer) in 100 μL of PBS were injected into the lateral tail vein of mice ($n=4$). For tumor model characterization by FLI, mice were imaged on days 5, 7, and 10 post implantation by epifluorescence imaging and on day 14 post implantation by FLIT, as described below.

For intratracheal application of polyplexes, 75 μL of polyplex solution (a N/P 9 of in HBG, containing 20 μg of plasmid) was applied using the MicroSprayer®/Syringe Assembly (MSA-250-M; Penn-Century, Inc.), as recently described.[3] On day 8 post

implantation of 4T1-iRFP720 cells, LPEI polyplexes (at N/P of 9) were intratracheally administered ($n = 3$). In brief, ketamin/xylazin (80 mg/kg and 5 mg/kg, respectively) anesthetized mice were placed on an intubation platform made in-house and intubated with a 18G 1″ catheter (BBraun, Melsungen, Germany). Polyplex solution was administered intratracheally right above the tracheal bifurcation, ensuring equal delivery into both lungs. Gooseneck light guides (white LED) were placed externally on the trachea (ventral side) so that the transmitted light ensured proper placement of the tube. On day 9 post implantation (24 h transfection), the mice were imaged first by FLI, followed by BLI and magnetic resonance imaging (MRI), as described below.

In vivo imaging

Optical imaging and CT was carried out on an IVIS Spectrum CT imaging system (PerkinElmer). Mice were shaved ventrally and dorsally to improve the signal quality for fluorescence and bioluminescence measurements. For FLIT imaging, mice received intraperitoneally 300 μl Scanlux (Iopamidol, Sanochemia, Vienna; 300 mg iodine/mL) in 5% glucose (w/v) at a ratio of 1:1.5. Fluorescence imaging was performed in epifluorescence mode, as described earlier,[3] with automated exposure time using the following excitation (Ex)/emission (Em) filter combination (excitation: 30 nm bandwidth; emission: 20 nm bandwidth): Ex: 640 nm with Em: 680 nm, 700 nm, 720 nm, 740 nm, 760 nm; and Ex: 675 nm with Em: 720 nm, 740 nm, 760 nm, 780 nm, 800 nm. All animals were imaged along with a control animal, and spectral unmixing was done for each image separately. For 3D measurement, mice were first scanned by CT in low resolution and afterwards measured for fluorescence emission in transillumination mode, according to the technique described previously.[3] Mice were anesthetized by 1.5–2% isoflurane in oxygen, placed ventral up on the grid plate, and fluorescence images were acquired at Ex: 675 nm (30 nm BW) and Em: 720 nm (20 nm BW). For BLI, luciferin (D-luciferin potassium salt VivoTrace™; Intrace Medical, Lausanne, Switzerland; dissolved in PBS at 30 mg/mL) was injected s.c. at a dose of 120 mg/kg. Bioluminescence signal was subsequently collected for 45 min at an exposure of 5 min in stage B to gain maximum signals after 20–40 min.

For MRI analysis, anesthetized animals were imaged by an Aspect Imaging™ M3 compact MRI system (AspectImaging, Shoham, Israel). T2 weighted images were acquired using a 50 mm × 30 mm body coil (time to repetition [TR]: 3,250 ms; time to echo [TE]: 63.47 ms; number of slices: 15; slice thickness: 1 mm; number of excitations: 7; slice orientation: coronal; center of slice position: 0; flip angle: 90°; scan time: 5 min 46 s). Analysis was performed by a veterinary clinical radiologist using VivoQuant™ (Invicro, Boston, MA).

Histology

After imaging, mice were sacrificed by an overdose of anesthesia and intubated. Ten percent formalin (4% formaldehyde in HBS, prepared using paraformaldehyde; Sigma–Aldrich) was instilled, as per a reported method.[17] Briefly, the intratracheal tube was connected to a bottle (filled with 10% formalin) at a height of 25 cm, and the lungs were instilled utilizing the pressure of the fluid over a time period of 5 min. The lungs were subsequently fixed in formalin for 22 h, dehydrated by gradient ethanol treatment (70%, 96%, and 100%), cleared by Xylene (Sigma–Aldrich), and embedded using Paraplast® (Sigma–Aldrich). After sectioning, the tissues were rehydrated in a descending ethanol row and stained using hematoxylin according to Harris (Carl Roth GmbH + Co. KG, Karlsruhe, Germany) and Eosin Y (Sigma–Aldrich; 3 min hematoxylin, 1 s acidified ethanol, 20 s NH_4OH, 10 min eosin) for morphological analysis.

Immunohistochemistry

Sections were boiled for at least 20 min in pH 8 EDTA-Tween buffer (1 mM of EDTA +0.05% Tween R 20 in PBS) in a water bath. EDTA-Tween buffer was prepared by mixing 1 mM of EDTA (Sigma–Aldrich) with 0.05% Tween® 20 (Sigma–Aldrich) in PBS, and the pH was adjusted to 8. The sections were allowed to cool for 30 min at room temperature, and endogenous peroxidase was blocked using 3% H_2O_2 (v/v) in PBS. Unspecific binding sites were blocked using normal rabbit serum (Vectastain ABC Kit; Vector Laboratories, Burlingame, CA) for 30 min. The polyclonal goat anti-firefly luciferase antibody (Abcam, Cambridge, United Kingdom) was diluted in 2% bovine serum albumin (Sigma–Aldrich) in PBS to a final concentration of 1 μg/mL, and the sections were treated overnight at 4°C. In parallel, control sections were incubated with an equivalent amount of buffer for secondary antibody control. After washing in PBS, the biotinylated rabbit anti-goat antibody (Vectastain ABC Kit; Vector Laboratories) was applied for 30 min and subsequently treated with ABC reagent of the same kit for 30 min. The sections were then treated with 0.5% Triton® X-100 (Sigma–Aldrich) in PBS followed by incubation in a 3,3-diaminobenzidine tetrahydrochloride (DAB; Sigma–Aldrich) substrate solution (10 tablets in 250 mL of PBS +1.25 mL of Triton® X-100) for 7 min. Counterstaining of the sections was done using hematoxylin.

RESULTS

The most NIR-shifted protein, namely iRFP720, with excitation/emission maxima of 710/760 nm, was selected for transfection studies. Within *in vitro* transfection studies, as can be seen in Fig. 1A and B, *iRFP720* plasmid showed similar expression profile when compared to *EGFP*-encoding plasmid. Both plasmids share the same backbone (N1) and promoter (CMV). There was no fluorescence overspill between the two fluorophores when using the 488 nm laser line for excitation and a 525–550 nm bandpass filter for EGFP, and 635 nm laser excitation and a 655–730 nm bandpass filter for iRFP720. Within co-transfection experiment (Fig. 1C), a high level of transgene expression for both *iRFP720* and *EGFP* reporter genes was observed, with good signal correlation. However, low EGFP-expressing cells were negative for iRFP720 expression. Further, the *iRFP720* cDNA was cloned into a pHIV7/SF-GFP-derived plasmid, replacing *EGFP* and the SF-promoter, and VSV-G pseudotyped self-inactivating (SIN) lentivirus was produced in HEK-293T cells. This lentivirus was used to transduce 4T1 cells stably. After cell sorting, 85–94% cells remained positive for iRFP720 expression (Supplementary Fig. S1; Supplementary Data are available online at www.liebertpub.com/hum).

Next, the influence of the microspraying process on biophysical properties (Fig. 2) and transfection efficiency of LPEI polyplexes (Fig. 3) was evaluated. With an increased N/P ratio (nine vs. six), particles appeared significantly smaller. After microspraying of polyplexes, both broadness of the size distribution and average size increased due to probable aggregation, thereby resulting in a decrease in particle concentration, as shown in Fig. 2A and B, respectively. Nevertheless, the fraction of particles up to 200 nm in size decreased only slightly (Fig. 2B). When comparing the *in vitro* transfection efficiency of native to microsprayed particles, A549 cells showed higher transfection than 4T1 cells with a N/P of 9, showing highest transfection efficiency in both cell types (Fig. 3). Microspraying of polyplexes affects transfection efficiency slightly in the case of A549 (at N/P of 9) and more significantly in the case of 4T1 cells for both treatment ratios (*i.e.*, at N/P of 6 and at N/P of 9).

Further on, the 4T1-iRFP720 disseminated tumor model (Fig. 4) was established, and it was compared to the already established 4T1-Luc model (Supplementary Fig. S2). iRFP720 fluorescence signal of 4T1-iRFP720 cell suspension was acquired with the imaging system, and optimal signal intensity was achieved with Ex 675/Em 720–740 nm as shown in Fig. 4A. In control experiments, the validity and high sensitivity of the 4T1-luc model could be confirmed. When 10^5 4T1-Luc cells were injected i.v. into Balb/c mice, a significant BLI signal (10-fold above background) was measured (Supplementary Fig. S2A), which further increased by three log units on day 8 after tumor cell injection (Supplementary Fig. S2A). Because of this high BLI signal, DLIT measurement and 3D signal reconstruction was possible. In the case of the 4T1-iRFP720 model, as expected, 4T1-iRFP720 cells resulted in a considerably lower signal/noise ratio when measured by epifluorescence imaging. Fluorescence signals clearly distinguishable from background appeared earliest at day 5 post injection (Supplementary Fig. S3), and required the application of the background unmixing technique.[3]

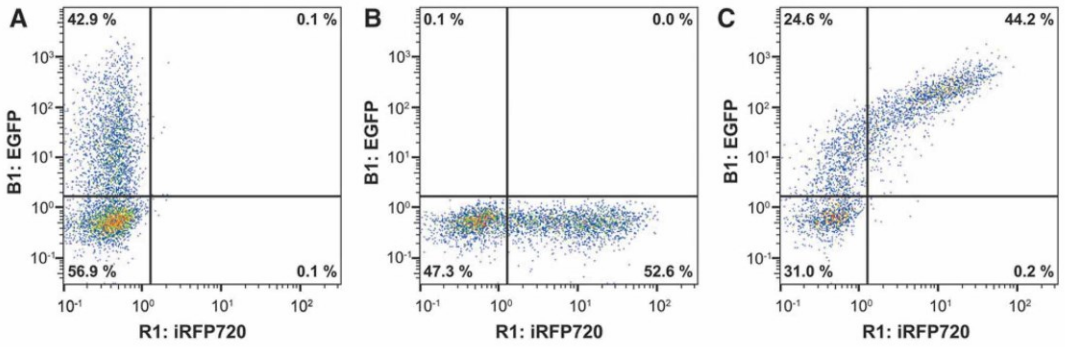

Figure 1. Combination of near infrared (NIR)-emitting *iRFP720* reporter gene with enhanced green fluorescent protein (*EGFP*) reporters for transient transfection studies. Cells were transfected with 400 ng of *pEGFP-N1* **(A)**, 400 ng of *piRFP720* **(B)**, or with a mixture of 200 ng of each plasmid **(C)** using linear polyethylenimine (LPEI), as described in the Materials and Methods. Live cells were gated after addition of 2-(4-amidinophenyl)-6-indolecarbamidine dihydrochloride (DAPI) and represented as density plots showing iRFP720 fluorescence on the *x*-axis and EGFP fluorescence on the *y*-axis.

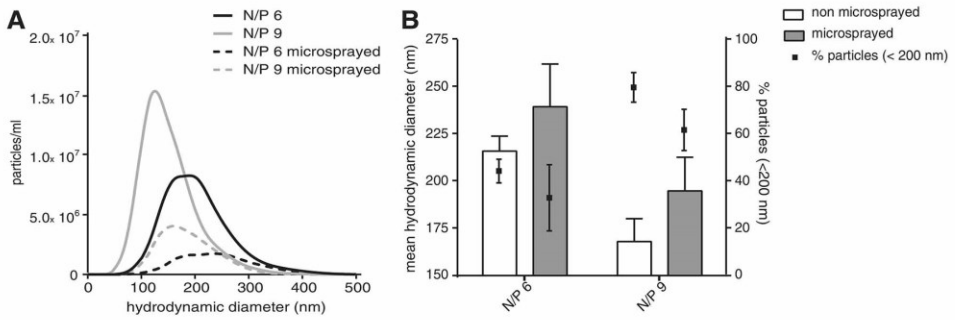

Figure 2. Influence of microspraying on biophysical properties of LPEI polyplexes. Polyplexes (N/P of 6 and N/P of 9) were generated in HEPES-buffered glucose (HBG) buffer at a final pDNA concentration of 267 μg/mL and underwent microspraying with a PennCentury microsprayer. They were then analyzed by nanoparticle tracking analysis (as described in the Materials and Methods) to plot particle size distribution **(A)**, and mean hydrodynamic diameter and percentage of particles within a range of up to 200 nm **(B)**. Data shown are representative of three different experiments.

With late-stage tumors (day 14 after injection), 3D signal analysis (FLIT) together with CT and contrast agent was feasible (4B). Distinct tumor areas could be identified in the lungs. Pathological evaluation of mouse lungs (21 days post tumor implantation) revealed macroscopic multiple pale nodules up to 2 mm in diameter (Fig. 4C). To examine the microanatomy of tumors and their invasion pattern, first the lung fixation technique was optimized to preserve the organ structure (Supplementary Fig. S4). Simply excising the lungs, followed by the standard fixation and embedding procedure, resulted in collapsed lung tissue without the possibility of studying bronchio-alveolar structure. Optimal structure conservation was achieved when instilling lungs of dead animals with formalin solution prior to formalin-fixed paraffin-embedded processing (Supplementary Fig. S4A and C). Hence, this fixation technology was also applied to tumor-bearing animals. 4T1-iRFP720 tumors exhibited a multifocal nodular-like appearance, with invasive parenchymal growth pattern and oligofocal single cell infiltrates (Fig. 4D and E), responsible for the macroscopic nodular structure. Notably, the tumor cells were located in the alveolar septs and could also be detected inside the alveolar space (Fig. 4E). Inside the compact tumor formations, the vascularization consisted only of capillaries, as larger vessels could not be detected.

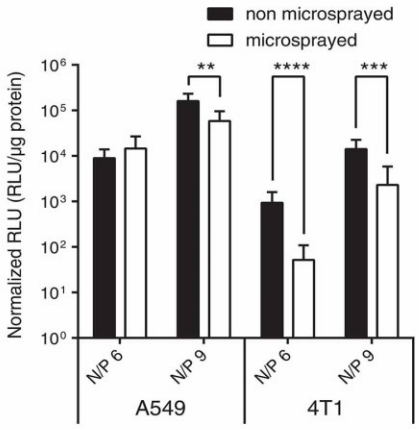

Figure 3. Influence of microspraying on *in vitro* transfection efficiency. A549 and 4T1 cells (10,000 cells/well) were treated with *pCpG-hCMV-EF1a*-LucSH-based polyplexes at a concentration of 200 ng of pDNA/well. The polyplex solution was tested before and after microspraying. Twenty-four hours later, luciferase expression was evaluated by luciferase assay protocol. Relative light unit (RLU) values were normalized based on total protein amount per well. Normalized RLU values are shown as mean values ($n=9$; error bars indicate standard deviation; *$p \leq 0.05$; **$p \leq 0.01$; ***$p \leq 0.001$; ****$p \leq 0.0001$; U test [Mann-Whitney]).

Furthermore, the transfection pattern of LPEI polyplexes in 4T1-iRFP720 tumor-bearing mice was investigated (Fig. 5). In all experiments, N/P 9 polyplexes were used due to their higher stability (Fig. 2) and reliability of *in vivo* transfection.[14] First, the tumor load and its spatial localization were evaluated using fluorescence imaging and spectral unmixing (Fig. 5A–C). Two animals showed highest signal intensities in the area of the right lung. In one animal, the overall signal intensity was less. However, the main signal was located in the left area of the lungs, with a less intense signal in the right lung (Fig. 5B). After spatially localizing the tumor via FLI signal, BLI imaging was performed on these animals to investigate the transfection pattern. Polyplex-treated animals exhibited significant BLI signals (Fig. 5D–F) when compared to control animals (data

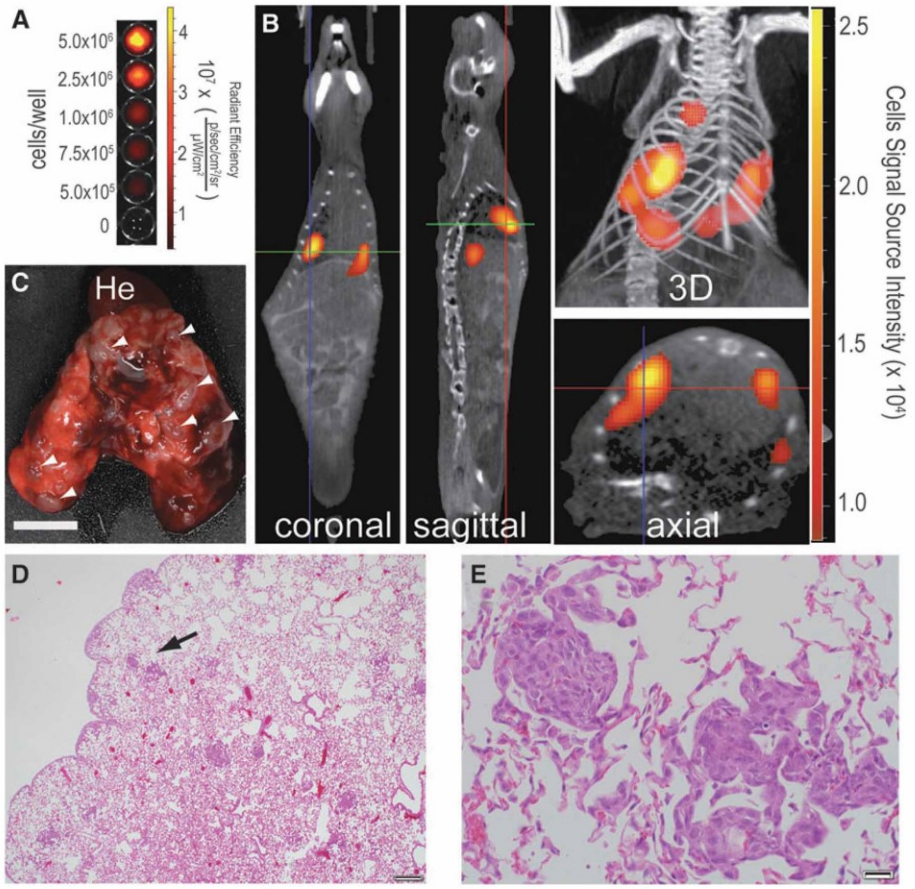

Figure 4. Characterization of 4T1-iRFP720 tumor model in Balb/c mice. **(A)** Epifluorescence imaging of 4T1-iRFP720 cell suspension (Ex 675 nm, Em 720 nm) on a 96-well plate, 5×10^5–5×10^6 cells/well. **(B)** Fluorescence imaging tomography (FLIT)/computed tomography (CT) analysis of 4T1-iRFP720 tumors 14 days after intravenous (i.v.) injection of 10^5 cells. Animals received iopamidol contrast agent i.v. prior to imaging. The CT picture (grayscale) is overlaid with the FLIT signal (color coded). Colored lines denote the position of the optical section in coronal (*red*), axial (*green*), or sagittal (*violet*) view. **(C)** Explanted lung/heart 21 days after tumor cell injection. He denotes heart. *White arrowheads* point at tumor nodules (pale appearance). Scale bar: 5 mm. **(D** and **E)** Instillation fixed, hematoxylin and eosin–stained tumor-infiltrated lungs 9 days after tumor cell injection. Scale bar: 200 μm **(D)** and 20 μm **(E)**. *Arrow* in **(D)** indicates the magnified area in **(E)**.

not shown). However, the BLI signals were low in signal intensity. Importantly, the localization of the BLI source not only matched the side of the FLI signal, but also partially overlapped with the fluorescence signals. Using MRI and histological analysis, tumor structures within the same localization could also be morphologically identified. Histological examination (Supplementary Fig. S5) revealed tumor nodules in all lobes. Interestingly, in the case of the animal with low FLI signal (Fig. 5B), no diffuse morphological alterations of the structure in MRI were seen, but a nodular structure of high echogenicity in the dorsal portion of the right caudal lobe, surrounded by finger-like structures of medium echogenicity, were observed only inside the left lung (Fig. 5H). The MRI of the control animal showed that all thoracic structures were of physiological appearance (i.e., no structures with high echogenicity; Fig. 5I). Histologically, tumors of this particular animal were also found in all lobes but with an area of presumably dystelectatic lung tissue inside the left lobe. For validation of LPEI polyplex-mediated luciferase gene delivery to 4T1-iRFP720 tumor, immunohistochemical staining for firefly luciferase protein of the tumor-bearing lungs was performed for both polyplex-transfected and untransfected mice (Supplementary Fig. S6). Immunohistochemical analysis revealed a pale but distinct homogenous

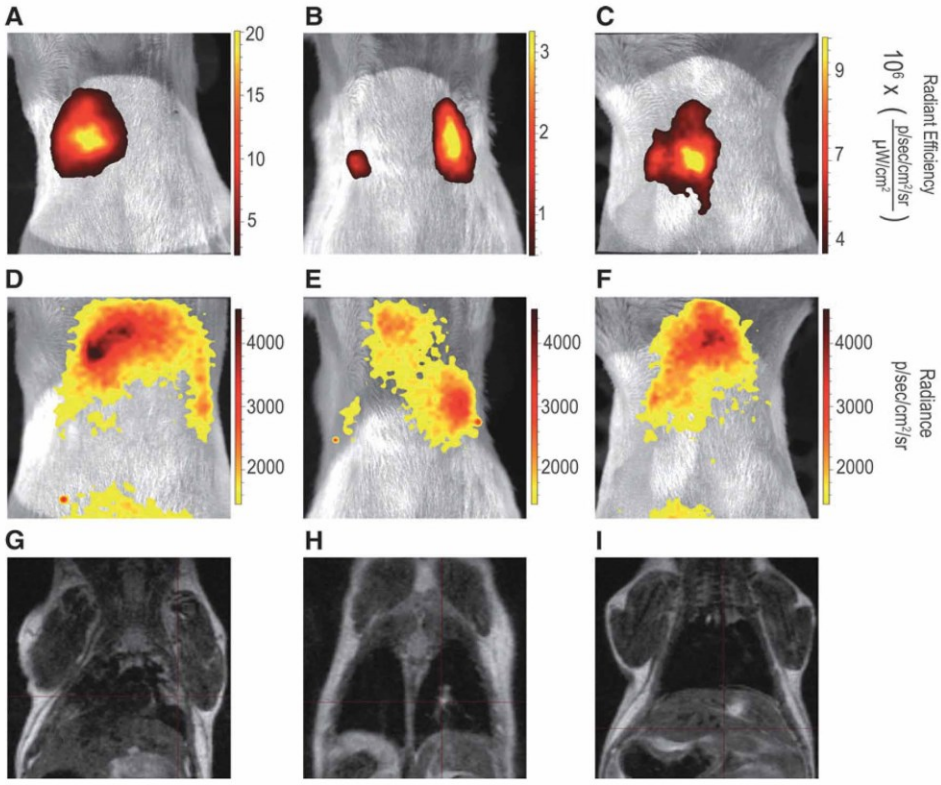

Figure 5. Transfection of 4T1-iRFP720 tumor after intratracheal instillation. Balb/c mice received 10^5 4T1-iRFP720 cells i.v. On day 8 after tumor cell injection, LPEI polyplexes (N/P 9) were applied intratracheally, and on day 9 (24 h transfection), mice were imaged by FLIT, bioluminescence imaging (BLI), and magnetic resonance imaging (MRI), as described in Materials and Methods. **(A–C)** 4T1-iRFP720 fluorescence signal (color coded, after spectral unmixing) is overlaid on a reflected light picture (B/W). **(D–F)** BLI signal (color coded) overlaid on a reflected light picture (B/W). **(G** and **H)** MRI picture (T2 weighted) of tumor-bearing animals. **(I)** MRI (T2) of healthy control animal. Note: data from the same animal shown in A, D, and G, in B, E, and H, and in C and F, respectively. $n=3$ for FLI/BLI imaging; $n=2$ for MRI imaging.

staining pattern similar to stably transfected control tumor (4T1-Luc)-bearing lungs expressing luciferase (data not shown), thereby indicating the presence of luciferase protein in polyplex-transfected tumor mice (Supplementary Fig. S6).

DISCUSSION

Tracking *in vivo* transgene expression with optical imaging via BLI of luciferase activity is a well-established method. Here, luciferases with a red-shifted emission spectrum offer optimal signal for deeper-seated signals, as there is an inverse correlation between tissue absorption and wavelength of the emitted light.[18] Also, for fluorescence imaging *in vivo*, the use of fluorophores emitting in the green to orange spectrum is precluded due to absorption at a lower wavelength (*e.g.*, by hemoglobin and skin melanin). An absorption minimum is possible within the so-called biological window, ranging from approximately 650 to 900 nm, enabling preclinical and clinical use of fluorophores emitting within this range.[19,20] The fluorescent spectrum of recombinant proteins has been considerably extended into the far red and NIR, with development of a whole series of NIR-shifted protein variants with high stability and quantum yield.[13] With iRFP720 being the most red-shifted variant, this reporter protein was utilized to label different cancer lines.

First, cells were co-transfected with *EGFP*-encoding plasmid with a similar backbone (N1 based). Separate excitation with 488 and 635 nm laser lines, respectively, did not give any spectral

overlap and hence need for signal compensation. In co-transfection, a good signal correlation was observed in cells with high levels of transgene expression. Notably, cells exhibiting low EGFP signals were negative for iRFP. This could be due to lower quantum yields of iRFP720 (in contrast to EGFP), as iRFP720 is excited only with approximately 50% efficiency when using the 635 nm laser. Nevertheless, the signal observed was specific and significant.

Next, a lentiviral vector was generated for efficient gene marking of 4T1 cells with *iRFP720*, and positive cells were selected by sorting. The 4T1 murine triple-negative breast cancer model syngeneic in Balb/c mice resembles several aspects of the human disease situation, such as receptor status and metastasis formation. Both orthotopically implanted tumors and direct i.v. injected tumor cells form intravascular tumors in the lungs,[21] and there is no significant difference in gene expression pattern between lung metastases derived from orthotopically implanted 4T1 cells when compared to lesions induced by i.v. injected cells.[22]

The study also directly compared the 4T1-iRFP720 cells to the commercialized 4T1-Luc cells in terms of growth kinetics and sensitivity of tumor detection (Supplementary Fig. S2). It is important to note that 4T1-luc cells grew considerably faster, with mice turning moribund already 6–7 days after injection of 10^5 cells (heavy breathing, weight loss >10%), with a notably higher sensitivity. In contrast, 4T1-iRFP720-injected mice remained clinically unaffected for 14–19 days post implantation, also when injecting 10^6 instead of 10^5 cells (data not shown).

To obtain detailed information on the tumor micromorphology, the lung fixation procedure had to be optimized, as shown in Supplementary Fig. S4. In the case of the lungs, the penetration of the diaphragm usually leads to lung collapse. Hence, *in situ* fixation by whole-body perfusion, instillation, and other methods can be applied.[17] Using formalin instillation fixation, based on a constant fluid pressure, very good preservation of alveolar structures was achieved. The histological studies revealed that 4T1-iRFP720 cells form small multifocal parenchymal nodular or nodular-like tumors, with single-cell infiltrates growing within the alveolar sept architecture, as well as occasional peribronchiolar colonialization with slight side preferences, when injected i.v. (Fig. 4D and Supplementary Fig. S5). This is in contrast to the pattern observed with 4T1-Luc, where i.v.-injected cells led to tumor infiltrated parenchyma without detectable isolated tumor nodules.[22] Interestingly, FLI imaging nevertheless showed a good sensitivity, as it was able to determine a significant tumor load.

These findings could not be entirely verified using morphological analysis with the MRI. In one mouse (Fig. 5G), diffuse infiltration of both sides of the lungs was observed, matching the histological findings (Supplementary Fig. S5A), whereas FLI only showed a signal in the right lung area. In contrast, the second mouse (Fig. 5B) showed FLI signals in both lungs, as also seen in histology, but with MRI (Fig. 5H), only a high echogenicity structure in the right lung was observed. Moreover, this structure could also be morphologically related to structures other than cancerous tissue. For that reason, it is important to consider that 2D imaging cannot be used for fine morphological analysis to determine the exact location of the signal, and in the case of one particularly high signal, smaller signals can appear invisible. Also, the second example shows that morphological *in vivo* imaging by MRI can be limited in terms of sensitivity.

It is important to note that epifluorescence in the case of deep-seated signals comes to a limit, and transfluorescence technique in 2D or FLIT would be advisable for a more accurate quantification, but this would also then be more time-consuming. Taken together, it is nevertheless important to consider the high value of FLI *in vivo* imaging of iRFP720 to monitor lung tumor load in mice in terms of relative signal quantification, and with that, animals could be signal-dependent treated before they become clinically affected or even moribund. Furthermore, in the case of sufficient fluorescence emission, FLIT imaging for absolute quantification and localization could also give additional information about the tumor load (Fig. 4B). As a consequence, refinement of animal procedures to improve the ethics of lung metastasis experiments could be achieved using this model. It is also possible that if all transduced cancerous cells express the fluorescence protein, tumor load–dependent treatment in a comparable tumor load could be gained. However, it is also important to note that the heterogeneity of iRFP720 expression within the whole tumor cannot be ruled out, as approximately 90% of 4T1-iRFP720 cells were fluorescent (Supplementary Fig. S1).

When analyzing the individual tumor nodules as well as nodular structures and their growth pattern along the alveolar septs and, with that, the interference with healthy, alveolar tissue, obviously tumor cells breached through the endothelium, basal membrane, and alveolar wall and reached the air side. Similar to the clinical situation, 4T1 cells from either orthotopically implanted tumors or i.v. injected ones form intravascular tumors, occluding vessels, and after prolonged growth invade the pa-

renchyma and reach the luminal side, as also observed in Fig. 4E.[21] This should make these tumors accessible for LPEI polyplexes when applied via the airways.

Accessibility is of key importance, as Hasenpusch *et al*. demonstrated that only lung tumors with access to the air side were accessible for aerosolized polyplexes.[6] In this case, only tumors that grew after intrabronchiolar cell application were transfected by polyplexes, whereas i.v.-applied cells (A549 human lung carcinoma xenografted in NSG-mice) exhibited a diffuse parenchymal infiltration pattern and could not be transfected by aerosolized polyplexes. In the case of optical imaging, sensitivity of detection was much lower for fluorescence imaging in comparison to bioluminescence. This is substantiated by the presence of a clear bioluminescence signal in the lung area (Supplementary Fig. S2) immediately after i.v. injection of 10^5 4T1-luc cells. On the other hand, with 4T1-iRFP a significant signal was only seen at the earliest at 5 days post implantation. However, the tumor growth rate was observed to be more aggressive in the luciferase-transfected tumor cells in comparison to 4T1-iRFP720 cells (Supplementary Figs. S2 and S3). Switching to a chlorophyll-free diet could reduce fluorescence from stomach and intestine, but the spectral unmixing procedure still had to be applied to improve detection of the lesion by 2D epifluorescence imaging.[3] Despite the spectral unmixing process, signals from the stomach were still detectable. This indicates the need to reduce background both by a reduced FL diet and also by the spectral unmixing procedure.

In a similar work by Shcherbakova and Verkhusha,[13] 3D tomographic imaging of deep-seated signals in the liver by FLIT was achieved using iRFP713 after transduction with *iRFP713*-encoding adenovirus. However, in the present study, FLIT was possible only in individual animals with high fluorescence signal and probably also high tumor load. Due to less sensitivity, 3D FLIT imaging with subsequent quantification based on a created database needs a critical threshold to gain a better signal-to-noise ratio. In the case of the presented mid-stage tumor load and a rather low expression rate of iRFP720 protein in 4T1-iRFP720 cells (data not shown), FLIT reconstruction was possible but not without excluding background from the stomach. Selecting and sorting of cells with even higher iRFP720 levels might help to increase the homogeneity of RFP expression within the whole tumor, but care has to be taken to avoid cytotoxic effects due to high reporter gene expression. In order to improve sensitivity, alternatives are also being considered, such as the use of luciferases with substrates other than luciferin and approaches based on bioluminescence resonance energy transfer.[23]

Consideration of biophysical properties of polyplexes is crucial for efficiency of transfection both *in vitro* and *in vivo*, and especially with respect to the influence of microspraying on size and transfection ability. NTA showed that N/P 9–based polyplexes had significantly higher percentage of particles up to 200 nm in size in comparison to N/P 6, which can be ascribed to the excess polymer, as also reported in other studies.[24,25] The microspraying process did not drastically change the fraction of particles up to 200 nm, which are important for transfection.[26] This is supported by the results of *in vitro* transfection of A549 cells, where there was only slight decrease in transfection efficiency (Fig. 3). However, in the case of 4T1 cells, detrimental effect of microspraying on transfection efficiency may be ascribed to their low transfectability, which can also be observed in comparison to A549 (Fig. 3). When compared to the very high bioluminescence signal observed with N/P 9 LPEI polyplexes in Balb/c mice,[14] transfection was very low when applying such polyplexes intratracheally (data not shown). This is in agreement with observations by Bragonzi *et al*., where a 100-fold lower luciferase activity was seen with LPEI polyplexes when comparing intratracheal to i.v. application.[27]

Additional barriers for lung delivery include mucus in the larger airways, surfactant in the alveolae, and clearance by the phagocytic system in the lungs, especially for nanoparticles bearing a cationic charge such as polyplexes. Albeit mucus-producing breast cancers are known, that is, mucinous (colloidal) breast cancer,[28] triple-negative breast cancer is not known for exuberant mucus production. With IT delivery, BLI signals could be detected in the lung area, overlapping at least partially with the iRFP720 signal using FLI imaging. Notably, the side of the animal with BLI signal matched in all cases with the side having the fluorescence signals. However, the signal was very low, and an untreated animal was needed to verify the BLI signal. Importantly, immunohistochemical evaluation showed the same staining pattern as could be observed in stably transduced 4T1-luc-bearing tumor lungs showing a rather pale homogenous staining pattern. Nevertheless, background staining and unspecific binding especially for the healthy tissue cannot fully be excluded (Supplementary Fig. S6). To investigate potential transfection of healthy tissue and especially the bronchiolar epithelium, further studies need to be conducted.

With the data presented here, the study successfully utilized LPEI polyplexes to transfect lung lesions after intratracheal delivery. As transfection levels were still rather low, and transfection of healthy tissue cannot be completely excluded, further improvements for the LPEI polyplex part are conceivable. Imaging-based biodistribution studies of these polyplexes can also help in tracking the transfection process. For instance, some studies show liver accumulation of nucleic acids after lung delivery. This possibility of liver accumulation cannot be ruled out in the present study. To pursue tumor selective transgene expression further, the authors plan to apply targeting strategies on the transcriptional level using tumor-selective promoter elements,[29] de-targeting transgene expression on the transcriptional level utilizing microRNA binding domains,[30] or for selectivity of tumor cell uptake combined de-targeting with PEG and re-targeting with ligand binding peptides.[31,32]

ACKNOWLEDGMENTS

Parts of this work have received support from the EU/EFPIA Innovative Medicines Initiative Joint Undertaking COMPACT grant no. 115363. J.M. is supported by the uni:docs fellowship program for doctoral candidates of the University of Vienna. We are very grateful to Gerald Schmauss and Karin Aumayr (Research Institute for Molecular Pathology GmbH, Vienna, Austria) for sorting of iRFP720 transduced cells. We are grateful to Sebastian Gehrig for help and discussions regarding MRI analysis.

AUTHOR DISCLOSURE

No competing financial interests exist.

REFERENCES

1. McLachlan G, Davidson H, Holder E, et al. Preclinical evaluation of three non-viral gene transfer agents for cystic fibrosis after aerosol delivery to the ovine lung. Gene Ther 2011;18:996–1005.
2. Mastorakos P, da Silva AL, Chisholm J, et al. Highly compacted biodegradable DNA nanoparticles capable of overcoming the mucus barrier for inhaled lung gene therapy. Proc Natl Acad Sci U S A 2015;112:8720–8725.
3. Geyer A, Lorenzer C, Gehrig S, et al. Fluorescence- and computed tomography for assessing the biodistribution of siRNA after intratracheal application in mice. Int J Pharm 2017;525:359–366.
4. Kuzmov A and Minko T. Nanotechnology approaches for inhalation treatment of lung diseases. J Control Release 2015;219:500–518.
5. Densmore CL. The re-emergence of aerosol gene delivery: a viable approach to lung cancer therapy. Curr Cancer Drug Targets 2003;3:275–286.
6. Hasenpusch G, Pfeifer C, Aneja MK, et al. Aerosolized BC-819 inhibits primary but not secondary lung cancer growth. PLoS One 2011;6:e20760.
7. Zintchenko A, Susha AS, Concia M, et al. Drug nanocarriers labeled with near-infrared-emitting quantum dots (quantoplexes): imaging fast dynamics of distribution in living animals. Mol Ther 2009;17:1849–1856.
8. Navarro G, Maiwald G, Haase R, et al. Low generation PAMAM dendrimer and CpG free plasmids allow targeted and extended transgene expression in tumors after systemic delivery. J Control Release 2010;146:99–105.
9. Medarova Z, Pham W, Farrar C, et al. *In vivo* imaging of siRNA delivery and silencing in tumors. Nat Med 2007;13:372–377.
10. Rabinovich BA, Ye Y, Etto T, et al. Visualizing fewer than 10 mouse T cells with an enhanced firefly luciferase in immunocompetent mouse models of cancer. Proc Natl Acad Sci U S A 2008;105:14342–14346.
11. Kuo C, Coquoz O, Troy TL, et al. Three-dimensional reconstruction of *in vivo* bioluminescent sources based on multispectral imaging. J Biomed Opt 2007;12:024007.
12. Hong H, Yang Y, Cai W. Imaging gene expression in live cells and tissues. Cold Spring Harb Protoc 2011;2011:pdb top103.
13. Shcherbakova DM, Verkhusha VV. Near-infrared fluorescent proteins for multicolor *in vivo* imaging. Nat Methods 2013;10:751–754.
14. Taschauer A, Geyer A, Gehrig S, et al. Up-scaled synthesis and characterization of nonviral gene delivery particles for transient *in vitro* and *in vivo* transgene expression. Hum Gene Ther Methods 2016;27:87–97.
15. Su B, Cengizeroglu A, Farkasova K, et al. Systemic TNFalpha gene therapy synergizes with liposomal doxorubicine in the treatment of metastatic cancer. Mol Ther 2013;21:300–308.
16. Rodl W, Schaffert D, Wagner E, et al. Synthesis of polyethylenimine-based nanocarriers for systemic tumor targeting of nucleic acids. Methods Mol Biol 2013;948:105–120.
17. Braber S, Verheijden KA, Henricks PA, et al. A comparison of fixation methods on lung morphology in a murine model of emphysema. Am J Physiol Lung Cell Mol Physiol 2010;299:L843–851.
18. Mezzanotte L, van 't Root M, Karatas H, et al. *In vivo* molecular bioluminescence imaging: new tools and applications. Trends Biotechnol 2017;35:640–652.
19. Owens EA, Henary M, El Fakhri G, et al. Tissue-specific near-infrared fluorescence imaging. Acc Chem Res 2016;49:1731–1740.
20. Vahrmeijer AL, Hutteman M, van der Vorst JR, et al. Image-guided cancer surgery using near-infrared fluorescence. Nat Rev Clin Oncol 2013;10:507–518.
21. Wong CW, Song C, Grimes MM, et al. Intravascular location of breast cancer cells after spontaneous metastasis to the lung. Am J Pathol 2002;161:749–753.
22. Rashid OM, Nagahashi M, Ramachandran S, et al. Is tail vein injection a relevant breast cancer lung metastasis model? J Thorac Dis 2013;5:385–392.
23. Rumyantsev KA, Turoverov KK, Verkhusha VV. Near-infrared bioluminescent proteins for two-color multimodal imaging. Sci Rep 2016;6:36588.
24. Boeckle S, von Gersdorff K, van der Piepen S, et al. Purification of polyethylenimine polyplexes highlights the role of free polycations in gene transfer. J Gene Med 2004;6:1102–1111.
25. Fahrmeir J, Gunther M, Tietze N, et al. Electrophoretic purification of tumor-targeted polyethylenimine--based polyplexes reduces toxic side effects *in vivo*. J Control Release 2007;122:236–245.

26. von Gersdorff K, Sanders NN, Vandenbroucke R, et al. The internalization route resulting in successful gene expression depends on polyethylenimine both cell line and polyplex type. Mol Ther 2006;14:745–753.

27. Bragonzi A, Dina G, Villa A, et al. Biodistribution and transgene expression with nonviral cationic vector/DNA complexes in the lungs. Gene Ther 2000;7:1753–1760.

28. Dumitru A, Procop A, Iliesiu A, et al. Mucinous breast cancer: a review study of 5 year experience from a hospital-based series of cases. Maedica (Buchar) 2015;10:14–18.

29. Haase R, Magnusson T, Su B, et al. Generation of a tumor- and tissue-specific episomal non-viral vector system. BMC Biotechnol 2013;13:49.

30. Kopp F, Schnoedt M, Haase R, et al. De-targeting by miR-143 decreases unwanted transgene expression in non-tumorigenic cells. Gene Ther 2013;20:1104–1109.

31. Schafer A, Pahnke A, Schaffert D, et al. Disconnecting the yin and yang relation of epidermal growth factor receptor (EGFR)-mediated delivery: a fully synthetic, EGFR-targeted gene transfer system avoiding receptor activation. Hum Gene Ther 2011;22:1463–1473.

32. Klutz K, Schaffert D, Willhauck MJ, et al. Epidermal growth factor receptor-targeted (131)I-therapy of liver cancer following systemic delivery of the sodium iodide symporter gene. Mol Ther 2011;19:676–685.

Received for publication July 29, 2017;
accepted after revision September 3, 2017.

Published online: September 5, 2017.

Supplementary Data

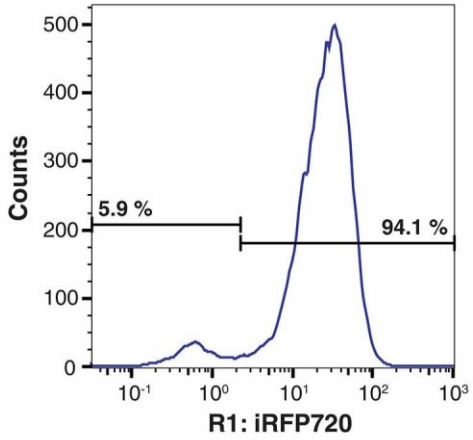

Supplementary Figure S1. Lentiviral-based transduction of 4T1 cells with iRFP720 gene under constitutive expression. iRFP720 expression of 4T1 cells as analyzed by flow cytometry.

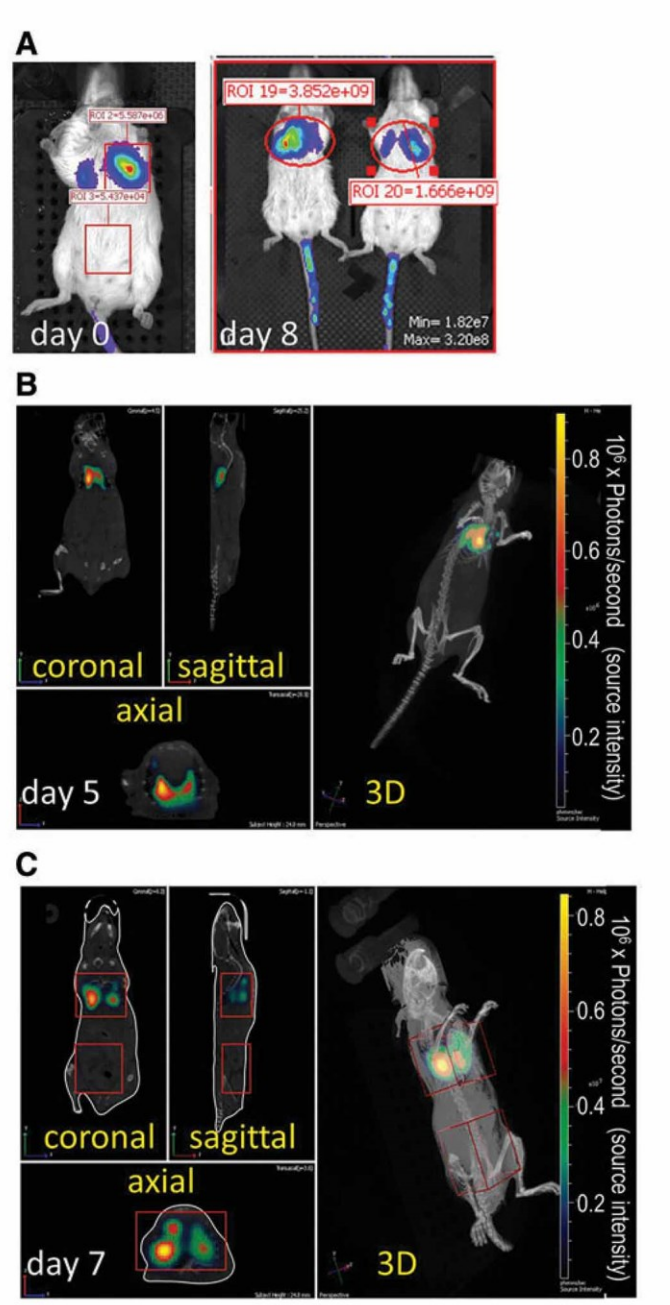

Supplementary Figure S2. BLI and DLIT measurements in the 4T1-Luc tumor model. Female Balb/c mice were injected with 1×10^5 4T1-Luc cells and imaged either immediately after injection, day 0 **(A),** after 5 days **(B)**, after 7 days **(C)**, or after 8 days **(A**, *right*) thereafter. Imaging was carried out after injection of Na-luciferin at a dose of 60 mg/kg intraperitoneally. **(A)** Color-coded BLI image overlaid in a reflected light picture (B/W). ROIs shown BLI signal in photons/s/ROI. **(B** and **C)** Color-coded DLIT signal overlaid on CT image (B/W). Coronal, sagittal, and axial section and maximum intensity projection 3D reconstructed model (3D) is shown.

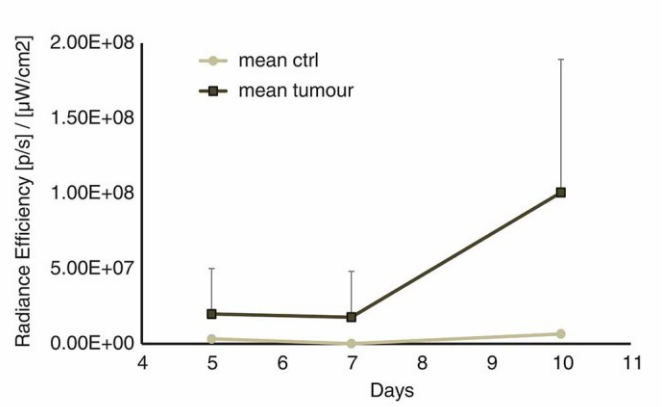

Supplementary Figure S3. Quantification of signal intensity at different time points of tumor growth in 4T1-iRFP720 tumor model. Balb/c mice received 10^5 4T1-iRFP720 cells i.v. and were imaged by epifluorescence imaging at different time points after cell implantation (days 5, 7, and 10; $n=3$).

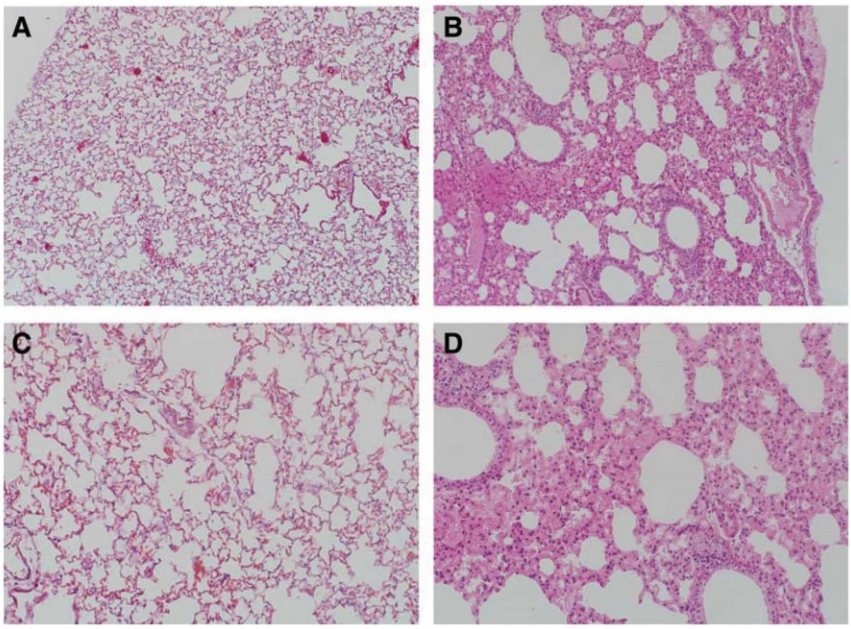

Supplementary Figure S4. Establishment of instillation fixation. Female Balb/c mice were sacrificed by an overdose of anesthesia, and either intubated and intratracheally fixed by in instillation of formalin **(A** and **C)** or immediately excised and fixed afterwards **(B** and **D)**. Magnification used: **(A** and **B)** 10×; **(C** and **D)** 20×.

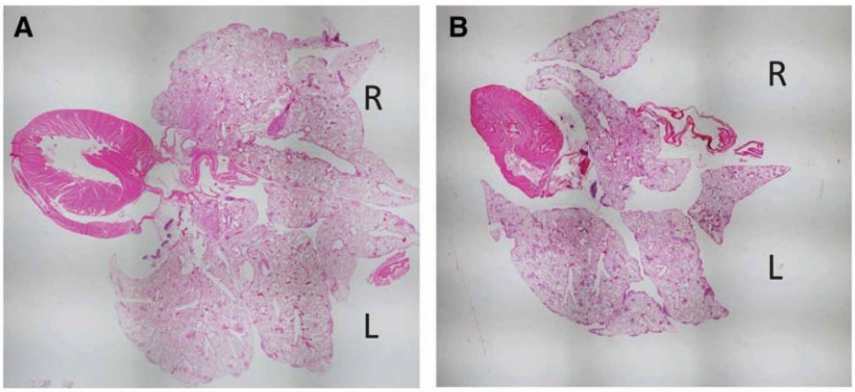

Supplementary Figure S5. Histology of whole lungs from transfected 4T1-iRFP720 tumor mice after intratracheal instillation corresponding to Fig. 5. Whole-section images after H&E staining are shown. **(A)** Histology for animal shown in Fig. 5A, D, and G. **(B)** histology for animal shown in Fig. 5B, E, and H. Figures were taken at 2×magnification and were stitched together using CellSens software (Olympus) to get the whole section from both lungs. R and L refer to right and left lung.

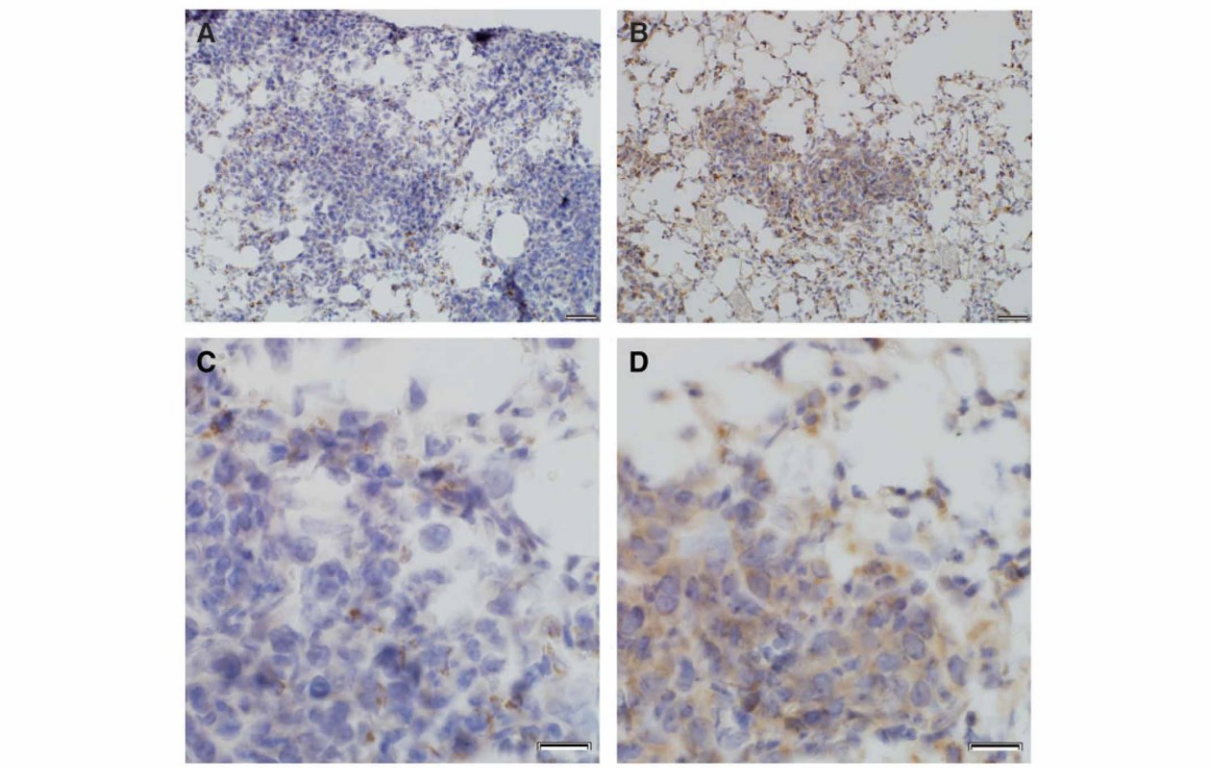

Supplementary Figure S6. Luciferase immunohistochemistry of tumor-bearing lung tissue. Luciferase immunohistochemistry of tumor-bearing lung tissue from untransfected tumor mice **(A** and **C)** and transfected tumor mice after polyplex instillation **(B** and **D)**. 4T1-iRFP720 tumor-bearing animals were transfected with LPEI polyplexes, as in Fig. 5. After BLI imaging, lungs were fixed by instillation fixation, processed and sectioned, and histological sections (3 μm) stained with polyclonal goat-anti luciferase antibody, followed by biotinylated rabbit-anti-goat antibody and stained with the Vectastain ABC kit followed by incubation in DAB, as described in the Materials and Methods (*brown staining*). Sections were counterstained with hematoxylin (*blue stain*). Scale bar in **(A** and **B)** 100 μm; in **(C** and **D)** 20 μm.

2.3. Peptide-targeted polyplexes for aerosol mediated gene delivery to CD49f overexpressing tumor lesions in lung

universität wien

Fakultät für Lebenswissenschaften

Univ.Prof. Dr. Manfred Ogris
Department für Pharmazeutische Chemie
Althanstraße 14
A-1090 Wien
m.ogris@univie.ac.at
T +43 (1) 4277-55551
F +43 (1) 4277-95 51

http://klinischepharmazie.univie.ac.at/mmctresearch/

To
Prof John Rossi
Editor Molecular Therapy - Nucleic Acids

Vienna, 25.05.2019

Dear Prof Rossi,

We would like to submit our manuscript entitled **‚Peptide-targeted polyplexes for aerosol mediated gene delivery to CD49f overexpressing tumor lesions in lung'** authored by Alexander Taschauer, Wolfram Polzer, Fatih Alioglu, Magdalena Billerhart, Simon Decker, Theresa Kittelmann, Emanuela Geppl, Salma Elmenofi, Martin Zehl, Ernst Urban, Haider Sami and Manfred Ogris, as a **research article**. Corresponding authorship should be shared between Manfred Ogris and Haider Sami.

In this work, we present the development and *in vivo* application of a peptide targeted gene delivery system for enhanced delivery of plasmid DNA to CD49f-overexpressing tumors. Using a short synthetic peptide (CYESIKVAVS), we could demonstrate improved cellular binding, uptake and reporter gene expression on CD49f (Integrin α6) overexpressing tumor cells. Prior to *in vivo* application, the stability of gene delivery particles was thoroughly characterized by nanoparticle tracking analysis (NTA) to study their behaviour after aerosolization. We also characterised a syngeneic, disseminated murine triple negative breast cancer model (4T1 in Balb/c) both by means of magnetic resonance imaging (MRI) and histopathological methods (morphology and immunohistochemistry). We could demonstrate significantly enhanced uptake and reporter gene expression of plasmid DNA when using CD49f targeted polyplexes *in vitro*. *In vivo*, intratracheally applied polyplexes were well tolerated, and when using CD49f targeted polyplexes, a significant transgene expression in tumor areas could be observed. In our view, this work covers several disciplines ranging from polymer chemistry, targeted nanoparticles, nucleic acid therapy, to *in vivo* studies for pulmonary delivery into tumor lesions by employing molecular and morphological

imaging. Therefore, we think that this manuscript fits into the scope of The Journal Molecular Therapy - Nucleic Acids.

Supporting information has been uploaded and contains additional experimental results supporting the content of the main manuscript. We would like to suggest the following potential reviewers:

Name	e-mail	Expertise
Olivia Merkel	olivia.merkel@lmu.de	Pulmonary delivery of nanosystems
Antoine Kichler	kichler@unistra.fr	Nanoparticle and polymer based nucleic acid delivery
Niek Sanders	Niek.Sanders@UGent.be	In vivo delivery of and therapy with DNA and RNA
Claus-Michael Lehr	lehr@mx.uni-saarland.de	Lung delivery of nanomedicines
S. Moein Moghimi	seyed.moghimi@newcastle.ac.uk	Nanomedicines and toxicological considerations

We confirm that the manuscript is being solely submitted to this journal and is not under consideration elsewhere. We also confirm that the manuscript has been approved and reviewed by all included authors.

We are looking forward for your favourable consideration!

Yours sincerely

Manfred Ogris

Professor for Pharmaceutical Sciences
Department of Pharmaceutical Chemistry
University of Vienna
Althanstraße 14
A-1090 Vienna, Austria
m.ogris@univie.ac.at

Haider Sami

Groupleader Nanobiomaterials
Department of Pharmaceutical Chemistry
University of Vienna
Althanstraße 14
A-1090 Vienna, Austria
haider.sami@univie.ac.at

Peptide-targeted polyplexes for aerosol mediated gene delivery to CD49f overexpressing tumor lesions in lung

Alexander Taschauer[1], Wolfram Polzer[1], Fatih Alioglu[1], Magdalena Billerhart[1], Simon Decker[1], Theresa Kittelmann[1], Emanuela Geppl[1], Salma Elmenofi[1], Martin Zehl[2], Ernst Urban[3], Haider Sami[1*], Manfred Ogris[1*]

[1] Laboratory of MacroMolecular Cancer Therapeutics (MMCT), Center of Pharmaceutical Sciences, Department of Pharmaceutical Chemistry, University of Vienna, Althanstrasse 14, A-1090 Vienna, Austria.

[2] Faculty of Chemistry, Department of Analytical Chemistry, University of Vienna, Währingerstrasse 38, 1090 Vienna, Austria.

[3] Department of Pharmaceutical Chemistry, Faculty of Life Sciences, University of Vienna, Althanstraße 14, 1090, Vienna, Austria.

[*]Corresponding authors

Email: m.ogris@univie.ac.at; haider.sami@univie.ac.at

Short title: CD49f targeted gene delivery to lung tumors

Abstract

Peptide ligands can enhance delivery of nucleic acid loaded nanoparticles to tumors by promoting their cell binding and internalization. Lung tumor lesions accessible from the alveolar side can be transfected, in principle, using gene vectors delivered as an aerosol. The cell surface marker CD49f (Integrin α6) is frequently upregulated in metastasizing, highly aggressive tumors. In this study, we utilize a CD49f binding peptide coupled to linear polyethylenimine (LPEI) promoting gene delivery into CD49f overexpressing tumor cells *in vitro* and into lung lesions *in vivo*.

We have synthesized a molecular conjugate based on LPEI covalently attached to the CD49f binding peptide CYESIKVAVS via a polyethylene glycol (PEG) spacer. Particles formed with plasmid DNA were small (<200 nm) and could be aerosolized without causing major aggregation or particle loss. *In vitro*, CD49f-targeting significantly improved plasmid uptake and reporter gene expression on both human and murine tumor cell lines. For evaluation *in vivo*, localization and morphology of 4T1 murine triple negative breast cancer tumor lesions in the lung of syngeneic Balb/c mice were identified by magnetic resonance imaging (MRI). Polyplexes applied via intratracheal aerosolization were well tolerated and resulted in measurable transgene activity of the reporter gene firefly luciferase in tumor areas by bioluminescence imaging. Transfectability of tumors correlated with their accessibility for the aerosol. With CD49f targeted polyplexes, luciferase activity was considerably increased and was restricted to the tumor area.

Keywords: Linear polyethylenimine, polyplexes, CD49f targeting, pulmonary delivery, lung tumor transfection

Introduction

Receptor mediated delivery of nucleic acids to tumor cells is an important issue in the development of viral and synthetic gene delivery systems. Besides increased accumulation in tumors when delivered systemically, their improved internalization into target cells via transfection-permissive uptake routes allows to significantly increase transfection rates and transgene expression. We and others have developed targeted delivery systems based on polycations for nucleic acid condensation, polyethylene glycol (PEG) for shielding purposes and peptidic ligands for receptor targeting.[1-4] Although the affinity of a rather small peptide can be considerably lower when compared to the whole protein, the high number of targeting peptides per transfection particle induce a cooperative binding mode.[5] When compared to their protein counterparts, such peptide ligands are advantageous by several means, i.e. being fully synthetic, less immunogenic and preferred for the nucleic acid condensation process due to their lower molecular weight.[1] Most of the potentially targetable antigens on tumor cells are not unique *de novo* antigens, but rather overexpressed compared to the surrounding, non-malignant tissue.[6] Integrin α6 (ITGA6, CD49f) is a glycosylated transmembrane protein which dimerizes preferentially with integrin β1 and β4 forming laminin binding heterodimers. It is expressed at low to medium levels on a broad range of human tissues, including stomach, intestine and kidney.[7] CD49f is expressed on almost all tissue stem cell populations including cancer stem cells[8] and has recently been described as a key signaling molecule in the maintenance and development of bone mesenchymal stem cells.[9] It is also associated with (PI3K)/Akt signaling and responsible to maintain stemness properties in other stem cells by interaction with OCT4 and SOX2.[10] Both, benign and malignant cells derived from the prostate capable of spheroid formation show a high CD49f expression, whereas other stem cell markers like CD133 seem to be less important.[11] In numerous studies it was demonstrated that CD49f overexpressing tumor cells show tumor initiating and metastasis forming potential in numerous solid cancers, including hemangioma[12], gastric cancer[13] and breast cancer[14]. In breast cancer patients, CD49f positive tumors have a dismal clinical prognosis.[15] Also in murine tumors, CD49f-high cells show tumor initiating properties[16] and formation of metastasis.[17] The murine triple negative breast cancer cell line 4T1 is a highly metastatic and aggressive cancer growing syngeneic in Balb/c mice forming lung metastasis accessible from the alveolar side.[18, 19] Stable knockdown of CD49f in 4T1 reduced proliferation and migration *in vitro*.[17] Hence, CD49f represents a valuable target for cancer therapeutics including nucleic acid based drugs (NABD). The small laminin peptide sequence IKVAV derived from the A-chain of laminin has been initially identified by Tashiro et al. for being responsible for cell interaction.[20] The sequence (expanded to SIKVAV) was later on

identified to bind to α3, α6, and β1 integrins.[21] The group of Len Seymour was the first to utilize this peptide as YESIKVAVS for targeting of an adenoviral vector to α6β1 overexpressing tumor cell both *in vitro* and *in vivo*.[22]

In this study, we show the transfection promoting properties of CD49f peptide targeted polymeric gene vectors both *in vitro* and in a syngeneic lung metastasis model in mice through intratracheal aerosolization of polyplex formulations.

Results:

Synthesis of LPEI-PEG-Peptide conjugate

LPEI was synthesized by acidic hydrolysis of poly(2-ethyl-2-oxazoline) with HCl (6 M). Complete cleavage of the side chains of poly(2-ethyl-2-oxazoline) was checked by ^{1}H-NMR where no remaining signals derived from the side chain of the polymer were found. GPC analysis of LPEI revealed a weight average molecular weight of 10 kDa and a polydispersity (Mw/Mn) of 1.55.

The peptide CYESIKVAVS was generated with a N-terminal L-cysteine by microwave assisted solid phase synthesis based on Fmoc strategy. A ChemMatrix® resin functionalized with a Rink amide linker was used to generate a C-terminal carboxamide functionality. The crude product was purified by reversed-phase HPLC with a linear gradient from 5-50 % acetonitrile resulting in a product purity of >95 %. High resolution mass spectrometry (HRMS) of the intact peptide as well as extensive series of CID-generated single and double charged y- and b-fragment ions confirmed both purity and the desired sequence CYESIKVAVS.

Conjugate synthesis and analysis was done in principle as described previously.[1, 23] In brief, CYESIKVAVS was coupled to LPEI via a heterobifunctional polyethylene glycol (Mw 2 kDa) linker with α-OPSS (3-(2-pyridyldithio)propionamide) and ω-NHS (N-hydroxysuccinimide) functionality. ^{1}H-NMR of the intermediate compound, LPEI-PEG-OPSS, revealed a LPEI to PEG ratio of 1:1.2. A solution of LPEI-PEG-OPSS in water with a concentration of 2 mg/mL showed an OPSS concentration of 84.65 nmol/mL. A three-fold molar amount of peptide was used for generating LPEI-PEG-CYESIKVAVS. Due to the weak absorption of CYESIKVAVS at 280 nm, no direct peptide quantification could be conducted in the conjugate. Nevertheless, near quantitative reaction of the free thiol group in CYESIKVAVS with α-OPSS was observed when measuring the increase in absorption at 343 nm generated by 2-thiopyridone released during the coupling reaction (ε = 8080 M^{-1}). Therefore, it was assumed that 1.2 mol PEG per LPEI molecule calculated by ^{1}H-NMR (described above) carry 1.2 mol peptide. The synthesized conjugate is later termed as LPEI-PEG-CD49f. For non-targeted formulation LPEI-PEG-cysteine (LPEI-PEG) conjugate was employed.

Nanoparticle tracking analysis (NTA)

Polyplex nanoparticles were prepared by complexing plasmid DNA with LPEI-PEG-CD49f or LPEI-PEG-cysteine at N/P 9 to form peptide-targeted or non-targeted formulations, respectively. Only LPEI based polyplexes served as control for PEGylated formulation. Nanoparticles were analyzed by NTA to determine the influence of PEGylation on size and ζ-potential of polyplexes and potential aggregation effects induced by microspraying (Figure 1).

Figure 1

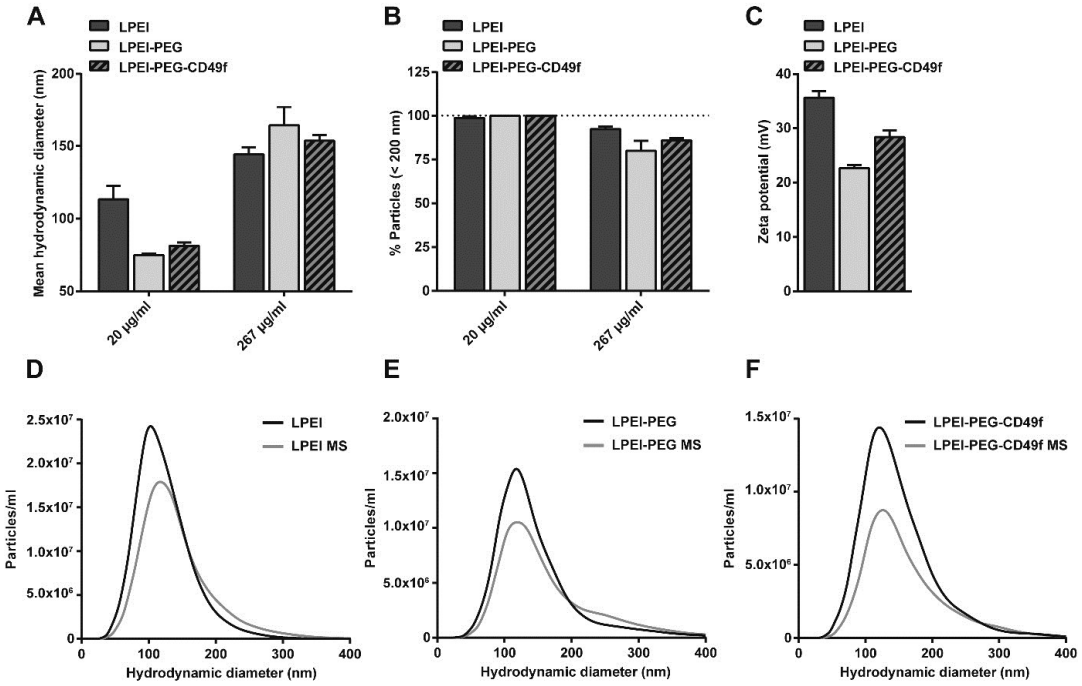

Figure 1: Size and ζ-potential of polyplexes evaluated by NTA. *(A) Hydrodynamic diameter and (B) changes in the percentage of particles below 200 nm of polyplexes prepared at pDNA concentrations of 20 µg/mL or 267 µg/mL at N/P 9 in HBG. (C) ζ-Potential of polyplexes generated with 267 µg/mL pDNA at N/P 9. (n=3 + stddev) (D-F) Representative particle size distribution of polyplexes based on LPEI (D), LPEI-PEG (E) and LPEI-PEG-CD49f (F) at pDNA concentration 267 µg/mL, N/P 9 before and after aerosolization by microspraying (MS).*

At 20 µg/mL, mean particle size of polyplexes based on both PEGylated formulations (LPEI-PEG; LPEI-PEG-CD49f) was approx. 30 % below the average size of LPEI polyplexes (Figure 1 A) (LPEI: 113 +/- 8 nm, LPEI-PEG: 75 +/- 1 nm, LPEI-PEG-CD49f: 81 +/- 2 nm. At 267 µg/mL, an increase of particle size of 6-14 % with PEGylated conjugates could be observed in comparison to LPEI polyplexes (LPEI: 144 +/- 4 nm, LPEI-PEG: 160 +/- 10nm, LPEI-PEG-CD49f: 154 +/- 3 nm). When generating polyplexes at 267 µg/mL, the fraction of particles below 200 nm in size was reduced by approx. 20 % when compared to their respective counterparts generated at 20 µg/mL pDNA (Figure 1 B).

LPEI based polyplexes had a ζ-potential of 35.6 nm +/- 1.01 mV, whereas with LPEI-PEG and LPEI-PEG-CD49f polyplexes this value was reduced (22.6 +/- 0.50 mV for LPEI-PEG, 28.4 +/- 0.98 mV for LPEI-PEG-CD49f) (Figure 1 C).

The influence of microspraying on particle size and aggregation effects was analyzed for polyplexes generated at 267 µg/mL (Figure 1 D-F and Supp. Figure 1). For all three formulations

(LPEI, LPEI-PEG, LPEI-PEG-CD49f), a slight reduction of nanoparticle concentration after microspraying for sizes up to 400 nm occurred (Figure 1 D-F). LPEI based polyplexes showed only a minor increase of mean particle size from 131 +/- 1 nm to 143 +/- 3 nm after microspraying procedure (Supp. Figure 1 A). In case of LPEI-PEG a change of particle size from 154 +/- 1 nm to 169 +/- 4 nm and LPEI-PEG-CD49f from 148 +/- 5 nm to 163 +/- 5 nm could be observed. Overall, a reduction of the percentage of particles below a size of 200 nm of 4 % for LPEI, 10 % for LPEI-PEG and 8 % for LPEI-PEG-CD49f could be detected (Supp. Figure 1 B).

Cellular binding and uptake of targeted polyplexes on CD49f expressing cells

Cell binding and internalization of fluorescently labelled polyplexes was evaluated on CD49f-overexpressing cells *in vitro* by flow cytometry and confocal laser scanning microscopy. First, CD49f expression was verified on human (MDA-MB-231) and murine (CT26 and 4T1-iRFP720) cancer cell lines by flow cytometry (Figure 2). For all three cell lines a shift of 1-2 log units could be observed indicating high CD49f expression for MDA-MB-231 (2 A) and medium for CT26 (2 B) and 4T1-iRFP720 (2 C). Geometric mean values of anti-CD49f stained cells were 43.3 for MDA-MB-231, 10.8 and 11.7 for CT26 and 4T1-iRFP720, respectively (2 D).

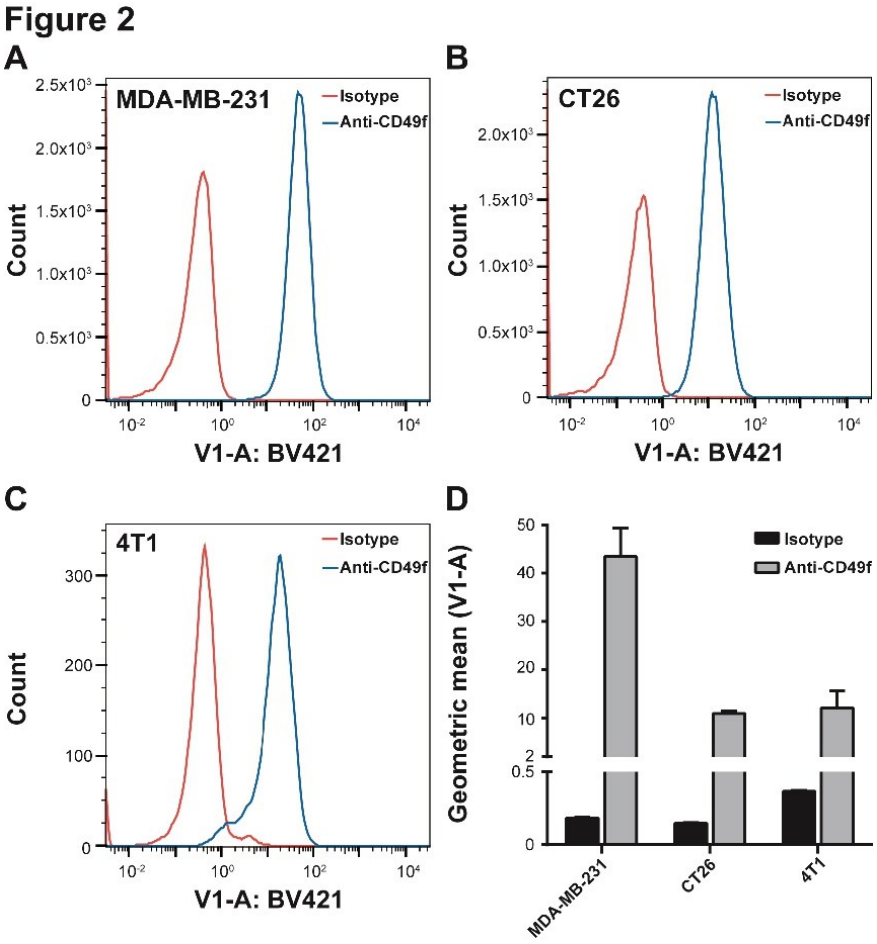

Figure 2: Evaluation of CD49f expression by flow cytometry. *MDA-MB-231, CT26 and 4T1-iRFP720 cells were harvested, stained with BV421-labelled rat anti-human CD49f antibody or rat IgG2a κ isotype control and gated cells were analyzed. A-C: representative histograms of MDA-MB-231 (A), CT26 (B) and 4T1-iRFP720 (C); (D) Geometric mean values for BV421 signal (n=3 + stddev).*

Analysis of cell binding and uptake was conducted on MDA-MB-231 cells utilizing polyplexes with Cy5-labelled plasmid pCMV-Gluc. Analysis by flow cytometry (Figure 3) revealed that total cellular association of LPEI-PEG polyplexes was clearly lower when compared to LPEI polyplexes at 1 µg/mL (for 30 min and 4 h incubation, Figure 3 A and 3 B) and 2 µg/mL (for 30 min incubation, Figure 3 C). In contrast, LPEI-PEG-CD49f polyplexes exhibited increased cell binding when compared with LPEI-PEG at all conditions evaluated. Although, at 4 h incubation with 2 µg/mL, there was no gross difference observed between all three polyplex types (Figure 3 D).

Figure 3

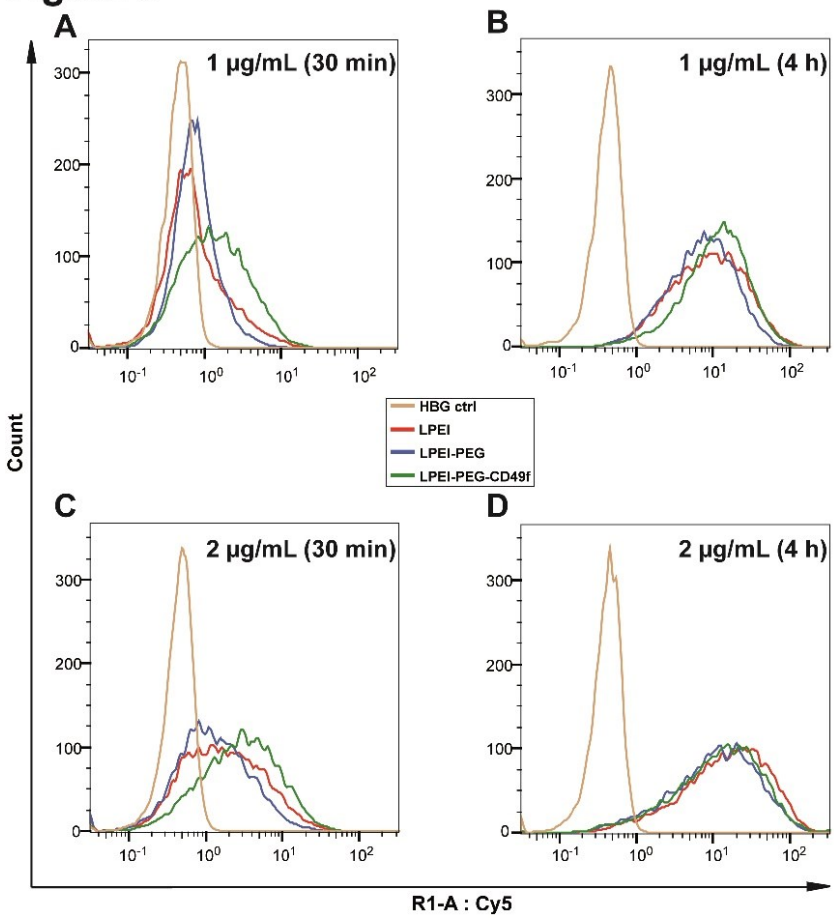

Figure 3: Cell association of polyplexes. *MDA-MB-231 cells were incubated with polyplexes prepared at 20 µg/mL and N/P 9 with Cy5-labelled pDNA diluted in basal medium at a final concentration of 1 µg/mL (A,B) or 2 µg/mL (C,D) for 30 min (A,C) or 4 h (B,D). After incubation, cells were harvested and analyzed by flow cytometry. Data is depicted as representative histograms showing the Cy5 derived fluorescence signal of live cells in the R1 channel (Cy5 fluorescence).*

When analyzing the geometric mean values, LPEI-PEG-CD49f polyplexes exhibited always higher values compared to LPEI-PEG, irrespective of polyplex concentration or incubation time. (Supp. Figure 2).

In order to unambiguously demonstrate intracellular localization of polyplexes, CLSM studies were conducted after 4 h of incubation at 2 µg/mL (Figure 4). Co-staining of actin filaments with AlexaFluor® 488-phalloidin enabled localization of particles both on the cellular surface and intracellularly, when visualizing the middle sections of cells.

Whereas LPEI particles were internalized to a considerable extent (Figure 4 A), there were far less internalized LPEI-PEG based particles observed (Figure 4 B). Employing LPEI-PEG-CD49f

conjugate for polyplex generation resulted in an enhanced cellular uptake of particles (Figure 4 C).

Figure 4

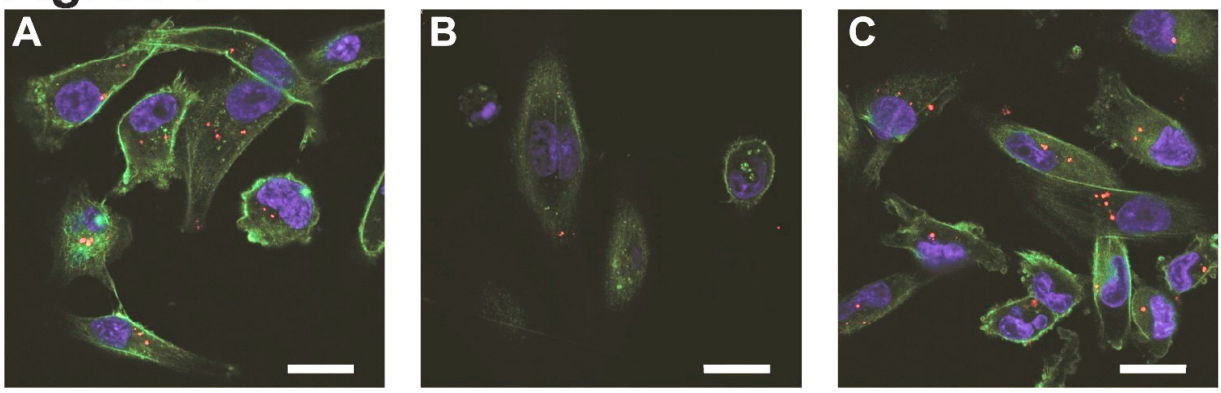

Figure 4: Cellular internalization of polyplexes studied by CLSM. *MDA-MB-231 cells were incubated in basal cell culture medium with Cy5-labelled polyplexes (red) prepared at N/P 9 at a pDNA concentration of 2 µg/mL for 4 h. Thereafter cells were fixed, stained with AlexaFluor® 488-phalloidin (green) and DAPI (blue). (A) LPEI, (B) LPEI-PEG and (C) LPEI-PEG-CD49f polyplexes. CLSM imaging was conducted with a 63X oil objective; representative middle sections of the cells are shown. Scale bars: 20 µm.*

Targeted gene delivery and biocompatibility profile

For evaluating *in vitro* transfection efficiency, polyplexes were generated with plasmid pCMV-Gluc. As Gaussia luciferase is secreted by the cells, we quantified its activity in the cellular supernatant by a bioluminescence assay using coelenterazine as substrate. In case of MDA-MB-231 and CT26 cells, remaining cells were harvested and cell numbers determined by flow cytometry. Total count of live cells was used for normalization of bioluminescence signal. In case of 4T1-iRFP720 cells, Gaussia activity was also measured in the supernatant, but its activity was normalized on protein content per well quantified by bicinchoninic acid assay. MDA-MB-231 and 4T1-iRFP720 cells were transfected with polyplexes generated at N/P 9 at pDNA concentrations of 0.5 µg/mL, 1 µg/mL, 2 µg/mL and 4 µg/mL (Figure 5 A and B).

Figure 5

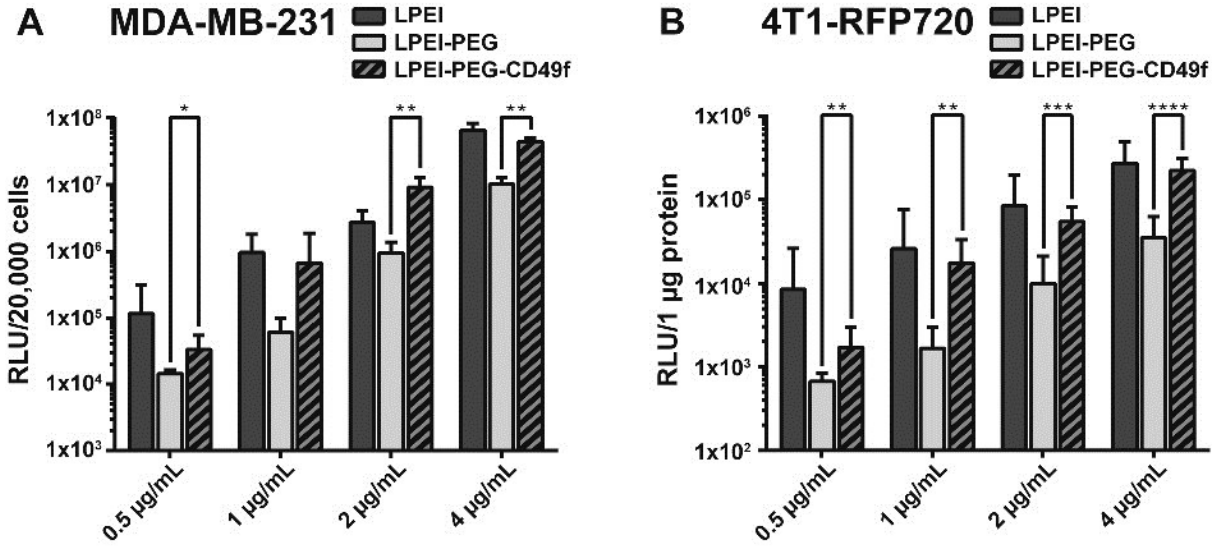

Figure 5: Transfection efficiency of polyplexes on MDA-MB-231 and 4T1-iRFP720 breast cancer cells. *MDA-MB-231 (A) and 4T1-iRFP720 cells (B) were seeded in 96-well plates and transfected with pCMV-Gluc polyplexes at indicated pDNA concentrations. Transfections were conducted in basal cell culture medium for 4 h followed by exchanging the supernatant with FCS supplemented medium. Gaussia luciferase was quantified in the supernatant 24 h after transfection and RLU values normalized on total count of live cells (MDA-MB-231) or on protein content (4T1-iRFP720); mean values from two independent experiments with n=3/experiment + stddev; *p≤0.05, ** p≤0.01, *** p≤0.001, **** p≤0.0001 (Mann-Whitney)).*

In case of LPEI-PEG-CD49f, this corresponds to a peptide concentration of 70.4 nM, 140.7 nM, 281.5 nM and 562.9 nM respectively. Transfection studies with CT26 were conducted with 2 µg/mL (Supp. Figure 3). For all three cell lines, Gaussia reporter gene activity obtained with LPEI-PEG polyplexes was at least 10-fold lower when compared with plain LPEI polyplexes. Also, at all concentrations evaluated and with all three cell types, except 1 µg/mL with MDA-MB-231 cells, a significant increase of transfection efficiency when using LPEI-PEG-CD49f conjugate could be observed compared to LPEI-PEG. Cell viability was evaluated on MDA-MB-231 with flow cytometry quantifying viable cells per well with buffer treated ones set to 100 % along with transfection efficiency (Supp. Figure 4). At all polyplex concentrations used, LPEI polyplex treatment resulted in the most prominent reduction of viable cells (53 % to 72 % compared to buffer control). Both, LPEI-PEG-CD49f and LPEI-PEG polyplex treatment exhibited a significantly higher cell viability.

Tumor model

The tumor model was established by intravenous injection of 4T1-iRFP720 cells as recently described[19] and tumor growth was monitored by T2 weighted MRI imaging (Figure 6). On all T2-weighted MR-images, tumor tissue could be visualized as hyperintense structure. A clear differentiation between tumor tissue and blood vessels could be made based on the comparison with untreated control animals (Figure 6 A and 6 B).

Figure 6

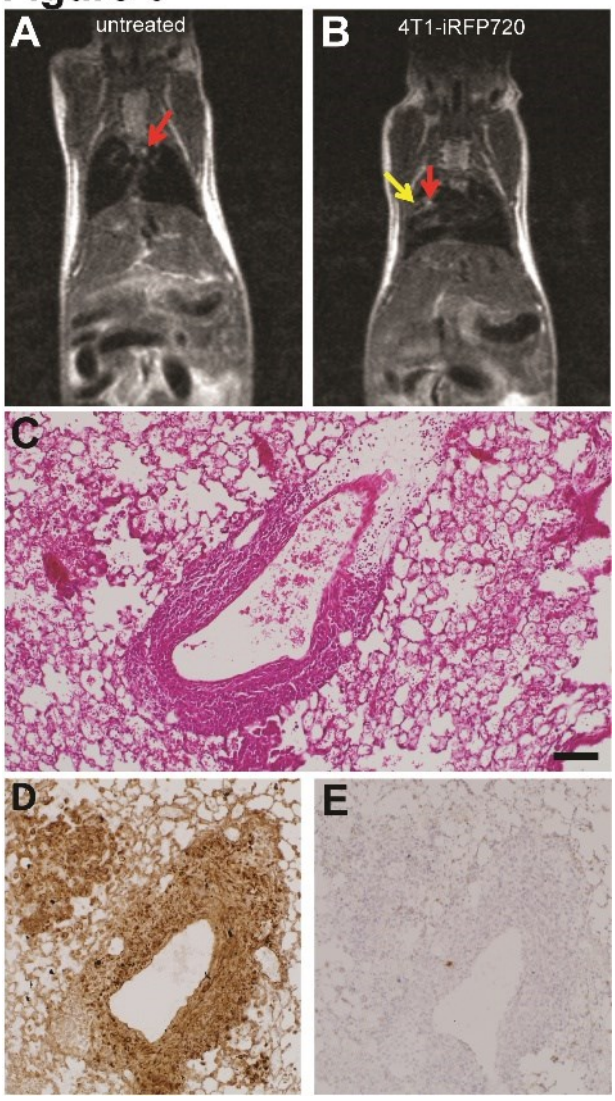

Figure 6: Morphological and histological evaluations of 4T1-iRFP720 tumor model. *A-B: Representative T2 weighted MRI images of tumor-free (A) and 4T1-iRFP720 tumor bearing Balb/c mice (B; day 10 post tumor cell injection); red arrows: blood vessels, yellow arrow: tumor tissue. C-E: Histopathology of an instillation fixed lung bearing 4T1-iRFP720 tumors: (C) HE staining, (D) IHC staining for CD49f (brown) and (E) isotype control antibody. Scale bar (common for C-E): 100 µm*

Whereas larger blood vessels in the lung appeared as hyperintense structures, lung parenchyma of tumor free animal exhibited an overall homogenously hypointense area. At 11 days post tumor cell implantation, tumor nodules appeared as hyperintense areas at various regions in the lung (Figure 6 B). Lung histopathology confirmed the findings by Geyer et al.[19] revealing both peribronchiolar and parenchymal tumor tissue with invasive growth pattern and accessibility from the alveolar side (Figure 6 C and D). Immunohistochemistry could proof CD49f overexpression of 4T1-iRFP720 tumors (Figure 6 D and E), but also a lower expression level in healthy lung tissue.

Figure 7

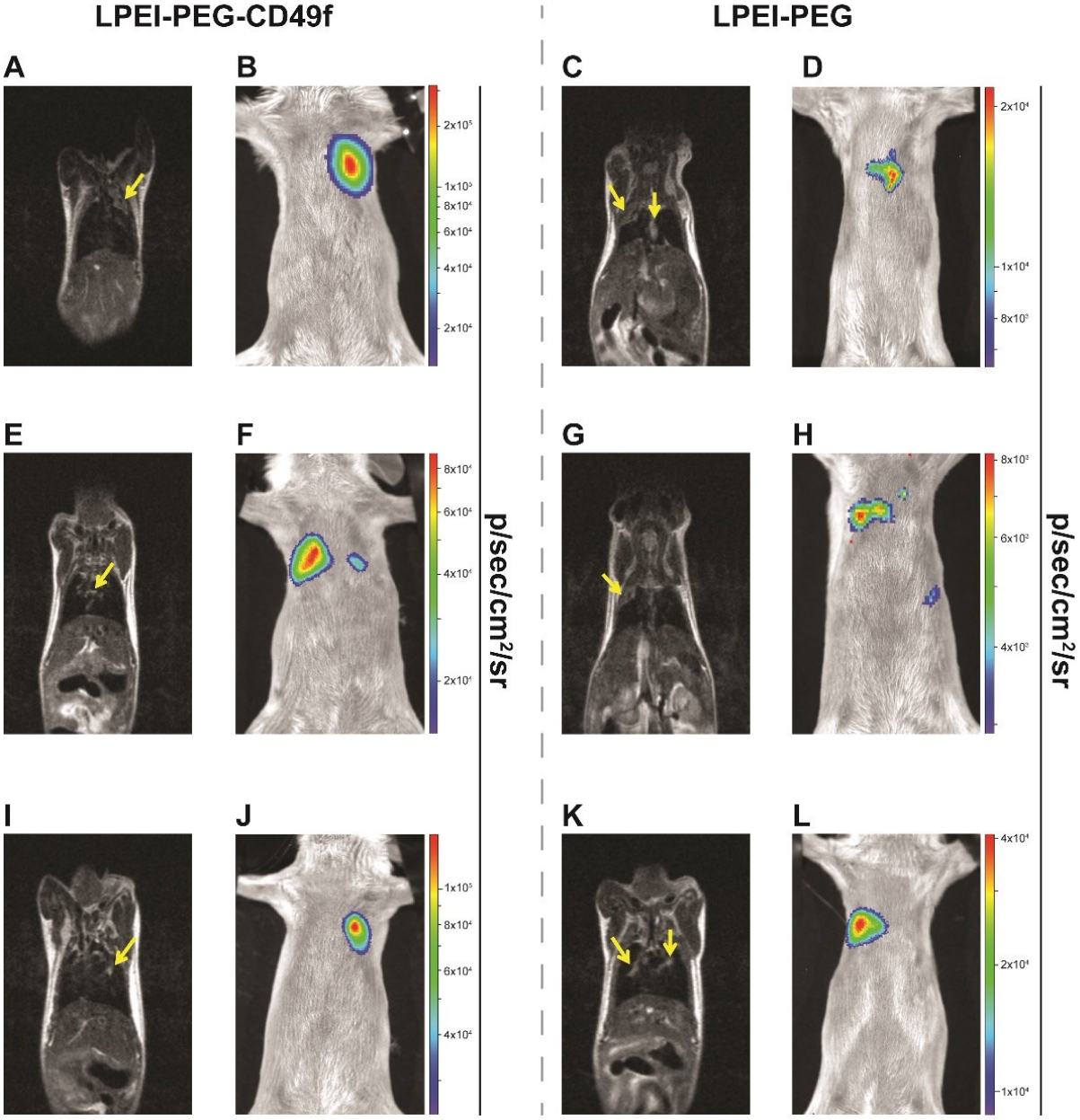

Figure 7: Intratracheal transfection of 4T1-iRFP720 tumor bearing lungs. *4T1-iRFP720 tumor bearing Balb/c mice were treated with polyplexes based on pCpG-hCMV-EF1α-LucSH and LPEI-PEG-CD49f or LPEI-PEG at N/P 9 and a concentration of 267 µg/ml. In total 20 µg of formulated pDNA was administered by i.t. aerosolization. 24 h post treatment firefly luciferase expression was analyzed by in vivo BLI imaging. T2 weighted MRI was conducted one or two days before treatment for evaluating the status of tumor growth. Both BLI and MRI were done in supine positioning of the animal. Three representative animals treated with LPEI-PEG-CD49f (animal 1: MRI (A)/BLI (B); animal 2 MRI (E)/BLI (F); animal 3 MRI (I)/BLI (J)) and LPEI-PEG (animal 1: MRI (C)/BLI (D); animal 2 MRI (G)/BLI (H); animal 3 MRI (K)/BLI (L)) polyplexes are depicted. Tumor growth is marked with yellow arrows in the MRI images. BLI signals (color coded) are overlaid on a reflected light picture.*

Aerosol mediated gene delivery to lung tumor lesions

Before transfection, tumor localization was analyzed by T2 weighted MRI (Figure 7 A, C, E, G, I, K). Both, the formation of a rather large homogenously structured, well margined tumor tissue (Figure 7 A, C and G) as well as diffuse small heterogeneous lesions (Figure 7 E, I and K) could be found. Such diffuse lesions were sometimes located along the tracheal bifurcation with infiltration into the bronchial airways (Figure 7 E and K). Animals were treated by microspray-based aerosolization of polyplexes on day 11 after tumor cell implantation. Twenty-four hours post transfection, luciferase activity was evaluated by 2D bioluminescence imaging (Figure 7 B, D, F, H, J, L). With both treatments, either LPEI-PEG-CD49f polyplexes (Figure 7 B, F and J) or LPEI-PEG polyplexes (Figure 7 D, H and L), distinct BLI signals could be detected in the lung area. When placing BLI images and MRI images of the same animal side by side, there was high degree of correlation between the tumor localization depicted by MRI and the site of the BLI signal. In animals with higher tumor load and reduced accessibility of lung tissue, application of sufficient volumes of aerosol was not possible and hence no reporter gene expression was detected after treatment. In the representative example shown (Supp. Figure 5 A and B), the left lung showed a homogeneous growth of tumor lesions, hence reducing accessibility of tumor tissue through the airways. The BLI signal in successfully treated animals was quantified by analyzing the BLI images (Figure 8). Here, BLI signals of animals treated with LPEI-PEG-CD49f polyplexes were significantly higher than background signal, which was not the case with the LPEI-PEG based formulation (Figure 8).

Figure 8

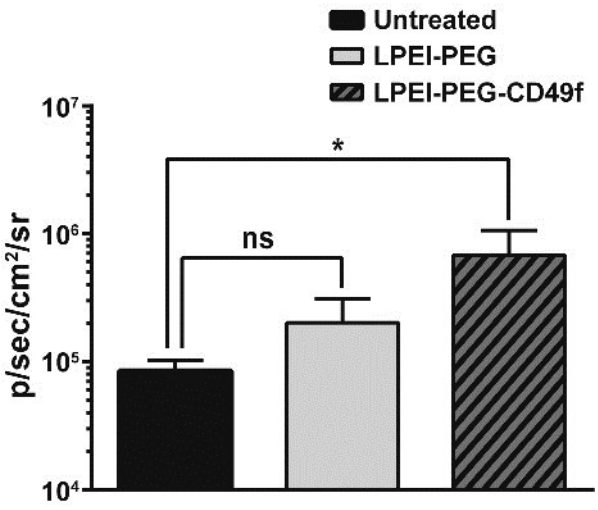

Figure 8: Quantification of BLI signal after intratracheal polyplex treatment. *4T1-iRFP720 tumor bearing Balb/c mice were treated with indicated polyplexes as described in Fig 7, the BLI signal was quantified in*

*the thoracic area 24h thereafter and compared to untreated animals; n=4 + stddev; *p≤0.05 (Mann-Whitney).*

Discussion

The peptide sequence SIKVAV (IKVAV) has initially been identified as the functional domain within the α-chain of laminin, which is responsible for cellular interaction.[20] Later on, α3, α6, and β1 integrins were identified as binding partners on the cell surface.[21] Upon binding, the peptide can activate PI3K/Akt downstream signaling, ERK1/2 and MMP expression[24], albeit at high concentrations of 0.1 mM and above.[21, 25] To achieve high local concentrations, it is included in polymeric carriers or nanogels and applied locally, for example in wound healing approaches.[26] Our approach here was to use the peptide as a targeting moiety covalently coupled to the nucleic acid carrier LPEI, but at low, non-activating concentrations (<0.6 µM). For this, we have generated a molecular conjugate with equimolar ratios of peptide, a heterobifunctional, 2 kDa PEG linker, which also serves as shielding agent[1, 27], and a 10 kDa LPEI for DNA binding and condensation. Already in our previous work we could demonstrate that coupling of the amine reactive NHS group in NHS-PEG-OPSS to secondary amines within the LPEI chain is efficient and controllable when carried out in water-free conditions either in DMSO or absolute EtOH resulting in a coupling efficiency of approx. 60 %.[27] The extended peptide sequence CYESIKVAVS was then coupled in a HEPES buffered aqueous solution at pH 7.4 to the proximal OPSS group. Whereas the N-terminal cysteine was added to enable thiol coupling, the other residues improve water solubility of the peptide.[28]

A thorough biophysical characterization was conducted to study effects of PEG linker, targeting peptide, higher particle concentrations for *in vivo* application and the shear stress during the nebulization procedure. For stability reasons, all polyplex formulations were prepared with positive charge excess at N/P 9. This ratio prevents aggregation during polyplex formation also at higher concentrations and is still well tolerated *in vivo.*[19, 29] The 2 kDa PEG linker is significantly reducing the ζ-potential, and in our previous studies we could demonstrate that such pDNA polyplexes are stable enough in the blood stream to transfect tumor tissue after systemic administration.[4, 30] No differences were observed in terms of average particle size or aggregation between polyplexes +/- PEG after microspraying indicating that the elevated N/P ratio is already ensuring enough stability.[31]

We could confirm the already observed high level of CD49f in human MDA-MB-231 and murine 4T1 triple negative breast cancer cells[17, 32], but also demonstrated this in the murine colon

carcinoma cell type CT26. The high level of CD49f expression in MDA-MB-231 cells is in line with previous observations, where in this and other highly malignant breast cancer cell lines ITGA6 expression was elevated and mediated radio-resistance via the activation of PI3K/Akt and MEK/Erk signaling pathways.[33]

Binding of polyplexes to the cell surface occurs either via electrostatic interaction, e.g. heparan sulfate proteoglycan binding, or receptor-ligand interaction. PEGylated polyplexes without ligand exhibit an overall lower cell association, at least when incubated for one hour or less.[34] Although total cell association of positively charged (unshielded) polyplexes and targeted ones (but with decreased positive surface charge) can be similar, they can differ in their internalization kinetics. Polyplexes with EGF as ligand are rapidly internalized within minutes, which is triggered after activation of downstream signaling (MAPK, Akt/Erk) followed by membrane ruffling.[1, 2, 34] In contrast, a receptor binding mode, which does not activate downstream signaling, is similarly efficient, but internalization is delayed and occurs via a rather slow, actin driven receptor recycling.[2] When comparing cell association (by flow cytometry) and internalization (by CLSM), CYESIKVAVS-polyplexes showed higher (at earlier timepoints and lower concentration) or similar (at later timepoints and higher concentration) association rates than LPEI polyplexes. Still, internalization was rather slow, as no significant intracellular signal of LPEI-PEG-CD49f polyplexes was seen with CLSM after 30 min of incubation (data not shown), but rather occurred at the 4 h time point. Hence, we do not expect rapid internalization due to pathway activation, like with EGF-EGFR, but rather slow actin driven receptor-ligand recycling. This would be also in line with the peptide concentrations applied: our highest concentration applied (4 µg/mL pDNA) corresponds to a peptide concentration of 0.563 µM (considering an N/P of 9 and a LPEI-PEG-peptide ration of 1:1.2:1.2 in the conjugate). This is still far below the concentration of 100 µM needed for Erk and Akt activation.[25] For evaluation of transfection efficiency *in vitro*, we utilized secreted Gaussia luciferase.[35] At all concentrations and cell lines tested, PEG-polyplexes without ligand reduced reporter activity by 90 % or more, whereas the peptide ligand could fully restore activity or induce an even higher activity when compared to 'naked' LPEI polyplexes. This also points out that the 2 kDa PEG linker does shield particles (as demonstrated by the lower ζ-potential), but does not negatively affect the intracellular transfection process, like endosomal release. Especially in case of excessive PEGylation, this can otherwise lead to an inhibitory effect called 'PEG dilemma'.[36]

For basal like and triple negative breast cancer (TNBC), the lung is the most common site of metastasis, and there are several studies indicating that the presence of cancer stem cells in

TNBC promote this metastasis formation.[37] Within the syngeneic 4T1 model, lung lesions can be induced either by orthotopic cell implantation and subsequent removal of the primary tumor, or by intravenous injection of the cell suspension.[38] As with both methods the genomic profile of lung lesions is similar, intravenous injection appears a useful and less invasive method. Whereas for the intravenous models using a luciferase labelled 4T1 subline, tumors were located parenchymally without the appearance of individual lesions, we observed also parenchymal infiltration, but with a clear nodular structure and also peribronchiolar localization using our own, iRFP720 labelled subline.[31] Immunohistochemical analysis of instillation fixed lungs revealed that both, parenchymal like and peribronchiolar lesions were overexpressing CD49f, and $CD49f^+$ cells appeared accessible from the air side. In line with the histomorphological analysis, the T2 weighted MRI analysis also reflected the situation of both margin-defined tumor lesions and also diffuse parenchymal infiltrations. Similar correlations could be shown in a model of orthotopically implanted 4T1 tumors followed by lung metastasis: here, mainly well-defined tumor lesions were seen both with histomorphology and T2 weighted MRI.[39]

Besides low molecular weight drugs, also macromolecules, including proteins and nucleic acids and nanostructured carriers, can be applied as an aerosol or by instillation to primary and secondary lung tumors.[40] Direct accessibility of the tumor, reduced distribution in non-target tissue and elevated local drug concentrations are major advantages of this method. Branched polyethylenimine was successfully used for aerosol mediated plasmid delivery, also in a therapeutic setting.[41, 42] We have recently used linear polyethylenimine and could observe a low, but tumor restricted expression of luciferase reportergene.[31] Due to the improved transfection *in vitro* and the accessibility of $CD49f^+$ cells, we evaluated both peptide-targeted and PEGylated only polyplexes. Although with PEGylated polyplexes a defined BLI signal could be measured, the signal was low and failed significance when compared to background. A comparably low, but locally restricted BLI signal was observed with similar settings using non-PEGylated LPEI polyplexes.[31] Still, the BLI signal could be correlated with the T2 weighted MRI signal. Such a correlation could also be observed by Adiseshaiah et al., where 4T1-luc cells were implanted orthotopically and the lung lesions imaged by BLI and T2 weighted MRI.[39] When compared to PEG polyplexes, transgene activity induced after application of peptide targeted polyplexes was clearly more pronounced, giving an in average three-fold higher value. Of note, transfection was only possible for tumors accessible via the intratracheal route. In case the tumor obstructed the airways, no transfection of tumor tissue could be achieved. With CD49f targeting, we could observe a strong luciferase signal in the area of the tumor lesion, whereas surrounding, healthy lung tissue appeared not transfected. We conclude that this difference is also due to the fact

that also untargeted, unshielded LPEI polyplexes, when applied intratracheally, only very inefficiently transfect healthy lung tissue.[43]

Taken together, CD49f targeting of polyplexes with the laminin derived peptide CYESIKVAVS significantly enhanced transgene expression. Due to its applicability *in vivo* by the intratracheal route, it opens the possibility of efficient transfection of lung tumor lesions also for therapeutic purposes.

Materials

The plasmid pCMV-Gluc was obtained from New England Biolabs (Frankfurt, Germany). The plasmid pCpG-hCMV-EF1α-LucSH encoding for a luciferase-bleomycin fusion protein was already described elsewhere.[44] For binding and uptake studies by flow cytometry and CLSM pCMV-Gluc was labelled with Cyanin 5 (Cy5) using a Mirus LabelIT kit (Mirus Bio; Madison, WI, USA) as described.[1]

MDA-MB-231 (human breast adenocarcinoma; HTB-26), CT26 (murine colon carcinoma; CRL-2638) and 4T1 (murine breast cancer; CRL-2539) cells were obtained from ATCC (LGC Standards GmbH, Wesel, Germany). Stably iRFP720 expressing 4T1 cells (4T1-iRFP720) were generated as previously published.[19] MDA-MB-231 were cultured in DMEM high glucose medium, CT26 in DMEM/F-12 Ham medium and 4T1-PGK-iRFP720 cells in RPMI1640 medium. All cell culture media were supplemented with 10 % fetal bovine serum (FBS; Sigma-Aldrich Austria), 2 % L-glutamine (L-gln; Sigma-Aldrich; Vienna, Austria) and 1 % antibiotics (Penicillin/Streptomycin; Sigma-Aldrich). Cell culture medium without any supplement is later termed as basal medium.

α-Methyl ω-hydroxy poly(2-ethyl-2-oxazoline) was obtained from Sigma-Aldrich (Austria) and α-OPSS (3-(2-pyridyldithio)propionamide) ω-NHS (N-hydroxysuccinimide) polyethylene glycol (Mw 2 kDa) from Rapp Polymere (Tübingen, Germany).

Fmoc protected L-amino acids used for solid phase peptide synthesis were obtained from Iris Biotech (Germany).

AlexaFluor®-488 phalloidin for actin staining used for CLSM, TrypLE® Express for cell detachment and bicinchoninic acid (BCA) assay kit for protein quantification were purchased from ThermoFisher Scientific (Vienna, Austria). Passive lysis buffer was obtained from Promega (Mannheim, Germany).

Native coelenterazine was purchased from Synchem (Felsberg, Germany) and used for evaluating *in vitro* Gaussia luciferase expression at a concentration of 20 µM in DPBS (supplemented with 5 mM NaCl) as per instructions in Tannous et al.[45] D-luciferin (potassium salt; VivoTrace®) was used for *in vivo* bioluminescence imaging (BLI) at a concentration of 30 mg/mL in DPBS and obtained from Intrace medical (Lausanne, Switzerland).

For all experiments water purified with a Sartorius Arium® Pro (Vienna, Austria) system was used.

All other reagents used for synthesis, physical and biological evaluation if not stated differently were obtained from Sigma Aldrich.

All diluents used for nanoparticle analysis by NTA as well as cell culture media were filtered through 0.1 µm cellulose acetate membranes.

Methods

Synthesis of LPEI-PEG-cysteine (LPEI-PEG) and LPEI-PEG-CYESIKVAVS (LPEI-PEG-CD49f)

Generation of LPEI-PEG-OPSS was done based on a previously described protocol.[27] Briefly, 60 mg of LPEI dissolved in 1.5 mL dry ethanol were mixed with a solution of NHS-PEG-OPSS (2 eq) in 100 µL DMSO and incubated at 35 °C for 3 h under vigorous mixing. The reaction was stopped with 100 µL TRIS.HCl buffer (1 M) set to pH 8. After adding 830 µL HEPES/3 M NaCl (pH 7.4) the solution was filled up to a final volume of 5 mL to reach a final NaCl concentration of 0.5 M. Purification of the product was conducted with an Äkta Pure system (GE Healthcare; Vienna, Austria) equipped with a cation exchange resin (MacroPrep High S (Bio-Rad; Vienna, Austria) in HR10/10 column). For removing impurities in the mixture a mobile phase containing 0.5 M NaCl in HEPES (pH 7.4) was used at a flow rate of 0.5 mL/min for 25 minutes. Elution of LPEI-PEG-OPSS was done with a NaCl gradient from 0.5 M to 3 M in HEPES (pH 7.4) over a total duration of 40 minutes. LPEI-PEG-OPSS containing fractions were pooled, dialyzed against water employing a regenerated cellulose membrane with a molecular weight cut-off (MWCO) of 6-8 kDa (SpectraPor; Repligen; Germany) and lyophilized. The ratio between LPEI and PEG in the product was evaluated by ^{1}H-NMR with a 200 MHz Bruker Avance system (Billerica, MA, USA). Therefore, 5 mg of LPEI-PEG-OPSS were dissolved in 1 mL D_2O and pH was set to 7 with DCl (1 M) and NaOD (1 M). The solvent derived signal was used as reference (δ=4.79 ppm) for analysis of signals derived from the conjugate. For determination of PEGylation degree the peak integral of the

signal derived from C**H**$_2$C**H**$_2$NH was set to 930 (based on a Mw of 10 kDa of LPEI). Based on the Mw of PEG of 2 kDa the ratio of LPEI:PEG within the conjugate was calculated. The total amount of intact OPSS groups in the conjugate was evaluated by adding 15 µL of DTT (1 M in water) to 150 µL of an aqueous LPEI-PEG-OPSS stock with a concentration of 2 mg/mL. The mixture was incubated at room temperature for 10 minutes and analyzed by UV/Vis spectrophotometry for its absorption at 343 nm generated by 2-thiopyridone released through reductive cleavage of OPSS groups.

For synthesis of LPEI-PEG or LPEI-PEG-CD49f a three-fold excess (based on amount of OPSS) of either L-cysteine or CYESIKVAVS dissolved in 30 % ACN (in 0.1 % TFA) was added to a solution of LPEI-PEG-OPSS in 30 % ACN (in 20 mM HEPES; pH 7.4). Unwanted oxidation of the N-terminal thiol group of the peptide was avoided by purging all diluents with argon. The mixture was incubated at room temperature under vigorous stirring. The reaction process was monitored by UV/Vis spectrophotometry and proceeded until no change in the absorption at 343 nm generated by 2-thiopyridone could be detected. 830 µL of 3 M NaCl (in 10 % ACN in 20 mM HEPES; pH 7.4) were added to the solution which was then filled up to a total volume of 5 mL with 10 % ACN (in 20 mM HEPES; pH 7.4) to reach a final NaCl concentration of 0.5 M. Purification was again conducted based on cation exchange chromatography using a MacroPrep High S resin (HR10/10 column) with an Äkta Pure system. Uncharged impurities were removed with 0.5 M NaCl (in 10 % ACN in 20 mM HEPES; pH 7.4) at a flow rate of 0.5 mL/min for 35 minutes. LPEI-PEG or LPEI-PEG-CD49f were eluted with a linear NaCl gradient from 0.5 M to 3 M (in 10 % ACN in 20 mM HEPES; pH 7.4) over 40 minutes. Conjugate containing fractions were pooled, dialyzed against water with a regenerated cellulose membrane (MWCO: 6 kDa-8 kDa) at 4 °C and lyophilized.

Polyplex synthesis

Preparation of polyplexes was conducted based on a previously described method.[46] Briefly, same volumes of a pDNA containing solution and a LPEI/LPEI-PEG/LPEI-PEG-CD49f containing solution were mixed by flash pipetting. The mixture was then incubated for 5 minutes at room temperature. For all experiments polyplexes were prepared at N/P ratio 9 in 20 mM 4-(2-Hydroxyethyl)piperazine-1-ethanesulfonic acid (HEPES)/5% glucose (HBG; pH 7.4). For *in vitro* experiments nanoparticles were generated at a final pDNA concentration of 20 µg/mL. For *in vivo* administration a concentration of 267 µg/mL of formulated pDNA was used.

Evaluation of nanoparticle properties (size and ζ-potential)

NTA was done based on the instructions by Taschauer et al.[29] Polyplex samples were analyzed for their particle size and ζ-potential on a Malvern NS500 system (UK). For all measurements dilution factors were chosen to reach 10 to 100 particles per frame corresponding to a concentration of 10^8 to 10^9 particles/mL. For size measurement samples were diluted in HBG and for ζ-potential measurements in 2.5 mM NaCl. Particle size was calculated based on 5 videos with a duration of 60 seconds. For analyzing the ζ-potential a capture duration of 90 seconds and a secondary duration of 30 seconds were chosen. All ζ-potential measurements used for evaluation showed a coefficient of correlation of at least 0.95. For analyzing the effect of microspraying with a PennCentury Microsprayer®/Syringe Assembly (MSA-250-M; PennCentruy, Inc; US) on particle properties samples were sprayed into centrifuge tubes and analyzed for particle size as described above.

Cell characterization (CD49f expression profile)

Cells (MDA-MB-231/CT26/4T1-iRFP720) were detached with Versene® (Thermo Fisher Scientific; Austria) based on manufacturer´s instructions. $2x10^5$ cells were transferred into 96-well v-bottom plates and washed with 2 mM EDTA/0.5 % (m/V) bovine serum albumin (BSA) in DPBS (PEB) to avoid non-specific binding of antibodies. The cell pellet was then resuspended in 20 µL of either PEB (untreated control), a dilution of rat IgG2a κ isotype control (BD Biosciences; Germany) in PEB or a dilution of rat anti-human CD49f antibody (BD Biosciences; Germany) in PEB. Both antibodies were labelled with BV (brilliant violet) 421. Antibody concentrations were chosen as per manufacturer´s instructions. After an incubation period of 30 minutes at 4 °C cells were washed twice with PEB and resuspended in 100 µL PEB. Flow cytometry was done with a MacsQuant® Analyzer 10 system (Miltenyi Biotec; Germany). Live cells were gated and analyzed for their fluorescence signal derived by BV421 in the V1 channel (excitation laser: 405 nm; emission band pass filter: 450/50 nm).

Cell association assay by flow cytometry

$5x10^4$ MDA-MB-231 cells were seeded into a transparent 96-well plate 24 h prior to treatment. Polyplex samples used for this experimental setup were based on pCMV-Gluc labelled with Cy5. Nanoparticles were prepared as described above. Before sample addition to cells, cell culture medium was exchanged with basal DMEM high glucose medium. Cells were treated with 1 µg/mL or 2 µg/mL of formulated pDNA. Both concentrations were tested for a total duration of 30 minutes and 4 h. Thereafter, cells were washed twice with DPBS, detached with TrypLE®

Express based on manufacturer´s protocol, resuspended in DPBS and transferred into a PCR plate (Nerbe; #04-083-0150; Germany). Flow cytometric analysis was conducted with a MacsQuant® Analyzer 10 system. For live/dead staining DAPI was automatically added with an autoinjector reaching a final concentration of 1 µg/mL. Until DAPI addition and automated injection into the flow cytometry system cell suspensions were permanently kept at 4 °C using a CPAC cooling unit (Inheco; Germany). $1x10^4$ live cells were analyzed per well for their Cy5 signal detected in the R1 channel (excitation laser: 635 nm; emission band pass filter: 655-730 nm). Data evaluation was conducted with FlowJo X software (version: 10.1r5).

Evaluation of cell binding and uptake by confocal laser scanning microscopy (CLSM)

$5x10^4$ MDA-MB-231 cells were seeded into chamber slides (Nunc® Lab-Tek® II 8-well slides; Thermo Fisher scientific; Germany) 24 h before treatment. Polyplexes were prepared based on Cy5 labelled pCMV-Gluc. Cells were treated with a concentration of 2 µg/mL of formulated pDNA for 4 h in basal DMEM high glucose medium. After treatment cells were washed 3 times with 1 % (m/V) BSA (in DPBS) and fixed with 4 % (m/V) formaldehyde (in HBS; pH 7.4) for 30 minutes at room temperature. After 3 washing steps with 1 % (m/V) BSA (in DPBS) cells were permeabilized with 0.1 % Triton X-100 (in DPBS) for 5 minutes and washed again with 1 % (m/V) BSA (in DPBS). Actin staining was done with AlexaFluor® 488-phalloidin as per manufacturer´s instructions. After 3 further washing steps with 1 % (w/V) BSA (in DPBS) nuclei were stained with DAPI at a concentration of 2 µg/mL for 5 minutes and objects were mounted with Vectashield® antifade mounting medium (Vector Laboratories; UK). Image acquisition was performed on a Leica TCS SPE microscope (Leica; Germany) with a 63X oil immersion objective. DAPI derived signal was imaged at 405 nm laser excitation, AlexaFluor488-phalloidin at 488 nm and Cy5 at 635 nm. Detection of emission signal was set for optimal collection of emitted light as per the respective fluorophore. For both magnifications z-scans with a vertical resolution of 0.1 µm were conducted. Data acquisition and analysis was done with LasX software (Version 3.1.2.16221).

In vitro transfection assay

For evaluation of transfection efficiency gene delivery agents (LPEI/LPEI-PEG/LPEI-PEG-CD49f) were tested on MDA-MB-231, CT26 and 4T1-iRFP720. For MDA-MB-231 a seeding density of $2x10^4$ cells/well was used. Due to their high growth rate both CT26 and 4T1-iRFP720 were seeded at a density of $1x10^4$ cells/well. Cell seeding was conducted 24 h before treatment. Polyplexes were based on pCMV-Gluc and tested at pDNA concentrations of 0.5 µg/mL, 1 µg/mL, 2 µg/mL and 4 µg/mL. Cell treatment was conducted in basal cell culture medium. 4 h after

compound addition supernatant was exchanged with cell culture medium supplemented with 10 % FBS, 2 % L-gln and antibiotics. After a total treatment time of 24 h expression of Gaussia luciferase (Gluc) was analyzed in 20 µL of supernatant. Quantification of light signal was conducted after automated injection of 50 µL of Coelenterazine (native; 20 µM in DPBS) with an Infinite® M200 Pro system (Tecan Life Sciences; Switzerland) set to an integration time of 10,000 ms. Relative light units (RLU) were normalized based on total cell count in case of MDA-MB-231 and CT26. Therefore, cells were washed with DPBS and detached with TrypLE® Express based on manufacturer´s protocol. After resuspension of cells in DPBS cell count was conducted on a MacsQuant Analyzer 10 system. DAPI was used for live/dead staining at a concentration of 1 µg/mL without incubation time. Until automated addition of DAPI followed by injection into the flow cytometer cell suspensions were permanently kept at 4 °C.

Gaussia luciferase expression signals of 4T1-iRFP720 were normalized to protein amount. Therefore, cells were washed with DPBS and lysed with 30 µL passive lysis buffer (Promega; Germany). Protein quantification was evaluated in 20 µL of cell lysate by BCA kit (Pierce; Thermo Fisher scientific; Germany) following manufacturer´s instructions.

In vivo transfection assay

In vivo transfection was evaluated on a 4T1-iRFP720 lung tumor model established by Geyer et al.[19] Therefore, female Balb/cJRj (Janvier Labs; France) were kept in individually ventilated Type 2L cages and kept on a low fluorescent diet (AIN-76A, gamma-irradiated; ssniff, Soest, Germany) for at least 10 days before treatment. All procedures were approved by local ethics committee and are in accordance with the Austrian law for the protection of animals and the EU directive 2010/63/EU.

4T1-iRFP720 cells were detached with TrypLE® Express based on manufacturer´s instructions, washed and resuspended in DPBS at a final concentration of 10^6 cells/mL. For generating 4T1-iRFP720 tumor model 10^5 cells were injected into the lateral tail vein. Tumor growth was monitored by MRI using a small 1.0 Tesla preclinical MRI – scanner, equipped with a homogenous permanent magnet unit (Aspect Imaging M3™ compact MRI – system; Israel) along with a 50 mm x 38 mm body coil (Mouse Body L50D38 Serial: 1, Aspect Imaging® Ltd, Shoham, Israel). For all animals native two dimensional fast spin echo T2 – weighted images were acquired in coronal slice orientation (Time to repetition (TR): 3250ms, Time to Echo (TE): 63.47ms, number of slices: 15, slice thickness: 1 mm, number of excitations: 7, slice orientation: coronal, center of slice position: 0 °, hor. FOV: 30 mm, vert. FOV: 60 mm, flip angle: 90°, scan

time: 5 min 46 seconds). Mice were anesthetized with 2 % isoflurane (Isoflurane CP 1 mL/mL, CP – Pharma; Germany) with an oxygen flow rate of 2 L/min and eyes were protected by an ointment (Vit A-POS®, Ursapharm Arzneimittel GmbH; Austria). For optimal acquisition respiratory movement was detected to suppress motion derived artifacts. A high intrapulmonal tumor load detected by MRI was taken as major criterion for starting the treatment. Image analysis was conducted with VivoQuant® software (Version 3.0.patch1, Invicro Imaging Service and Software; US).

Intratracheal administration of polyplex samples was conducted using a Microsprayer®/Syringe Assembly (MSA-250-M; PennCentruy, Inc; US) as described by Geyer et al.[19, 47] Both LPEI-PEG-CD49f or LPEI-PEG were tested as polyplex formulations with pCpG-hCMV-EF1α-LucSH. Polyplexes were prepared at a final pDNA concentration of 267 µg/mL. In total 20 µg of formulated pDNA were administered into tumor bearing animals. For microspraying animals were anesthetized with a mixture of ketamine (80 mg/kg) and xylazine (5 mg/kg). 24 h after treatment animals were imaged for bioluminescence signal. Therefore, animals were anesthetized with 2 % isoflurane followed by subcutaneous injection of D-luciferin (potassium salt; 30 mg/mL in DPBS; dosage: 120 mg/kg). Bioluminescence signal was collected at an exposure of 3 minutes in Stage B with an IVIS spectrum CT system (PerkinElmer; US) over a duration of 30 min to 45 min. Data was analyzed with Living Image software (version 4.5.2.18424). For evaluation of light signal a rectangular region of interest (ROI) was placed over the thoracic region.

Histology

Histological evaluation of lungs was conducted based on previously described protocol.[19, 48] Briefly, animals were sacrificed directly after bioluminescence imaging (BLI) and intubated. Instillation fixation was done with 4 % formaldehyde (in HBS; pH 7.4). Lungs were subsequently fixed in 4 % formaldehyde for 22 h, dehydrated with increasing ethanol concentrations (70 %; 96 %; 100 %) followed by clearing with xylene and embedding in Paraplast®. Tissue was rehydrated and sectioned on a microtome (Slee; Germany) with 2 µm thickness. For morphological analysis tissue was stained for 3 minutes with Harris modified hematoxylin (Carl Roth GmbH + Co. KG; Germany) followed by treatment with acidified ethanol (1 seconds), ammonium hydroxide (20 seconds) and Eosin Y (10 minutes; Sigma– Aldrich; Austria). For IHC staining, FFPE sections were prewarmed for 2h at 55°C, deparaffinized, dehydrated and heat induced epitope retrieval (HIER) was performed for 30 min in TRIS-EDTA Buffer (pH 9). After normal serum blockage for 30 min, endogenous avidin and biotin were blocked with Avidin/Biotin Blocking Reagent (BIO-RAD,

BUF016) for 15 min each. The samples were incubated with Anti-Integrin α6 antibody [EPR18124] (Abcam, ab181551; UK) (1:100) or Rabbit IgG, monoclonal [EPR25A] - Isotype Control (Abcam, ab172730; UK) in PBS + 2% BSA over night at 4 °C. Endogenous peroxidase was blocked with 0,3% H_2O_2/PBS for 15min. Samples were further treated via VECTASTAIN® ABC HRP Kit (Peroxidase, Rabbit IgG, PK-4001) and counterstained with Hematoxylin. The sections were mounted in Entellan® (Merck Millipore; Austria) and coverslipped. Images were acquired on an Olympus BX53 light microscope (Olympus; Austria) equipped with an Olympus DP-73 colour camera.

Acknowledgements

We would like to thank Dr Michal Pechar (Institute of Macromolecular Chemistry, Czech Academy of Science) for help with GPC analysis, Susanne Wiederkum for technical assistance and Dr Antonia Geyer for helpful advice concerning intratracheal application. Open access funding was provided by University of Vienna.

References

1. Schafer, A, Pahnke, A, Schaffert, D, van Weerden, WM, de Ridder, CM, Rodl, W*, et al.* (2011). Disconnecting the yin and yang relation of epidermal growth factor receptor (EGFR)-mediated delivery: a fully synthetic, EGFR-targeted gene transfer system avoiding receptor activation. *Hum Gene Ther* **22**: 1463-1473.

2. Mickler, FM, Mockl, L, Ruthardt, N, Ogris, M, Wagner, E, and Brauchle, C (2012). Tuning nanoparticle uptake: live-cell imaging reveals two distinct endocytosis mechanisms mediated by natural and artificial EGFR targeting ligand. *Nano Lett* **12**: 3417-3423.

3. Ge, Z, Chen, Q, Osada, K, Liu, X, Tockary, TA, Uchida, S*, et al.* (2014). Targeted gene delivery by polyplex micelles with crowded PEG palisade and cRGD moiety for systemic treatment of pancreatic tumors. *Biomaterials* **35**: 3416-3426.

4. Urnauer, S, Klutz, K, Grunwald, GK, Morys, S, Schwenk, N, Zach, C*, et al.* (2017). Systemic tumor-targeted sodium iodide symporter (NIS) gene therapy of hepatocellular carcinoma mediated by B6 peptide polyplexes. *J Gene Med* **19**.

5. Abourbeh, G, Shir, A, Mishani, E, Ogris, M, Rodl, W, Wagner, E*, et al.* (2012). PolyIC GE11 polyplex inhibits EGFR-overexpressing tumors. *IUBMB Life* **64**: 324-330.

6. Boonstra, MC, de Geus, SW, Prevoo, HA, Hawinkels, LJ, van de Velde, CJ, Kuppen, PJ*, et al.* (2016). Selecting Targets for Tumor Imaging: An Overview of Cancer-Associated Membrane Proteins. *Biomark Cancer* **8**: 119-133.

7. Human Protein Atlas (2019). https://www.proteinatlas.org/ENSG00000091409-ITGA6/tissue.

8. Krebsbach, PH, and Villa-Diaz, LG (2017). The Role of Integrin alpha6 (CD49f) in Stem Cells: More than a Conserved Biomarker. *Stem Cells Dev* **26**: 1090-1099.

9. Yang, Z, Dong, P, Fu, X, Li, Q, Ma, S, Wu, D*, et al.* (2015). CD49f Acts as an Inflammation Sensor to Regulate Differentiation, Adhesion, and Migration of Human Mesenchymal Stem Cells. *Stem Cells* **33**: 2798-2810.

10. Yu, KR, Yang, SR, Jung, JW, Kim, H, Ko, K, Han, DW*, et al.* (2012). CD49f enhances multipotency and maintains stemness through the direct regulation of OCT4 and SOX2. *Stem Cells* **30**: 876-887.

11. Yamamoto, H, Masters, JR, Dasgupta, P, Chandra, A, Popert, R, Freeman, A*, et al.* (2012). CD49f is an efficient marker of monolayer- and spheroid colony-forming cells of the benign and malignant human prostate. *PLoS One* **7**: e46979.

12. Smadja, DM, Guerin, CL, Boscolo, E, Bieche, I, Mulliken, JB, and Bischoff, J (2014). alpha6-Integrin is required for the adhesion and vasculogenic potential of hemangioma stem cells. *Stem Cells* **32**: 684-693.

13. Fukamachi, H, Seol, HS, Shimada, S, Funasaka, C, Baba, K, Kim, JH*, et al.* (2013). CD49f(high) cells retain sphere-forming and tumor-initiating activities in human gastric tumors. *PLoS One* **8**: e72438.

14. Vassilopoulos, A, Chisholm, C, Lahusen, T, Zheng, H, and Deng, CX (2014). A critical role of CD29 and CD49f in mediating metastasis for cancer-initiating cells isolated from a Brca1-associated mouse model of breast cancer. *Oncogene* **33**: 5477-5482.

15. Ye, F, Qiu, Y, Li, L, Yang, L, Cheng, F, Zhang, H*, et al.* (2015). The Presence of EpCAM(-)/CD49f(+) Cells in Breast Cancer Is Associated with a Poor Clinical Outcome. *J Breast Cancer* **18**: 242-248.

16. Saha, A, Blando, J, Fernandez, I, Kiguchi, K, and DiGiovanni, J (2016). Linneg Sca-1high CD49fhigh prostate cancer cells derived from the Hi-Myc mouse model are tumor-initiating cells with basal-epithelial characteristics and differentiation potential in vitro and in vivo. *Oncotarget* **7**: 25194-25207.

17. Wang, Y, Shenouda, S, Baranwal, S, Rathinam, R, Jain, P, Bao, L*, et al.* (2011). Integrin subunits alpha5 and alpha6 regulate cell cycle by modulating the chk1 and Rb/E2F pathways to affect breast cancer metastasis. *Mol Cancer* **10**: 84.

18. DuPre, SA, Redelman, D, and Hunter, KW, Jr. (2007). The mouse mammary carcinoma 4T1: characterization of the cellular landscape of primary tumours and metastatic tumour foci. *Int J Exp Pathol* **88**: 351-360.

19. Geyer, A, Taschauer, A, Alioglu, F, Anton, M, Maier, J, Drothler, E*, et al.* (2017). Multimodal Fluorescence and Bioluminescence Imaging Reveals Transfection Potential of Intratracheally Administered Polyplexes for Breast Cancer Lung Metastases. *Human gene therapy* **28**: 1202-1213.

20. Tashiro, K, Sephel, GC, Weeks, B, Sasaki, M, Martin, GR, Kleinman, HK*, et al.* (1989). A synthetic peptide containing the IKVAV sequence from the A chain of laminin mediates cell attachment, migration, and neurite outgrowth. *J Biol Chem* **264**: 16174-16182.

21. Freitas, VM, Vilas-Boas, VF, Pimenta, DC, Loureiro, V, Juliano, MA, Carvalho, MR*, et al.* (2007). SIKVAV, a laminin alpha1-derived peptide, interacts with integrins and increases protease activity of a human salivary gland adenoid cystic carcinoma cell line through the ERK 1/2 signaling pathway. *Am J Pathol* **171**: 124-138.

22. Stevenson, M, Hale, AB, Hale, SJ, Green, NK, Black, G, Fisher, KD*, et al.* (2007). Incorporation of a laminin-derived peptide (SIKVAV) on polymer-modified adenovirus permits tumor-specific targeting via alpha6-integrins. *Cancer Gene Ther* **14**: 335-345.

23. Rodl, W, Taschauer, A, Schaffert, D, Wagner, E, and Ogris, M (2019). Synthesis of Polyethylenimine-Based Nanocarriers for Systemic Tumor Targeting of Nucleic Acids. *Methods Mol Biol* **1943**: 83-99.

24. Kikkawa, Y, Hozumi, K, Katagiri, F, Nomizu, M, Kleinman, HK, and Koblinski, JE (2013). Laminin-111-derived peptides and cancer. *Cell Adh Migr* **7**: 150-256.

25. Li, B, Qiu, T, Zhang, P, Wang, X, Yin, Y, and Li, S (2014). IKVAV regulates ERK1/2 and Akt signalling pathways in BMMSC population growth and proliferation. *Cell Prolif* **47**: 133-145.

26. Chen, X, Fu, W, Cao, X, Jiang, H, Che, X, Xu, X*, et al.* (2018). Peptide SIKVAV-modified chitosan hydrogels promote skin wound healing by accelerating angiogenesis and regulating cytokine secretion. *Am J Transl Res* **10**: 4258-4268.

27. Schaffert, D, Kiss, M, Rodl, W, Shir, A, Levitzki, A, Ogris, M*, et al.* (2011). Poly(I:C)-Mediated Tumor Growth Suppression in EGF-Receptor Overexpressing Tumors Using EGF-Polyethylene Glycol-Linear Polyethylenimine as Carrier. *Pharm Res* **28**: 731-741.

28. Crosas, E, Egea, MA, and Reig, F (2006). Spectroscopic techniques applied to the study of laminin fragments inserted into model membranes. *J Colloid Interface Sci* **295**: 264-269.

29. Taschauer, A, Geyer, A, Gehrig, S, Maier, J, Sami, H, and Ogris, M (2016). Up-Scaled Synthesis and Characterization of Nonviral Gene Delivery Particles for Transient In Vitro and In Vivo Transgene Expression. *Hum Gene Ther Methods* **27**: 87-97.

30. Klutz, K, Schaffert, D, Willhauck, MJ, Grunwald, GK, Haase, R, Wunderlich, N*, et al.* (2011). Epidermal growth factor receptor-targeted (131)I-therapy of liver cancer following systemic delivery of the sodium iodide symporter gene. *Mol Ther* **19**: 676-685.

31. Geyer, A, Taschauer, A, Alioglu, F, Anton, M, Maier, J, Drothler, E*, et al.* (2017). Multimodal Fluorescence and Bioluminescence Imaging Reveals Transfection Potential of Intratracheally Administered Polyplexes for Breast Cancer Lung Metastases. *Hum Gene Ther* **28**: 1202-1213.

32. Brooks, DL, Schwab, LP, Krutilina, R, Parke, DN, Sethuraman, A, Hoogewijs, D*, et al.* (2016). ITGA6 is directly regulated by hypoxia-inducible factors and enriches for cancer stem cell activity and invasion in metastatic breast cancer models. *Mol Cancer* **15**: 26.

33. Hu, T, Zhou, R, Zhao, Y, and Wu, G (2016). Integrin alpha6/Akt/Erk signaling is essential for human breast cancer resistance to radiotherapy. *Sci Rep* **6**: 33376.

34. de Bruin, K, Ruthardt, N, von Gersdorff, K, Bausinger, R, Wagner, E, Ogris, M*, et al.* (2007). Cellular dynamics of EGF receptor-targeted synthetic viruses. *Mol Ther* **15**: 1297-1305.

35. Degeling, MH, Bovenberg, MS, Lewandrowski, GK, de Gooijer, MC, Vleggeert-Lankamp, CL, Tannous, M*, et al.* (2013). Directed molecular evolution reveals Gaussia luciferase variants with enhanced light output stability. *Anal Chem* **85**: 3006-3012.

36. Shorter, SA, Gollings, AS, Gorringe-Pattrick, MAM, Coakley, JE, Dyer, PDR, and Richardson, SCW (2017). The potential of toxin-based drug delivery systems for enhanced nucleic acid therapeutic delivery. *Expert Opin Drug Deliv* **14**: 685-696.

37. Jin, L, Han, B, Siegel, E, Cui, Y, Giuliano, A, and Cui, X (2018). Breast cancer lung metastasis: Molecular biology and therapeutic implications. *Cancer Biol Ther* **19**: 858-868.

38. Rashid, OM, Nagahashi, M, Ramachandran, S, Dumur, CI, Schaum, JC, Yamada, A*, et al.* (2013). Is tail vein injection a relevant breast cancer lung metastasis model? *J Thorac Dis* **5**: 385-392.

39. Adiseshaiah, PP, Patel, NL, Ileva, LV, Kalen, JD, Haines, DC, and McNeil, SE (2014). Longitudinal imaging of cancer cell metastases in two preclinical models: a correlation of noninvasive imaging to histopathology. *Int J Mol Imaging* **2014**: 102702.

40. Storti, C, Le Noci, V, Sommariva, M, Tagliabue, E, Balsari, A, and Sfondrini, L (2015). Aerosol Delivery in the Treatment of Lung Cancer. *Curr Cancer Drug Targets* **15**: 604-612.

41. Jia, SF, Worth, LL, Densmore, CL, Xu, B, Duan, X, and Kleinerman, ES (2003). Aerosol gene therapy with PEI: IL-12 eradicates osteosarcoma lung metastases. *Clin Cancer Res* **9**: 3462-3468.

42. Hasenpusch, G, Pfeifer, C, Aneja, MK, Wagner, K, Reinhardt, D, Gilon, M*, et al.* (2011). Aerosolized BC-819 inhibits primary but not secondary lung cancer growth. *PLoS One* **6**: e20760.

43. Bragonzi, A, Dina, G, Villa, A, Calori, G, Biffi, A, Bordignon, C*, et al.* (2000). Biodistribution and transgene expression with nonviral cationic vector/DNA complexes in the lungs. *Gene Ther* **7**: 1753-1760.

44. Magnusson, T, Haase, R, Schleef, M, Wagner, E, and Ogris, M (2011). Sustained, high transgene expression in liver with plasmid vectors using optimized promoter-enhancer combinations. *The journal of gene medicine* **13**: 382-391.

45. Tannous, BA (2009). Gaussia luciferase reporter assay for monitoring biological processes in culture and in vivo. *Nat Protoc* **4**: 582-591.

46. Rödl, W, Schaffert, D, Wagner, E, and Ogris, M (2013). Synthesis of polyethylenimine-based nanocarriers for systemic tumor targeting of nucleic acids. *Methods Mol Biol* **948**: 105-120.

47. Geyer, A, Lorenzer, C, Gehrig, S, Simlinger, M, Winkler, J, Sami, H*, et al.* (2017). Fluorescence- and computed tomography for assessing the biodistribution of siRNA after intratracheal application in mice. *International journal of pharmaceutics* **525**: 359-366.

48. Braber, S, Verheijden, KAT, Henricks, PAJ, Kraneveld, AD, and Folkerts, G (2010). A comparison of fixation methods on lung morphology in a murine model of emphysema. *Am J Physiol-Lung Cell Mol Physiol* **299**: L843-L851.

Supplemental Figures

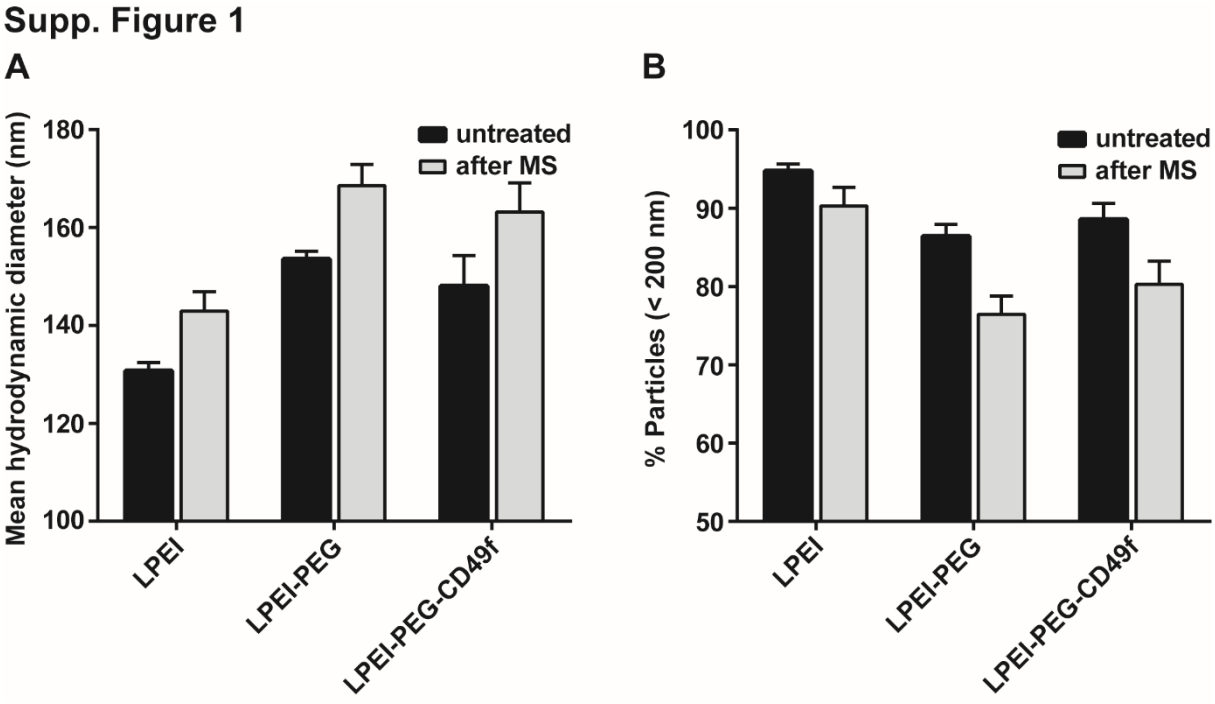

Supp. Figure 1: NTA analysis of polyplexes after aerosolization. *Both mean hydrodynamic diameter (A) and percentage of particles <200 nm (B) were evaluated with polyplexes based on LPEI, LPEI-PEG and LPEI-PEG-CD49f at N/P 9 before and after aerosolization. Values are depicted as mean values (n=3 + stddev).*

Supp. Figure 2

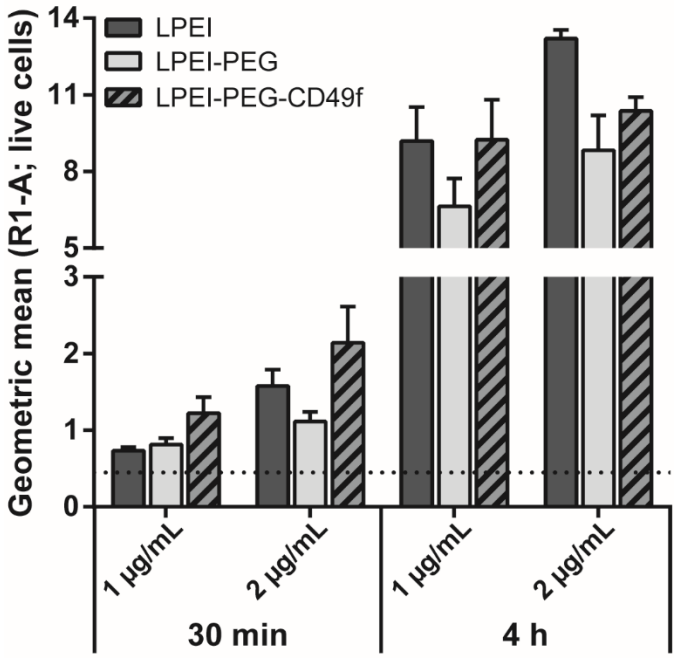

Supp. Figure 2: Geometric mean values of cell association study of polyplexes. *MDA-MB-231 cells were incubated with polyplexes based on Cy5-labelled pDNA prepared at N/P 9. Cells were treated in basal cell culture medium with two different concentrations and durations (1 µg/mL for 30 min and 4 h; 2 µg/mL for 30 min and 4 h) and analyzed by flow cytometry. Data is depicted as mean values (n=3 + stddev). The background signal is depicted as dotted line.*

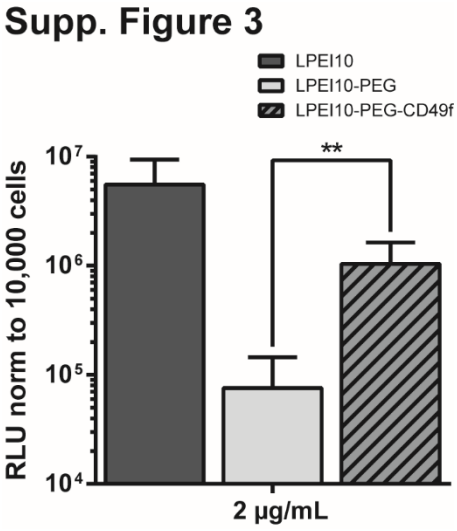

Supp. Figure 3: Transfection study with CT26 cells. *CT26 were seeded in 96-well plates and treated with polyplexes based on pCMV-Gluc at 2 µg/mL. 4 h after polyplex addition cellular supernatant was exchanged with cell culture medium supplemented with FCS, L-gln and antibiotics. 24 h after starting cell treatment Gaussia luciferase was quantified in the supernatant and RLU values were normalized based on total count of live cells. Data is depicted as mean values (n=3 + stddev; data from 2 independent experiments; ** p≤0.01 (Mann-Whitney))*

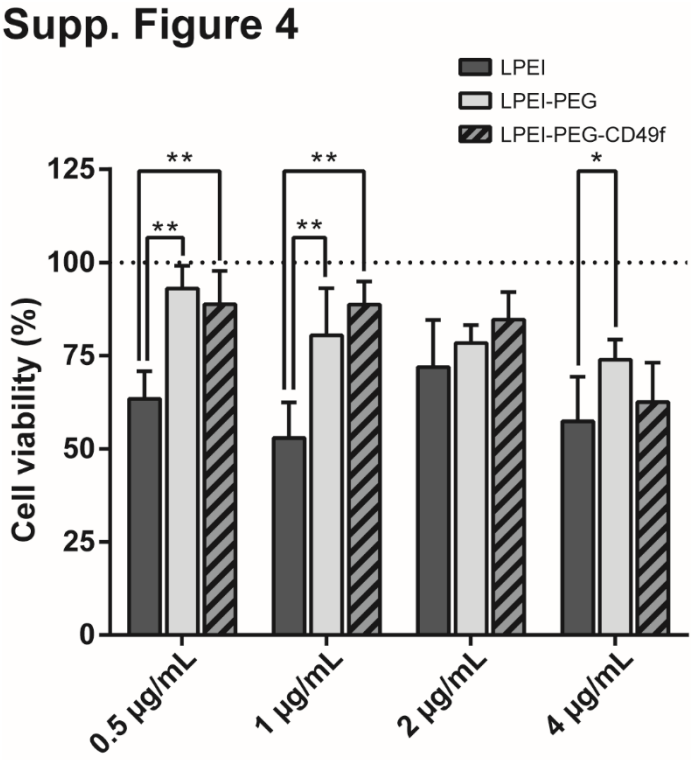

Supp. Figure 4: Cell viability studies by flow cytometry. *MDA-MB-231 cells were treated with polyplexes at 4 different concentrations (0.5 µg/mL; 1 µg/mL; 2 µg/mL; 4 µg/mL). 24 h post treatment live cells were counted by flow cytometry after DAPI addition. DAPI derived fluorescence signal was detected in the V1 channel. Total count of live cells was normalized based on buffer treated cells. Data is depicted as mean values (n=3 + stddev; data from 2 independent experiments; *p≤0.05, ** p≤0.01 (Mann-Whitney))*

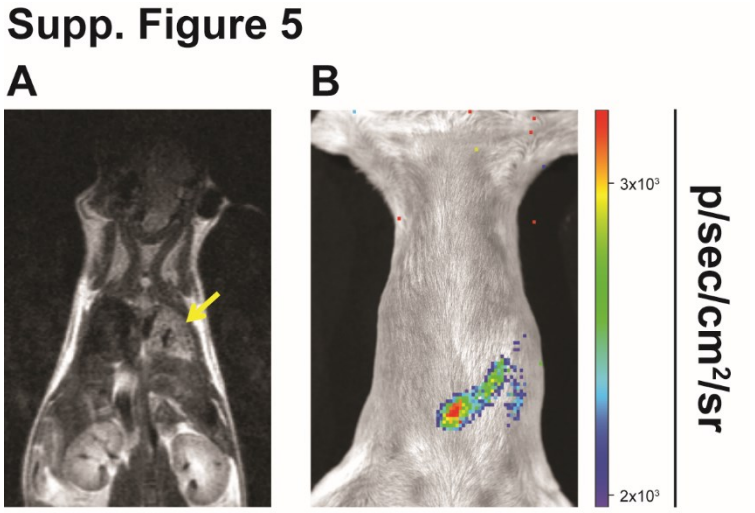

Supp. Figure 5: Representative example of intratracheal polyplex treatment of 4T1-iRFP720 tumor bearing animal with inaccessible tumor tissue. *MRI shows intense tumor growth in the whole left lung (marked with yellow arrow) (A). Treatment with LPEI-PEG-CD49f based polyplexes of this animal didn´t result in sufficient transfection (B). Background BLI signal (color coded) in the abdominal region is depicted as overlay on a reflected light picture.*

Supplemental methods

Synthesis of linear polyethylenimine (LPEI; Mw 10 kDa)

α-Methyl ω-hydroxy LPEI (Mw 10 kDa) was generated based on a previously described protocol.[1] 2 g α-Methyl ω-hydroxy poly(2-ethyl-2-oxazoline) was dissolved in 50 mL HCl (7 M) and heated overnight under reflux. LPEI precipitated as HCl salt and was purified by centrifugation with HCl (7 M). After dissolving the precipitate in 30 mL water the solution was again heated under reflux and pH was adjusted to 12 with NaOH (1 M). The mixture was cooled to room temperature where LPEI formed a white precipitate as free base. The precipitate was then washed by centrifugation with NaOH (1 M) and water. After resuspending in water the product was lyophilized. Analysis of both structure and purity of LPEI was conducted by ^{1}H-NMR on a Bruker Avance (200 MHz; US) system. Therefore, 5 mg of the product were dissolved in $CDCl_3$. The peak derived from the solvent was used as reference (δ [chemical shift]=7.24 ppm) for evaluation of signals derived from C**H$_2$**-C**H$_2$**-NH and CH_2-CH_2-N**H**. α-Methyl ω-hydroxy poly(2-ethyl-2-oxazoline) was used as control compound for showing complete hydrolysis. GPC analysis was conducted with a GPC/HPLC system equipped with a Catsec-300 column, a UV-Vis and a multiangle light scattering DAWN EOS (Wyatt; Germany) detector. GPC was done with 0.1 % TFA at a flow rate of 0.2 mL/min. For preparing stock solutions used for conjugate synthesis or polyplex generation LPEI was resuspended in water and pH was set to 7.4 with HCl and NaOH. The resulting product was then filtered through a 0.2 µm cellulose acetate membrane. Concentration of LPEI content in aqueous solutions was determined by $CuSO_4$ assay based on UV/Vis spectrophotometry like described elsewhere.[2] For long term storage LPEI was either stored as lyophilized powder under dry conditions at room temperature or dissolved in water at pH 7.4 at -80 °C.

Peptide synthesis

The peptide with the amino acid sequence CYESIKVAVS was synthesized on a semi-automated Biotage Initiator+ system (Sweden). The synthesis setup was based on using Fmoc protected L-amino acids and a ChemMatrix® resin functionalized with Rink-amide linker as solid phase. For every coupling step amino acids were C-terminally activated with 1-hydroxybenzotriazole hydrate (HOBt; 1 eq based on amino acid) and 2-(1H-Benzotriazole-1-yl)-1,1,3,3-tetramethylaminium tetrafluoroborate (TBTU; 1 eq based on amino acid) under addition of N,N-Diisopropylethylamine (DIPEA; 2 eq based on amino acid). The C-terminal amino acid (Fmoc-L-Serin-tBu) was used in a five-fold excess based on the binding capacity of the resin. All following activated amino acids were used in a 2.5-fold excess. Coupling steps of all activated amino acids

except activated Fmoc-L-cysteine-Trt were conducted at a temperature of 75 °C for 10 minutes. Coupling of activated Fmoc-L-cysteine-Trt was done twice at 45 °C for 10 minutes. For detection of free terminal primary amino groups Kaiser (ninhydrin) test was conducted after each coupling step.[3] Deprotection of the N-terminus of the growing peptide chain was conducted with piperidine (20 % (V/V) in DMF) twice for 3 minutes at a temperature of 75 °C. Cleavage of the peptide from the resin was done with trifluoracetic acid (TFA):phenol:water:triisopropylsilane (88:5:5:2) for 4 hours at room temperature under vigorous mixing. The solution was then concentrated under vacuum and the product was precipitated with cold diethyl ether. After washing the precipitate with diethyl ether by centrifugation the product was redissolved in water and lyophilized. Purification was conducted by reversed phase chromatography on a Shimadzu HPLC system (Austria) equipped with a Zorbax® 5B-C18 column (21.2 mm x 25 cm). For purification a linear gradient with an increasing concentration of acetonitrile (acidified with 0.1 % TFA) in water (acidified with 0.1 % TFA) starting from 5 to 50 % over 30 minutes at a flow rate of 21 mL/min was chosen. Detection was done at a wavelength of 215 nm. Fractions containing CYESIKVAVS were pooled and lyophilized. Peptide purity was analyzed both by HPLC and high resolution mass spectrometry (HRMS). The analytical HPLC system was equipped with a Thermoquest hypersil division C18 column (Thermo Fisher scientific; Germany) and the same gradient as described before at a flow rate of 1 mL/min was used. HRMS was employed for analysis of purity and amino acid sequence at a sample concentration of 10 µg/mL in 50 % (V/V) ACN (in 0.1 % (V/V) formic acid) with a Bruker maXis Hd system (US). Peptide sequencing was conducted based on single and double charged b- and y-fragments. For further procedure only CYESIKVAVS with a purity of >95 % (based on HPLC) was used.

Supplemental References

1. Rödl, W, Schaffert, D, Wagner, E, and Ogris, M (2013). Synthesis of polyethylenimine-based nanocarriers for systemic tumor targeting of nucleic acids. *Methods Mol Biol* **948**: 105-120.

2. Ungaro, F, De Rosa, G, Miro, A, and Quaglia, F (2003). Spectrophotometric determination of polyethylenimine in the presence of an oligonucleotide for the characterization of controlled release formulations. *J Pharm Biomed Anal* **31**: 143-149.

3. Kaiser, E, Colescott, RL, Bossinger, CD, and Cook, PI (1970). Color test for detection of free terminal amino groups in the solid-phase synthesis of peptides. *Analytical Biochemistry* **34**: 595-598.

2.4. Auropolyplex: a versatile nanotherapeutic platform for efficient nucleic acid delivery in vitro and in vivo

*Cover Letter

universität wien

Fakultät für Lebenswissenschaften

Univ.Prof. Dr. Manfred Ogris
Department für Pharmazeutische Chemie
Althanstraße 14
A-1090 Wien
m.ogris@univie.ac.at
T +43 (1) 4277-55551
F +43 (1) 4277-95 51

http://klinischepharmazie.univie.ac.at/mmctresearch/

To
Prof Stefaan De Smedt
Editor Journal of Controlled Release

Vienna, 22.10.2018

Dear Prof De Smedt,

We would like to submit our manuscript entitled **‚Auropolyplex: a versatile nanotherapeutic platform for efficient nucleic acid delivery in vitro and in vivo'** authored by Alexander Taschauer, Wolfram Polzer, Stefan Pöschl, Slavica Metz, Nathalie Tepe, Simon Decker, Norbert Cyran, Julia Maier, Hermann Bloß, Martina Anton, Thilo Hofmann, Manfred Ogris and Haider Sami, as a **research article**. Corresponding authorship should be shared between Manfred Ogris and Haider Sami.

In this work, we present a nanotherapeutic platform based on gold nanoparticles for efficient siRNA delivery, target knockdown and in vivo siRNA release, which overcomes several shortcomings associated with current nanoformulations for nucleic acid therapy. Polycation is directly attached to the gold surface by chemisorption, and in two consecutive complexation steps, nanoparticles (termed auropolyplexes) are formed with exceptionally high and tunable loading capacity. This nanotherapeutic platform enabled us to develop upscaled formulations also suitable for in vivo delivery and potential preclinical testing. Auropolyplexes were comprehensively characterized for biophysical properties, cell uptake and intracellulary delivery. Target knockdown was highly efficient in vitro. When auropolyplexes were applied intratracheally into the lungs of mice, siRNA was clearly released from the gold nanoparticles as tracked by optical tomography and mass spectrometry. Thus, auropolyplexes are a facile and versatile nano-formulation with high and tunable siRNA loading, superior gene knockdown attributes, and possess the potential to be an efficacious multifunctional nanomedicine platform for siRNA delivery. In our view, this work covers several disciplines ranging from polymer chemistry, nanotechnology, nucleic acid therapy, to in vivo studies for pulmonary delivery by employing

molecular and morphological imaging. Therefore, we think that this manuscript fits into the scope of The Journal of Controlled Release.

Supporting information has been uploaded and contains additional experimental results supporting the content of the main manuscript. We would like to suggest the following potential reviewers:

Name	e-mail	Expertise
Tom Anchordoquy	Tom.Anchordoquy@ucdenver.edu	Lipid based nanoparticle and their in vivo application
Claus-Michael Lehr	lehr@mx.uni-saarland.de	Lung delivery of nanomedicines
Antoine Kichler	kichler@unistra.fr	Nanoparticle and polymer based nucleic acid delivery
Olivia Merkel	olivia.merkel@lmu.de	Pulmonary delivery of nanosystems
S. Moein Moghimi	seyed.moghimi@newcastle.ac.uk	Nanomedicines and toxicological considerations

We confirm that the manuscript is being solely submitted to this journal and is not under consideration elsewhere. We also confirm that the manuscript has been approved and reviewed by all included authors.

We are looking forward for your favourable consideration!

Yours sincerely

Manfred Ogris

Professor for Pharmaceutical Sciences
Department of Pharmaceutical Chemistry
University of Vienna
Althanstraße 14
A-1090 Vienna, Austria
m.ogris@univie.ac.at

Haider Sami

Groupleader Nanobiomaterials
Department of Pharmaceutical Chemistry
University of Vienna
Althanstraße 14
A-1090 Vienna, Austria
haider.sami@univie.ac.at

Auropolyplex: a versatile nanotherapeutic platform for efficient nucleic acid delivery in vitro and in vivo

Alexander Taschauer[1], Wolfram Polzer[1], Stefan Pöschl[1], Slavica Metz[1], Nathalie Tepe[2], Simon Decker[1], Norbert Cyran[3], Julia Maier[1], Hermann Bloß[1], Martina Anton[4], Thilo Hofmann[2], Manfred Ogris[1,5*], Haider Sami[1*]

[1] Laboratory of MacroMolecular Cancer Therapeutics (MMCT), Center of Pharmaceutical Sciences, Department of Pharmaceutical Chemistry, University of Vienna, Althanstrasse 14, A-1090 Vienna, Austria

[2] Department of Environmental Geosciences, University of Vienna, Althanstraße 14, 1090 Vienna, Austria

[3] Core Facility Cell Imaging and Ultrastructure Research (CIUS), University of Vienna, Vienna, Austria

[4] Institutes of Molecular Immunology and Experimental Oncology, Klinikum rechts der Isar, Technische Universität München, Munich, Germany

[5] Center for NanoScience (CeNS), Ludwig Maximilians University, Munich, Germany.

*Corresponding authors

Email: haider.sami@univie.ac.at; m.ogris@univie.ac.at

Abstract

Nanomedicine has significant potential to achieve the goals of nucleic acid therapy. Current nucleic acid nanotherapeutic approaches face challenges because of shortcomings in terms of either loading control/efficiency and yield, or limited intracellular uptake, endosomal-trapping, and hampered release. Here we report a versatile nanotherapeutic platform, termed auropolyplexes, for improved and efficient delivery of small interfering RNA (siRNA). A simple two-step complexation method offers tunable loading of siRNA at concentrations relevant for *in vivo* studies and the flexibility for inclusion of multiple functionalities, like shielding polymers. Semitelechelic, thiolated linear polyethylenimine was chemisorbed onto gold nanoparticles to endow them with positive charge. siRNA was electrostatically complexed with these cationic gold nanoparticles and further condensed with polycation or conjugates with polyethylene glycol. The resulting auropolyplexes ensured complete complexation of siRNA into nanoparticles with high load of approx. 15,500 siRNA molecules/nanoparticle. After efficient internalization into tumor cell, 80 % knockdown of luciferase reporter gene was achieved. Auropolyplexes labelled with near infrared fluorescent dye were applied intratracheally into the lung of Balb/c mice and their biodistribution studied spatiotemporally by optical tomography. Auropolyplexes were well tolerated with 20 % of the siRNA dose remaining in lungs after 24 h. Importantly, released siRNA also crossed the air-blood barrier and was excreted via kidneys, whereas >97 % of the gold nanoparticles were retained in the lung. Taken together, auropolyplexes represent a versatile and upscalable nanogold based platform for siRNA delivery *in vitro* and *in vivo*. Using molecular conjugates, shielding and targeting moieties can be conveniently added.

Keywords: Gold nanoparticle, linear polyethylenimine, siRNA knockdown, pulmonary delivery, intratracheal, tomographic optical imaging, biodistribution

Introduction

Nanotechnology has the potential to overcome current challenges associated with nucleic acid based therapeutics and is an active area of nanomedicine application. Pre-clinical and clinical translation of nucleic acid based nanomedicines is decisively dependent on factors including, but not limited to, loading efficiency, yield and scale-up, effective delivery to target organ/cells and successful endosomal escape. [1-3] These crucial factors should be considered already during the design and development phase of formulations to ensure translation at later stages. Most of the existing nano-formulations for short nucleic acids, like short interfering RNA (siRNA) fall in one of the following categories- 1) layer-by-layer (LBL) self-assembly to include siRNA as one of the layers, 2) encapsulation/conjugation of siRNA within/to the carrier system, and 3) electrostatic complexation of siRNA with cationic moieties to form complexes (polyplexes, lipoplexes, etc.). In case of LBL, despite the versatility and other advantages for designing nanosized vehicles for siRNA delivery [4, 5], it is associated with challenges like low yield and repeated purification steps at each layer synthesis thereby drastically limiting scale-up [6] and control on siRNA loading efficiency. Additionally, in case of LBL-coated nanoparticles (NPs) it is preferable to have reduced number of layers [7, 8] which further limits the total amount of loaded siRNA. Within the second category, siRNA can be encapsulated within lipid based nanoparticles which are considered clinically relevant and potent delivery systems [9] or chemically conjugated to the nano-carrier or polymer or ligand. [10] The chemisorption of thiolated-siRNA directly onto the surface of gold nanoparticles to form spherical nucleic acids is a very promising approach. [11] However, in this case intracellular release of siRNA can be limiting as it has been observed that thiolated nucleic acid is still bound to the gold NP surface after delivery into cells, [12] hence limiting access to the cytoplasmic transcriptional machinery. Polyplexes can overcome such limitations by offering desirable yields, scalability [13] and control on loading efficiency, as all of the nucleic acid is complexed. Also, polyplexes can be generated at high concentrations for *in vivo* applications [13] and enable multiple functionalization with shielding domains (like polyethylene glycol), targeting ligands and endosomolytic agents [14] for pre-clinical and clinical relevance. Endosomal escape is achieved with polymers like polyethyleneimine (PEI), both in linear (LPEI) or branched (BPEI) formats. For siRNA knockdown studies, BPEI based polyplexes often show better results in comparison to LPEI. [15] However, LPEI is preferable due to a more biocompatible profile, [16] although this also highly depends on the molecular weight used. [17] Considering these current approaches and their associated challenges, it is desirable to have formulations which can address these limitations so as to deliver required amounts of siRNA to the target organ. *In vivo* imaging can significantly assist in

development of nucleic acid based therapies by deciphering important delivery and therapy concepts like quantification of retention in target organ, bio-distribution events, transfection efficiency, etc. This helps in optimizing delivery agents and their routes of administration, and also identifying bottlenecks. We have established an imaging based method for spatiotemporal tracking of non-encapsulated siRNA *in vivo* by near infrared fluorescence imaging, along with fluorescence imaging tomography (FLIT) and X-ray absorption computed tomography (CT). [18] The present study combines the advantages of electrostatic complexation approach with chemisorption on gold nanoparticles to develop a LPEI based novel formulation, termed as auropolyplexes, for efficient siRNA delivery *in vitro* and *in vivo* (Scheme 1). Towards this, gold nanoparticles were functionalized with thiolated LPEI to make a cationic nanocarrier and used for complexing with siRNA to generate auropolyplexes by a facile and convenient two-step complexation procedure. This ensures complexation of total siRNA as confirmed by gel retardation studies, thereby giving precise control on loading efficiency. The second complexation step is also for inclusion of excess LPEI to provide enough cationic charge for sufficient cell uptake and appropriate endosomal escape rate, as these are crucial rate-limiting steps in siRNA delivery. [1, 19] Nanoparticle tracking analysis and transmission electron microscopy ensured detailed biophysical characterization (size and ζ-potential) of the process of auropolyplex formation. Tunability of siRNA loading is demonstrated by preparing auropolyplexes at siRNA concentration of 10 µg/mL and 133 µg/mL for *in vitro* and *in vivo* experiments respectively, which also corresponded to a high loading of siRNA per nanoparticle. To demonstrate the flexibility of the formulation approach, PEGylated LPEI (instead of LPEI) was used at the second complexation step to provide 'stealth' attributes for potential *in vivo* applications. Flow cytometry and confocal microscopy based studies established successful cellular uptake of auropolyplexes indicating successful intracellular delivery of siRNA. Luciferase gene reporter assay revealed superior gene knockdown efficiency for auropolyplexes (in comparison to polyplexes) demonstrating their functionality for gene regulation. AlexaFluor® 750 (AF750)-siRNA based auropolyplexes were microsprayed intratracheally and biodistribution of AF750-siRNA was spatiotemporally tracked by employing three-dimensional imaging techniques based on near-infrared fluorescence imaging and contrast agent enhanced X-ray absorption computed tomography (Scheme 1). Biodistribution of gold was studied by inductively coupled plasma mass spectrometry to compare with siRNA's biodistribution, so as to decipher *in vivo* release of siRNA from the auropolyplexes. This work presents auropolyplexes as a facile and versatile nano-formulation with tunable siRNA loading for both *in vitro* and *in vivo* experiments

and superior gene knockdown attributes, which has the potential to be an efficacious multifunctional nanomedicine platform for siRNA delivery.

Scheme 1

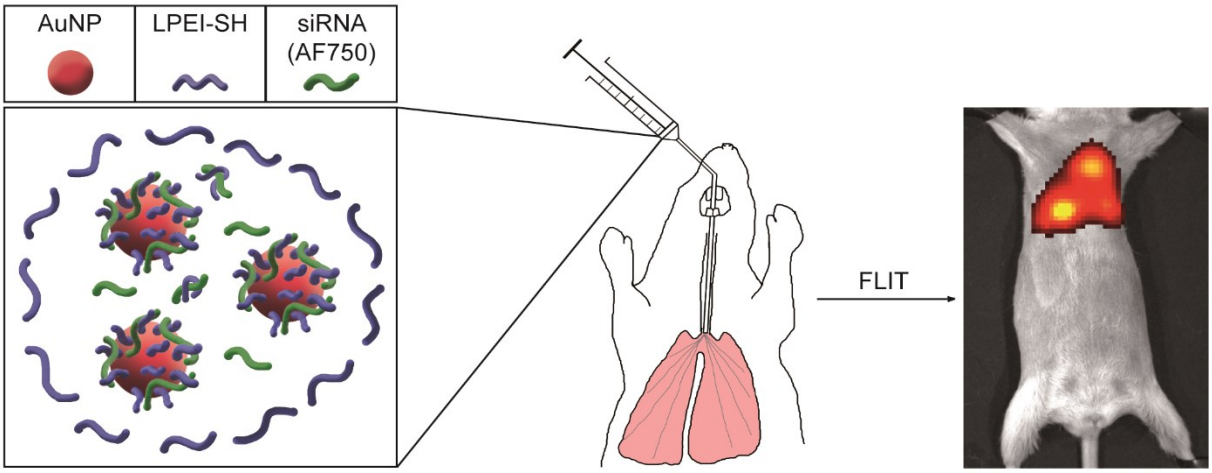

Scheme 1: *Schematic illustration of auropolyplexes and their pulmonary delivery by microspray-based aerosolization. In vivo biodistribution of the fluorescently labeled auropolyplexes was studied by fluorescence imaging tomography (FLIT), X-ray absorption computed tomography, and inductively coupled plasma mass spectrometry.*

Materials and Methods

Materials

All siRNA samples used in this study were kindly supplied by GlaxoSmithKline (GSK; UK). The siRNA for knockdown of firefly luciferase (anti-luc siRNA) with the sequence 5´-CUUACGCUGAGUACUUCGAdTdT-3´ (sense strand) has two phosphorothioate bonds on the 3´ terminus of the sense strand and one 3´ terminal phosphorothioate bond on the antisense strand (MW (duplex): 14,384 Da). The siRNA used as a negative control (control siRNA) with the sequence 5´-AUCGUACGUACCGUCGUAUdTdT-3´ (sense strand) shows two phosphorothioate bonds on the 3´ terminus of both sense and antisense strand (MW (duplex): 14,468 Da). Labelled negative control siRNA was generated by coupling AF647 or AF750 to the 3´ terminus of the sense strand using N-hydroxysuccinimide (NHS) based chemistry. In the following sections labelled siRNA is described as AF647-siRNA and AF750-siRNA. OPSS-PEG-NHS (3-(2-pyridyldithio)propionamide-PEG-N-hydroxysuccinimide ester) (Mw 2,000 Da) was purchased from Rapp Polymere (Germany). All further compounds used for synthesis, for physicochemical and biological evaluation were purchased from Sigma Aldrich (Austria). All polymer and buffer solutions were filtered through 0.22 µm cellulose acetate filters prior to use. Water was purified with a Sartorius Arium Pro system (Germany). TrypLE® Express for cell detachment was purchased from ThermoFisher Scientific (Germany) and passive lysis buffer from Promega (Germany).

Methods

Synthesis of LPEI.HCl (linear polyethylenimine as HCl salt)

Both α-Benzyl-ω-thiol LPEI (Mn 5,000 Da).HCl and α-Methyl-ω-hydroxy LPEI (Mw 10,000 Da).HCl were synthesized based on a previously described method. [20] The molecular weights stated refer to free base of the respective polymer. Briefly, 2 g of either α-Benzyl-ω-thiol poly(2-ethyl-2-oxazoline) or α-Methyl-ω-hydroxy poly(2-ethyl-2-oxazoline) were dissolved in 50 mL HCl (7 M) and heated under reflux for 16 hours. α-Benzyl-ω-thiol LPEI.HCl (described later as LPEI5-SH.HCl) or α-Methyl-ω-hydroxy LPEI.HCl (described later as LPEI10.HCl) formed a white precipitate which was further purified by centrifugation. After three washing steps with 7 M HCl, the precipitate was dissolved in 100 mL water and lyophilized. Quality control of compounds dissolved in D_2O was conducted by ^{1}H-NMR on a Bruker Avance 200 MHz system (Bruker, Billerica, USA). Chemical shifts (δ) expressed in parts per million (ppm) were analyzed using the peak derived

from the solvent as reference. In case of α-Benzyl-ω-thiol LPEI.HCl the ratio between LPEI and free thiol groups was evaluated by copper assay and Ellman´s assay as described. [20, 21] LPEI5-SH.HCl was stored for long term under dry conditions at room temperature to reduce the probability of thiol oxidation. Stock solutions in water were stored at -20 °C for not longer than 2 months, where no decrease of free thiol content could be detected.

Synthesis of LPEI (Mw 10,000 Da)-PEG (Mw 2,000 Da)-cysteine conjugate (LPEI10-PEG)

Conjugation of PEG to LPEI was conducted based on the protocol by Schaffert et al. [22] In brief, 1 g LPEI10.HCl was suspended in 20 mL NaOH (1 M). LPEI10 precipitated as free base. The mixture was heated under reflux and NaOH (1 M) was added in small portions until LPEI10 was entirely dissolved. After cooling down to room temperature, the white precipitate was purified by centrifugation and washed with 1 M NaOH and water. LPEI10 was resuspended in 30 mL water and lyophilized. For PEGylation, LPEI10 was dissolved in 1.5 mL dry ethanol, mixed with 100 µl NHS-PEG-OPSS (2 equivalents based on LPEI) in dry dimethyl sulfoxide and incubated for 3 h at 35 °C under continuous mixing. The reaction was quenched with 100 µl Tris.HCl (1 M; pH 8.0). The product was purified by ion exchange chromatography (MacroPrep High S; BioRad, US; column HR10/10) using an ÄktaPure system (GE Healthcare; Germany) applying a NaCl gradient of 0.5 M to 3 M in 20 mM aqueous HEPES solution (pH 7.4). Fractions containing LPEI-PEG-OPSS were pooled, dialyzed against water for 24 h and lyophilized. Thereafter, LPEI-PEG-OPSS was dissolved in 2 mL 20 mM HEPES/10 % acetonitrile (pH 7.4; degassed) and mixed with a solution of L-cysteine (5 equivalents based on OPSS) in 20 mM HEPES/10 % acetonitrile (pH 7.4; degassed). The reaction was monitored by analyzing the amount of released 2-thiopyridone (absorption maximum at 343 nm) by UV/Vis spectrophotometry every 30 minutes until no change in the absorption could be detected. The conjugate was purified by ion exchange chromatography, dialyzed and lyophilized as described above. LPEI10-PEG was analyzed by ^{1}H-NMR on a Bruker Avance 200 MHz system. PEGylation degree was evaluated correlating the integral of PEG signal [C**H$_2$**-C**H$_2$**-O; δ (ppm)=3.72] with the integral of LPEI signal [C**H$_2$**-C**H$_2$**-N; δ (ppm)=3.06].

Synthesis of cationic gold nanoparticles

Synthesis of gold nanoparticles was conducted based on the modified procedure by Frens [23, 24] For this, 25 mL of a 0.01 % (w/V) $HAuCl_4$ solution in water was heated to 100 °C and then mixed with 180 µL of an aqueous sodium citrate solution (1 % [w/V]). The color of the solution changed gradually from faint yellow to red. The reaction mixture was stirred at 100 °C until no

further color change could be observed. After cooling down to room temperature the product quality was evaluated by analyzing the particle size by nanoparticle tracking analysis (NTA) with a NanoSight NS500 system (Malvern, UK). The solution was kept at room temperature until further usage. For surface functionalization of gold nanoparticles (AuNP) with LPEI5-SH, the AuNP solution was adjusted to pH 8 by adding small portions (3-5 µl) of NaOH (1 M) under vigorous stirring. Thereafter, a stock solution of LPEI5-SH dissolved in water (pH 8) was added under constant stirring to obtain a final LPEI5-SH concentration of 0.229 mM. This mixture was incubated at room temperature for 72 h. Changes in the AuNP derived SPR before and after coating was analyzed by UV-Vis spectrophotometry of the undiluted samples. For purification, 18 mL of this solution were centrifuged in 1 mL aliquots for 10 min at 5,000 x *g* and 4 °C and washed with 1 mL water per aliquot till there was no free LPEI detected in the supernatant applying the copper assay [21]. Finally, pellets were pooled and reconstituted in water with a final volume of 400 µl. The resulting cationic AUNP are referred to "AL". Nanoparticles were stored until further usage at room temperature for up to one week.

Auropolyplex generation

For *in vitro* experiments, complexation was conducted using water as diluent for siRNA and LPEI, whereas for *in vivo* experiments HBG (HEPES buffered glucose; 20 mM HEPES/5 % glucose at pH 7.4) was used. For auropolyplex synthesis, equal volumes of a solution containing siRNA (conc. [*in vitro*] 40 µg/mL siRNA; conc. [*in vivo*] 533 µg/mL) and AL stock (described above) were mixed by flash pipetting. The mixture of AL with siRNA is termed "ALS". After an incubation for 45 minutes at room temperature, equal volumes of ALS and a solution containing LPEI (conc. [*in vitro*]: 10 µg/mL; conc. [*in vivo*]: 267 µg/mL) were mixed by flash pipetting. The mixture was again incubated for 45 min at room temperature until further usage. The resulting solution is described as "ALSL5-SH" (for LPEI5-SH as last layer), "ALSL10" (for LPEI10 as last layer) or "ALSL10-PEG" (for LPEI10-PEG as last layer). To reach the same final siRNA and AL concentration a 1:2 dilution of "ALS" was used as control substance both for physicochemical as well as for *in vitro* evaluation of components.

Polyplex generation

Polyplex synthesis was conducted in principle as described. [20] Water was used as diluent for all components. In brief, equal volumes of a siRNA containing solution (20 µg/mL) and a LPEI (LPEI5-SH or LPEI10) containing solution were mixed at a N/P ratio of 4 by flash pipetting. For LPEI based polyplexes water was used as a diluent. Polyplexes based on branched polyethylenimine

(BPEI; Mw: 25,000 Da) were used as control compound for cell binding/uptake and for knock down studies at N/P 10 in HBS (HEPES buffered saline; 20 mM HEPES/150 mM NaCl at pH 7.4).

Gel retardation assay

Auropolyplexes were generated using different concentrations of siRNA (anti-luciferase siRNA or AF750-siRNA) and different amounts of LPEI (LPEI5-SH or LPEI10). Auropolyplexes with anti-luciferase siRNA and LPEI5-SH were prepared in water reaching a final siRNA concentration of 10 µg/mL. For *in vivo* setup, AF750-siRNA and LPEI10 were prepared in HBG at a final siRNA concentration of 133 µg/mL. 200 ng of free or complexed siRNA were loaded onto a 1.5 % agarose gel sodium borate buffer (pH 8) together with $1/6^{th}$ volume of 60 % (V/V) glycerol as loading buffer. For nucleic acid staining ethidium bromide (EtBr) was used at a concentration of 0.5 µg/mL. Gel electrophoresis was carried out in sodium borate buffer (pH 8) at 80 V for 60 minutes. Imaging was conducted on a ChemiDoc MP system (Biorad, Vienna, Austria).

Nanoparticle tracking analysis (NTA)

Size and ζ-potential measurement by NTA was carried out in principle as described. [13] For size and concentration measurements, nanoparticles were diluted in the medium used for synthesis (water or HBG), for ζ-potential measurements in 2.5 mM NaCl. A dilution factor was chosen to obtain a particle concentration of 10^8 to 10^9 nanoparticles/mL, which correlates to 10 to 100 nanoparticles per frame. For size measurement, five videos with a duration of 60 seconds were acquired. In case of ζ-potential measurement capture duration was 90 seconds and secondary duration was 30 seconds. ζ-potential was measured applying 24 V. For evaluating ζ-potential of nanoparticles, only measurements with a coefficient of correlation of at least 0.95 were considered for further analysis. AL were analyzed by NTA after purification (by centrifugation) while all other samples were analyzed directly without purification.

TEM (Transmission electron microscopy)

For TEM every formulation was prepared in water as described above. 5 µL undiluted sample was deposited onto formvar coated copper grids and dried overnight at room temperature. Imaging was done on a Libra 120 system (Zeiss, Germany) with LaB^6 filament and in column filter operating at 120 kV, using a bottom mount camera Sharp:eye TRS (2 × 2 k) and an in column camera Morada G2 (11 MP). Magnifications ranged from 8,000 – 200,000-fold.

Cell culture and transduction

MDA-MB-231 human breast cancer cells (ATCC HTP-26) were cultured in DMEM (Dulbecco´s modified Eagle medium) supplemented with 10 % fetal bovine serum, L-glutamine and antibiotics (penicillin/streptomycin) and lentivirally transduced with PGK-EGFPLuc as described previously [25] to obtain MDA-MB-231Luc cells. EGFP-positive cells were sorted using a BD FACSAria II cell sorter (Becton-Dickinson, US). MDA-MB-231Luc cells were used for all cell culture experiments.

Flow cytometry

$5x10^4$ MDA-MB-231Luc cells per well were seeded into a transparent 96 well plate 24 h prior to treatment. All formulations were prepared using AF647-siRNA and added to cells at 2 or 4 µg/mL (based on siRNA) in basal DMEM high glucose medium. Medium supplemented with 10 % FCS, L-glutamine and antibiotics (Penicillin/Streptomycin) was added after 4 h incubation. After total 24 h, cells were washed twice with DPBS, trypsinized with TrypLE® Express as per manufacturer´s instructions, resuspended in DPBS and transferred into a PCR plate (Nerbe, #04-083-0150; Germany). Plates were kept at 4 °C for the whole measurement using an Inheco CPAC cooling unit (INHECO, Germany) when analyzed on a MacsQuant® Analyzer 10 (Miltenyi Biotec, Bergisch-Gladbach, Germany). For live/dead analysis, DAPI was used at a concentration of 1 µg/mL (405 nm excitation; 450/50 nm band pass emission filter). In total 15,000 gated live cells were analyzed per well. AF647 signal was acquired in the R1 channel (635 nm excitation, 655-730 nm band pass emission filter). Data were analyzed using FlowJo 10.1r5 (FlowJo LLC, Ashland OR 97520, USA).

Binding-/Uptake analysis by CLSM (Confocal Laser Scanning Microscopy)

$5x10^4$ MDA-MB-231Luc cell per well were seeded into chamber slides (Nunc® Lab-Tek® II 8-well slides; ThermoFisher Scientific, Germany) 24 h before treatment. Cells were incubated with formulations based on AF647 labelled siRNA (4 µg/mL) further treated as described above for flow cytometry. After 24h cells were washed thoroughly with DPBS and fixed with 4 % formaldehyde in HBS (pH 7.4) for 30 minutes at room temperature. Cell nuclei were stained with DAPI (2 µg/mL) and samples mounted with Vectashield® antifade mounting medium. Image acquisition was performed on a Leica TCS SPE microscope (Leica, Wetzlar, Germany) with a 63X oil immersion objective (NA 1.3) using a 405 nm laser excitation for DAPI, 488 nm for EGFP and 635 nm for AF647. Emission ranges were tuned for optimal collection of emitted light as per the respective fluorophore. Z-scans were conducted with a vertical resolution of 0.1 µm. Differential

interference contrast (DIC) was used for transmitted light pictures. Further analysis of the acquired pictures was done with LasX software Version 3.1.2.16221 (Leica).

In vitro gene knock-down by firefly luciferase assay

$2x10^4$ MDA-MB-231Luc cells per well were seeded into a transparent 96-well plate 24 h before treatment. All formulations were prepared using anti-luc siRNA or control siRNA and added to cells at 2 or 4 µg/mL (based on siRNA) and further treated as described above for flow cytometry. After a total of 48 h, cells were washed with DPBS and lysed with 30 µl passive lysis buffer. 10 µl of the lysate were analyzed for luciferase activity using luciferase assay reagent (LAR). [26] Luminescence was measured using an Infinite® M200 system (Tecan, Grödig, Austria).

In vivo biodistribution by fluorescence imaging tomography (FLIT) and X-ray absorption computed tomography (CT)

All animal procedures were approved by local ethics committee and are in accordance with the Austrian law for the protection of animals and the EU directive 2010/63/EU. Female Balb/cJRj mice (Janvier Labs, Le-Genest, France) were housed under specified pathogen free (SPF) conditions in individually ventilated cages (Type 2L, Tecniplast, Hohenpeißenberg, Germany) with food and water ad libitum and a 12 h/12 h light/dark cycle. Mice were kept on low fluorescent diet (AIN-76A; Brogaarden Korn & Foder ApS; Denmark) for at least 10 days before treatment. ALSL containing total 10 µg of AF750-siRNA was applied by intratracheal administration using a Microsprayer®/Syringe Assembly (MSA-250-M; PennCentruy, Inc; USA). Before administration to animals influence of the microspraying process on auropolyplexes was analyzed by NTA. Animals were imaged on an IVIS Spectrum CT system (PerkinElmer, USA) immediately after drug administration and 24 h thereafter in principle as described. [18] 2D imaging was conducted in epifluorescence mode using the following excitation (Ex) and emission (Em) filter settings: Ex 640 nm with Em 680 nm, 700 nm, 720 nm, 740 nm, 760 nm; and Ex 675 nm with Em 720 nm, 740 nm, 760 nm, 780 nm, 800 nm. To ensure proper background subtraction, treated and untreated animals were imaged side-by-side. Analysis was done by spectral unmixing. For 3D CT imaging the following fluorescence filter settings were used in transillumination mode: Ex 675 nm (30 nm BW) and Em 720 nm (20 nm BW). 300 µl of a 1:1.5 mixture of Scanlux® (active component: Iopamidol [300 mg iodine/mL]; Sanochemia, Vienna, Austria) with 5 % glucose were used as CT contrast agent. After the last imaging session, animals were sacrificed and *ex vivo* organ imaging was done in 2D epifluorescence mode using settings

described above but without spectral unmixing. Lungs, liver, spleen, kidneys and stomach were stored at -80 °C until further analysis by ICP-MS.

Inductively coupled plasma-Mass spectrometry (ICP-MS)

Lungs, heart, liver, spleen, kidneys and stomach were cut into 3-5 mm fragments and digested in 8 mL inverse aqua regia at 100 °C for 1 h. Each sample was then treated with 15 mL HNO_3 conc. at 180 °C for one further hour. For dissolving gold nanoparticles 10 mL of aqua regia were added and the mixture incubated at 100 °C for 1 h. All samples were finally diluted to a total mass of 40 g with purified water. Samples prepared following the same procedure without any tissue were used as blank for ICP-MS measurements. Total dissolved gold concentration (^{197}Au) measurements were conducted with a 7900 ICP-MS unit (Agilent; US) and ^{209}Bi was used as internal standard. To evaluate total dissolved gold concentrations, the ICP-MS was calibrated with dissolved gold standards ranging from 5 ng/L to 50 µg/L prepared from a single element gold standard (1000 µg/mL; CGAUN1-125ML; Inorganic Ventures, Christiansburg, VA, USA). The acid blanks show a lower limit of detection (LOD; 3 x standard deviation + mean) of 5.09 ng/L and a lower limit of quantification (LOQ; 10 x standard deviation + mean) of 11.4 ng/L.

Results and discussion:

Gold nanoparticles are often surface modified by ligand exchange reaction using thiol containing organic compounds. For example, use of 11-mercaptoundecanoic acid (MUA) results in a negatively charged surface. [27] For use in nucleic acid delivery, cationic nanoparticles are employed for binding polyanionic nucleic acids, e.g. siRNA. Here, we employed thiol terminated LPEI to synthesize cationic gold nanoparticles (Figure 1A) for auropolyplex generation. This allowed direct ionic complexation of siRNA, thereby avoiding extensive purification steps and also enabling a simpler formulation approach.

Cationic gold nanocarrier for auropolyplex generation

Citrate stabilized gold nanoparticles were synthesized according to a protocol from Wurster et al. [8], originally based on the report by Frens. [23] Synthesis reproducibly resulted in monodisperse AuNPs with an average size of 68.5 +/- 2.8 nm as measured by NTA and visualized by TEM (Figure 1B-C). UV-Vis spectroscopy of AuNPs demonstrated the presence of characteristic surface plasmon resonance (SPR) with absorption wavelength maximum at 530nm (Figure S1), which matches with the reported data. [8] Gold nanoparticles were directly surface functionalized with thiol terminated LPEI (LPEI5-SH) (Figure 1A). LPEI-SH with a number average molecular weight of 5,000 Da was synthesized as hydrochloride salt by acidic hydrolysis of ω-thiol terminated poly(2-ethyl-2-oxazoline) with 6 M HCl. ^{1}H-NMR analysis of LPEI5-SH.HCl revealed complete cleavage of the side chain from α-Benzyl-ω-thiol poly(2-ethyl-2-oxazoline), C**H$_3$**-CH$_2$-CO [δ (ppm)=1.12-1.05] and CH$_3$-C**H$_2$**-CO [δ (ppm)=2.45-2.33], therefore showing full conversion of the precursor to thiol terminated LPEI (Figure S2). Thiol content of LPEI was evaluated by Ellman´s assay showing a thiol:LPEI ratio of 1:6. Surface functionalization of AuNPs with LPEI5-SH was carried out by ligand exchange method and the successful formation of cationic AuNPs (here referred to as “AL”) characterized by UV-Vis spectroscopy, NTA and TEM. On addition of LPEI5-SH to AuNPs, the characteristic SPR band shifted to an absorption maximum of 535nm (Figure S1) indicating an increase of particle size and/or the chemisorption of LPEI5-SH to the surface. Centrifugation based purification allowed the removal of all unbound LPEI and increased the concentration to an average of 2.32 x 10^{11} +/- 6.28 x 10^{09} nanoparticles/mL. Cationic AuNPs (AL) remained small (71 +/- 2.8 nm by NTA) indicating absence of any aggregation during the ligand exchange and purification step (Figure 1B). A change of the average ζ-potential from -27 mV for citrate stabilized AuNPs to +37 mV for cationic AuNPs indicated successful assembly of LPEI5-SH on surface of AuNPs (Figure 1B). More than 90 % of the gold nanoparticles were positively charged (Figure S3), indicating a homogeneous preparation of cationic AuNPs. TEM based visualization indicated an average coating thickness of

6 nm +/- 1.8 nm (29 fields of view analyzed) (Figure 1D). As there was only a minor size increase, we speculate that the LPEI layer rather appears in a 'mushroom' state, i.e. not stretched like it would be in a 'brush' like structure. This is in accordance with the published literature: the hydrodynamic radius of non-aggregated LPEI (Mw 2,500 Da) has been reported to be 2.5 nm, while the calculated contour length (stretched out) of a 5 kDa LPEI molecule is approx. 38 nm. [28] In case of PEG attached to AuNP it has been observed that with increasing PEG density the hydrodynamic diameter increases and the brush structure occurs. [29, 30] Nevertheless, in our case the coating density was appropriate to sufficiently stabilize the purified nanoparticles for at least 5 days at room temperature, indicating considerable stability. Positive ζ-potential (Figure 1B) along with TEM visualization (Figure 1D) confirmed successful synthesis of cationic AuNP. Due to the post-grafting with LPEI5-SH, AuNP remained spherical and homogeneous in size. This is in contrast to a one-step synthesis process, where thiolated PEI is already mixed with $HAuCl_4$ during the nucleation process. [31] The latter procedure rather leads to nanoparticles heterogeneous in size and shape.

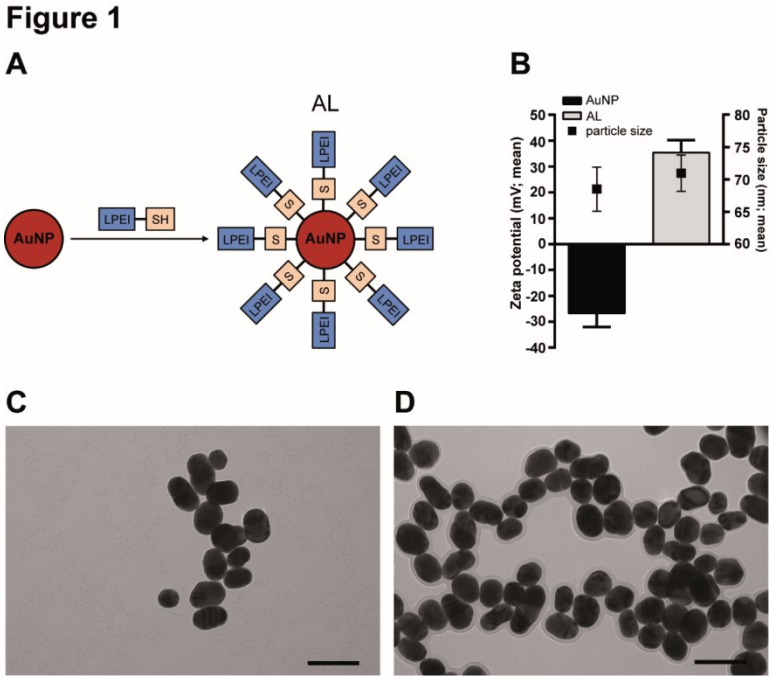

Figure 1: Synthesis and characterization of cationic gold nanoparticles. *(A) Schematic illustration of synthesis of cationic gold nanoparticles (AL) by chemisorption of thiol terminated linear polyethyleneimine (LPEI5-SH) to gold nanoparticles (AuNP). (B) Nanoparticle tracking analysis-based characterization of AuNP and AL for ζ-potential (bars, left y-axis) and particle size (boxes, right y-axis). (C-D) TEM micrographs of AuNPs (C) and AL NPs (D). Scale bar: 100nm.*

Auropolyplexes: a facile and tunable siRNA-nanotherapeutic platform

Cationic AuNPs (AL) were used in a concentrated state to generate siRNA based auropolyplexes by a simple two-step complexation process. The first step was to mix AL with siRNA giving siRNA coated cationic AuNPs (ALS). In the second mixing step, the desired cationic polymer (LPEI5-SH, LPEI10 or LPEI10-PEG; for details see Methods section) was added to ensure total complexation giving respective auropolyplexes (ALSL5-SH; ALSL10; ALSL10-PEG). The complexation process was characterized in detail by gel retardation studies, NTA and TEM analysis. Gel retardation studies were conducted for different concentrations (10 and 133 µg/mL) and buffer conditions (water vs HBG [20 mM HEPES pH 7.4, 5% glucose w/v], Figure 2). When preparing ALS at 10 µg/mL in water, no retardation of siRNA was observed (Figure 2A), but a black precipitate in the loading well could be seen visually and indicated the presence of gold nanoparticles in the well. In the second complexation step, increasing amounts of LPEI5-SH (from 10ng to 400ng) were added to ALS forming ALSL5-SH. At low N/P ratios (N/P 0.4-1, corresponding to 10-25 ng of LPEI5-SH per 200 ng siRNA), the intensity of the siRNA band gradually decreased indicating partial retardation. At N/P 2 (50 ng LPEI5-SH) and above, complete siRNA retardation occurred. Similarly, with free (untethered) LPEI5-SH, siRNA was also completely retarded at N/P 2 and above (Figure S4). It is to be noted that for the N/P ratio calculation, the LPEI5-SH bound to AuNP was not considered. Similar studies were conducted with a formulation intended for later *in vivo* use, using AF750 labelled siRNA in HBG buffer at a siRNA concentration of 133 µg/mL and LPEI10 for complexation (Figure 2B). Almost complete retardation was observed at N/P 2 and above (625 ng LPEI per 2500 ng siRNA). Sufficient surplus of positive charge ensures nanoparticle stability and transfection efficiency. [32] Hence, for all further studies we used formulations with higher N/P ratios: N/P 4 (corresponding to a w/w ratio of 0.5/1 PEI/siRNA) for *in vitro* studies and N/P 8 (corresponds to a 1/1 w/w ratio of siRNA/LPEI) for *in vivo* studies. Thus, gel retardations studies of auropolyplexes confirmed total siRNA loading at N/P 2 and above.

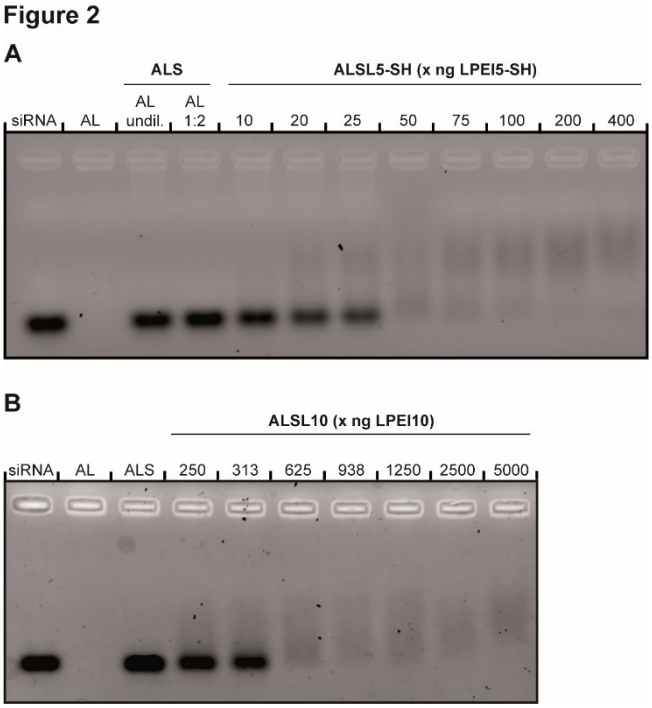

Figure 2: Gel retardation assay for siRNA complexation studies. *siRNA alone, AL alone, ALS or ALS condensed with indicated amounts of (A) LPEI5-SH (resulting in ALSL5-SH) or (B) LPEI10 (resulting in ALSL10) were loaded onto a 1.5 % agarose gel (200 ng siRNA/lane) and underwent electrophoresis, staining with EtBr and visualization as described in materials and methods. (A) Samples generated in water at a final concentration of 10 µg/mL anti-luciferase siRNA. ALS generated with undiluted (undil.) or 1:2 diluted (1:2) AL; ALS (containing 200 ng siRNA in water) were condensed with indicated amounts of LPEI5-SH giving ALSL5-SH. (B) Samples generated in HBG at a final concentration of 133 µg/mL AF750-siRNA. ALS (containing 2500 ng siRNA) were condensed with indicated amounts of LPEI10 giving ALSL10, and aliquots containing 200 ng AF750-siRNA each were loaded onto the gel.*

We also applied ζ-potential measurements to further characterize the individual complexation steps. In the first step, the addition of siRNA to AL at a concentration of 10 µg/mL decreased the ζ-potential from +37 mV to -18 mV indicating successful attachment of negatively charged siRNA to the AL surface (Figure 3A). Apparently, the electrostatic interaction of the cationic AuNP surface with siRNA is sufficient to bind siRNA in solution. However, this interaction appears not strong enough under conditions of gel retardation, as siRNA was observed to be non-retarded (Figure 2). This could be due to limited accessibility of LPEI5-SH tethered to the AuNP surface and/or low density of LPEI5-SH on the AuNP. In the second step, the addition of LPEI5-SH or LPEI10 to ALS increased the ζ-potential to +24 mV, indicating complexation of siRNA into positively charged auropolyplexes and appears in line with the results obtained from the gel retardation assay. In case of auropolyplexes for *in vivo* set-up (133 µg/mL AF750 siRNA, LPEI10), ζ-potentials of -26 mV (for ALS) and +31 mV (for ALSL) were recorded showing similar

complexation behavior. Considering the complexation was without additional purification steps, there is in principle the possibility of polyplex formation (in addition to, or instead of auropolyplexes). We visualized the auropolyplexes by TEM, where only nanoparticles with high contrast similar to AuNPs were observed (4 fields of view analyzed at magnification 200k; Figure S5A-B). On the other hand, siRNA/LPEI5-SH polyplexes appeared to be of low contrast with a size of 50-100 nm in diameter (Figure S5C). Such low contrast structures were not observed in case of both ALS and ALSL, which indicates absence of any detectable polyplexes during the process of auropolyplex generation.

Size based characterization was conducted by NTA analysis: all formulations generated in water, AL, ALS and ALSL, exhibited average particle sizes between 60 and 75 nm (Figure 3B) in case of both, LPEI5-SH and LPEI10 auropolyplexes. Using HBG as synthesis medium (relevant for *in vivo* application), ALS and auropolyplexes were >100 nm in size. To determine, whether this size increase is due to aggregation or due to increased hydrodynamic diameter, NTA tracks of single nanoparticles in a defined volume were considered to give concentration of nanoparticles. This can provide valuable information on size distribution data along with concentration of nanoparticles. Total particle count for ALSL10 generated in water was 2.98×10^{11} +/- 5.00×10^{09} nanoarticles/mL, while in HBG buffer it was 2.18×10^{11} +/- 1.32×10^{10} nanoparticles/mL (Figure S6). This indicates that the hydrodynamic diameter increased, but also approx. one third of nanoparticles were prone to aggregation when using 20 mM HEPES and 5% glucose as buffer. To demonstrate the versatility of auropolyplex formulation, LPEI10-PEG was used instead of LPEI10 to prepare PEGylated auropolyplexes at 133 µg/mL with AF750-siRNA in HBG. Hydrodynamic diameter of PEGylated auropolyplexes was below 100 nm and smaller in comparison to their non-PEGylated version and ζ-potential was lower for PEGylated auropolyplexes (Figure S7). This masking of surface charge and prevention of aggregation on inclusion of PEG is in accordance with the effects of PEGylation on gold- and other nanoparticles. [29, 33]

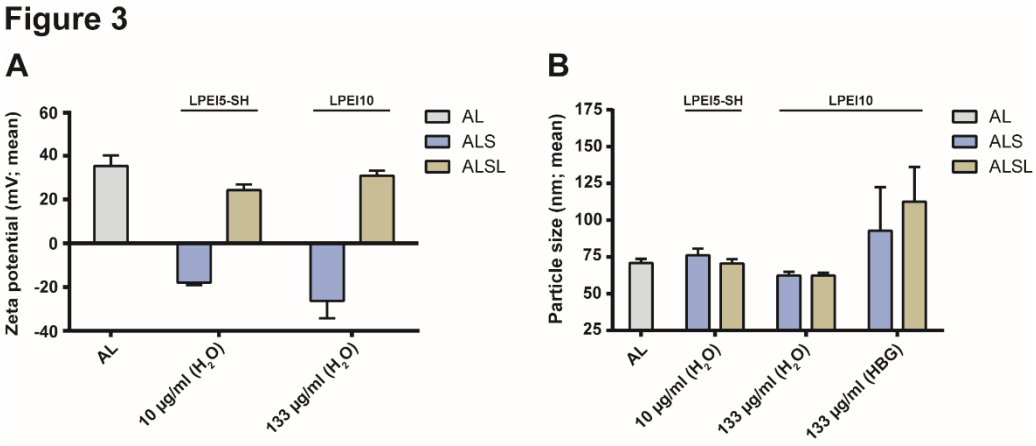

Figure 3: Nanoparticle tracking analysis at different steps of auropolyplex generation. (A) *ζ-potential and* ***(B)*** *mean size of nanoparticles at different steps of auropolyplex generation (AL-cationic gold nanoparticles, ALS-after complexation of siRNA with AL, ALSL-auropolyplex after complexation of ALS with LPEI (LPEI5-SH or LPEI10). ALS and ALSL were prepared in the indicated buffer (water or HBG); ALSL were generated at final siRNA concentration of 10 or 133 µg/mL, as indicated; n=3 + stddev*

The amount of siRNA loaded per nanoparticle can be crucial for effective knockdown. We estimated approx. 15,500 siRNA duplex molecules per auropolyplex particle (in case of ALSL10 generated with AF750-siRNA at 133 µg/mL in water, considering complete association of siRNA). This is considerably higher when compared to LBL techniques (3,500 duplex molecules per particle [4]) or with covalently attached siRNA, which was approx. 38 duplexes for a 13 nm particle. [34, 35]

Auropolyplexes for successful intracellular siRNA delivery and gene knockdown

Cell binding, internalization and endosomal release are key steps in siRNA delivery. Here we employed net positively charged nanoparticles, which usually bind via heparansulfate proteoglycans and are internalized by adsorptive endocytosis. [36] AF647-labelled siRNA based auropolyplexes were employed to detect their binding and uptake by flow cytometry and CLSM. Cell association of AF647-siRNA based nanoparticles significantly increased when the dose was doubled from 200 ng/well (64 nM siRNA) to 400 ng/well (128 nM siRNA) (Figure 4 A-C). Auropolyplexes showed similar or even higher cell association than corresponding polyplexes (BPEI or LPEI5-SH), whereas negatively charged ALS exhibited least cell association (Figure 4C). Confocal laser scanning microscopy (CLSM) was used to validate uptake and visualize intracellular distribution at a concentration of 128 nM siRNA (Figure 4D-I). The fluorescent signal of EGFP from EGFP-Luc fusion protein) was utilized to visualize the cytoplasmic area. As observed in the middle sections of cells, AF647-labelled siRNA was found intracellularly in all

treatments, ALS (Figure 4D), Auropolyplexes (Figure 4E) and BLEI polyplexes (Figure 4F). In transmitted light DIC pictures (overlaid onto fluorescence micrographs), dense structures (appearing black) were visible within ALS and ALSL5-SH treated cells, but not with BPEI polyplex transfected ones (Figure 4G-I). Comparing DIC- and CLSM pictures, there is an intriguing correlation between the dark structures in DIC and the absence of EGFP signal in the corresponding areas in the CLSM picture (highlighted by arrows), which indicates the presence of gold nanoparticles intracellularly. These structures also resembled the same distribution pattern as the AF647 signal indicating presence of siRNA intracellularly near to gold NPs. In case of ALS, although the total cellular association of siRNA was significantly lower (4C), internalization was still observed (4D and 4G). Patel et al reported a similar observation, where negatively charged AuNP covalently decorated with siRNA were internalized after binding to scavenger receptors. [37] Taken together, we conclude from these data that cationic gold nanoparticles and siRNA are efficiently delivered intracellularly.

Figure 4

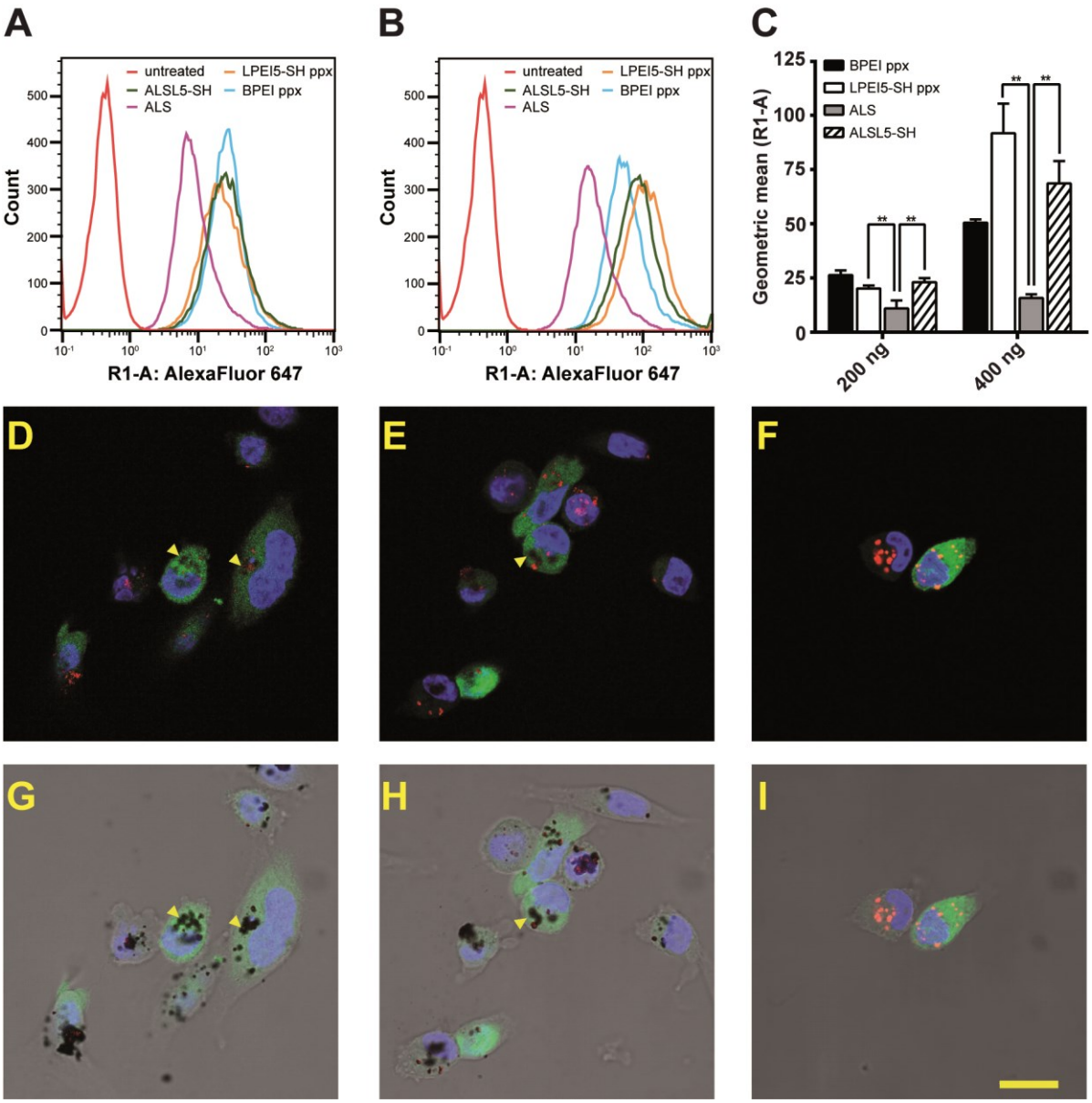

Figure 4: Cell association and uptake of auropolyplexes and polyplexes. *MDA-MB-231Luc cells were incubated with AF647-siRNA based auropolyplexes (ALSL5-SH), polyplexes (LPEI5-SH ppx and BPEI ppx) or ALS complexes for 24 h and analyzed by flow cytometry (A-C) or CLSM (D-I). (A-B) Representative histograms for AF647 signal in R1 channel at a siRNA dose of 200 (A) or 400 (B) ng/well. (C) Geometric mean values for AF647 signal in R1 channel for different treatments (n=3 + stddev, data from 2 independent experiments; *p≤0.05; **p≤0.01; U-test (Mann-Whitney). (D-I) CLSM based imaging of the middle section of the cells showing fluorescence images (D-F) or DIC overlay with fluorescence images (G-I) after incubation with ALS (D, G), ALSL5-SH (E, H), or BPEI polyplexes (F,I). DAPI staining is depicted in blue, the EGFP signal in green and the AF647 signal derived from siRNA in red; arrowheads in D and E denote areas without EGFP signal and in G and H the corresponding area in the figure with DIC overlay; scale bar: 20 µm.*

Several uptake routes for siRNA and formulations thereof have been described, but only a few lead to efficient target knockdown. [38] After establishing the successful intracellular siRNA delivery, we therefore assessed gene knock-down efficiency of auropolyplexes on MDA-MB-231Luc cells stably expressing EGFP-Luc reporter gene. Cells were treated with different formulations based on anti-luc siRNA or control siRNA (400 ng / well, corresponding to 140 nM) for 48 h and the luciferase activity was quantified by firefly luciferase assay. The luciferase signal from cells treated with anti-luc siRNA based formulations was normalized to cells treated with formulations loaded with non-coding control siRNA (Figure 5). BPEI (Mw 25,000 Da) polyplexes were used as positive control. Both, ALSL5-SH and ALSL10 auropolyplexes caused a significantly reduced luciferase expression in comparison to BPEI polyplexes. Comparing auropolyplexes with the corresponding polyplexes using the same polymer (LPEI5-SH and LPEI10, respectively), the knockdown was either similar (LPEI5-SH) or further strongly improved (LPEI10). This indicates the role of gold nanoparticles in assisting siRNA delivery and knockdown. A similar assisting role of nanoparticles in gene delivery was described for BPEI based plasmid delivery. [31] ALSL10 auropolyplex performed superiorly with 80 % knockdown, however, ALS did not induce any knockdown of luciferase expression. Very recently, SNAs (siRNA attached to 13 nm AuNP) were complexed with 25 kDa BPEI and used for *in vitro* transfection studies. [35] Based on siRNA, 60 nM were necessary to achieve 70 % reporter gene (EGFP) knockdown at a concentration of 34 µg/mL of BPEI (giving an N/P ratio of approx. 630 and a siRNA/BPEI w/w ratio of 41/1). Although the formulation was very well tolerated *in vitro*, BPEI dosages of 2 mg/kg and above induce acute toxicity with approx. 50% lethality,[32] hence limiting the treatment dosage of siRNA *in vivo* with BPEI based formulations.

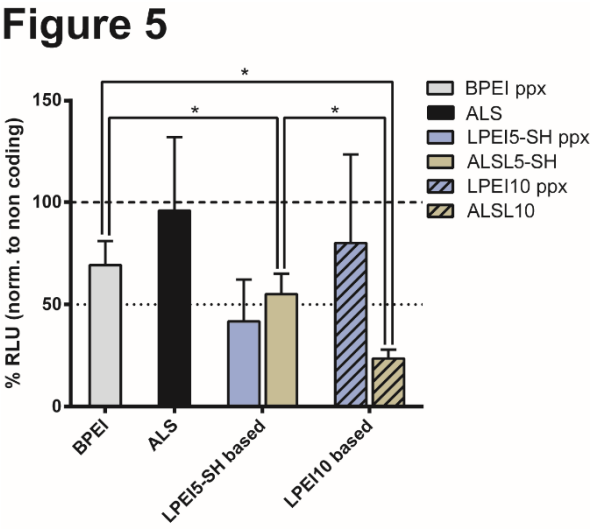

Figure 5: Functional evaluation of siRNA based knockdown. *MDA-MB-231Luc cells seeded in 96-well plates were treated with 400 ng siRNA/well (140 nM) anti-luc-siRNA or control siRNA for 24 h formulated as auropolyplexes (ALSL5-SH and ALSL10), polyplexes (LPEI5-SH ppx, LPEI10 ppx, and BPEI ppx). Relative knockdown in percent is calculated by the formula 100* (RLU anti-luc siRNA / RLU control siRNA); (n=3 + stddev, data from 2 independent experiments; *p≤0.05;U-test (Mann-Whitney)).*

As a proof of principle, we also evaluated PEGylated auropolyplexes generated with LPEI10-PEG for cell uptake and gene knockdown at 70 and 140 nM (Figure S8). Despite the presence of PEG, ALSL10-PEG auropolyplexes showed similar cell association/uptake as in case of ALSL10 auropolyplexes (Figure S8A). As expected, knockdown by PEGylated auropolyplexes was less pronounced, but still significant (Figure S8B). Thus, PEGylated auropolyplexes are potentially suitable for targeted siRNA delivery, e.g. to EGFR overexpressing cells, similar to our work on targeted gene delivery by LPEI based conjugates with distally attached peptide ligands. [39, 40] Thus, this auropolyplexes system can be in principle used for developing targeted and shielded nucleic acid delivery formulations.

Pulmonary siRNA delivery by aerosolization of auropolyplexes: FLIT/CT based spatio-temporal and non-invasive tracking of siRNA delivery process

Pulmonary delivery of nucleic acids is very relevant for treatment of lung related disorders as it offers local distribution and higher lung retention, thereby circumventing accumulation in non-target organs and avoiding side-effects. Delivery by microspray-based aerosolization via intratracheal administration route is generally employed for proof-of-concept animal studies. [41] We have recently applied 'naked' siRNA intratracheally demonstrating partial lung retention, but also crossing of the air-blood barrier and renal excretion of intact siRNA. [18] Also,

we could confirm, that the AF750 dye remains attached to siRNA and the siRNA remains intact when analyzed in urine, making this a suitable method for tracking siRNA *in vivo*. Here, we evaluated the biodistribution and biocompatibility of ALSL10 auropolyplexes with AF750-siRNA in HBG (133 µg/mL) *in vivo* via this administration route. Microspraying of formulations is associated with increased pressure as well as shear forces and can considerably influence the size and stability of nanoparticular agents. Therefore, we determined size and possible aggregation of auropolyplexes after microspraying by NTA analysis of size and particle concentration. The size distribution was clearly broader ranging from 50-400 nm in size, and also the absolute particle concentration decreased (Figure S9). However, 40 % of the nanoparticles were still below 200 nm hydrodynamic diameter based on NTA, which should still allow sufficient lung deposition when applied as an aerosol. Post intratracheal application of ALSL10 auropolyplexes formulated with 10 µg AF750-siRNA, the signal was found in the thoracic area within minutes, indicating deposition in lung (0 h, Figure 6A and 6C). After 24 h of administration, a strong signal was also observed in the abdominal area, depicting signal in kidneys (when imaged in prone position, Figure 6B) and in the bladder area (when imaged in supine position, Figure 6D), indicating distribution from lungs to excretory organs. When applying tomographic analysis together with contrast agent enhanced CT, the distribution of the fluorescence signal from the respiratory tract to the renal system 24 h after administration was confirmed corroborating the 2D analysis (Figure S10). Similarly, *ex vivo* imaging of organs corroborated the observation with a significant signal in both kidneys and in the lung (Figure S11).

Figure 6

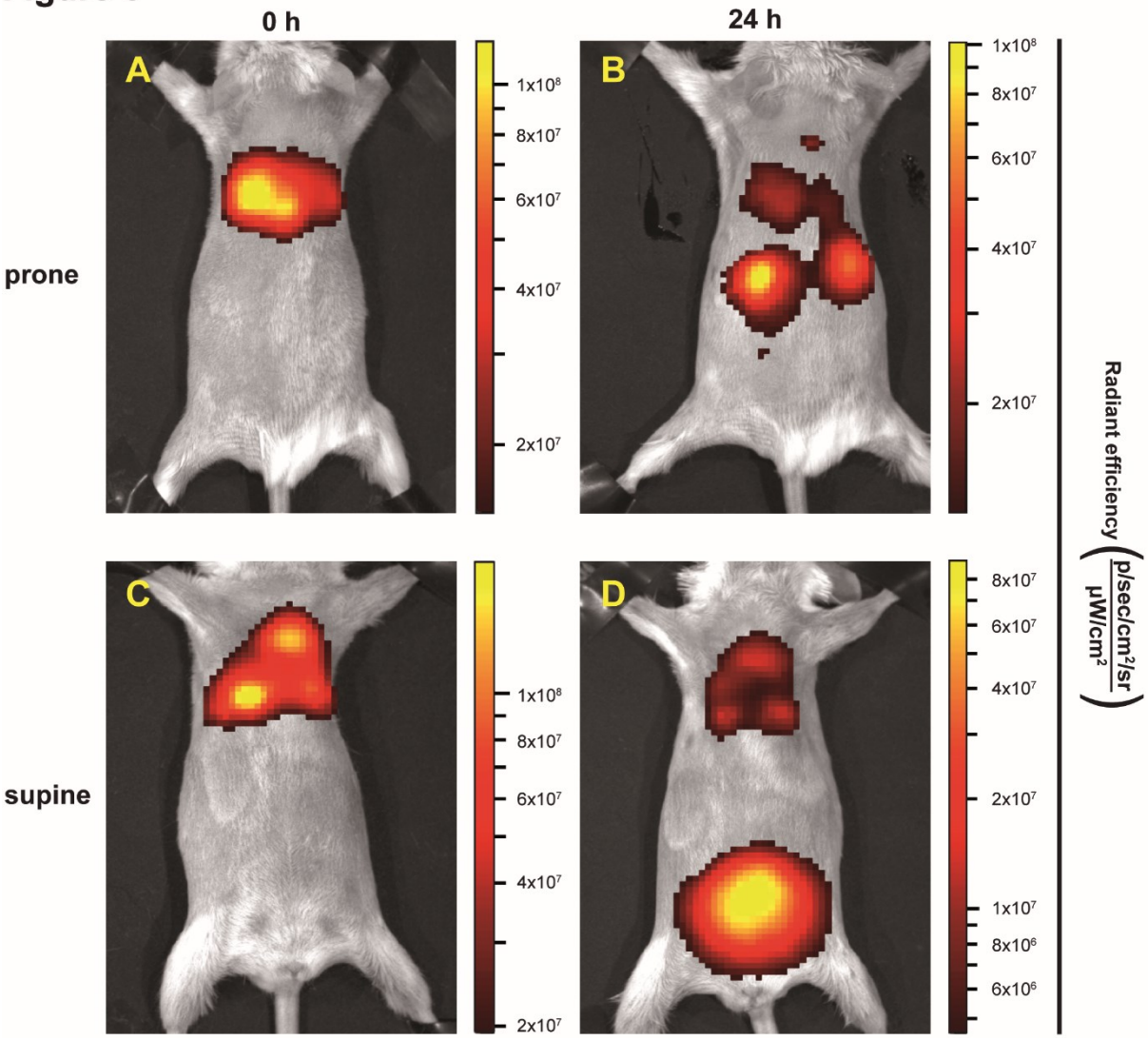

Figure 6: 2D epifluorescence imaging of auropolyplexes after intratracheal pulmonary delivery. *Balb/c mice were treated with ALSL10 auropolyplexes (containing 10 µg AF750-siRNA) intratracheally by microspray based aerosolization and imaged immediately after application (0 h, A, C) and 24 h thereafter (B, D) either in dorsal up (prone, A, B) or ventral up (supine, C, D) position for AF750 signal. Color coded fluorescence radiance images are overlaid onto reflected light images; n=3 per group, representative animals are shown.*

FLIT imaging also allowed a quantitative analysis of lung signal at 0 h and 24 h after i.t. administration (Figure 7A). Quantification was done by employing a standard curve based on different concentrations of AF750 siRNA and placing appropriate cuboid ROIs. [18] Based on a Mw of 15,700 Da, 10 µg AF750 siRNA correspond to 637 pmol AF750. Immediately after spraying 686 +/- 216 pmol AF750 were found in the lung area, indicating complete lung delivery of the dosage applied (recovery rate approx. 108 %). 24 h thereafter, 20 % of the dosage (129 +/- 26 pmol) was found in the lung, whereas the remaining material was apparently excreted renally.

After sacrificing the animals, we also quantified the amount of gold remaining in the respective organs using ICP-MS (Figure 7B). ICP-MS measurements showed that 24 h after auropolyplex administration, >97 % of the detected gold remained in the lungs at a concentration of 4970 +/- 469 ppb. In the stomach, 1.8 % of the dose was found, whereas in all other organs values were below 0.5 %, which was in the range of acid blank measurements. The amount of gold in stomach was very low and can be due to the activity of the mucociliar escalator. Comparable results were reported for non-cationized 22 nm AuNP, where values of >3 % stomach retention were observed already 2 h after intratracheal application. [42] The biodistribution pattern of gold is different from the siRNA biodistribution as measured by fluorescence, indicating no apparent air-blood transfer of AuNP and strong retention of the gold in lungs. This difference cannot be explained only due to sheer differences in size: 2 nm, citrate capped AuNPs remained in the lung with only minute amounts found in the liver as per Sadauskas et al. [43] In contrast, siRNA of similar size (2 nm, when considering the hydrodynamic diameter) [44] crosses the air-blood barrier rapidly and efficiently and is excreted via kidneys. [18, 45] Thus, in case of auropolyplexes, release of siRNA from gold AuNP seems unhampered, which can be advantageous from the standpoint of functionality. In contrast, covalently attached nucleic acid to the gold NP surface is not completely released, where approx. 60 % remain surface bound [12] and might not be accessible to the cellular machinery. The rationale of using thiol terminated LPEI (as in case of auropolyplexes) rather than thiolated-siRNA (as in case of SNAs) was to avoid trapping of siRNA onto the gold nanoparticles after intracellular delivery, thereby ensuring release of siRNA also inside the cells. Functionality testing, i.e. target knockdown *in vivo*, was not conducted with the current version of auropolyplexes as targeting moieties are needed for enabling knockdown in healthy lungs. Also, mucus represents a strong biobarrier for cationic nanoparticles usually hindering their access to lung cells. [46] However, in principle, cationic auropolyplexes might be applicable in lung cancer models based on our recent results, where we could demonstrate accessibility of breast cancer lung metastases for gene transfection via intratracheal administration, due to the invasive growth of cancer cells. [47]

Figure 7

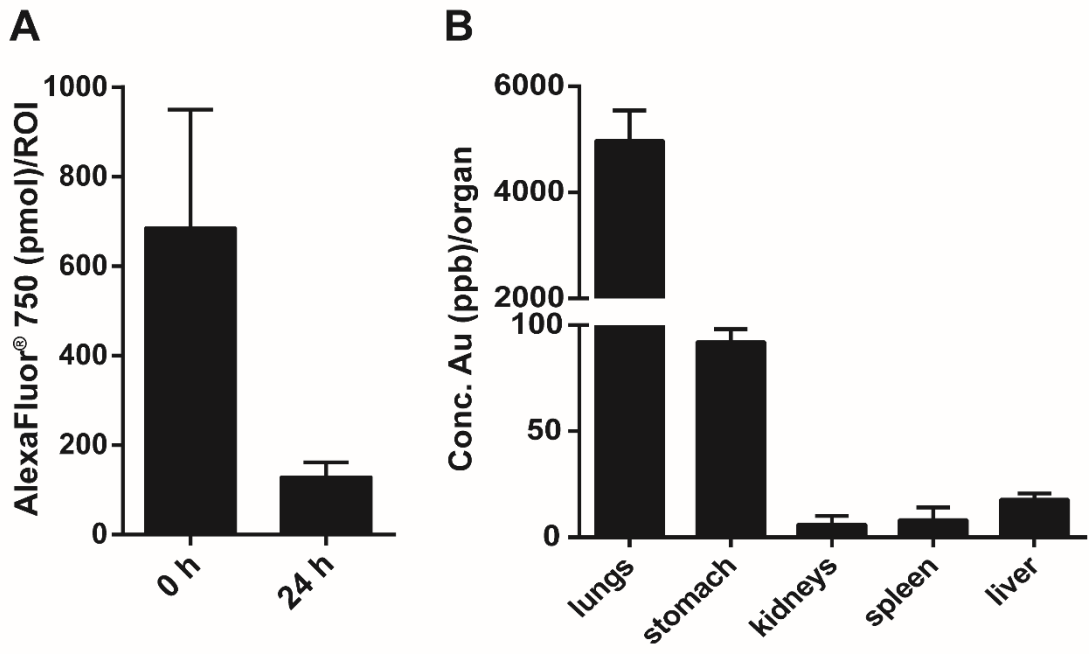

Figure 7: Biodistribution of AF750-siRNA and gold nanoparticle after intratracheal application. *Animals were treated with ALSL (10 µg Alexa750-siRNA) as described. (A) Quantification of AF750 by FLIT in the lung region at 0 h and 24 h after intratracheal application of auropolyplexes. (B) ICP-MS based quantification of gold per organ 24 h after intratracheal application of auropolyplexes; (n=3 + stddev).*

Conclusions

Taken together, auropolyplexes represent a highly versatile platform for delivery of siRNA and in principle also other nucleic acids. They offer effective siRNA delivery with exceptional high loading capacity, efficient cellular uptake and intracellular release of siRNA. A good knock down efficiency can be obtained using low amounts of polycation indicating the synergistic role of gold nanoparticles and polycation. The modular structure allows the use of shielding and potentially also targeting agents for cell specific siRNA delivery. The robust synthesis protocol enables generation of formulations for *in vivo* delivery with sufficient siRNA concentration in physiological buffers. It also allowed the spatiotemporal tracking of siRNA and its unhampered release *in vivo* from the nanocarrier.

Acknowledgements

The research leading to these results has received support from the Innovative Medicines Initiative Joint Undertaking under grant agreement no. [115363], resources of which are composed of financial contribution from the European Union's Seventh Framework Programme (FP7/2007–2013) and EFPIA companies' in kind contribution. Antonia Geyer and Theresa Kittelmann are gratefully acknowledged for help in setting up the initial *in vivo* measurements. The Oligonucleotides used in this work were supplied by GSK (GSK Medicines Research Centre, Stevenage, UK; synthesis by Glynn Williams and Jonathan Northall) as part of their contribution to the EU funded IMI project COMPACT.

Supporting information available: Additional results (figures S1-S11 and supporting videoS1).

References

[1] J. Gilleron, W. Querbes, A. Zeigerer, A. Borodovsky, G. Marsico, U. Schubert, K. Manygoats, S. Seifert, C. Andree, M. Stoter, H. Epstein-Barash, L. Zhang, V. Koteliansky, K. Fitzgerald, E. Fava, M. Bickle, Y. Kalaidzidis, A. Akinc, M. Maier, M. Zerial, Image-based analysis of lipid nanoparticle-mediated siRNA delivery, intracellular trafficking and endosomal escape, Nat Biotechnol, 31 (2013) 638-646 10.1038/nbt.2612.

[2] S.W. Morton, K.P. Herlihy, K.E. Shopsowitz, Z.J. Deng, K.S. Chu, C.J. Bowerman, J.M. Desimone, P.T. Hammond, Scalable manufacture of built-to-order nanomedicine: spray-assisted layer-by-layer functionalization of PRINT nanoparticles, Adv Mater, 25 (2013) 4707-4713 10.1002/adma.201302025.

[3] A. Wei, J.G. Mehtala, A.K. Patri, Challenges and opportunities in the advancement of nanomedicines, J Control Release, 164 (2012) 236-246 10.1016/j.jconrel.2012.10.007.

[4] Z.J. Deng, S.W. Morton, E. Ben-Akiva, E.C. Dreaden, K.E. Shopsowitz, P.T. Hammond, Layer-by-layer nanoparticles for systemic codelivery of an anticancer drug and siRNA for potential triple-negative breast cancer treatment, ACS Nano, 7 (2013) 9571-9584 10.1021/nn4047925.

[5] A. Elbakry, A. Zaky, R. Liebl, R. Rachel, A. Goepferich, M. Breunig, Layer-by-layer assembled gold nanoparticles for siRNA delivery, Nano Lett, 9 (2009) 2059-2064 10.1021/nl9003865.

[6] S. Correa, K.Y. Choi, E.C. Dreaden, K. Renggli, A. Shi, L. Gu, K.E. Shopsowitz, M.A. Quadir, E. Ben-Akiva, P.T. Hammond, Highly scalable, closed-loop synthesis of drug-loaded, layer-by-layer nanoparticles, Adv Funct Mater, 26 (2016) 991-1003 10.1002/adfm.201504385.

[7] Y.F. Tan, R.C. Mundargi, M.H. Chen, J. Lessig, B. Neu, S.S. Venkatraman, T.T. Wong, Layer-by-layer nanoparticles as an efficient siRNA delivery vehicle for SPARC silencing, Small, 10 (2014) 1790-1798 10.1002/smll.201303201.

[8] E.C. Wurster, R. Liebl, S. Michaelis, R. Robelek, D.S. Wastl, F.J. Giessibl, A. Goepferich, M. Breunig, Oligolayer-coated nanoparticles: impact of surface topography at the nanobio interface, ACS Appl Mater Interfaces, 7 (2015) 7891-7900 10.1021/am508435j.

[9] H. Yin, R.L. Kanasty, A.A. Eltoukhy, A.J. Vegas, J.R. Dorkin, D.G. Anderson, Non-viral vectors for gene-based therapy, Nat Rev Genet, 15 (2014) 541-555 10.1038/nrg3763.

[10] R. Kanasty, J.R. Dorkin, A. Vegas, D. Anderson, Delivery materials for siRNA therapeutics, Nat Mater, 12 (2013) 967-977 10.1038/nmat3765.

[11] S.N. Barnaby, A. Lee, C.A. Mirkin, Probing the inherent stability of siRNA immobilized on nanoparticle constructs, Proc Natl Acad Sci U S A, 111 (2014) 9739-9744 10.1073/pnas.1409431111.

[12] N.L. Rosi, D.A. Giljohann, C.S. Thaxton, A.K. Lytton-Jean, M.S. Han, C.A. Mirkin, Oligonucleotide-modified gold nanoparticles for intracellular gene regulation, Science, 312 (2006) 1027-1030 10.1126/science.1125559.

[13] A. Taschauer, A. Geyer, S. Gehrig, J. Maier, H. Sami, M. Ogris, Up-Scaled Synthesis and Characterization of Nonviral Gene Delivery Particles for Transient In Vitro and In Vivo Transgene Expression, Hum Gene Ther Methods, 27 (2016) 87-97 10.1089/hgtb.2016.027.

[14] U. Lachelt, E. Wagner, Nucleic Acid Therapeutics Using Polyplexes: A Journey of 50 Years (and Beyond), Chem Rev, 115 (2015) 11043-11078 10.1021/cr5006793.

[15] S. Hobel, A. Aigner, Polyethylenimines for siRNA and miRNA delivery in vivo, Wiley Interdiscip Rev Nanomed Nanobiotechnol, 5 (2013) 484-501 10.1002/wnan.1228.

[16] M.E. Bonnet, P. Erbacher, A.L. Bolcato-Bellemin, Systemic delivery of DNA or siRNA mediated by linear polyethylenimine (L-PEI) does not induce an inflammatory response, Pharm Res, 25 (2008) 2972-2982 10.1007/s11095-008-9693-1.

[17] S. Di Gioia, M. Conese, Polyethylenimine-mediated gene delivery to the lung and therapeutic applications, Drug Des Devel Ther, 2 (2009) 163-188.

[18] A. Geyer, C. Lorenzer, S. Gehrig, M. Simlinger, J. Winkler, H. Sami, M. Ogris, Fluorescence- and computed tomography for assessing the biodistribution of siRNA after intratracheal application in mice, Int J Pharm, 525 (2017) 359-366 10.1016/j.ijpharm.2017.02.025.

[19] Z. ur Rehman, D. Hoekstra, I.S. Zuhorn, Mechanism of polyplex- and lipoplex-mediated delivery of nucleic acids: real-time visualization of transient membrane destabilization without endosomal lysis, ACS Nano, 7 (2013) 3767-3777 10.1021/nn3049494.

[20] W. Rodl, D. Schaffert, E. Wagner, M. Ogris, Synthesis of polyethylenimine-based nanocarriers for systemic tumor targeting of nucleic acids, Methods Mol Biol, 948 (2013) 105-120 10.1007/978-1-62703-140-0_8.

[21] F. Ungaro, G. De Rosa, A. Miro, F. Quaglia, Spectrophotometric determination of polyethylenimine in the presence of an oligonucleotide for the characterization of controlled release formulations, J Pharm Biomed Anal, 31 (2003) 143-149.

[22] D. Schaffert, M. Kiss, W. Rodl, A. Shir, A. Levitzki, M. Ogris, E. Wagner, Poly(I:C)-mediated tumor growth suppression in EGF-receptor overexpressing tumors using EGF-polyethylene glycol-linear polyethylenimine as carrier, Pharm Res, 28 (2011) 731-741 10.1007/s11095-010-0225-4.

[23] G. Frens, Controlled Nucleation for the Regulation of the Particle Size in Monodisperse Gold Suspensions, Nature Physical Science, 241 (1973) 20 10.1038/physci241020a0.

[24] E.C. Wurster, A. Elbakry, A. Gopferich, M. Breunig, Layer-by-layer assembled gold nanoparticles for the delivery of nucleic acids, Methods Mol Biol, 948 (2013) 171-182 10.1007/978-1-62703-140-0_12.

[25] B. Su, A. Cengizeroglu, K. Farkasova, J.R. Viola, M. Anton, J.W. Ellwart, R. Haase, E. Wagner, M. Ogris, Systemic TNFalpha gene therapy synergizes with liposomal doxorubicine in the treatment of metastatic cancer, Mol Ther, 21 (2013) 300-308 10.1038/mt.2012.229.

[26] K. Mueller, M. Ogris, H. Sami, Firefly luciferase based reporter gene assay for investigating nanoparticle mediated nucleic acid delivery, Methods Mol Biol, 948 (2018) in press 10.1007/978-1-62703-140-0_8.

[27] A.C. Templeton, M.J. Hostetler, E.K. Warmoth, S. Chen, C.M. Hartshorn, V.M. Krishnamurthy, M.D.E. Forbes, R.W. Murray, Gateway Reactions to Diverse, Polyfunctional Monolayer-Protected Gold Clusters, Journal of the American Chemical Society, 120 (1998) 4845-4849 10.1021/ja980177h.

[28] K.A. Curtis, D. Miller, P. Millard, S. Basu, F. Horkay, P.L. Chandran, Unusual Salt and pH Induced Changes in Polyethylenimine Solutions, PLoS One, 11 (2016) e0158147 10.1371/journal.pone.0158147.

[29] H. Chen, H. Paholak, M. Ito, K. Sansanaphongpricha, W. Qian, Y. Che, D. Sun, 'Living' PEGylation on gold nanoparticles to optimize cancer cell uptake by controlling targeting ligand and charge densities, Nanotechnology, 24 (2013) 355101 10.1088/0957-4484/24/35/355101.

[30] C.S. Levin, S.W. Bishnoi, N.K. Grady, N.J. Halas, Determining the conformation of thiolated poly(ethylene glycol) on Au nanoshells by surface-enhanced Raman scattering spectroscopic assay, Anal Chem, 78 (2006) 3277-3281 10.1021/ac060041z.

[31] M. Thomas, A.M. Klibanov, Conjugation to gold nanoparticles enhances polyethylenimine's transfer of plasmid DNA into mammalian cells, Proc Natl Acad Sci U S A, 100 (2003) 9138-9143 10.1073/pnas.1233634100.

[32] J. Fahrmeir, M. Gunther, N. Tietze, E. Wagner, M. Ogris, Electrophoretic purification of tumor-targeted polyethylenimine-based polyplexes reduces toxic side effects in vivo, J Control Release, 122 (2007) 236-245 10.1016/j.jconrel.2007.05.013.

[33] J.V. Jokerst, T. Lobovkina, R.N. Zare, S.S. Gambhir, Nanoparticle PEGylation for imaging and therapy, Nanomedicine (Lond), 6 (2011) 715-728 10.2217/nnm.11.19.

[34] D.A. Giljohann, D.S. Seferos, A.E. Prigodich, P.C. Patel, C.A. Mirkin, Gene regulation with polyvalent siRNA-nanoparticle conjugates, J Am Chem Soc, 131 (2009) 2072-2073 10.1021/ja808719p.

[35] J.R. Melamed, N.L. Kreuzberger, R. Goyal, E.S. Day, Spherical Nucleic Acid Architecture Can Improve the Efficacy of Polycation-Mediated siRNA Delivery, Mol Ther Nucleic Acids, 12 (2018) 207-219 10.1016/j.omtn.2018.05.008.

[36] I. Kopatz, J.S. Remy, J.P. Behr, A model for non-viral gene delivery: through syndecan adhesion molecules and powered by actin, J Gene Med, 6 (2004) 769-776 10.1002/jgm.558.

[37] P.C. Patel, D.A. Giljohann, W.L. Daniel, D. Zheng, A.E. Prigodich, C.A. Mirkin, Scavenger receptors mediate cellular uptake of polyvalent oligonucleotide-functionalized gold nanoparticles, Bioconjug Chem, 21 (2010) 2250-2256 10.1021/bc1002423.

[38] R.L. Juliano, X. Ming, O. Nakagawa, Cellular uptake and intracellular trafficking of antisense and siRNA oligonucleotides, Bioconjug Chem, 23 (2012) 147-157 10.1021/bc200377d.

[39] K. Klutz, D. Schaffert, M.J. Willhauck, G.K. Grunwald, R. Haase, N. Wunderlich, C. Zach, F.J. Gildehaus, R. Senekowitsch-Schmidtke, B. Goke, E. Wagner, M. Ogris, C. Spitzweg, Epidermal growth factor receptor-targeted (131)I-therapy of liver cancer following systemic delivery of the sodium iodide symporter gene, Mol Ther, 19 (2011) 676-685 10.1038/mt.2010.296.

[40] A. Schafer, A. Pahnke, D. Schaffert, W.M. van Weerden, C.M. de Ridder, W. Rodl, A. Vetter, C. Spitzweg, R. Kraaij, E. Wagner, M. Ogris, Disconnecting the yin and yang relation of epidermal growth factor receptor (EGFR)-mediated delivery: a fully synthetic, EGFR-targeted gene transfer system avoiding receptor activation, Hum Gene Ther, 22 (2011) 1463-1473 10.1089/hum.2010.231.

[41] D.P. Feldmann, O.M. Merkel, The advantages of pulmonary delivery of therapeutic siRNA, Ther Deliv, 6 (2015) 407-409 10.4155/tde.15.8.

[42] C. Schleh, U. Holzwarth, S. Hirn, A. Wenk, F. Simonelli, M. Schaffler, W. Moller, N. Gibson, W.G. Kreyling, Biodistribution of inhaled gold nanoparticles in mice and the influence of surfactant protein D, J Aerosol Med Pulm Drug Deliv, 26 (2013) 24-30 10.1089/jamp.2011.0951.

[43] E. Sadauskas, N.R. Jacobsen, G. Danscher, M. Stoltenberg, U. Vogel, A. Larsen, W. Kreyling, H. Wallin, Biodistribution of gold nanoparticles in mouse lung following intratracheal instillation, Chem Cent J, 3 (2009) 16 10.1186/1752-153X-3-16.

[44] C. Troiber, J.C. Kasper, S. Milani, M. Scheible, I. Martin, F. Schaubhut, S. Kuchler, J. Radler, F.C. Simmel, W. Friess, E. Wagner, Comparison of four different particle sizing methods for siRNA polyplex characterization, Eur J Pharm Biopharm, 84 (2013) 255-264 10.1016/j.ejpb.2012.08.014.

[45] S.A. Moschos, M. Frick, B. Taylor, P. Turnpenny, H. Graves, K.G. Spink, K. Brady, D. Lamb, D. Collins, T.D. Rockel, M. Weber, O. Lazari, L. Perez-Tosar, S.A. Fancy, C. Lapthorn, M.X. Green, S. Evans, M. Selby, G. Jones, L. Jones, S. Kearney, H. Mechiche, D. Gikunju, R. Subramanian, E. Uhlmann, M. Jurk, J. Vollmer, G. Ciaramella, M. Yeadon, Uptake, efficacy, and systemic distribution of naked, inhaled short interfering RNA (siRNA) and locked nucleic acid (LNA) antisense, Mol Ther, 19 (2011) 2163-2168 10.1038/mt.2011.206.

[46] N. Sanders, C. Rudolph, K. Braeckmans, S.C. De Smedt, J. Demeester, Extracellular barriers in respiratory gene therapy, Adv Drug Deliv Rev, 61 (2009) 115-127 10.1016/j.addr.2008.09.011.

[47] A. Geyer, A. Taschauer, F. Alioglu, M. Anton, J. Maier, E. Drothler, M. Simlinger, S. Yavuz, H. Sami, M. Ogris, Multimodal Fluorescence and Bioluminescence Imaging Reveals Transfection Potential of Intratracheally Administered Polyplexes for Breast Cancer Lung Metastases, Hum Gene Ther, 28 (2017) 1202-1213 10.1089/hum.2017.137.

Supporting information for:

Auropolyplex: a versatile nanotherapeutic platform for efficient nucleic acid delivery in vitro and in vivo

Alexander Taschauer[1], Wolfram Polzer[1], Stefan Pöschl[1], Slavica Metz[1], Nathalie Tepe[2], Simon Decker[1], Norbert Cyran[3], Julia Maier[1], Hermann Bloß[1], Martina Anton[4], Thilo Hofmann[2], Manfred Ogris[1,5*], Haider Sami[1*]

[1] Laboratory of MacroMolecular Cancer Therapeutics (MMCT), Center of Pharmaceutical Sciences, Department of Pharmaceutical Chemistry, University of Vienna, Althanstrasse 14, A-1090 Vienna, Austria

[2] Department of Environmental Geosciences, University of Vienna, Althanstraße 14, 1090 Vienna, Austria

[3] Core Facility Cell Imaging and Ultrastructure Research (CIUS), University of Vienna, Vienna, Austria

[4] Institutes of Molecular Immunology and Experimental Oncology, Klinikum rechts der Isar, Technische Universität München, Munich, Germany

[5] Center for NanoScience (CeNS), Ludwig Maximilians University, Munich, Germany.

*Corresponding authors

Email: haider.sami@univie.ac.at; m.ogris@univie.ac.at

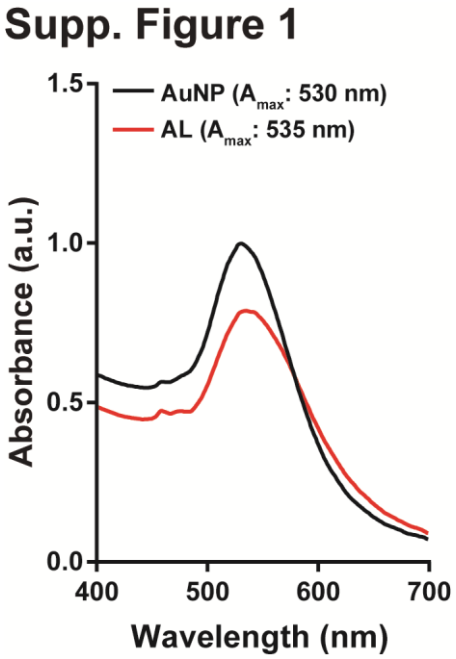

Figure S1: *UV-Vis absorbance spectra of synthesized gold nanoparticles (AuNP) and gold nanoparticles after chemisorption of LPEI5-SH (AL).*

Supp. Figure 2

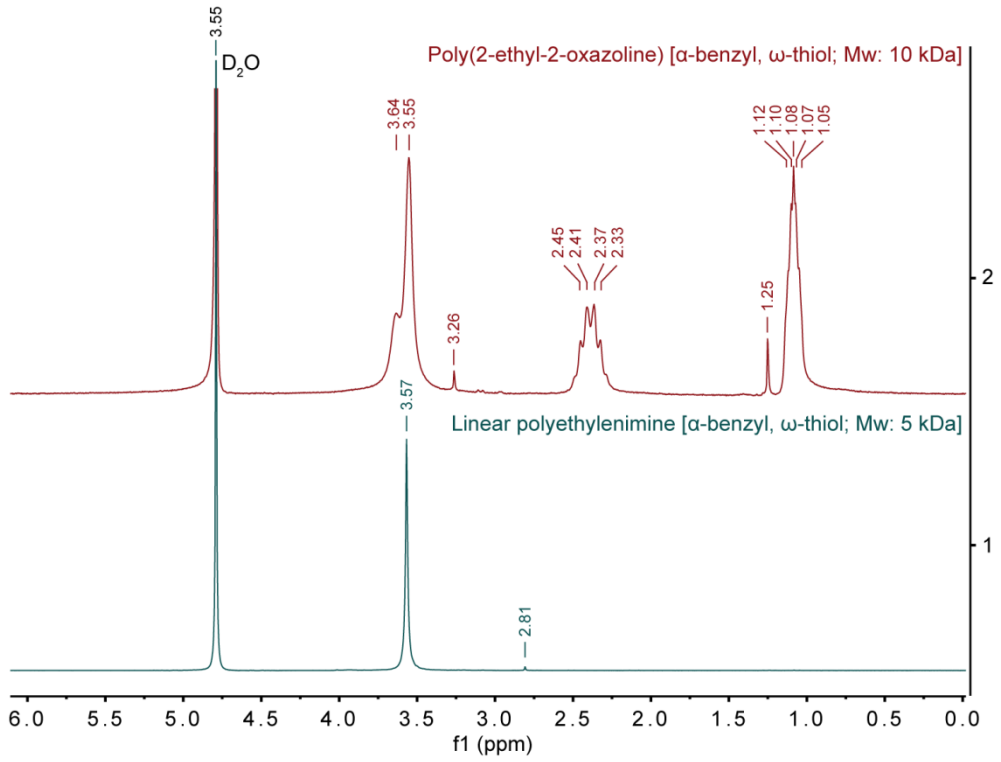

Figure S2: *^{1}H-NMR analysis (200 MHz) of α-benzyl-ω-thiol poly(2-ethyl-2-oxazoline) (Mn 10,000 Da) and α-benzyl-ω-thiol LPEI (Mn 5,000 Da). The polymeric subunits of α-benzyl-ω-thiol poly(2-ethyl-2-oxazoline) show signals derived by C**H3**-CH2-CO [δ (ppm)=1.12-1.05], CH3-C**H2**-CO [δ (ppm)=2.45-2.33] and C**H2**-C**H2**-N [δ (ppm)=3.64-3.55]. The subunits of α-benzyl-ω-thiol LPEI show a signal derived by C**H2**-C**H2**-NH [δ (ppm)=3.57].*

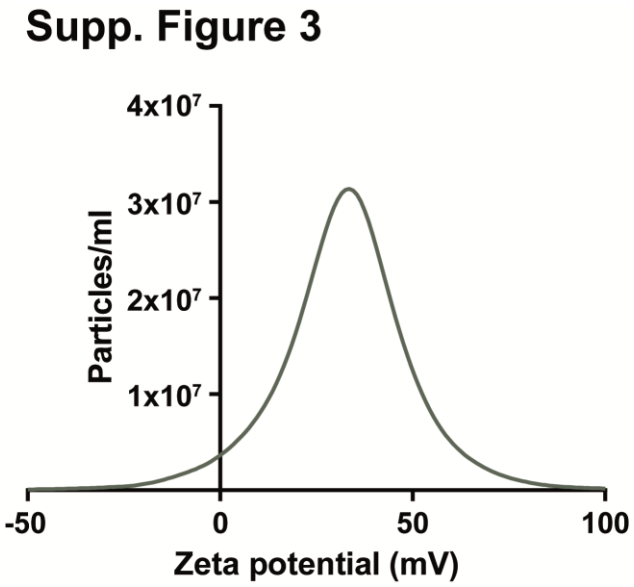

Figure S3: *Nanoparticle tracking analysis based characterization of gold nanoparticles after chemisorption of LPEI5-SH (AL) for ζ-potential.*

Supp. Figure 4

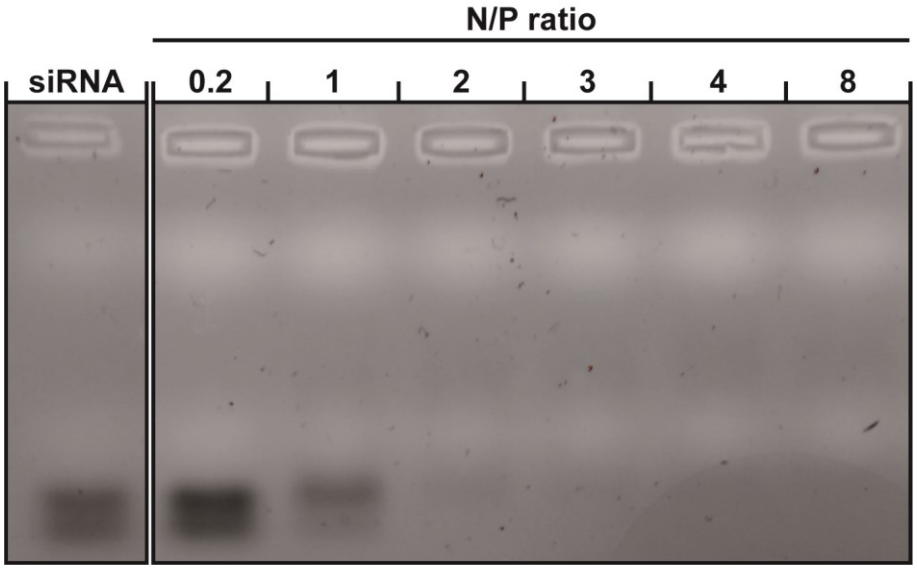

Figure S4: *Gel retardation studies for complexation of siRNA by LPEI5-SH at different N/P ratios.*

Supp. Figure 5

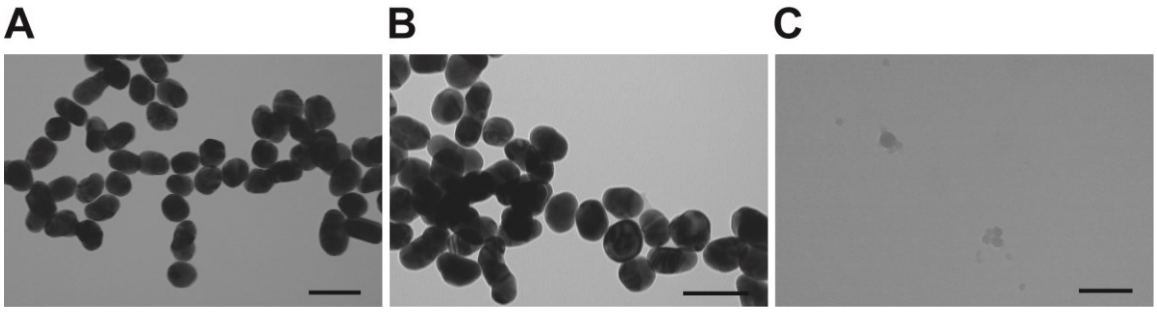

Figure S5: *TEM based visualization of (A) ALS complexes, (B) ALSL5-SH auropolyplexes, and (C) LPEI polyplexes. Scale bar: 100nm.*

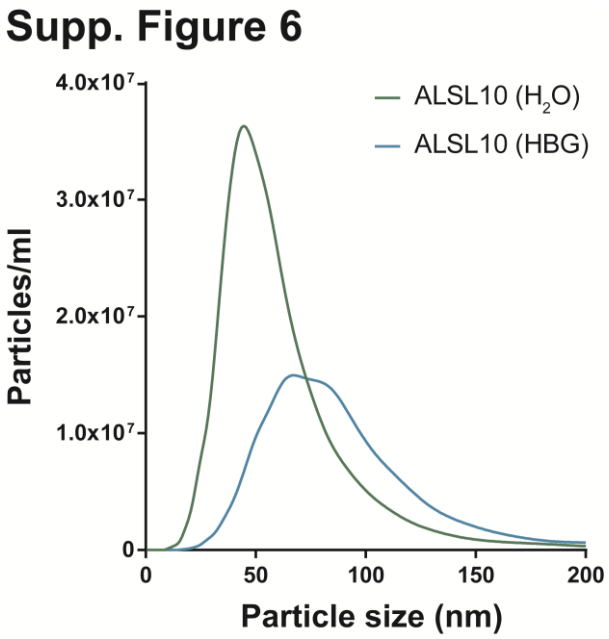

Figure S6: *NTA based particle size distribution of ALSL10 auropolyplexes generated in water or HBG.*

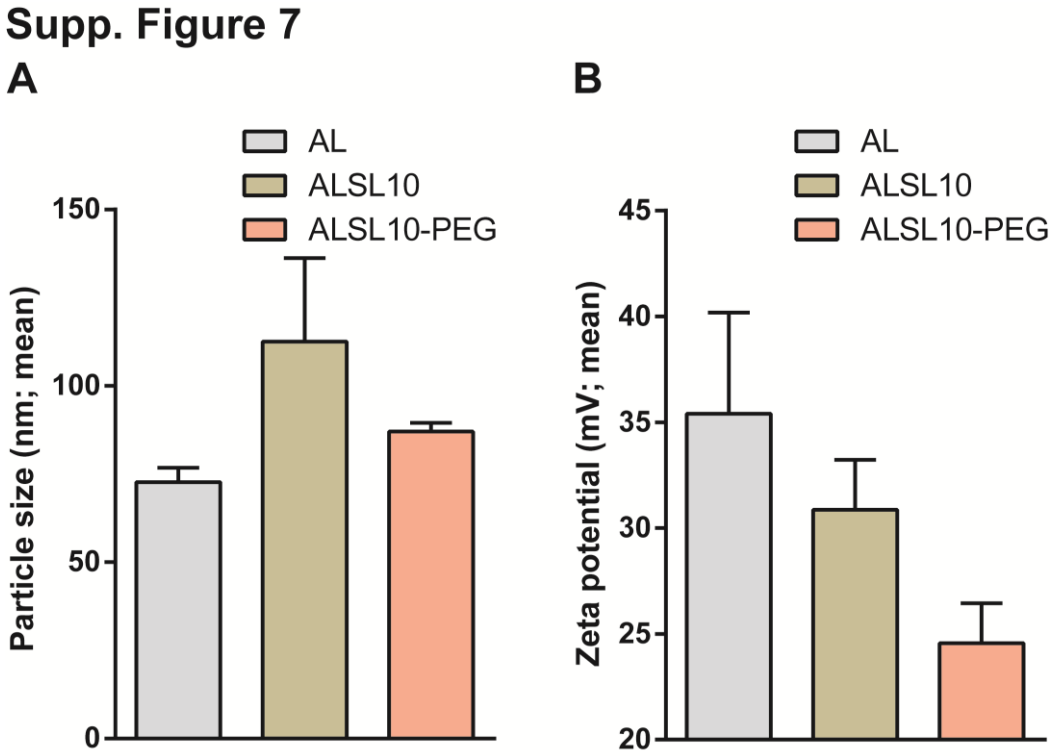

Figure S7: *NTA based characterization of (A) particle size and (B) ζ-potential for PEGylated auropolyplexes (ALSL10-PEG), corresponding auropolyplexes (ALSL10) and cationic gold nanoparticles (AL).*

Supp. Figure 8

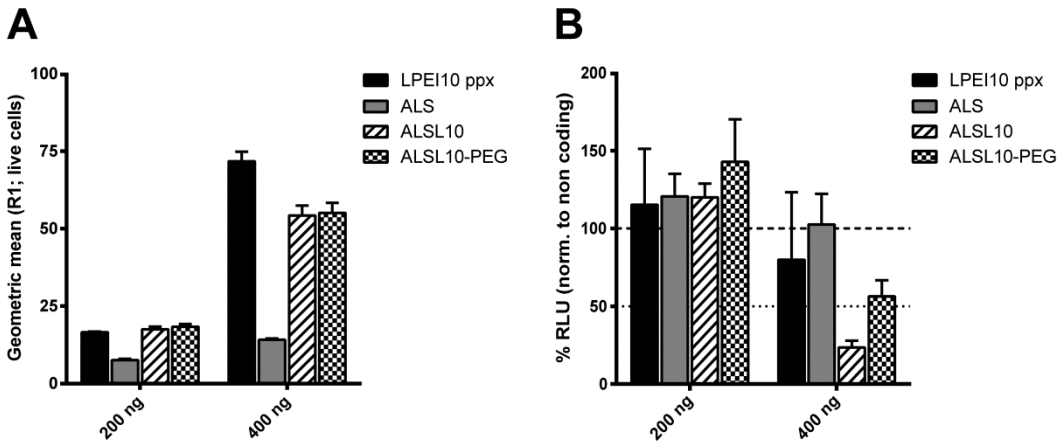

Figure S8: *PEGylated auropolyplexes (ALSL10-PEG), auropolyplexes (ALSL10), polyplexes (LPEI10 ppx) and ALS complexes were employed at two treatment doses (siRNA amount per well- 200ng or 400 ng) for cell association/uptake by flow cytometry (A; geometric mean values for AF647 signal in R1) and gene knockdown studies by firefly luciferase assay (B) in EGFP-Luc expressing MDA-MB 231 cells. In case of knockdown studies, for normalization of RLUs from luciferase signal, the same formulations based on non-coding siRNA were used. Data is depicted as mean values with standard deviation shown as error bars (n=3).*

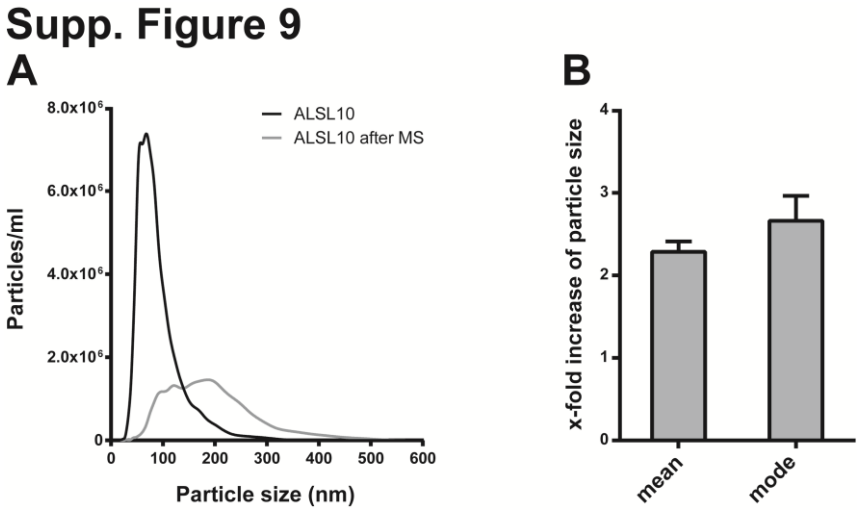

Figure S9: *NTA based size evaluation of auropolyplexes (final siRNA conc. 133 µg/mL in HBG) for (A) particle size distribution before (ALSL10) and after microspraying (ALSL10 after MS) and (B) x-fold increase of mean and mode particle size for microsprayed auropolyplexes, in comparison to non-microsprayed. Data is shown as mean values with standard deviation depicted as error bars (n=3).*

Supp. Figure 10

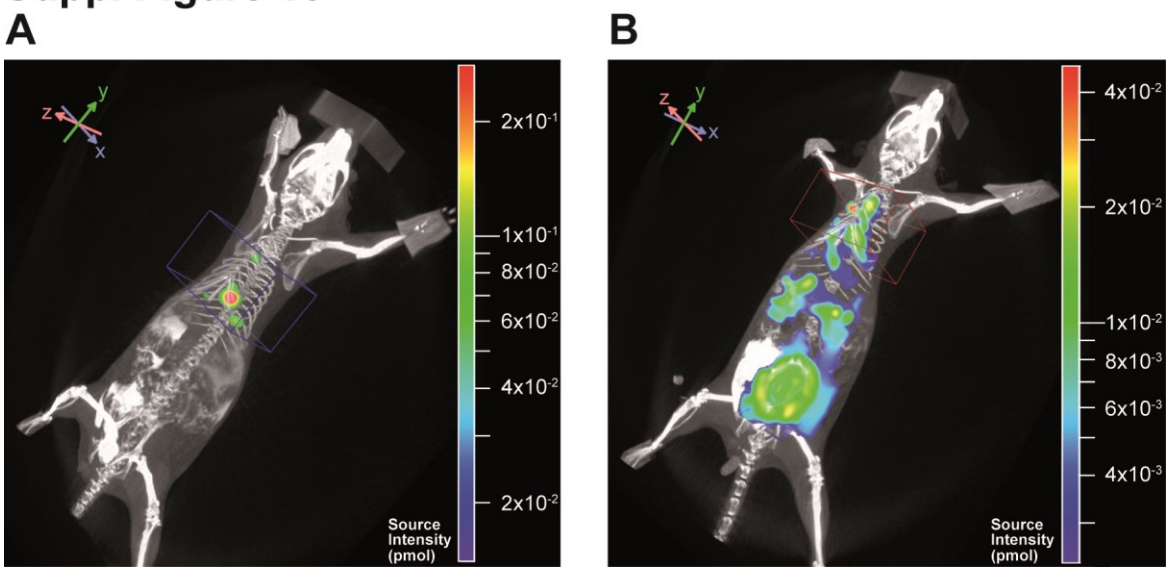

Figure S10: *Evaluation of fluorescence intensity (AF750 signal) from FLIT for amount of AF750-siRNA in the lung region at 0h (A) and 24h (B) after intratracheal application of auropolyplexes. For quantification of fluorescence signal in lungs a cuboid ROI was set over the thoracic area.*

Supp. Figure 11

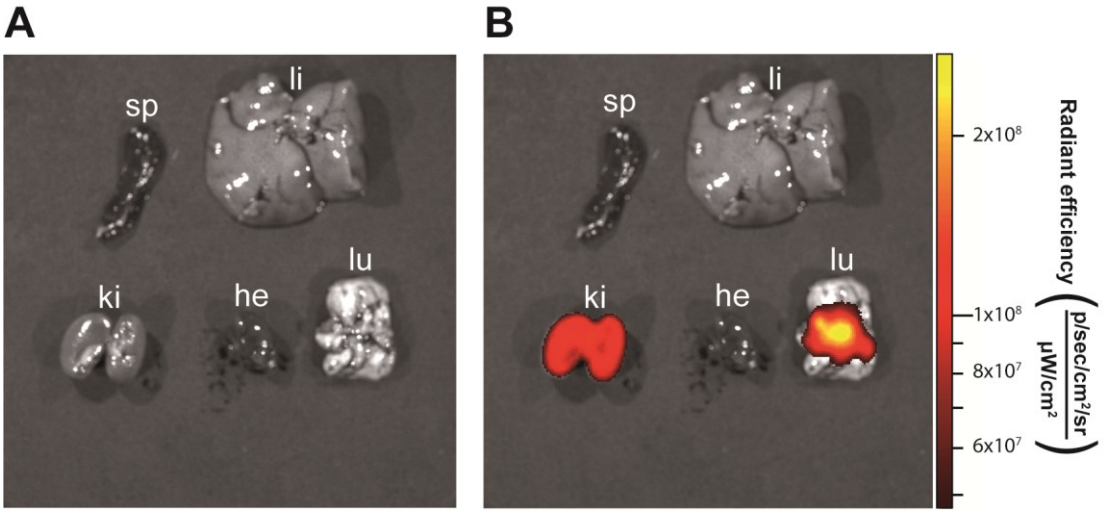

Figure S11: *Epifluorescence ex vivo organ imaging 24 h after intratracheal administration of auropolyplexes. Organs were analyzed for their AF750 signal derived from AF750-siRNA. Images are shown in grey scale picture (A) as well as an overlay of the grey scale picture with the pseudocolor fluorescence radiance image (B). Abbreviations: sp (spleen), li (liver), ki (kidneys), he (heart), lu (lungs)*

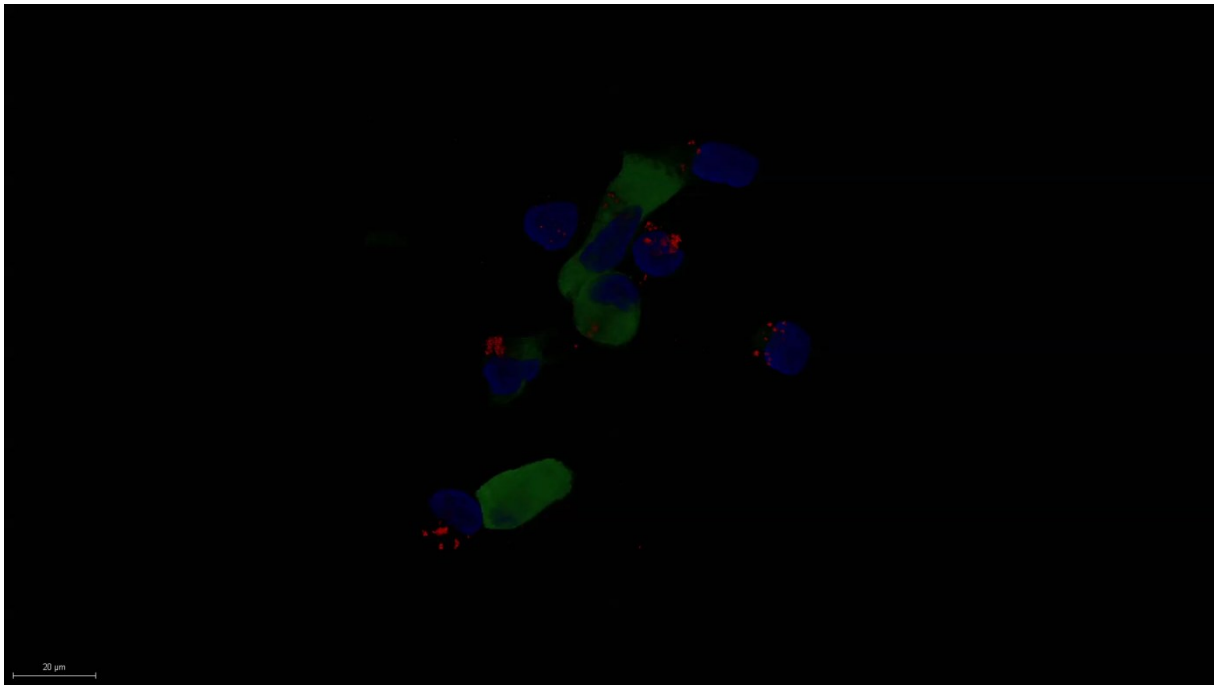

Video S1: *CLSM 3D reconstruction of EGFP-Luc expressing MDA-MB-231 treated with auropolyplexes based on AF647-labeled siRNA and LPEI5-SH. Z-scan was conducted at 63X magnification with a vertical resolution of 0.1 µm. DAPI signal is shown in blue, EGFP in green and AF647 in red.*

VI. Summary and conclusions

1. Optimization of LPEI polyplex generation

Section 2.1. (chapter "Results") is mainly dedicated to one of the major drawbacks of manual preparation of LPEI polyplexes which is possible operator dependent variations amongst different synthesis batches.[80] Furthermore, the standard procedure which is based on flash pipetting is limited to relatively small volumes.[81] Direct correlation of this operator dependent product quality with physical properties of nanoparticles like size and ζ-potential might therefore result in more or less significant changes of their biological behavior, such as transfection efficiency. The high dependency of transfection abilities of LPEI both *in vitro* and *in vivo* was described by other working groups which bring an average hydrodynamic diameter of <200 nm as important criterion for sufficient cellular uptake of LPEI polyplexes.[156] Hence, our main target was the optimization of a method for a fast and reproducible production of polyplexes characterized by small size and low polydispersity. For this and all other studies generation of polyplexes was always done under NaCl free conditions to avoid any negative influence of the buffer on particle stability. HEPES buffered glucose (HBG) was therefore used as standard medium as it supports the formation of small particles with low risk for particle aggregation over at least 30 minutes (data not shown). As the whole technique was based on employing a syringe pump for controlled mixing of LPEI and pDNA containing solutions even high volumes of the final formulation could be prepared which was especially needed for i.v. injections. Physical evaluation of nanoparticles was done by NTA which in comparison to dynamic light scattering systems (DLS) brings high resolution measurements of both hydrodynamic diameter and ζ-potential of nanoparticular fomulations giving the possibility of analyzing certain particle populations within one sample.[157]

By testing three different N/P ratios (3, 6, 9) further investigation on the influence of a surplus of free LPEI in the solution on particle stability could be made. At N/P 3, which is slightly above the electroneutrality point, polyplexes showed high tendency for particle aggregation and low pDNA recovery resulting in weak transfection efficiency which is also in accordance with literature.[75, 158, 159] Both N/P 6 and N/P 9 showed high particle stability and good *in vitro* transfection efficiency comparable to the one achieved with commercially available transfection agents. Testing both types of luciferases *in vitro* further revealed an advantage of the secreted Gaussia luciferase over intracellularly expressed firefly luciferase which is the possibility of investigating the cell viability post treatment besides the quantification of bioluminescence signal in the cell

culture medium. Additionally the application of Gaussia luciferase also better simulates the therapeutic aspect, as cancer gene therapy is often based on the use of secreted proteins, such as TNFα and the monocyte chemoattractant protein 1 (MCP-1) which even with a small amount of transfected cells allows an efficient by-stander effect.[160, 161]

As described above, the total amount of free LPEI in the formulation correlates with the transfection efficiency.[75] A comparison of N/P 6 and N/P 9 was therefore also done after i.v. administration. Both treatments resulted in lung specific luciferase expression with higher signal intensity for N/P 9. This unspecific transfection of lung tissue also due to the aggregation behaviour of particles based on unmodified LPEI after i.v. administration is supported by literature.[1, 96]

Taken together, the results presented in section 2.1. (chapter "Results") show the clear advantages of a syringe pump based mixing method for the generation of LPEI based polyplexes especially when it comes to the generation of higher formulation volumes. As most non-viral gene delivery formulations are in general based on mixing of the gene transfer agent with the nucleic acid fraction the protocol could in principle be directly adapted. Both the particle analysis by NTA and the evaluation of the transfection efficiency based on Gaussia luciferase assay showed high sensitivity and were therefore applied as standard methods in the following publications. *In vitro* and *in vivo* treatment with particles prepared at N/P 9 resulted in the highest transfection efficiency compared to both N/P 3 and 6 and was therefore always used in section 2.2 and 2.3 (chapter "Results"). As LPEI with a weight average molecular weight of 10 kDa resulted in the formation of stable particles with good transfection ability it was used in the following sections as either main transfection agent or as a control for positive transfection for pDNA delivery.

2. Application of iRFP720 as reporter for transfection studies

In vivo application of fluorescent reporter proteins shows some limitations mainly due to strong absorption of emitted light at lower wavelength.[115] Reporter proteins with emission below 600 nm like EGFP have clear restrictions in the use for *in vivo* imaging. In the range from 650 nm to 900 nm a minimum of light absorption by body tissue exists.[116] Therefore, near infrared fluorescent dyes like AlexaFluor® 750 could successfully be applied for detailed *in vivo* evaluation of pharmacokinetics of macromolecular formulations like modified siRNA.[20, 60, 162, 163] This advantage of near infrared fluorescent material for *in vivo* fluorescence imaging could also be

found for reporter proteins with near infrared emission profile enabling investigations on cancer growth.[115, 164] We therefore tested iRFP720 with an excitation maximum at 710 nm and an emission maximum at 760 nm for *in vitro* and *in vivo* gene delivery studies for LPEI mediated transfection. Due to its red shifted emission spectrum co-transfection studies with polyplexes based on LPEI and the plasmids piRFP720-N1 and pEGFP-N1 were done and evaluated by flow cytometry without signal compensation. However, fluorescence based transfection assays showed significantly reduced sensitivity compared to the application of bioluminescent reporter proteins.

Applicability of NIR reporter proteins *in vivo* were tested with 4T1 lung tumor cells which stably expressed iRFP720 with around 90 % positive cells. Despite the low fluorescence signal which might be due to a very diffuse growth of rather small metastasis in the lung tissue *in vivo* monitoring of cancer growth could be conducted and was therefore used in section 2.2. (chapter "Results") for finding the optimal tumor load for i.t. administration of LPEI polyplexes. Based on its controllable growth this tumor model was later on applied for testing the *in vivo* transfection efficiency of modified LPEI based gene delivery particles.

3. Passive and active targeting for treating lung metastasis with LPEI/pDNA polyplexes

The high potential of topical delivery of gene transfer particles into lungs for the treatment of primary tumors or metastasis has already been shown in previous publications.[147] Therefore, we optimized a procedure for the administration of nanoparticle containing solutions as aerosol via the i.t. route. Aerosolization was done with a Penn-Century MicroSprayer®/Syringe assembly which allows the generation of an aerosol under pressure without the additional need of gas. With that technique an average drop diameter ranging from 16 µm to 22 µm can be achieved using water as diluent.[165] Equal distribution of the formulation applied via i.t. microspraying could be shown by Geyer et al. with fluorescently labelled siRNA.[20] However, both the high pressure and the creation of shear forces which are generated during microspraying procedure showed influence on the hydrodynamic diameter of particles. Formation of aggregates and with that reduction of particle concentration could be detected. The impact on biological nanoparticle properties was tested with LPEI polyplexes *in vitro* where we could show a decreased but still sufficient transfection efficiency on tumor cells especially at N/P 9 (see section 2.2. (chapter "Results")).

Particle modifications are often needed in order to enhance stability and transfection efficiency when applied on lung tissue. Especially mucus which is permanently produced in respiratory pathways embodies a strong barrier for gene delivery formulations due to its high viscosity and the presence of nucleases.[100, 152, 153] Besides the particle size also their surface charge has strong influence on the ability of particles to traverse their payload through mucus to the targeted tissue.[153, 155] This problem could be shown in section 2.2. (chapter "Results") where we tested the transfection efficiency of LPEI/pDNA polyplexes after i.t. administration on a 4T1-iRFP720 lung tumor model. Sufficient tissue transfection was detected based on luciferase expression. iRFP720 expression enabled both monitoring of cancer growth and *in vivo* co-localization of fluorescence and the transfection induced luminescence signal. 24 h after polyplex administration a partial overlap of luciferase derived BLI signal and iRFP720 fluorescence signal could be detected. That indicates that the morphological structure of 4T1 tumor nodules which reach through the endothelium, the basal membrane and the alveolar wall into the air side contributes to good transfectability via topical administration. However, the application of unmodified LPEI polyplexes brought only very low luminescence signals which might be due to non-specific electrostatic interactions with mucus components leading to reduced stability of the particles.

Both a small hydrodynamic diameter and high stability of nanoparticular formulations are needed to overcome steric hindrances created by the dense mucin fiber network. Additionally, as mentioned above both electrostatic and hydrophobic interactions with mucus components might contribute to weak particle diffusion. Therefore, it is not surprising that the introduction of a shielding domain, such as PEG, could lead to a significant reduction of particle interactions with the environment resulting in an improvement of the diffusion rate of particles through lung mucus. Previous publications revealed efficient penetration of PEGylated polymeric nanoparticle formulations with hydrodynamic diameters of up to 200 nm through respiratory mucus.[155] Also in case of PEI polyplexes PEGylation brought a significant improvement of particle performance after i.t. instillation.[166] We therefore hypothesized in section 2.3. (chapter "Results") that the introduction of PEG on LPEI polyplexes might also lead to better transfection after aerosolization.[167] For that we generated a LPEI(10 kDa)-PEG(2kDa) conjugate following the synthetic route described by Schaffert et al. where a simple modification of LPEI with PEG (Mw 2 kDa) could be achieved with NHS based chemistry resulting in the formation of a stable carboxamide bond between LPEI and PEG.[125] A PEGylation degree of 1:1.2 led to the generation of pDNA polyplexes with small size and a sufficient reduction of the ζ-potential. The reduced cell association and transfection abilities *in vitro* of LPEI(10 kDa)-PEG(2kDa) polyplexes compared to

unmodified LPEI polyplexes stands in accordance to literature.[125, 127] I.t. administration in 4T1-iRFP720 lung tumor bearing animals under the same conditions used for LPEI polyplexes described in section 2.2. (chapter "Results") revealed increased transfection efficiency of PEGylated LPEI compared to unmodified LPEI of approx. 1 log potency. In case of this study, MRI and not the tumor derived fluorescence signal was used for evaluating tumor growth and its location in the lung tissue due to its higher sensitivity. Comparison of MRI and BLI images revealed that treatment with LPEI-PEG polyplexes results in a transfection of regions where tumor could be detected. Overall those results indicate that improved particle dissociation through the lung mucus layer can be achieved through PEGylation of LPEI.

However, some examples showed absolutely no transfection due to reduced accessibility of tumor tissue. This influence coming from the morphological heterogeneity of cancer tissue is besides other barriers a strong limiting factor for gene delivery agents and should therefore always be taken into consideration when it comes to designing nanoparticular formulations.[168]

As using LPEI-PEG might also result in transfection of healthy tissue through non-specific interactions we followed the strategy of introducing a targeting moiety for active targeting of CD49f. Stevenson et al. designed a peptide based on initial findings about the specific interaction between the E8 region of the α1 chain of laminin and CD49f with the sequence YESIKVAVS for targeted gene delivery with adenoviral formulations.[141] In their experiments YESIKVAVS brought both an increased transduction efficiency and high specificity *in vitro*.

For our experiments we modified YESIKVAVS with an N-terminal L-cystein to enable coupling of the targeting moiety to LPEI-PEG via a disulfide bridge. As the SIKVAV motif activates PI3k/Akt signaling at high treatment concentrations starting from 0.1 mM[145, 169] it was important for us to keep the treatment concentrations both *in vitro* and *in vivo* significantly lower.

Also here, the conjugate (described as LPEI-PEG-CD49f) was tested for both physical and biological properties. NTA of both particle size and ζ-potential showed only slight differences between LPEI-PEG-CD49f and LPEI-PEG polyplexes. *In vitro* experiments showed a clearly improved cell association and transfection efficiency of LPEI-PEG-CD49f compared to LPEI-PEG. As 4T1 cells have mediate to high expression of CD49f the 4T1-iRFP720 lung tumor model was used for evaluating *in vivo* particle performance of LPEI-PEG-CD49f polyplexes after i.t. aerosolization. Almost every treatment resulted in a distinct bioluminescence signal overlapping with tumor areas detected by MRI. Compared to LPEI-PEG treatment with LPEI-PEG-CD49f polyplexes resulted in BLI signals significantly higher than background. Same as with LPEI-PEG

polyplexes exceptions with almost no bioluminescence could be found in case of tumor areas with significantly reduced accessibility.

4. Combination of LPEI with gold nanoparticles for efficient siRNA delivery

Surface modifications of gold nanoparticles can be conducted via chemisorption of thiol containing compounds.[36] Via this route so called spherical nucleic acids based on thiolated siRNA bound on gold nanoparticles were generated and used for gene knock-down experiments in previous publications.[170] Main drawback of this formulation was that a big fraction of siRNA stayed bound on the gold surface after internalization hindering its accessibility for the transcriptional machinery.[56] Therefore, we followed another approach which was based on chemisorption of thiol terminated LPEI on gold nanoparticles as starting point for the generation of a formulation for efficient siRNA delivery which we called “auropolyplex” (see section 2.4. (chapter “Results”)).

Poly(2-alkyl-2-oxazoline) is normally used as initiating compound for LPEI generation. We synthesized α-benzyl ω-thiol LPEI (5 kDa; LPEI5-SH) of commercially available α-benzyl ω-thiol poly(2-ethyl-2-oxazoline) by acidic hydrolysis. Under slightly basic conditions coupling of LPEI5-SH on gold nanoparticles was done.

Quantitative size and ζ-potential analysis by NTA revealed the formation of stable and highly positively charged nanoparticles. Qualitative analysis by TEM enabled the visualization of the polymeric layer which had an average thickness of 6 nm. Additionally, coating of gold nanoparticles with LPEI resulted in a significant increase of particle stability in water after particle purification when compared to citrate stabilized particles. Therefore, those cationic gold nanoparticles could be stored after purification for at least 5 days at room temperature and used as “ready-to-use compound” for the following synthesis steps. This enabled the fast generation of complexes with siRNA and additional LPEI. This is one of the major advantages of this formulation compared to strategies like layer-by-layer assembly of gold nanoparticles which is characterized by a time consuming synthesis.

Further LPEI was added to the mixture of cationic gold nanoparticles and siRNA for complete condensation of the nucleic acid fraction in the formulation and the generation of positive surface charge which is needed for sufficient cell uptake. Gel retardation assays revealed efficient siRNA complexation also with LPEI with different molecular weights and LPEI modified

with PEG. TEM micrographs of auropolyplexes didn´t show impurities based on LPEI/siRNA polyplexes.

LPEI is known for its low efficiency in the transfection of cells with siRNA partly due to weaker interactions with nucleic acids compared to BPEI. Nevertheless, detailed analysis of biological properties of auropolyplexes showed good binding/uptake and high transfection efficiency. *In vitro* luciferase knock-down assays showed reductions of the light signal of up to 80 %. Knock-down efficiency directly correlated with the molecular weight of LPEI used for the last complexation step. LPEI with a weight average molecular weight of 10 kDa brought a 2fold improvement when compared to 5 kDa. Due to the synthetic approach also LPEI conjugates like LPEI10-PEG could be applied for preparation of auropolyplexes with reduced ζ-potential leading to decreased *in vitro* transfection efficiency.

In vivo biodistribution analysis of auropolyplexes was conducted via pulmonary delivery by aerosolization. Experiments were conducted with AlexaFluor® 750 labelled siRNA to enable *in vivo* monitoring of biodistribution processes. Initial experiments showed that using water as diluent for the formulation sometimes resulted in intense contraction of the chest area followed by expectoration of most of the administered solution. Therefore, for *in vivo* administration the whole preparation of auropolyplexes was conducted in HBG where complexes showed slight aggregation resulting in decrease of particle concentration of approx. one third. Microspraying of particles in HBG brought a 2-fold increase of the mean hydrodynamic diameter. However, *in vivo* administration was conducted as 40 % of nanoparticles had a size below 200 nm necessary for efficient lung deposition. 24 h after administration of the formulation a significant reduction of the fluorescence signal in lungs and a strong signal in kidneys and bladder could be detected. *Ex vivo* analysis of digested organs by ICP-MS revealed that the gold fraction was not able to traverse the air-blood barrier. Those findings indicate the efficient release of siRNA.

Taken together the generation of auropolyplexes and their advantageous physical and biological properties are further proof for the versatile applicability of LPEI as non-viral gene delivery agent. With those initial experiments the high potential of auropolyplexes as siRNA transfection agent could be shown. Further investigation especially based on the use of LPEI-PEG for the last complexation step are planned for the evaluation of a possible improvement of particle behavior in lung tissue linked to an increased transfection efficiency as observed after administration of LPEI-PEG polyplexes for pDNA delivery. Furthermore, using LPEI-PEG-PEPTIDE constructs for auropolyplex synthesis might give the possibility of sufficient targeting of cancer tissue.

VII. Appendix

1. Synthesis of polyethylenimine-based nanocarriers for systemic tumor targeting of nucleic acids

Chapter 6

Synthesis of Polyethylenimine-Based Nanocarriers for Systemic Tumor Targeting of Nucleic Acids

Wolfgang Rödl, Alexander Taschauer, David Schaffert, Ernst Wagner, and Manfred Ogris

Abstract

Nucleic acid-based therapies offer the option to treat tumors in a highly selective way, while toxicity towards healthy tissue can be avoided when proper delivery vehicles are used. We have recently developed carrier systems based on linear polyethylenimine, which after chemical coupling of protein- or peptide-based ligands can form nanosized polyplexes with plasmid DNA (pDNA) or RNA and deliver their payload into target cells by receptor-mediated endocytosis. This chapter describes the synthesis of LPEI from a precursor polymer and the current coupling techniques and purification procedure for peptide conjugates with linear polyethylenimine. A protocol is also given for the formation and characterization of polyplexes formed with LPEI conjugate and pDNA.

Key words Polyethylenimine, Polyethylene glycol, Molecular conjugates, EGF receptor, Targeting, Gene delivery

1 Introduction

The standard treatment for solid cancers is usually surgery, followed by radiotherapy and treatment with chemotherapeutic drugs. Dose-limiting toxicity and resistance mechanisms often preclude a successful treatment of relapsing disease. Nucleic acid-based therapeutics offer the possibility to develop highly specific, tailor made therapies for the treatment of malignant diseases taking into account the genetic aberrations occurring in tumor cells compared to healthy body tissue. For gene therapy approaches, the gene of interest is cloned into an appropriate expression cassette and can either be incorporated into a viral vector, for example the widely used adenovirus; as an alternative, plasmids are cloned and produced in *E. coli* for nonviral delivery approaches [1, 2]. Several physical delivery methods for plasmid are also applicable in vivo, like electroporation, particle bombardment, or ultrasound

Manfred Ogris and Haider Sami (eds.), *Nanotechnology for Nucleic Acid Delivery: Methods and Protocols*, Methods in Molecular Biology, vol. 1943, https://doi.org/10.1007/978-1-4939-9092-4_6,

enhanced delivery with microbubbles (*see* also Chapter 15 in this book, Vlaskou et al.). For systemic delivery, particle-mediated systems are commonly used, either based on lipids, polycations, or combinations thereof [3]. For polycation-based transfection systems, polyethylenimine (PEI) represents a kind of "golden standard" [4, 5]. PEIs are polymers with one of the highest charge densities: 1 mg of PEI contains approx. 23 μmol potentially protonatable amines, of which approx. 50% are protonated at pH 7 [6]. Due to its high positive charge density, nanosized particles, so called polyplexes, can be formed by electrostatic interaction after mixing PEI with nucleic acids containing a negatively charged phosphate backbone. PEI polyplexes, usually carrying a positive surface charge, bind to negatively charged cell surfaces mainly by interaction with proteoglycans and are thereafter internalized by adsorptive endocytosis [3, 7]. After internalization into endosomes and acidification by ATP driven proton pumps, additional amines become protonated leading to a so called proton sponge effect [8–10]: protons absorbed by PEI trigger the influx of chloride ions, which in turn leads to attraction of water molecules and the osmotic imbalance causes vesicle disruption and subsequent release of its payload into the cytoplasm. Besides branched PEI, linear PEI (LPEI) has been used for transfection studies in vitro and in vivo [11, 12]. Compared to branched PEI, LPEI exhibits a clearly improved transfection performance both in vitro and *in vivo* [13]. The synthesis of LPEI can be carried out by hydrolysis of the precursor polymer poly(2-ethyl-2-oxazoline) under highly acidic conditions [14, 15]. In order to obtain a product with fully biofunctional LPEI, care has to be taken that complete hydrolysis of the precursor is achieved, as residual N-acyl groups negatively affect the transfection efficiency [16]. Albeit being nonbiodegradable, LPEI-based vectors can be designed in a way that renders them well biocompatible. When polyplexes between LPEI and plasmid DNA are formed, they usually exhibit a positive surface charge and excess of free, not polyplex bound LPEI [17]. After intravenous injection, LPEI polyplexes rapidly interact with blood components and aggregate within the first vascular bed encountered, namely the lung [11, 12, 18]. This makes LPEI an excellent transfection reagent to achieve high transgene expression levels in the lung, where after crossing the endothelial barrier mostly pulmonary cells at the basolateral site are transfected [19]. At least two important parameters for this efficient transfection of lung tissue have been identified, namely the aggregation with blood platelets [20] and the presence of free, non-polyplex bound LPEI [17]. Although similar aggregation occurs with polyplexes based on branched PEI (BPEI), the latter polyplexes are far less efficient in lung transfection compared to LPEI [13]. Major reasons for this effect are the differences in the aggregation behavior and the dissociation behavior between PEI and plasmid DNA [21]. For optimal

transfection via the systemic route, LPEI polyplexes have to be rather small. After intravenous injection, LPEI polyplexes rapidly aggregate in the blood stream, which causes their entrapment in the lung. On the cellular level, a reduced binding strength towards plasmid DNA of LPEI compared to BPEI has been observed: LPEI polyplexes are dissociated after endocytosis within intracellular vesicles [22] and release intact plasmid [23], which then is accessible for the translation machinery. In vivo, LPEI polyplexes initially aggregating in the lung redistribute to a considerable extent to the liver within the first minutes after injection [24], whereas BPEI polyplexes do not. To reduce the interaction with blood components and aggregation in blood, LPEI can be, similarly as described for stealth liposomes, chemically modified with the hydrophilic polymer polyethylene glycol (PEG) [25, 26]. Coupling of PEG to LPEI is on the one hand beneficial when it comes to systemic application of polyplexes in vivo, where the PEG component significantly reduces protein binding, allows blood circulation and passive accumulation in well vascularized tumors [24, 27–29]. After cellular internalization, excessive PEGylation can be disadvantageous, as it negatively affects the endosomal release of polyplexes [25]. Such limitations can be overcome by designing pH-responsive PEI conjugates, for example by coupling PEG via chemical bonds which are cleaved after acidification of the endosome [30, 31]. Alternatively, rather short PEG molecules can be used, which prevent aggregation in blood and still allow transfection of tumor cells in vivo [32]. As for PEG, protein ligands like transferrin or EGF can hamper endosomal release of targeted polyplexes when coupled to PEI polyplexes, but also interfere with proper particle condensation [33–35]. Hence, we developed a platform for the development of targeted, LPEI polyplexes, where short, peptidic ligands are utilized [36]. Here, the peptidic ligand is coupled to LPEI via a rather short 2 kDa PEG spacer. To ensure the formation of LPEI-PEG-peptide conjugates without crosslinking of LPEI molecules, a heterobifunctional PEG linker 3-(2-pyridyldithio)propionamide-PEG-*N*-hydroxysuccinimide ester (short: OPSS-PEG-NHS) is used. In the first coupling step, the NHS group reacts with one of the secondary amines in the LPEI chain forming a stable amide bond. In order to improve the reactivity of the NHS ester with secondary amines and to reduce ester hydrolysis, this reaction step is best carried out under water-free conditions in absolute ethanol or other suitable solvents. After purification by cation exchange chromatography, which removes unreacted PEG, the distal OPSS group on the PEG linker is available for coupling to free thiols by forming a reducible disulfide bond [10, 36]. The thiopyridone group released during this reaction strongly absorbs at 343 nm, allowing UV control of the reaction. After a second cation exchange chromatography step, unreacted peptide and 2-thiopyridone are removed. The resulting LPEI-PEG-peptide conjugate forms nanosized polyplexes with

plasmid DNA, but also with RNA. With such polyplexes, targeted delivery and high transfection efficiency can be obtained both in vitro and in vivo in tumors after intratumoral [36] or intravenous polyplex administration [32]. For a further preclinical development it is of note that LPEI-based polyplexes have already been applied in clinical trials [37], and that LPEI is available in GMP grade from the company Polyplus in France (www.polyplus-transfection.com).

2 Materials

With the exception of the materials mentioned below, all reagents can be obtained from standard lab suppliers. Please choose the quality grade "per synthesis" if available. For all reactions in aqueous solution use desalted and highly purified water.

The precursor polymer for linear polyethylenimine (LPEI), poly(2-ethyl-2-oxazoline) (M_w 50 kDa) is obtained from Aldrich (Aldrich Cat. No. 37,284-6). Alternatively, LPEI with a molecular weight of 22 kDa can be purchased as ExGen 500 from Fermentas (Burlington, Canada). The heterobifunctional 2 kDa poly(ethylene glycol) (PEG) linker OPSS-PEG-NHS has been synthesized by Rapp Polymere GmbH (Tübingen, Germany); a 3 kDa version is available from IRIS Biotech (Marktredwitz, Germany). Peptides used in this study were synthesized by standard fmoc solid phase synthesis and obtained with more than 95% purity from Biosyntan (Berlin, Germany). Ion exchange resin MacroPrep HighS was purchased from Bio-Rad (Munich, Germany).

2.1 For LPEI Synthesis, the Following Equipment Is Needed

Round bottom flask (NS 29/32, 100 mL).

Reflux condenser (NS 29/32, 200–300 mm length).

Silicone oil bath.

Magnetic stirrer with heating function and stir bar.

50 mL centrifuge tubes

Centrifuge system.

Lyophilization system.

2.2 For Conjugate Synthesis the Following Lab Equipment Is Needed

Lab-shaker with controllable temperature.

Vortex mixer.

Glass vial (5–10 mL) equipped with stir bar.

Magnetic stirrer.

Sterile polypropylene tubes (2 mL and 15 mL).

Conjugates are purified on a HPLC/FPLC system running under aqueous conditions. A gradient mixer with at least two channels, a multiline UV/VIS detector, and a fraction collector are needed. pH

is checked by using a micro pH electrode; for photometric measurements a standard UV/VIS photometer is sufficient.

3 Methods

The following assays are used for quantification of LPEI conjugate components.

3.1 Quantification of LPEI (Copper Assay)

This assay has been first described by Ungaro et al. [38]. After adding a solution of Cu^{2+} to LPEI solutions a dark blue cuprammonium complex is formed, which absorbs strongly at 285 nm enabling quantification of the LPEI content in an aqueous solution.

1. Prepare 100 mL of Cu^{2+} solution by dissolving 23 mg of $CuSO_4$ in 0.1 M Na-acetate buffer (pH 5.4).
2. For creating a standard curve prepare LPEI standard solutions in water with a final volume of 100 μL at concentrations ranging from 10–100 μg/mL. Use 100 μL water as blank. Standard solutions should always be analyzed in duplicates.
3. Dilute your LPEI sample to be analyzed also to a final volume of 100 μL with water. Use duplicates and different dilutions of sample in water.
4. Mix 100 μL Cu^{2+} solution with the blank, the standard solutions and the samples and incubate at room temperature for 5 min.
5. Set the absorption wavelength to 285 nm on a standard UV/Vis spectrophotometer and set the absorption of the blank to zero.
6. Measure the absorption of LPEI solutions and LPEI samples to be analyzed and calculate the LPEI concentration with the help of the standard curve (*see* **Note 1**).

3.2 Determination of OPSS Content

After addition of excess DTT (Dithiothreitol; 1 M stock in water) to a sample containing an OPSS group, 2-thiopyridone gets released and induces UV absorption at 343 nm ($\varepsilon_{343\ nm} = 8080\ M^{-1}\ cm^{-1}$).

1. Dilute the OPSS containing sample in 150 μL water, add 15 μL 1 M DTT solution, mix well, and incubate for 10 min. Use 15 μL 1 M DTT diluted with 150 μL water as blank.
2. Transfer to a micro cuvette suitable for UV measurement and measure the absorption at 343 nm against the blank. Calculate the OPSS concentration with $\varepsilon_{343\ nm} = 8080\ M^{-1}\ cm^{-1}$ taking into account the dilution factor.

3.3 Quantification of LPEI/PEG Ratio by ^{1}H-NMR

In addition to the copper and DTT assay, ^{1}H-NMR analysis allows nondestructive determination of the molar ratio between LPEI and PEG in a conjugate. By comparison of the distinct proton signals of ethylene glycol units of PEG and ethyleneimine units of LPEI the yield of the PEGylation reaction can be calculated.

1. Dissolve 5 mg of LPEI-PEG-OPSS (synthesis described in Subheading 3.7) in 1 mL D_2O.
2. Adjust the pH of the solution to pH 7 based on pH paper using 1 M stock solutions of DCl or NaOD (*see* **Note 2**).
3. Analysis is then carried out on a ≥200 MHz NMR with 3-(trimethyl silyl) propionic-2,2,3,3-d_4 acid (TSP) as internal reference. Alternatively, the residual solvent peak can be used to correct the spectrum.

The spectrum is characterized by two major signals, a rather broad LPEI signal at 2.9–3.1 ppm (derived from –C**H$_2$**–C**H$_2$**–N) and a sharp PEG signal (derived from –C**H$_2$**–C**H$_2$**–O) at 3.7 ppm (*see* **Note 3**). The signals of the OPSS moiety can be observed above 7 ppm, but with lower PEGylation rates these signals are normally too weak to allow quantification.

To quantify the degree of PEGylation use the integral of the LPEI derived –C**H$_2$**–C**H$_2$**–N signal (2.9–3.1 ppm) to normalize the other signals. In the representative example (Fig. 1) the integral of the LPEI derived signal was set to 2047 ($N = [22{,}000(M_{w(\mathrm{LPEI})})/43(M_{w(\mathrm{ethyleneimine\ monomer})})] \times 4$ (Protons per –C**H$_2$**–C**H$_2$**–N unit). Calculate the number of protons in the PEG-chain using $N = [\mathrm{PEG}(M_{w(\mathrm{PEG})})/44$ ($M_{w(\mathrm{ethylene\ glycol\ monomer})}$)] × 4 (Protons per –C**H$_2$**–C**H$_2$**–O unit). For PEG with a M_w of 2 kDa this yields 182. Divide the integral value of the PEG-signal (3.7 ppm) by 182 to obtain the average number of PEG chains per PEI molecule. In the representative example (Fig. 1) the integral value of the PEG derived signal is 192 which results in a PEG/LPEI ratio of 1.05:1.

3.4 Quantification of Free Thiols (Ellman's Assay)

This assay is based on the thiol-specific reactivity of Ellman's reagent (5,5′-dithiobis-(2-nitrobenzoic acid), short DTNB) forming mixed disulfides. During the reaction, 2-nitro-5-thiobenzoate (TNB) is released, which can be quantified by measuring the absorption at 412 nm [39].

1. Dissolve 2 mg DTNB in 0.1 M HEPES pH 7.4 (*see* **Note 4**).
2. Dilute 5 µL of the solution from **step 1**, fill up to 500 µL with 0.1 M HEPES pH 7.4 and use as a blank on a photometer set to an absorption wavelength of 412 nm.
3. Dilute your sample (using different amounts) in the solution from **step 1**, incubate for 20 min at ambient temperature and measure the absorption at 412 nm.

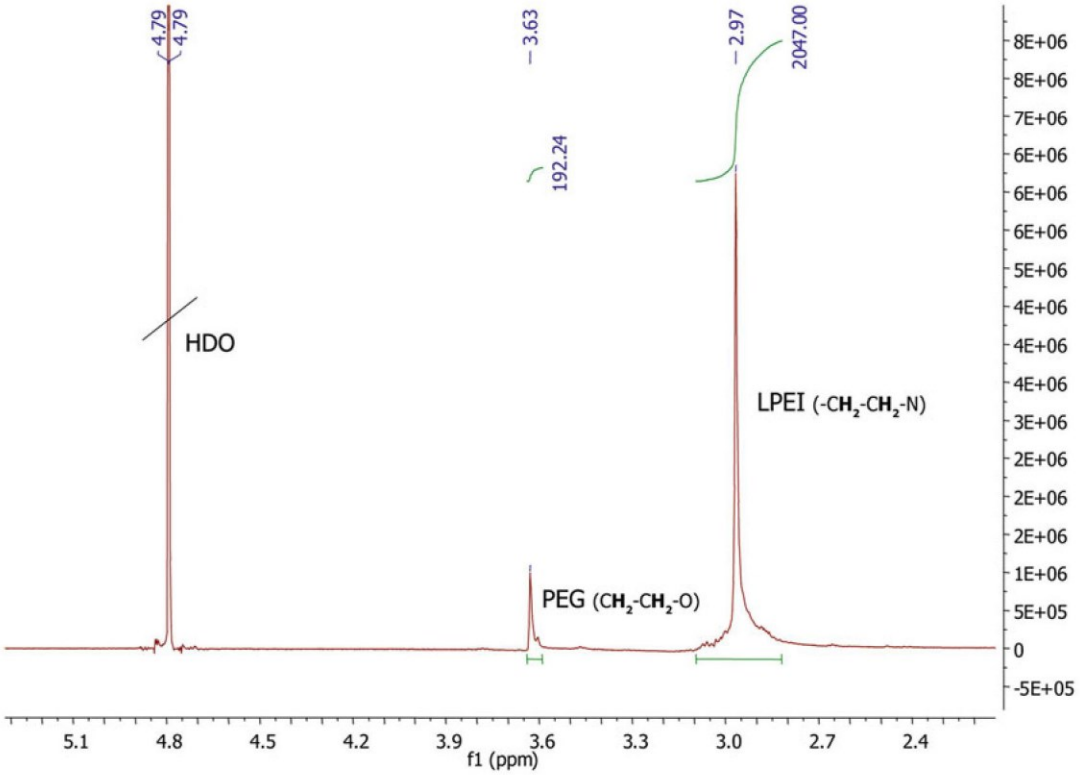

Fig. 1 ^{1}H NMR profile of LPEI-PEG-OPSS. OPSS-PEG-NHS (M_w 2 kDa) has been coupled to LPEI (M_w 22 kDa) as described in Subheading 3.7 and the integral of the –CH_2–CH_2–N signal (LPEI derived) (green line at 2.97 ppm) set to 2047. The number of protons in PEG (M_w 2 kDa) are (2000/44) × 4 = 182. The molar ratio PEG/LPEI is calculated by dividing the integral value of the –CH_2–CH_2–O signal (PEG derived; green line at 3.63 ppm) by the number or protons in PEG: 192/182 = 1.05 PEG_{2kDa}/$LPEI_{22kDa}$ M/M

4. Calculate the thiol content using the molar extinction coefficient $\varepsilon_{412nm} = 14{,}100\ M^{-1}\ cm^{-1}$).

3.5 Peptide Quantification by A_{280} Measurement

Prior to coupling, the absorption coefficient of the peptide has to be estimated, as the peptide content in conjugates is calculated according to the absorption of aromatic amino acids within the peptide. For this purpose, a useful online tool from the Expasy Bioinformatics tool portal (expasy.org) can be utilized (*see* http://web.expasy.org/protparam/). The molar extinction coefficient (ε) is calculated with the following formula:

$$\varepsilon_{(\text{Peptide})} = \text{Number(Tyr)} \times \varepsilon_{(\text{Tyr})} + \text{Number(Trp)} \times \varepsilon_{(\text{Trp})} + \text{Number(Cys)} \times \varepsilon_{(\text{Cys})}$$

For proteins in water measured at 280 nm use the following extinction coefficients:

$$\varepsilon_{(\mathrm{Tyr})} = 1{,}490\ \mathrm{M}^{-1}\ \mathrm{cm}^{-1};\ \varepsilon_{(\mathrm{Trp})} = 5{,}500\ \mathrm{M}^{-1}\ \mathrm{cm}^{-1};\ \varepsilon_{(\mathrm{Cys})} = 125\ \mathrm{M}^{-1}\ \mathrm{cm}^{-1}$$

For the GE11 peptide (**C<u>Y</u>HW<u>Y</u>G<u>YT</u>PQNVI**; GE11 sequence in bold letters; amino acids taken for calculating extinction coefficient are underlined) the extinction coefficient $\varepsilon_{280\mathrm{nm}} = 9970\ \mathrm{M}^{-1}\ \mathrm{cm}^{-1}$ is calculated.

Nevertheless, it is of note that the theoretical calculation of $\varepsilon_{280\mathrm{nm}}$ has to be amended by absorption measurements at 280 nm with the actual peptide used.

In the following subheadings, the synthesis of LPEI from the precursor molecule and the conjugate synthesis are described.

3.6 Synthesis of LPEI (M_w 22 kDa) from Poly (2-Ethyl-2-Oxazoline) (M_w 50 kDa)

3.6.1 Synthesis of LPEI–HCl

1. Dissolve 5 g poly(2-ethyl-2-oxazoline) 50 kDa (100 μmol) in 50 mL HCl (30% v/v) in a 100 mL round bottom flask (*see* **Note 5**).
2. Attach the round bottom flask to the reflux condenser and connect the reflux condenser to the cooling system. Boil the reaction under reflux and constant stirring for 16 h (*see* **Note 6**).
3. Cool the reaction to room temperature.
4. Transfer the content of the round bottom flask including the fine, white precipitate into a 50 mL centrifuge tube.
5. Centrifuge at 4000 × *g* for 5 min and remove the supernatant.
6. Carry out three repeated washes of the precipitate with 40 mL 30% (v/v) HCl per washing cycle as in **step 5** (*see* **Note 7**). The isolated precipitate is LPEI as HCl salt.
7. Dissolve the precipitate in 200 mL water and lyophilize the product (*see* **Note 8**).

3.6.2 Synthesis of LPEI (Free Base)

1. Transfer 2 g LPEI–HCl to a round bottom flask and resuspend it in 30 mL 1 M NaOH.
2. Attach the round bottom flask to the reflux condenser and connect the reflux condenser to the cooling system. Boil the reaction under reflux using an oil bath under constant stirring. Carefully add 1 M NaOH (in 10 mL portions) to the still hot solution until the solution is clear (*see* **Note 5**); then switch off the heating.
3. Transfer the content of the round bottom flask including white precipitate into 50 mL centrifuge tubes.
4. Centrifuge at 4000 × *g* for 5 min and remove the supernatant.
5. Carry out three repeated washes of the precipitate with 40 mL 1 M NaOH (per tube) per washing cycle as in **step 5**. Conduct 5 further washing cycles with 40 mL water (per tube).

6. Resuspend the precipitate in 50 mL water and transfer into a 100 mL round bottom flask.
7. Lyophilize product.
8. The resulting LPEI can be stored at room temperature in a desiccator protected from light.

3.7 Synthesis and Purification of LPEI-PEG-OPSS

1. Dissolve 75 mg (3.4 μmol) LPEI (free base; M_w 22,000) in 1.5 mL absolute ethanol in a 2 mL polypropylene reaction vial with lid and incubate on a standard lab mixer for 15 min at 800 rpm and 35 °C (*see* **Note 9**).
2. Dissolve OPSS-PEG-NHS linker (6.8 μmol; 2 eq based on LPEI) in 100 μL DMSO (water free), add to the reaction mixture from step 1 and incubate again for 3 h at 35 °C with 800 rpm.
3. Quench the reaction by adding 100 μL 1 M Tris (pH 8.0) and incubating for 15 min at 35 °C with 800 rpm.
4. Transfer the reaction mixture to a 15 mL polypropylene tube and add approximately 2 mL of a 20 mM HEPES solution pH 7.4 (pH 7.4) and 20 mM HEPES–3 M NaCl (pH 7.4), so that in the final volume of 5 mL the NaCl concentration reaches 0.5 M (the starting NaCl concentration during ion exchange purification, *see* below) (*see* **Notes 10** and **11**).
5. Adjust the pH with 1 M HCl and check the pH with a micro pH probe until pH 7 is reached. Thereafter fill up the reaction mix to 5 mL with 20 mM HEPES (pH 7.4) (*see* **Notes 12** and **13**).
6. Equip the HPLC system with a column (HR10/10, i.e., 10 cm in length, 10 mm diameter) filled with cation exchange resin (MacroPrep High S). Set the UV detector to 240, 280 and 343 nm. Equilibrate the system with 83.3% solution A (20 mM HEPES; pH 7.4) and 16.7% solution B (20 mM HEPES–3 M NaCl; pH 7.4) for at least 1 h at a flow rate of 0.5 mL/min; this corresponds to a concentration of 500 mM NaCl and 20 mM HEPES at pH 7.4.
7. Program a gradient (flow rate: 0.5 mL/min) with 16.7% A and 83.3% B from 0 to 25 min, and linear change to 100% B over 40 min (25–65 min), followed by 100% B for 20 min.
8. Load the product from **step 4** onto the column and run the gradient. Fractions eluting during the first 25 min (at 500 mM NaCl, 20 mM HEPES pH 7.4) contain unreacted OPSS-PEG-NHS and by-products from the reaction between the NHS ester in PEG and amines in LPEI. A representative chromatogram is shown in Fig. 2. Fractions eluting between 2.0 and 2.8 M NaCl contain LPEI modified with PEG (LPEI-PEG-

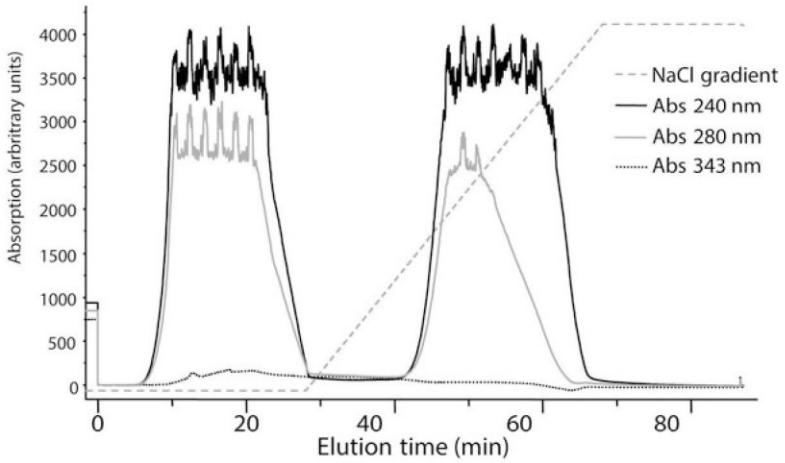

Fig. 2 Cation exchange chromatography profile of LPEI-PEG-OPSS. 5 mL reaction mixture from **step 5**, Subheading 3.7, were loaded onto a HR10/10 cation exchange column and purified as described in the text. Fraction eluting from 40 to 60 min were pooled and further processed as described

OPSS), these fractions are pooled and subsequently dialyzed against 5 L water at 4 °C under constant stirring overnight.

9. Lyophilize product (*see* **Note 14**).

3.8 Coupling of Peptide to LPEI-PEG-OPSS

The peptide C**YHWYGYTPQNVI** (sequence of GE11 in bold letters, *see* ref. 36) used in this study was synthesized by standard Fmoc solid phase peptide synthesis and purified on a C18 reversed phase HPLC column. The product was eluted with an acetonitrile gradient (A: 0.05% (v/v) TFA in water, B: 0.05% TFA (v/v) in 80% acetonitrile in water), 0.6 mL/min flow, linear gradient 2.5% B/min, detection at 220 nm) the peptide eluted at 13.1 min) and thereafter lyophilized (*see* **Note 15**).

1. For this reaction always use 2 equivalents of peptide based on OPSS in the sample.
2. The whole reaction can be conducted in a glass vial equipped with a magnetic stir bar.
3. Purge all solvents used for this synthesis (30% acetonitrile–-water–0.1% TFA; 20 mM HEPES–30% acetonitrile [pH 7.4]; 20 mM HEPES–3 M NaCl–10% (v/v) acetonitrile [pH 7.4]) with argon.
4. Dissolve the peptide in 100 μL 30% acetonitrile–water–0.1% TFA.
   (a) To ensure that the thiol residue has not been oxidized or dimerized, quantify the free thiol content by Ellman's assay. For this purpose, dilute 1 μL peptide sample 1:100

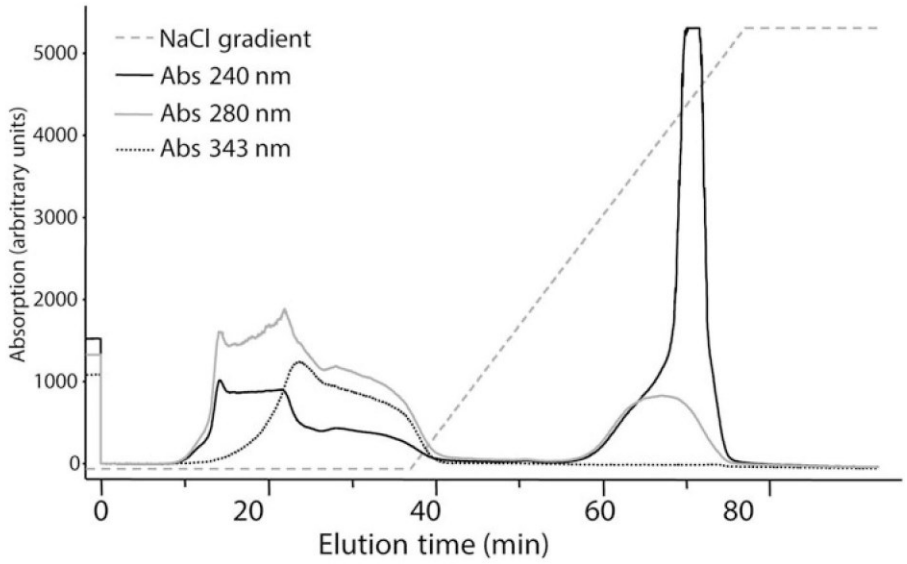

Fig. 3 Cation exchange chromatography profile of LPEI-PEG-GE11. 10 mL reaction mixture from **step 11**, Subheading 3.8, were loaded onto a HR10/10 cation exchange column and purified as described in the text. Fraction eluting from 57 to 77 min were pooled and further processed as described

with water and use 15 μL dilution for the assay, proceed as described in Subheading 3.4.

5. Dissolve LPEI-PEG-OPSS in 20 mM HEPES–30% acetonitrile (pH 7.4) (*see* **Note 16**).
   (a) The final concentration of LPEI in the reaction mix should be between 4 and 5 mg/mL.
6. For online reaction monitoring, check the absorption of the LPEI-PEG-OPSS solution at 343 nm prior to mixing.
7. Add the peptide solution (2 eq in 100 μL, *see* above) to the LPEI-PEG-OPSS solution and incubate at room temperature under constant stirring.
8. Thereafter (approx. 1 min) transfer a 150 μL sample from the reaction mix into a cuvette and measure A_{343} with a UV/Vis spectrophotometer. From then on A_{343} is measured every 30 min, until there is no more increase in absorption observed.
9. Calculate the 2-thiopyridone released as described in Subheading 3.2.
10. Add 20 mM HEPES–3 M NaCl–10% (v/v) acetonitrile (pH 7.4) to obtain a final concentration of 500 mM NaCl in a final volume of 5 mL.
11. Fill up to 5 mL with 20 mM HEPES–10% (v/v) acetonitrile (pH 7.4) (*see* **Note 13**).

12. Equip a HPLC/FPLC system with a 10/10 MacroPrep column (MacroPrep High S; HR10/10; Bio-Rad, München, Germany). Set the UV detector to 240, 280, and 343 nm. Equilibrate the system with 83.3% solution A (20 mM HEPES–10% (v/v) acetonitrile; pH 7.4) and 16.7% solution B (20 mM HEPES–3 M NaCl–10% (v/v) acetonitrile; pH 7.4) for at least 1 h at a flow rate of 0.5 mL/min; this corresponds to a concentration of 500 mM NaCl.
13. Program a gradient (flow rate: 0.5 mL/min) with 16.7% A and 83.3% B from 0 to 35 min, and linear change to 100% B over 40 min followed by 100% B for 20 min.
14. Load the product from **step 11** onto the column and run the gradient. The product elutes between 2.0 and 2.8 M NaCl (Fig. 2). A chromatogram from this purification step is depicted in Fig. 3.
15. Pool the fractions eluting between 2 and 2.8 M NaCl and dialyze them against 5 L water at 4 °C under constant stirring overnight.
16. Lyophilize product.
17. At this stage the product can be stored under dry conditions at −80 °C.
18. For analyzing LPEI and peptide content reconstitute conjugate in water and set pH to 7.
19. Analyze the LPEI content in the conjugate by copper assay.
20. Calculate the peptide concentration as described in Subheading 3.5. For the measurement, take a 150 µL aliquot of your sample (undiluted, can be reused, so use sterile, clean cuvettes) and measure the absorption at 280 nm.
21. For further storage of conjugate containing solutions freeze aliquots (snap freezing) and store at −80 °C.

3.9 Polyplex Formation

The LPEI-PEG-peptide conjugates have been developed for local or systemic delivery of nucleic acids in vivo. For this purpose, polyplexes are generated in a low salt buffer (HBG: HEPES buffered glucose, 20 mM HEPES–5% glucose w/v [pH 7.4]). This allows the formation of rather small, colloidal stable polyplexes.

The HBG buffer is sterile filtered (0.2 µm pore size) and stored in aliquots either at 4 °C or frozen at −20 °C. Plasmid DNA is usually produced in suitable *E. coli* strains and the plasmid isolated after alkaline lysis of bacterial cells using commercially available purification kits. Please make sure to use kits which result in a low endotoxin contamination in the purified plasmid. Alternatively, plasmids can be produced by companies specialized in plasmid production (*see* **Note 17**).

LPEI/pDNA polyplexes are defined by their molar ratio of phosphate in plasmid and nitrogen in LPEI (N/P ratio). The N/P ratio is transformed into a w/w ratio by the following formula:

$$\mu g \text{ PEI} = \mu g \text{ DNA} \times 43 \times (\text{N/P ratio})/330.$$

Forty-three is the molecular weight of one repeating [CH_2–CH_2–NH] unit in PEI (N), and 330 is the average molecular weight of one nucleotide (P). Polyplexes with N/P ratios ranging from 5 to 10 are recommended.

Here, an example is given to obtain 500 μL polyplexes containing 100 μg plasmid DNA at an N/P ratio of 6.

1. Prepare 250 μL plasmid diluted in HBG (final plasmid concentration 400 μg/mL).
2. Prepare 250 μL LPEI-PEG-peptide conjugate solution in HBG (amount of LPEI in 250 μL total volume: $100 \times 43 \times 6/330 = 78.18$ μg).
3. Transfer the LPEI-PEG-peptide dilution to the plasmid dilution and immediately pipet the solution 10 times up and down (*see* **Note 18**).
4. For quality control, measure polyplex size and zeta potential by dynamic light scattering (DLS) or nanoparticle tracking analysis (NTA). The average particle size should be below 300 nm.
5. Store polyplex containing solution at ambient temperature for no longer than 20 min prior to use.

4 Notes

1. The absorption value of your sample should be between 0.1 and 1.2 to ensure linear correlation between absorption and LPEI concentration.
2. Adjusting the pH to 7.0 with deuterated hydrochloric acid (DCl) or deuterated sodium hydroxide (NaOD) is important at this step to obtain comparable results, as acidic pH can cause a shift of the LPEI peak towards 3.5 ppm.
3. One has to be aware of the possibility of additional peaks due to incomplete deprotection of the LPEI-precursor, especially signals of propionamidyl residues (1.2–1.3 ppm; 2.1–2.3 ppm; 3.5–3.8 ppm) can lead to a overestimation of PEGylation [40]. When dissolved in D_2O secondary amines of LPEI-PEG-OPSS do not show a signal in ^1H NMR.
4. Always prepare the Ellman's reagent fresh, do not exceed storage for longer than 1 day.

5. Take safety measures (protective goggles, gloves, lab coat) when handling highly concentrated acids or alkaline.
6. Carry out the reaction in a fume hood and take proper safety measures when carrying out the reaction overnight. The reaction mixture appears first clear, after approximately 5 h a white precipitate is formed (LPEI–HCl).
7. Washings steps have to be repeated until the supernatant is clear and odorless. The residual propionic acid can develop a strong odor.
8. LPEI–HCl is well soluble in water at pH >2, but remains insoluble in >25% (v/v) HCl. At this step, LPEI–HCl can be neutralized with concentrated NaOH to pH 7 and thereafter used as transfection reagent. To calculate the LPEI, content, please note that LPEI–HCl has a molecular weight of 79.6 Da per repeating unit ($[CH_2–CH_2–NH].HCl$).
9. LPEI dissolves fast, but constant mixing is necessary to achieve a homogeneous solution, which is highly viscous.
10. When adding in 10 μL aliquots HCl in, do this under constant vortexing to avoid local low pH, which could result in LPEI precipitation. Cave: the solutions heats up if HCl is added too fast.
11. All solutions used for diluting the sample have to be purged with argon or nitrogen for at least 15 min prior to use.
12. This is necessary to reduce the EtOH concentration prior to loading of the mix onto the ion exchange columns, where otherwise a too high EtOH concentration results in pressure increase and compression of the column material.
13. Before loading the sample on the HPLC/FPLC the sample should always be filtered at least through a 0.45 μm filter.
14. At this step, the resulting LPEI-PEG-OPSS conjugate can be stored at −80 °C until further use.
15. Peptides containing free thiols, like the terminal Cys residue, should be stored under argon at −80 °C for no longer than a month, depending on the peptide. After extended storage, dimerization or oxidation of thiol groups occurs.
16. Make sure that the final reaction mixture contains at least a concentration of acetonitrile needed for dissolving the peptide, otherwise the peptide can precipitate. In case of C**YHWY-GYTPQNVI** (GE11 sequence in bold letters) it is 30% (v/v) acetonitrile.
17. Elevated levels of high molecular weight bacterial genomic DNA can be present in the plasmid preparation using commercialized isolation kits [41], especially when using for example low copy plasmid [42]. In such cases, preparations methods

using additional purification steps are recommended [41]. For example, the company PlasmidFactory (www.plasmidfactory.com) offers plasmid in "ccc" grade, that is, supercoiled plasmid structure and absence of bacterial genomic DNA impurities. Besides biological effects, the presence of high molecular weight DNA impurities can lead to excessive particle aggregation during the mixing process. For the generation of well-defined larger batches of polyplexes, methods using controllable mixing devices are recommended (*see* refs. 18, 43 and Chapter 14 in this book).

18. Mixing should be done immediately, to avoid formation of aggregates; the appearance of aggregates correlates positively with an increase in the final concentration of polyplexes and the salt concentration in the dilution buffer; there is a negative correlation with the increase in the N/P ratio, *see* also ref. 44).

Acknowledgments

This work was supported by the Center for Nanoscience (CeNS) and the German Research Foundation (SFB824) to M.O., and the Nanosystems Initiative Munich (NIM) to E.W.

References

1. Gehrig S, Sami H, Ogris M (2014) Gene therapy and imaging in preclinical and clinical oncology: recent developments in therapy and theranostics. Ther Deliv 12:1275–1296
2. El-Aneed A (2004) An overview of current delivery systems in cancer gene therapy. J Control Release 94:1–14
3. Pack DW, Hoffman AS, Pun S, Stayton PS (2005) Design and development of polymers for gene delivery. Nat Rev Drug Discov 4:581–593
4. Boussif O, Lezoualc'h F, Zanta MA, Mergny MD, Scherman D, Demeneix B, Behr JP (1995) A versatile vector for gene and oligonucleotide transfer into cells in culture and in vivo: polyethylenimine. Proc Natl Acad Sci U S A 92:7297–7301
5. Kircheis R, Wightman L, Wagner E (2001) Design and gene delivery activity of modified polyethylenimines. Adv Drug Deliv Rev 53:341–358
6. Tang MX, Szoka FC (1997) The influence of polymer structure on the interactions of cationic polymers with DNA and morphology of the resulting complexes. Gene Ther 4:823–832
7. Kopatz I, Remy JS, Behr JP (2004) A model for non-viral gene delivery: through syndecan adhesion molecules and powered by actin. J Gene Med 6:769–776
8. Sonawane ND, Szoka FC Jr, Verkman AS (2003) Chloride accumulation and swelling in endosomes enhances DNA transfer by polyamine-DNA polyplexes. J Biol Chem 278:44826–44831
9. Nguyen J, Szoka FC (2012) Nucleic acid delivery: the missing pieces of the puzzle? Acc Chem Res 45:1153–1162
10. Schaffert D, Ogris M (2013) Nucleic acid carrier systems based on polyethylenimine conjugates for the treatment of metastatic tumors. Curr Med Chem 20:3456–3470
11. Ferrari S, Moro E, Pettenazzo A, Behr JP, Zacchello F, Scarpa M (1997) ExGen 500 is an efficient vector for gene delivery to lung epithelial cells in vitro and in vivo. Gene Ther 4:1100–1106
12. Goula D, Benoist C, Mantero S, Merlo G, Levi G, Demeneix BA (1998) Polyethylenimine-based intravenous delivery of transgenes to mouse lung. Gene Ther 5:1291–1295

13. Wightman L, Kircheis R, Rossler V, Carotta S, Ruzicka R, Kursa M, Wagner E (2001) Different behavior of branched and linear polyethylenimine for gene delivery in vitro and in vivo. J Gene Med 3:362–372
14. Brissault B, Kichler A, Guis C, Leborgne C, Danos O, Cheradame H (2003) Synthesis of linear polyethylenimine derivatives for DNA transfection. Bio Conjug Chem 14:581–587
15. Ogris M, Wagner E (2012) Synthesis of linear polyethylenimine and use in transfection. Cold Spring Harb Protoc 2012:246–250
16. Thomas M, Lu JJ, Ge Q, Zhang C, Chen J, Klibanov AM (2005) Full deacylation of polyethylenimine dramatically boosts its gene delivery efficiency and specificity to mouse lung. Proc Natl Acad Sci U S A 102:5679–5684
17. Boeckle S, von Gersdorff K, van der Piepen S, Culmsee C, Wagner E, Ogris M (2004) Purification of polyethylenimine polyplexes highlights the role of free polycations in gene transfer. J Gene Med 6:1102–1111
18. Taschauer A, Geyer A, Gehrig S, Maier J, Sami H, Ogris M (2016) Up-scaled synthesis and characterization of nonviral gene delivery particles for transient in vitro and in vivo transgene expression. Hum Gene Ther Methods 27:87–97
19. Goula D, Becker N, Lemkine GF, Normandie P, Rodrigues J, Mantero S, Levi G, Demeneix BA (2000) Rapid crossing of the pulmonary endothelial barrier by polyethylenimine/DNA complexes 965. Gene Ther 7:499–504
20. Chollet P, Favrot MC, Hurbin A, Coll JL (2002) Side-effects of a systemic injection of linear polyethylenimine-DNA complexes. J Gene Med 4:84–91
21. Kwok A, Hart SL (2011) Comparative structural and functional studies of nanoparticle formulations for DNA and siRNA delivery. Nanomedicine 7:210–219
22. Itaka K, Harada A, Yamasaki Y, Nakamura K, Kawaguchi H, Kataoka K (2004) In situ single cell observation by fluorescence resonance energy transfer reveals fast intra-cytoplasmic delivery and easy release of plasmid DNA complexed with linear polyethylenimine. J Gene Med 6:76–84
23. de Bruin KG, Fella C, Ogris M, Wagner E, Ruthardt N, Brauchle C (2008) Dynamics of photoinduced endosomal release of polyplexes. J Control Release 130:175–182
24. Zintchenko A, Susha AS, Concia M, Feldmann J, Wagner E, Rogach AL, Ogris M (2009) Drug nanocarriers labeled with near-infrared-emitting quantum dots (quantoplexes): imaging fast dynamics of distribution in living animals. Mol Ther 17:1849–1856
25. Kursa M, Walker GF, Roessler V, Ogris M, Roedl W, Kircheis R, Wagner E (2003) Novel shielded transferrin-polyethylene glycol-polyethylenimine/DNA complexes for systemic tumor-targeted gene transfer. Bioconjug Chem 14:222–231
26. Fitzsimmons REB, Uludag H (2012) Specific effects of PEGylation on gene delivery efficacy of polyethylenimine: Interplay between PEG substitution and N/P ratio. Acta Biomater 8:3941–3955
27. Smrekar B, Wightman L, Wolschek MF, Lichtenberger C, Ruzicka R, Ogris M, Rodl W, Kursa M, Wagner E, Kircheis R (2003) Tissue-dependent factors affect gene delivery to tumors in vivo. Gene Ther 10:1079–1088
28. Ogris M, Brunner S, Schuller S, Kircheis R, Wagner E (1999) PEGylated DNA/transferrin-PEI complexes: reduced interaction with blood components, extended circulation in blood and potential for systemic gene delivery. Gene Ther 6:595–605
29. Schwerdt A, Zintchenko A, Concia M, Roesen N, Fisher K, Lindner LH, Issels R, Wagner E, Ogris M (2008) Hyperthermia-induced targeting of thermosensitive gene carriers to tumors. Hum Gene Ther 19:1283–1292
30. Fella C, Walker GF, Ogris M, Wagner E (2008) Amine-reactive pyridylhydrazone-based PEG reagents for pH-reversible PEI polyplex shielding. Eur J Pharm Sci 34:309–320
31. Walker GF, Fella C, Pelisek J, Fahrmeir J, Boeckle S, Ogris M, Wagner E (2005) Toward synthetic viruses: endosomal pH-triggered deshielding of targeted polyplexes greatly enhances gene transfer in vitro and in vivo. Mol Ther 11:418–425
32. Klutz K, Schaffert D, Willhauck MJ, Grunwald GK, Haase R, Wunderlich N, Zach C, Gildehaus FJ, Senekowitsch-Schmidtke R, Goke B, Wagner E, Ogris M, Spitzweg C (2011) Epidermal growth factor receptor-targeted (131) I-therapy of liver cancer following systemic delivery of the sodium iodide symporter gene. Mol Ther 19:676–685
33. Kircheis R, Wightman L, Schreiber A, Robitza B, Rossler V, Kursa M, Wagner E (2001) Polyethylenimine/DNA complexes shielded by transferrin target gene expression to tumors after systemic application. Gene Ther 8:28–40

34. Ogris M, Steinlein P, Carotta S, Brunner S, Wagner E (2001) DNA/polyethylenimine transfection particles: Influence of ligands, polymer size, and PEGylation on internalization and gene expression. AAPS Pharm Sci 3: E21
35. Ogris M, Walker G, Blessing T, Kircheis R, Wolschek M, Wagner E (2003) Tumor-targeted gene therapy: strategies for the preparation of ligand-polyethylene glycol-polyethylenimine/DNA complexes. J Control Release 91:173–181
36. Schafer A, Pahnke A, Schaffert D, van Weerden WM, de Ridder CM, Rodl W, Vetter A, Spitzweg C, Kraaij R, Wagner E, Ogris M (2011) Disconnecting the Yin and Yang relation of epidermal growth factor receptor (EGFR)-mediated delivery: a fully synthetic, EGFR-targeted gene transfer system avoiding receptor activation. Hum Gene Ther 22:1463–1473
37. Sidi AA, Ohana P, Benjamin S, Shalev M, Ransom JH, Lamm D, Hochberg A, Leibovitch I (2008) Phase I/II marker lesion study of intravesical BC-819 DNA plasmid in H19 over expressing superficial bladder cancer refractory to bacillus calmette-guerin. J Urol 180:2379–2383
38. Ungaro F, De Rosa G, Miro A, Quaglia F (2003) Spectrophotometric determination of polyethylenimine in the presence of an oligonucleotide for the characterization of controlled release formulations. J Pharm Biomed Anal 31:143–149
39. Eyer P, Worek F, Kiderlen D, Sinko G, Stuglin A, Simeon-Rudolf V, Reiner E (2003) Molar absorption coefficients for the reduced Ellman reagent: reassessment. Anal Biochem 312:224–227
40. Jeong JH, Song SH, Lim DW, Lee H, Park TG (2001) DNA transfection using linear poly (ethylenimine) prepared by controlled acid hydrolysis of poly(2-ethyl-2-oxazoline). J Control Release 73:391–399
41. Schleef M, Schmidt T (2004) Animal-free production of ccc-supercoiled plasmids for research and clinical applications. J Gene Med 6(Suppl 1):S45–S53
42. Magnusson T, Haase R, Schleef M, Wagner E, Ogris M (2011) Sustained, high transgene expression in liver with plasmid vectors using optimized promoter-enhancer combinations. J Gene Med 13:382–391
43. Kasper JC, Schaffert D, Ogris M, Wagner E, Friess W (2011) The establishment of an up-scaled micro-mixer method allows the standardized and reproducible preparation of well-defined plasmid/LPEI polyplexes. Eur J Pharm Biopharm 77:182–185
44. Ogris M, Steinlein P, Kursa M, Mechtler K, Kircheis R, Wagner E (1998) The size of DNA/transferrin-PEI complexes is an important factor for gene expression in cultured cells. Gene Ther 5:1425–1433

VIII. References

1. Rödl, W, Taschauer, A, Schaffert, D, Wagner, E, and Ogris, M (2019). Synthesis of Polyethylenimine-Based Nanocarriers for Systemic Tumor Targeting of Nucleic Acids. In: Ogris, M and Sami, H (eds). *Nanotechnology for Nucleic Acid Delivery: Methods and Protocols*. Springer New York: New York, NY. pp 83-99.

2. Giornelli, GH (2016). Management of relapsed ovarian cancer: a review. *SpringerPlus* **5**, 11.

3. Gehrig, S, Sami, H, and Ogris, M (2014). Gene therapy and imaging in preclinical and clinical oncology: recent developments in therapy and theranostics. *Therapeutic delivery*, 1275-1296.

4. Das, SK, Menezes, ME, Bhatia, S, Wang, XY, Emdad, L, Sarkar, D*, et al.* (2015). Gene Therapies for Cancer: Strategies, Challenges and Successes. *J Cell Physiol* **230**, 259-271.

5. Shanker, M, Jin, J, Branch, CD, Miyamoto, S, Grimm, EA, Roth, JA*, et al.* (2011). Tumor suppressor gene-based nanotherapy: from test tube to the clinic. *Journal of drug delivery* **2011**, 465845-465845.

6. Vogelstein, B, and Kinzler, KW (2004). Cancer genes and the pathways they control. *Nature medicine* **10**, 789-799.

7. Vogelstein, B, Lane, D, and Levine, AJ (2000). Surfing the p53 network. *Nature* **408**, 307-310.

8. Werth, S, Urban-Klein, B, Dai, L, Hobel, S, Grzelinski, M, Bakowsky, U*, et al.* (2006). A low molecular weight fraction of polyethylenimine (PEI) displays increased transfection efficiency of DNA and siRNA in fresh or lyophilized complexes. *JControl Release* **112**, 257-270.

9. Dirin, M, and Winkler, J (2013). Influence of diverse chemical modifications on the ADME characteristics and toxicology of antisense oligonucleotides. *Expert Opin Biol Ther* **13**, 875-888.

10. Ballarín-González, B, Ebbesen, MF, and Howard, KA (2014). Polycation-based nanoparticles for RNAi-mediated cancer treatment. *Cancer letters* **352**, 66-80.

11. Walther, W, and Stein, U (2000). Viral vectors for gene transfer - A review of their use in the treatment of human diseases. *Drugs* **60**, 249-271.

12. Macpherson, JL, and Rasko, JEJ (2014). Clinical potential of gene therapy: towards meeting the demand. *Intern Med J* **44**, 224-233.

13. Yin, H, Kanasty, RL, Eltoukhy, AA, Vegas, AJ, Dorkin, JR, and Anderson, DG (2014). Non-viral vectors for gene-based therapy. *Nat Rev Genet* **15**, 541-555.

14. Jonsson, F, Hagedorn, C, and Kreppel, F (2018). Combined Genetic and Chemical Capsid Modifications of Adenovirus-Based Gene Transfer Vectors for Shielding and Targeting. *J Vis Exp*, 10.

15. Gruntman, AM, and Flotte, TR (2018). The rapidly evolving state of gene therapy. *Faseb J* **32**, 1733-1740.

16. Lawler, SE, Speranza, MC, Cho, CF, and Chiocca, EA (2017). Oncolytic Viruses in Cancer Treatment A Review. *JAMA Oncol* **3**, 841-849.

17. Thomas, CE, Ehrhardt, A, and Kay, MA (2003). Progress and problems with the use of viral vectors for gene therapy. *Nat Rev Genet* **4**, 346-358.

18. Dunbar, CE, High, KA, Joung, JK, Kohn, DB, Ozawa, K, and Sadelain, M (2018). Gene therapy comes of age. *Science* **359**, 175-+.

19. Mintzer, MA, and Simanek, EE (2009). Nonviral Vectors for Gene Delivery. *Chem Rev* **109**, 259-302.

20. Geyer, A, Lorenzer, C, Gehrig, S, Simlinger, M, Winkler, J, Sami, H*, et al.* (2017). Fluorescence- and computed tomography for assessing the biodistribution of siRNA after intratracheal application in mice. *International journal of pharmaceutics* **525**, 359-366.

21. Kawabata, K, Takakura, Y, and Hashida, M (1995). The fate of plasmid DNA after intravenous injection in mice: involvement of scavenger receptors in its hepatic uptake. *PharmRes* **12**, 825-830.

22. Voit, T, Topaloglu, H, Straub, V, Muntoni, F, Deconinck, N, Campion, G*, et al.* (2014). Safety and efficacy of drisapersen for the treatment of Duchenne muscular dystrophy (DEMAND II): an exploratory, randomised, placebo-controlled phase 2 study. *Lancet Neurol* **13**, 987-996.

23. Juliano, RL, Ming, X, Carver, K, and Laing, B (2014). Cellular Uptake and Intracellular Trafficking of Oligonucleotides: Implications for Oligonucleotide Pharmacology. *Nucl Acid Ther* **24**, 101-113.

24. Vermeulen, LMP, Brans, T, De Smedt, SC, Remaut, K, and Braeckmans, K (2018). Methodologies to investigate intracellular barriers for nucleic acid delivery in non-viral gene therapy. *Nano Today* **21**, 74-90.

25. Tauhardt, L, Kempe, K, Knop, K, Altuntas, E, Jager, M, Schubert, S*, et al.* (2011). Linear Polyethyleneimine: Optimized Synthesis and Characterization - On the Way to "Pharmagrade" Batches. *Macromol Chem Phys* **212**, 1918-1924.

26. Lostale-Seijo, I, and Montenegro, J (2018). Synthetic materials at the forefront of gene delivery. *Nat Rev Chem* **2**, 258-277.

27. Pack, DW, Hoffman, AS, Pun, S, and Stayton, PS (2005). Design and development of polymers for gene delivery. *Nat Rev Drug Discov* **4**, 581-593.

28. Kopatz, I, Remy, JS, and Behr, JP (2004). A model for non-viral gene delivery: through syndecan adhesion molecules and powered by actin. *The journal of gene medicine* **6**, 769-776.

29. Felgner, PL, Gadek, TR, Holm, M, Roman, R, Chan, HW, Wenz, M*, et al.* (1987). Lipofection: a highly efficient, lipid-mediated DNA-transfection procedure. *Proc Natl Acad Sci U S A* **84**, 7413-7417.

30. Zhang, X-X, McIntosh, TJ, and Grinstaff, MW (2012). Functional lipids and lipoplexes for improved gene delivery. *Biochimie* **94**, 42-58.

31. de Ilarduya, CT, Sun, Y, and Duezguenes, N (2010). Gene delivery by lipoplexes and polyplexes. *Eur J Pharm Sci* **40**, 159-170.

32. Hirko, A, Tang, FX, and Hughes, JA (2003). Cationic lipid vectors for plasmid DNA delivery. *Current Medicinal Chemistry* **10**, 1185-1193.

33. Li, W, and Szoka, FC, Jr. (2007). Lipid-based nanoparticles for nucleic acid delivery. *PharmRes* **24**, 438-449.

34. Al-Dosari, MS, and Gao, X (2009). Nonviral gene delivery: principle, limitations, and recent progress. *The AAPS journal* **11**, 671-681.

35. Sokolova, V, and Epple, M (2008). Inorganic nanoparticles as carriers of nucleic acids into cells. *Angew Chem-Int Edit* **47**, 1382-1395.

36. Giljohann, DA, Seferos, DS, Daniel, WL, Massich, MD, Patel, PC, and Mirkin, CA (2010). Gold Nanoparticles for Biology and Medicine. *Angew Chem-Int Edit* **49**, 3280-3294.

37. Salas, G, Costo, R, and Morales, MdP (2012). Chapter 2 - Synthesis of Inorganic Nanoparticles. In: de la Fuente, JM and Grazu, V (eds). *Frontiers of Nanoscience*, vol. 4. Elsevier. pp 35-79.

38. Valizadeh, A, Mikaeili, H, Samiei, M, Farkhani, SM, Zarghami, N, Kouhi, M*, et al.* (2012). Quantum dots: synthesis, bioapplications, and toxicity. *Nanoscale Res Lett* **7**, 14.

39. Shi, L, Buhler, E, Boue, F, and Carn, F (2017). How does the size of gold nanoparticles depend on citrate to gold ratio in Turkevich synthesis? Final answer to a debated question. *J Colloid Interf Sci* **492**, 191-198.

40. Turkevich, J, Stevenson, PC, and Hillier, J (1951). A STUDY OF THE NUCLEATION AND GROWTH PROCESSES IN THE SYNTHESIS OF COLLOIDAL GOLD. *Discussions of the Faraday Society*, 55-&.

41. Chithrani, BD, Ghazani, AA, and Chan, WCW (2006). Determining the size and shape dependence of gold nanoparticle uptake into mammalian cells. *Nano Lett* **6**, 662-668.

42. Westcott, SL, Oldenburg, SJ, Lee, TR, and Halas, NJ (1998). Formation and adsorption of clusters of gold nanoparticles onto functionalized silica nanoparticle surfaces. *Langmuir* **14**, 5396-5401.

43. Jeong, EH, Jung, G, Hong, CA, and Lee, H (2014). Gold nanoparticle (AuNP)-based drug delivery and molecular imaging for biomedical applications. *Arch Pharm Res* **37**, 53-59.

44. Cole, LE, Ross, RD, Tilley, JMR, Vargo-Gogola, T, and Roeder, RK (2015). Gold nanoparticles as contrast agents in x-ray imaging and computed tomography. *Nanomedicine* **10**, 321-341.

45. Eck, W, Nicholson, AI, Zentgraf, H, Semmler, W, and Bartling, S (2010). Anti-CD4-targeted Gold Nanoparticles Induce Specific Contrast Enhancement of Peripheral Lymph Nodes in X-ray Computed Tomography of Live Mice. *Nano Lett* **10**, 2318-2322.

46. Amendola, V, Pilot, R, Frasconi, M, Marago, OM, and Iati, MA (2017). Surface plasmon resonance in gold nanoparticles: a review. *J Phys-Condens Mat* **29**, 48.

47. Wurster, E-C, Elbakry, A, Göpferich, A, and Breunig, M (2013). Layer-by-Layer Assembled Gold Nanoparticles for the Delivery of Nucleic Acids. In: Ogris, M and Oupicky, D (eds). *Nanotechnology for Nucleic Acid Delivery: Methods and Protocols*. Humana Press: Totowa, NJ. pp 171-182.

48. Whitesides, GM, and Grzybowski, B (2002). Self-assembly at all scales. *Science* **295**, 2418-2421.

49. Decher, G (1997). Fuzzy nanoassemblies: Toward layered polymeric multicomposites. *Science* **277**, 1232-1237.

50. Correa, S, Choi, KY, Dreaden, EC, Renggli, K, Shi, A, Gu, L*, et al.* (2016). Highly Scalable, Closed-Loop Synthesis of Drug-Loaded, Layer-by-Layer Nanoparticles. *Adv Funct Mater* **26**, 991-1003.

51. Tan, YF, Mundargi, RC, Chen, MHA, Lessig, J, Neu, B, Venkatraman, SS*, et al.* (2014). Layer-by-Layer Nanoparticles as an Efficient siRNA Delivery Vehicle for SPARC Silencing. *Small* **10**, 1790-1798.

52. Wurster, E-C, Liebl, R, Michaelis, S, Robelek, R, Wastl, DS, Giessibl, FJ*, et al.* (2015). Oligolayer-Coated Nanoparticles: Impact of Surface Topography at the Nanobio Interface. *ACS Applied Materials & Interfaces* **7**, 7891-7900.

53. Barnaby, SN, Lee, A, and Mirkin, CA (2014). Probing the inherent stability of siRNA immobilized on nanoparticle constructs. *Proc Natl Acad Sci U S A* **111**, 9739-9744.

54. Hurst, SJ, Lytton-Jean, AKR, and Mirkin, CA (2006). Maximizing DNA loading on a range of gold nanoparticle sizes. *Anal Chem* **78**, 8313-8318.

55. Mirkin, CA (2017). Spherical nucleic acids as a powerful new platform for cancer immunotherapy. *Cancer research* **77**, 2.

56. Rosi, NL, Giljohann, DA, Thaxton, CS, Lytton-Jean, AKR, Han, MS, and Mirkin, CA (2006). Oligonucleotide-modified gold nanoparticles for intracellular gene regulation. *Science* **312**, 1027-1030.

57. de Araujo, RV, Santos, SD, Ferreira, EI, and Giarolla, J (2018). New Advances in General Biomedical Applications of PAMAM Dendrimers. *Molecules* **23**, 27.

58. Santos, SD, Ferreira, EI, and Giarolla, J (2016). Dendrimer Prodrugs. *Molecules* **21**, 22.

59. Tomalia, DA, Baker, H, Dewald, J, Hall, M, Kallos, G, Martin, S*, et al.* (1985). A NEW CLASS OF POLYMERS - STARBURST-DENDRITIC MACROMOLECULES. *Polym J* **17**, 117-132.

60. Navarro, G, Maiwald, G, Haase, R, Rogach, AL, Wagner, E, de Ilarduya, CT*, et al.* (2010). Low generation PAMAM dendrimer and CpG free plasmids allow targeted and extended transgene expression in tumors after systemic delivery. *Journal of controlled release : official journal of the Controlled Release Society* **146**, 99-105.

61. Jain, K, Kesharwani, P, Gupta, U, and Jain, NK (2010). Dendrimer toxicity: Let's meet the challenge. *International journal of pharmaceutics* **394**, 122-142.

62. Nyitrai, G, Heja, L, Jablonkai, I, Pal, I, Visy, J, and Kardos, J (2013). Polyamidoamine dendrimer impairs mitochondrial oxidation in brain tissue. *J Nanobiotechnol* **11**, 9.

63. Pryor, JB, Harper, BJ, and Harper, SL (2014). Comparative toxicological assessment of PAMAM and thiophosphoryl dendrimers using embryonic zebrafish. *International journal of nanomedicine* **9**, 1947-1956.

64. Boussif, O, Lezoualc'h, F, Zanta, MA, Mergny, MD, Scherman, D, Demeneix, B*, et al.* (1995). A versatile vector for gene and oligonucleotide transfer into cells in culture and in vivo: polyethylenimine. *ProcNatlAcadSciUSA* **92**, 7297-7301.

65. Schaffert, D, and Ogris, M (2013). Nucleic Acid Carrier Systems Based on Polyethylenimine Conjugates for the Treatment of Metastatic Tumors. *Current Medicinal Chemistry* **20**, 3456-3470.

66. von Harpe, A, Petersen, H, Li, Y, and Kissel, T (2000). Characterization of commercially available and synthesized polyethylenimines for gene delivery. *Journal of controlled release : official journal of the Controlled Release Society* **69**, 309-322.

67. Dick, CR, and Ham, GE (1970). CHARACTERIZATION OF POLYETHYLENIMINE. *J Macromol Sci Chem* **A 4**, 1301-&.

68. Clamme, JP, Krishnamoorthy, G, and Mely, Y (2003). Intracellular dynamics of the gene delivery vehicle polyethylenimine during transfection: investigation by two-photon fluorescence correlation spectroscopy. *BiochimBiophysActa* **1617**, 52-61.

69. Borkovec, M, and Koper, GJM (1997). Proton binding characteristics of branched polyelectrolytes. *Macromolecules* **30**, 2151-2158.

70. Godbey, WT, Wu, KK, and Mikos, AG (1999). Tracking the intracellular path of poly(ethylenimine)/DNA complexes for gene delivery 840. *ProcNatlAcadSciUSA* **96**, 5177-5181.

71. Remy-Kristensen, A, Clamme, JP, Vuilleumier, C, Kuhry, JG, and Mely, Y (2001). Role of endocytosis in the transfection of L929 fibroblasts by polyethylenimine/DNA complexes. *Bba-Biomembranes* **1514**, 21-32.

72. Benjaminsen, RV, Mattebjerg, MA, Henriksen, JR, Moghimi, SM, and Andresen, TL (2013). The Possible "Proton Sponge" Effect of Polyethylenimine (PEI) Does Not Include Change in Lysosomal pH. *Mol Ther* **21**, 149-157.

73. Ogris, M, Brunner, S, Schuller, S, Kircheis, R, and Wagner, E (1999). PEGylated DNA/transferrin-PEI complexes: reduced interaction with blood components, extended circulation in blood and potential for systemic gene delivery. *Gene therapy* **6**, 595-605.

74. Erbacher, P, Bettinger, T, Belguise-Valladier, P, Zou, SM, Coll, JL, Behr, JP*, et al.* (1999). Transfection and physical properties of various saccharide, poly(ethylene glycol), and antibody-derivatized polyethylenimines (PEI). *J Gene Med* **1**, 210-222.

75. Boeckle, S, von Gersdorff, K, van der Piepen, S, Culmsee, C, Wagner, E, and Ogris, M (2004). Purification of polyethylenimine polyplexes highlights the role of free polycations in gene transfer. *The journal of gene medicine* **6**, 1102-1111.

76. Brissault, B, Kichler, A, Guis, C, Leborgne, C, Danos, O, and Cheradame, H (2003). Synthesis of linear polyethylenimine derivatives for DNA transfection. *BioconjugChem* **14**, 581-587.

77. Kagiya, T, Narisawa, S, Maeda, T, and Fukui, K (1966). RING-OPENING POLYMERIZATION OF 2-SUBSTITUTED 2-OXAZOLINES. *Journal of Polymer Science Part B-Polymer Letters* **4**, 441-&.

78. Luxenhofer, R, Han, YC, Schulz, A, Tong, J, He, ZJ, Kabanov, AV*, et al.* (2012). Poly(2-oxazoline)s as Polymer Therapeutics. *Macromolecular Rapid Communications* **33**, 1613-1631.

79. Glassner, M, Vergaelen, M, and Hoogenboom, R (2018). Poly(2-oxazoline)s: A comprehensive overview of polymer structures and their physical properties. *Polym Int* **67**, 32-45.

80. Talsma, H, Cherng, J, Lehrmann, H, Kursa, M, Ogris, M, Hennink, WE*, et al.* (1997). Stabilization of gene delivery systems by freeze-drying. *International journal of pharmaceutics* **157**, 233-238.

81. Anchordoquy, TJ, Allison, SD, Molina, MC, Girouard, LG, and Carson, TK (2001). Physical stabilization of DNA-based therapeutics. *Drug Discov Today* **6**, 463-470.

82. Kasper, JC, Schaffert, D, Ogris, M, Wagner, E, and Friess, W (2011). The establishment of an up-scaled micro-mixer method allows the standardized and reproducible preparation of well-defined plasmid/LPEI polyplexes. *Eur J Pharm Biopharm* **77**, 182-185.

83. Davies, LA, Nunez-Alonso, GA, Hebel, HL, Scheule, RK, Cheng, SH, Hyde, SC*, et al.* (2010). A novel mixing device for the reproducible generation of nonviral gene therapy formulations. *Biotechniques* **49**, 666-668.

84. Beyerle, A, Irmler, M, Beckers, J, Kissel, T, and Stoeger, T (2010). Toxicity Pathway Focused Gene Expression Profiling of PEI-Based Polymers for Pulmonary Applications. *Mol Pharmaceut* **7**, 727-737.

85. Moghimi, SM, Symonds, P, Murray, JC, Hunter, AC, Debska, G, and Szewczyk, A (2005). A two-stage poly(ethylenimine)-mediated cytotoxicity: implications for gene transfer/therapy. *Molecular therapy : the journal of the American Society of Gene Therapy* **11**, 990-995.

86. Breunig, M, Hozsa, C, Lungwitz, U, Watanabe, K, Umeda, I, Kato, H*, et al.* (2008). Mechanistic investigation of poly(ethylene imine)-based siRNA delivery: Disulfide bonds boost intracellular release of the cargo. *J Control Release* **130**, 57-63.

87. Kunath, K, von Harpe, A, Fischer, D, Petersen, H, Bickel, U, Voigt, K*, et al.* (2003). Low-molecular-weight polyethylenimine as a non-viral vector for DNA delivery: comparison of physicochemical properties, transfection efficiency and in vivo distribution with high-molecular-weight polyethylenimine. *Journal of controlled release : official journal of the Controlled Release Society* **89**, 113-125.

88. Gebhart, CL, and Kabanov, AV (2001). Evaluation of polyplexes as gene transfer agents. *Journal of controlled release : official journal of the Controlled Release Society* **73**, 401-416.

89. Goula, D, Benoist, C, Mantero, S, Merlo, G, Levi, G, and Demeneix, BA (1998). Polyethylenimine-based intravenous delivery of transgenes to mouse lung. *Gene therapy* **5**, 1291-1295.

90. Ferrari, S, Moro, E, Pettenazzo, A, Behr, JP, Zacchello, F, and Scarpa, M (1997). ExGen 500 is an efficient vector for gene delivery to lung epithelial cells in vitro and in vivo. *Gene therapy* **4**, 1100-1106.

91. Bragonzi, A, Boletta, A, Biffi, A, Muggia, A, Sersale, G, Cheng, SH*, et al.* (1999). Comparison between cationic polymers and lipids in mediating systemic gene delivery to the lungs. *Gene therapy* **6**, 1995-2004.

92. Wiseman, JW, Goddard, CA, McLelland, D, and Colledge, WH (2003). A comparison of linear and branched polyethylenimine (PEI) with DCChol/DOPE liposomes for gene delivery to epithelial cells in vitro and in vivo. *Gene Ther* **10**, 1654-1662.

93. Wightman, L, Kircheis, R, Rossler, V, Carotta, S, Ruzicka, R, Kursa, M*, et al.* (2001). Different behavior of branched and linear polyethylenimine for gene delivery in vitro and in vivo. *The journal of gene medicine* **3**, 362-372.

94. Pezzoli, D, Giupponi, E, Mantovani, D, and Candiani, G (2017). Size matters for in vitro gene delivery: investigating the relationships among complexation protocol, transfection medium, size and sedimentation. *Sci Rep* **7**, 11.

95. Taschauer, A, Geyer, A, Gehrig, S, Maier, J, Sami, H, and Ogris, M (2016). Up-Scaled Synthesis and Characterization of Nonviral Gene Delivery Particles for Transient In Vitro and In Vivo Transgene Expression. *Hum Gene Ther Methods* **27**, 87-97.

96. Goula, D, Becker, N, Lemkine, GF, Normandie, P, Rodrigues, J, Mantero, S*, et al.* (2000). Rapid crossing of the pulmonary endothelial barrier by polyethylenimine/DNA complexes 965. *Gene therapy* **7**, 499-504.

97. Cun, D, Jensen, LB, Nielsen, HM, Moghimi, M, and Foged, C (2008). Polymeric Nanocarriers for siRNA Delivery: Challenges and Future Prospects. *J Biomed Nanotechnol* **4**, 258-275.

98. Lodish, HF, Zhou, B, Liu, G, and Chen, CZ (2008). Micromanagement of the immune system by microRNAs. *Nat Rev Immunol* **8**, 120-130.

99. Obbard, DJ, Gordon, KHJ, Buck, AH, and Jiggins, FM (2009). The evolution of RNAi as a defence against viruses and transposable elements. *Philos Trans R Soc B-Biol Sci* **364**, 99-115.

100. Merkel, OM, Rubinstein, I, and Kissel, T (2014). siRNA Delivery to the lung: What's new? *Advanced drug delivery reviews* **75**, 112-128.

101. Liu, JD, Carmell, MA, Rivas, FV, Marsden, CG, Thomson, JM, Song, JJ*, et al.* (2004). Argonaute2 is the catalytic engine of mammalian RNAi. *Science* **305**, 1437-1441.

102. Elbashir, SM, Lendeckel, W, and Tuschl, T (2001). RNA interference is mediated by 21- and 22-nucleotide RNAs. *Genes Dev* **15**, 188-200.

103. Grayson, AC, Doody, AM, and Putnam, D (2006). Biophysical and structural characterization of polyethylenimine-mediated siRNA delivery in vitro. *PharmRes* **23**, 1868-1876.

104. Wagner, M, Rinkenauer, AC, Schallon, A, and Schubert, US (2013). Opposites attract: influence of the molar mass of branched poly(ethylene imine) on biophysical characteristics of siRNA-based polyplexese. *RSC Adv* **3**, 12774-12785.

105. Ziebarth, JD, Kennetz, DR, Walker, NJ, and Wang, YM (2017). Structural Comparisons of PEI/DNA and PEI/siRNA Complexes Revealed with Molecular Dynamics Simulations. *J Phys Chem B* **121**, 1941-1952.

106. Lungwitz, U, Breunig, M, Blunk, T, and Gopferich, A (2005). Polyethylenimine-based non-viral gene delivery systems. *EurJPharmBiopharm* **60**, 247-266.

107. Neu, M, Fischer, D, and Kissel, T (2005). Recent advances in rational gene transfer vector design based on poly(ethylene imine) and its derivatives. *JGene Med* **7**, 992-1009.

108. Fischer, D, von Harpe, A, Kunath, K, Petersen, H, Li, Y, and Kissel, T (2002). Copolymers of ethylene imine and N-(2-hydroxyethyl)-ethylene imine as tools to study effects of polymer structure on physicochemical and biological properties of DNA complexes 1. *BioconjugChem* **13**, 1124-1133.

109. Niu, G, and Chen, XY (2012). Molecular Imaging with Activatable Reporter Systems. *Theranostics* **2**, 413-423.

110. Alam, J, and Cook, JL (1990). Reporter genes: Application to the study of mammalian gene transcription. *Analytical Biochemistry* **188**, 245-254.

111. Damdindorj, L, Karnan, S, Ota, A, Hossain, E, Konishi, Y, Hosokawa, Y*, et al.* (2014). A Comparative Analysis of Constitutive Promoters Located in Adeno-Associated Viral Vectors. *Plos One* **9**, 10.

112. Qin, JY, Zhang, L, Clift, KL, Hulur, I, Xiang, AP, Ren, BZ*, et al.* (2010). Systematic Comparison of Constitutive Promoters and the Doxycycline-Inducible Promoter. *Plos One* **5**, 4.

113. Sun, JH, Kelemen, GH, Fernandez-Abalos, JM, and Bibb, MJ (1999). Green fluorescent protein as a reporter for spatial and temporal gene expression in Streptomyces coelicolor A3(2). *Microbiology-(UK)* **145**, 2221-2227.

114. Haas, J, Park, EC, and Seed, B (1996). Codon usage limitation in the expression of HIV-1 envelope glycoprotein. *Curr Biol* **6**, 315-324.

115. Shcherbakova, DM, and Verkhusha, VV (2013). Near-infrared fluorescent proteins for multicolor in vivo imaging. *Nat Methods* **10**, 751-754.

116. Weissleder, R (2001). A clearer vision for in vivo imaging. *Nature biotechnology* **19**, 316-317.

117. Simeonov, A, Jadhav, A, Thomas, CJ, Wang, YH, Huang, RL, Southall, NT*, et al.* (2008). Fluorescence spectroscopic profiling of compound libraries. *J Med Chem* **51**, 2363-2371.

118. Thorne, N, Inglese, J, and Auldl, DS (2010). Illuminating Insights into Firefly Luciferase and Other Bioluminescent Reporters Used in Chemical Biology. *Chem Biol* **17**, 646-657.

119. Maguire, CA, Deliolanis, NC, Pike, L, Niers, JM, Tjon-Kon-Fat, LA, Sena-Esteves, M*, et al.* (2009). Gaussia Luciferase Variant for High-Throughput Functional Screening Applications. *Anal Chem* **81**, 7102-7106.

120. Wurdinger, T, Badr, C, Pike, L, de Kleine, R, Weissleder, R, Breakefield, XO*, et al.* (2008). A secreted luciferase for ex vivo monitoring of in vivo processes. *Nat Methods* **5**, 171-173.

121. Kursa, M, Walker, GF, Roessler, V, Ogris, M, Roedl, W, Kircheis, R*, et al.* (2003). Novel shielded transferrin-polyethylene glycol-polyethylenimine/DNA complexes for systemic tumor-targeted gene transfer. *Bioconjug Chem* **14**, 222-231.

122. Fitzsimmons, REB, and Uludag, H (2012). Specific effects of PEGylation on gene delivery efficacy of polyethylenimine: Interplay between PEG substitution and N/P ratio. *Acta Biomater* **8**, 3941-3955.

123. Schwerdt, A, Zintchenko, A, Concia, M, Roesen, N, Fisher, KD, Lindner, LH*, et al.* (2008). Hyperthermia induced targeting of thermosensitive gene carriers to tumors. *Human gene therapy*.

124. Smrekar, B, Wightman, L, Wolschek, MF, Lichtenberger, C, Ruzicka, R, Ogris, M*, et al.* (2003). Tissue-dependent factors affect gene delivery to tumors in vivo. *Gene therapy* **10**, 1079-1088.

125. Schaffert, D, Kiss, M, Rodl, W, Shir, A, Levitzki, A, Ogris, M*, et al.* (2011). Poly(I:C)-Mediated Tumor Growth Suppression in EGF-Receptor Overexpressing Tumors Using EGF-Polyethylene Glycol-Linear Polyethylenimine as Carrier. *Pharm Res* **28**, 731-741.

126. Hatakeyama, H, Akita, H, and Harashima, H (2013). The Polyethyleneglycol Dilemma: Advantage and Disadvantage of PEGylation of Liposomes for Systemic Genes and Nucleic Acids Delivery to Tumors. *Biol Pharm Bull* **36**, 892-899.

127. Schafer, A, Pahnke, A, Schaffert, D, van Weerden, WM, de Ridder, CM, Rodl, W*, et al.* (2011). Disconnecting the Yin and Yang Relation of Epidermal Growth Factor Receptor (EGFR)-Mediated Delivery: A Fully Synthetic, EGFR-Targeted Gene Transfer System Avoiding Receptor Activation. *Human gene therapy* **22**, 1463-1473.

128. Li, Z, Zhao, R, Wu, X, Sun, Y, Yao, M, Li, J*, et al.* (2005). Identification and characterization of a novel peptide ligand of epidermal growth factor receptor for targeted delivery of therapeutics. *Faseb J* **19**, 1978-1985.

129. Smith, GP (1985). FILAMENTOUS FUSION PHAGE - NOVEL EXPRESSION VECTORS THAT DISPLAY CLONED ANTIGENS ON THE VIRION SURFACE. *Science* **228**, 1315-1317.

130. Yum, LY, and Robyn, LW (2002). Application of Phage Display Technology to Cancer Research. *Current Pharmaceutical Biotechnology* **3**, 29-43.

131. Abourbeh, G, Shir, A, Mishani, E, Ogris, M, Rodl, W, Wagner, E*, et al.* (2012). PolyIC GE11 polyplex inhibits EGFR-overexpressing tumors. *IUBMB life* **64**, 324-330.

132. Kuo, WT, Lin, WC, Chang, KC, Huang, JY, Yen, KC, Young, IC*, et al.* (2015). Quantitative Analysis of Ligand-EGFR Interactions: A Platform for Screening Targeting Molecules. *Plos One* **10**, 11.

133. Ogris, M, and Sami, H (2015). Receptor Crosslinking in Drug Delivery: Detour to the Lysosome? *Molecular therapy : the journal of the American Society of Gene Therapy* **23**, 1802-1804.

134. Mickler, FM, Mockl, L, Ruthardt, N, Ogris, M, Wagner, E, and Brauchle, C (2012). Tuning Nanoparticle Uptake: Live-Cell Imaging Reveals Two Distinct Endocytosis Mechanisms Mediated by Natural and Artificial EGFR Targeting Ligand. *Nano Lett*.

135. Diller, DJ, Swanson, J, Bayden, AS, Jarosinski, M, and Audie, J (2015). Rational, computer-enabled peptide drug design: principles, methods, applications and future directions. *Future Med Chem* **7**, 2173-2193.

136. Song, SX, Liu, D, Peng, JL, Deng, HW, Guo, Y, Xu, LX*, et al.* (2009). Novel peptide ligand directs liposomes toward EGF-R high-expressing cancer cells in vitro and in vivo. *Faseb J* **23**, 1396-1404.

137. Williams, TM, Sable, R, Singh, S, Vicente, MGH, and Jois, SD (2018). Peptide ligands for targeting the extracellular domain of EGFR: Comparison between linear and cyclic peptides. *Chem Biol Drug Des* **91**, 605-619.

138. Bofinger, R, Zaw-Thin, M, Mitchell, NJ, Patrick, PS, Stowe, C, Gomez-Ramirez, A*, et al.* (2018). Development of lipopolyplexes for gene delivery: A comparison of the effects of differing modes of targeting peptide display on the structure and transfection activities of lipopolyplexes. *J Pept Sci* **24**, 12.

139. Fu, S, Xu, X, Ma, Y, Zhang, S, and Zhang, S (2019). RGD peptide-based non-viral gene delivery vectors targeting integrin αvβ3 for cancer therapy. *Journal of Drug Targeting* **27**, 1-11.

140. Plow, EF, Haas, TK, Zhang, L, Loftus, J, and Smith, JW (2000). Ligand binding to integrins. *J Biol Chem* **275**, 21785-21788.

141. Stevenson, M, Hale, ABH, Hale, SJ, Green, NK, Black, G, Fisher, KD*, et al.* (2007). Incorporation of a laminin-derived peptide (SIKVAV) on polymer-modified adenovirus permits tumor-specific targeting via alpha 6-integrins. *Cancer gene therapy* **14**, 335-345.

142. Lin, CS, Zhang, K, and Kramer, R (1993). ALPHA-6 INTEGRIN IS UP-REGULATED IN STEP INCREMENTS ACCOMPANYING NEOPLASTIC TRANSFORMATION AND TUMORIGENIC CONVERSION OF HUMAN FIBROBLASTS. *Cancer research* **53**, 2950-2953.

143. Krebsbach, PH, and Villa-Diaz, LG (2017). The Role of Integrin α6 (CD49f) in Stem Cells: More than a Conserved Biomarker. *Stem cells and development* **26**, 1090-1099.

144. Lathia, JD, Gallagher, J, Heddleston, JM, Wang, J, Eyler, CE, Macswords, J*, et al.* (2010). Integrin alpha 6 regulates glioblastoma stem cells. *Cell stem cell* **6**, 421-432.

145. Kikkawa, Y, Hozumi, K, Katagiri, F, Nomizu, M, Kleinman, HK, and Koblinski, JE (2013). Laminin-111-derived peptides and cancer. *Cell adhesion & migration* **7**, 150-256.

146. Feldmann, DP, and Merkel, OM (2015). The advantages of pulmonary delivery of therapeutic siRNA. *Therapeutic delivery* **6**, 407-409.

147. Kuzmov, A, and Minko, T (2015). Nanotechnology approaches for inhalation treatment of lung diseases. *J Control Release* **219**, 500-518.

148. McLachlan, G, Davidson, H, Holder, E, Davies, LA, Pringle, IA, Sumner-Jones, SG*, et al.* (2011). Pre-clinical evaluation of three non-viral gene transfer agents for cystic fibrosis after aerosol delivery to the ovine lung. *Gene therapy* **18**, 996-1005.

149. Densmore, CL (2006). Advances in noninvasive pulmonary gene therapy. *Curr Drug Deliv* **3**, 55-63.

150. Olmsted, SS, Padgett, JL, Yudin, AI, Whaley, KJ, Moench, TR, and Cone, RA (2001). Diffusion of macromolecules and virus-like particles in human cervical mucus. *Biophys J* **81**, 1930-1937.

151. Huckaby, JT, and Lai, SK (2018). PEGylation for enhancing nanoparticle diffusion in mucus. *Advanced drug delivery reviews* **124**, 125-139.

152. Lai, SK, O'Hanlon, DE, Harrold, S, Man, ST, Wang, YY, Cone, R*, et al.* (2007). Rapid transport of large polymeric nanoparticles in fresh undiluted human mucus. *Proc Natl Acad Sci U S A* **104**, 1482-1487.

153. Leal, J, Smyth, HDC, and Ghosh, D (2017). Physicochemical properties of mucus and their impact on transmucosal drug delivery. *International journal of pharmaceutics* **532**, 555-572.

154. Dames, PL, E.; Rudolph, C. (2007). Aerosol Gene Delivery to the Lungs of Mice Guided by Magnetic Forces. *Mol Ther* **15**, S348.

155. Schuster, BS, Suk, JS, Woodworth, GF, and Hanes, J (2013). Nanoparticle diffusion in respiratory mucus from humans without lung disease. *Biomaterials* **34**, 3439-3446.

156. von Gersdorff, K, Sanders, NN, Vandenbroucke, R, De Smedt, SC, Wagner, E, and Ogris, M (2006). The internalization route resulting in successful gene expression depends on both cell line and polyethylenimine polyplex type. *Molecular therapy : the journal of the American Society of Gene Therapy* **14**, 745-753.

157. Malloy, A (2011). Count, size and visualize nanoparticles. *Materials Today* **14**, 170-173.

158. Finsinger, D, Remy, JS, Erbacher, P, Koch, C, and Plank, C (2000). Protective copolymers for nonviral gene vectors: synthesis, vector characterization and application in gene delivery 995. *Gene Ther* **7**, 1183-1192.

159. Clamme, JP, Azoulay, J, and Mely, Y (2003). Monitoring of the Formation and Dissociation of Polyethylenimine/DNA Complexes by Two Photon Fluorescence Correlation Spectroscopy. *BiophysJ* **84**, 1960-1968.

160. Lenter, MC, Garidel, P, Pelisek, J, Wagner, E, and Ogris, M (2004). Stabilized nonviral formulations for the delivery of MCP-1 gene into cells of the vasculoendothelial system. *PharmRes* **21**, 683-691.

161. Su, B, Cengizeroglu, A, Farkasova, K, Viola, JR, Anton, M, Ellwart, JW*, et al.* (2013). Systemic TNFalpha gene therapy synergizes with liposomal doxorubicine in the treatment of metastatic cancer. *Molecular therapy : the journal of the American Society of Gene Therapy* **21**, 300-308.

162. Zintchenko, A, Susha, AS, Concia, M, Feldmann, J, Wagner, E, Rogach, AL*, et al.* (2009). Drug nanocarriers labeled with near-infrared-emitting quantum dots (quantoplexes): imaging fast dynamics of distribution in living animals. *Molecular therapy : the journal of the American Society of Gene Therapy* **17**, 1849-1856.

163. Medarova, Z, Pham, W, Farrar, C, Petkova, V, and Moore, A (2007). In vivo imaging of siRNA delivery and silencing in tumors. *Nature medicine* **13**, 372-377.

164. Piatkevich, KD, Suk, H-J, Kodandaramaiah, SB, Yoshida, F, DeGennaro, EM, Drobizhev, M*, et al.* (2017). Near-Infrared Fluorescent Proteins Engineered from Bacterial Phytochromes in Neuroimaging. *Biophys J* **113**, 2299-2309.

165. http://penncentury.com/products/liquid-aerosol-devices/microsprayer-msa-250/model-msa-250-mouse/ (23.12.2018).

166. Merkel, OM, Beyerle, A, Librizzi, D, Pfestroff, A, Behr, TM, Sproat, B*, et al.* (2009). Nonviral siRNA Delivery to the Lung: Investigation of PEG−PEI Polyplexes and Their In Vivo Performance. *Mol Pharmaceut* **6**, 1246-1260.

167. Ahmad, J, Akhter, S, Rizwanullah, M, Amin, S, Rahman, M, Ahmad, MZ*, et al.* (2015). Nanotechnology-based inhalation treatments for lung cancer: state of the art. *Nanotechnology, science and applications* **8**, 55-66.

168. Weiss, DJ (2002). Delivery of gene transfer vectors to lung: Obstacles and the role of adjunct techniques for airway administration. *Mol Ther* **6**, 148-152.

169. Freitas, VM, Vilas-Boas, VF, Pimenta, DC, Loureiro, V, Juliano, MA, Carvalho, MR*, et al.* (2007). SIKVAV, a laminin alpha1-derived peptide, interacts with integrins and increases protease activity of a human salivary gland adenoid cystic carcinoma cell line through the ERK 1/2 signaling pathway. *The American journal of pathology* **171**, 124-138.

170. Cutler, JI, Auyeung, E, and Mirkin, CA (2012). Spherical Nucleic Acids. *Journal of the American Chemical Society* **134**, 1376-1391.

IX. Disclaimer

I hereby confirm that this thesis was written following common citation rules. In case of any copyright violation, please do not hesitate to contact me.